# Development of Low Temperature Plasma as a Novel Focal Therapy for Prostate Cancer

Adam Michael Hirst

## PhD

University of York

Physics

April 2016

## Abstract

Cancer of the prostate is the most common male malignancy. Despite continual refinement, the treatment of localised prostate cancer remains unsatisfactory. Patients are often faced with the choice between invasive radical surgery and the risk of impotence, or radiological techniques with associated off-target toxicity and incomplete tumour ablation. Low temperature plasma (LTP) may present a completely new approach for the focal treatment of localised prostate cancer. LTPs create a rich source of reactive oxygen and nitrogen species, plus energetic photons, charged particles, and localised electric fields. Long-established radio- and chemo-therapies are known to exploit the ability of reactive species to induce cytopathic effects.

The effects of LTP were first investigated in two commonly used prostate cell lines: BPH-1 and PC-3 cells. It was found that LTP treatment induced high levels of DNA damage, reduced cell viability and clonogenicity, and both apoptotic and necrotic cell death. The study then moved on to evaluate the effects of LTP in clinically relevant prostate models through the treatment of normal and cancer primary prostate cells derived directly from patient tissues. Whilst the immediate effects of LTP mirrored those found in cell lines, it was found that primary prostate cells do not undergo apoptosis; dying entirely via necrotic mechanisms. Evidence of an autophagic response was also observed following LTP treatment, and it was found that LTP showed no selectivity between normal and tumour cells. The treatment of three-dimensional aggregate and spheroid models was also evaluated, where it was found that the cytopathic effect of LTP occurred at the surface of treated spheres. Finally, the study concludes by speculating how LTP may compare with and overcome some of the issues encountered with current prostate cancer therapies, and outlines how focal LTP could be applied to patients in the clinic.

# Table of Contents

## List of Figures

## List of Tables

## Acknowledgements

First and foremost, my sincere thanks go to my team of supervisors Dr. Deborah O'Connell, Professor Norman Maitland and Dr. Fiona Frame. Thank you to Deborah, for allowing me the freedom and support to carry out this work under my own steam, and to Norman and Fiona for their encouragement and patience, especially at the start of this project when I was just "a physicist" who knew next-to-nothing about biology!

I owe my thanks to Dr. Kari Niemi and Richard Armitage for their technical expertise, and to Phil Roberts for his assistance in creating the graphics and illustrations used in both my publications and in this thesis. Thanks also to Dr. Jérôme Bredin for his help with the needle plasma presented in this work and to Andy West for offering his advice on optical spectroscopy measurements. Thank you to the surgical staff, and especially the patients, of Castle Hill Hospital, for the donation and provision of tissue samples. Without you, studies of this nature would not be possible.

I would like thank Hannah, Michelle, Fiona and Dominika for the endless laughs and eyebrow-raising quotes over coffee and lunch. Thanks also to all the post-docs and students at the York Plasma Institute and Cancer Research Unit for making both laboratories such enjoyable places to work.

Em, your support has been unwavering and you have helped me to achieve things I did not think I was capable of. Also, I am indebted to you for your assistance with the intricacies of formatting this thesis!

Finally, Mum and Dad, for your continued support and belief in me, through the good times and the bad, I will be forever grateful.

## Author's Declaration

I declare that this thesis and the research presented within has been generated as a result of my own work and has not been submitted previously in consideration for a degree at this, or any other University. The contents of several chapters have been published in scientific journals, and are included in Appendix C of this thesis.

Consenting of patients and provision of primary prostate tissue was conducted by tissue procurement officer Dr. Vincent Mann. Subsequent primary tissue dissection and digestion was conducted by members of the Cancer Research Unit laboratory (including the author) on a rota system. Routine subculture of all cell types presented in this thesis was conducted by the author. The optical emission spectrum presented in Figure 14B was performed with assistance on the experimental setup from Dr. Andrew West, with subsequent data collection and analyses performed by the author. The raw data presented in Figure 18A was kindly provided by Dr. Fiona Frame, which was plotted graphically and analysed by the author. The irradiation treatment of cells in Figure 18 was also conducted by Dr. Fiona Frame. The power supply and plasma jet presented in Chapter 7 and Figures 51 and 52 were designed and operated by Dr. Jérôme Bredin. All other experimental procedures and subsequent data analysis were performed solely by the author. All sources are acknowledged as references.

# Chapter 1
## The Prostate and Treatment of Prostate Cancer

# 1. The Prostate and Treatment of Prostate Cancer

## 1.1 Morphology of the Prostate Gland

The normal human prostate gland is a small, walnut-sized organ, which is sited at the base of the bladder and surrounds the urethra. According to the widely adopted classification devised by McNeal [1], the prostate is composed of four separate regions, or 'zones', as depicted in Figure 1. The majority of the prostate glandular volume is made up by the peripheral zone (~70%), which surrounds the urethra. Over two-thirds of all carcinomas are believed to arise within this region [2]. The central zone surrounds the ejaculatory ducts and comprises ~25% of the total organ volume. Around ~5% is attributed to the transition zone, which is located in the centre of the prostate, grows throughout life and from which benign prostatic hyperplasia is believed to arise [3]. Finally, the anterior zone is a thick layer of fibrous and muscular tissue that possesses no glandular structure or function.
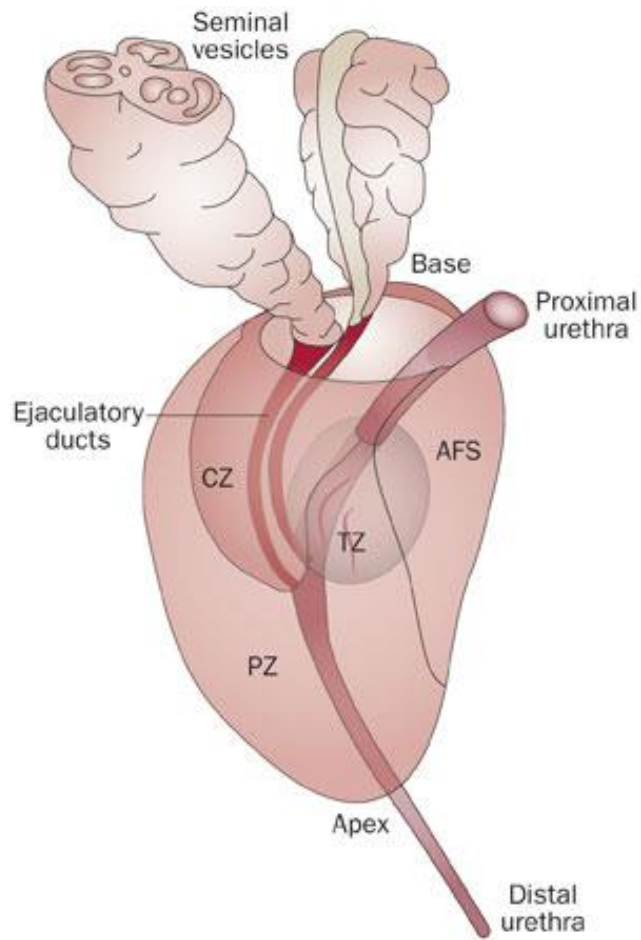
**Figure 1: Morphology of the human prostate gland**.

Sited at the base of the bladder, the prostate envelops the urethra. The gland comprises four main zones; the transition zone (TZ), peripheral zone (PZ), central zone (CZ) and anterior fibromuscular stroma (AFS). Reprinted with permission from Wadhera[a] [4].

## 1.2 Cellular Organisation of the Prostate Epithelium

The normal prostate consists of a double-layered epithelium, which comprises three phenotypically different cell types: secretory luminal cells, basal cells and neuroendocrine cells. Luminal cells constitute the inner layer of the epithelium, are terminally differentiated, and secrete products such as prostate specific antigen (PSA) and prostatic acid phosphatase (PAP) [5]. They have a high rate of apoptosis [6], are reliant on androgens for their survival and hence express high levels of androgen receptor (AR) [7].
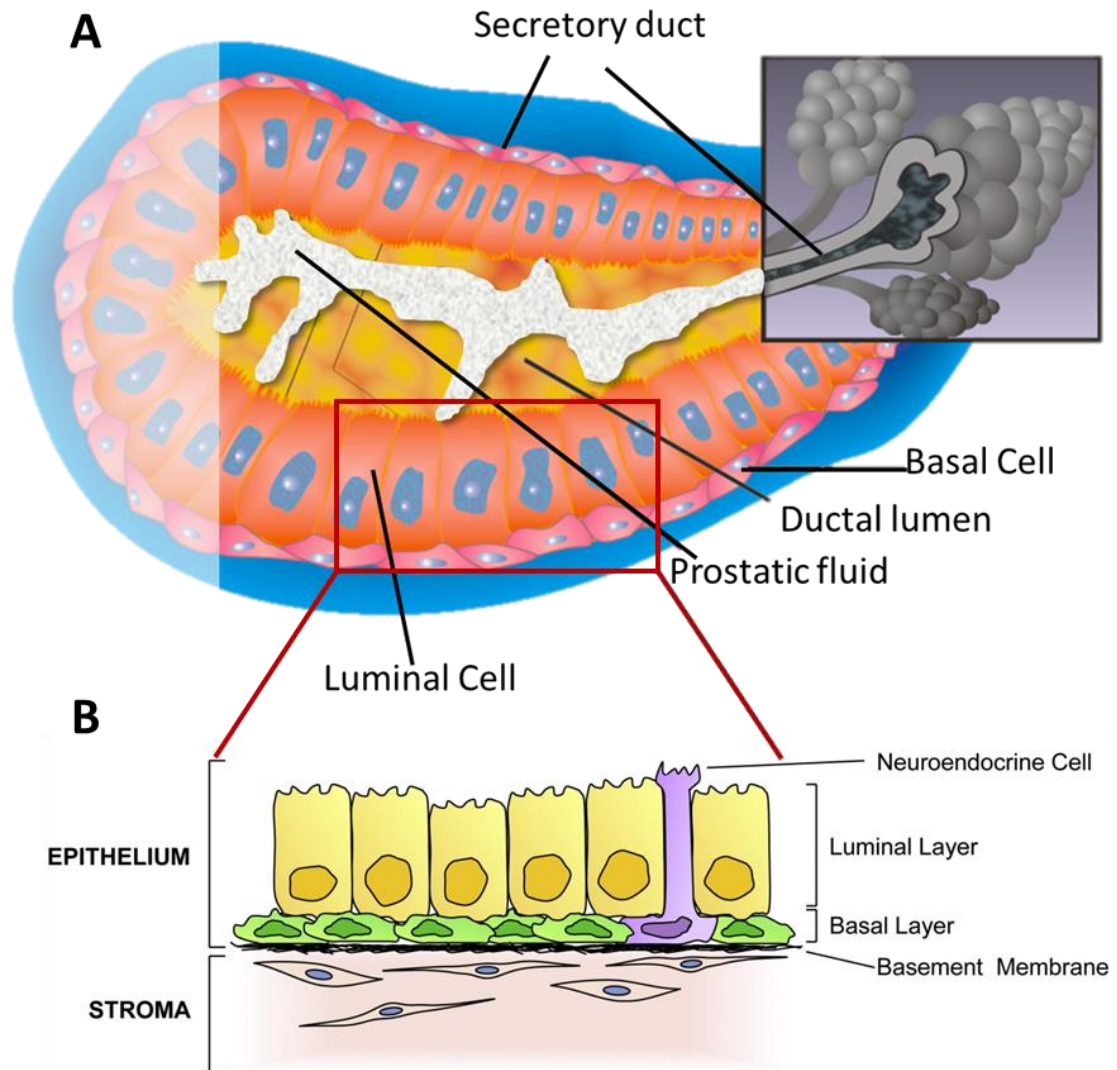
**Figure 2: Organisation of the prostate epithelium.**

A cross-section of a single duct within the prostate is shown in **A**, which is expanded in **B** to indicate the organization of luminal and basal cell layers and their proximity to stromal tissue. Reprinted with permission from Collins and Maitland[β] [8], and Oldridge et al[γ] [9]. *[β] Reprinted from Eur J Cancer 42(9), Collins A. T. and Maitland N. J., Prostate cancer stem cells, Pages 1213-1218, Copyright 2006, with permission from Elsevier. [γ]Reprinted from Mol Cell Endocrinol. 360(1-2), Oldridge E. E. et al., Prostate cancer stem cells: are they androgen responsive?, Pages 14-24, Copyright 2012, with permission from Elsevier.*

Basal cells form the outer layer of the epithelium and express p63, CD 44 and low levels of AR [10, 11]. They are strongly anchored to the basement membrane, which forms a dividing boundary between epithelial structures within the prostate and surrounding stromal tissue. Unlike luminal cells, basal cells have low secretory activity. They are also relatively undifferentiated compared to their luminal counterparts. Basal and luminal cells can be further distinguished by their expression of unique cytokeratin (CK) pairs [12]. Basal cells have been shown to express CK 5 and CK 14, whereas luminal cells express CK 8 and CK 18 [13]. A rare population of neuroendocrine cells are found scattered within the basal layer of the epithelium, which are terminally differentiated and AR-independent [14]. They secrete a number of bioactive products including chromogranin and serotonin [15], and are thought to play a regulatory role in the growth and maintenance of the prostate epithelium [16]. Stromal cells, which lie beneath the basement membrane, also secrete products which are essential for epithelial cell maintenance and differentiation, namely epidermal growth factor (EGF) and fibroblast growth factor (FGF) [17, 18]. The cells in the basal layer can be further subdivided based on their differentiation state, into stem cells (SC), transit amplifying (TA) cells and committed basal (CB) cells. Largely quiescent SCs give rise to rapidly dividing TA cells, which differentiate to form CB cells. These cells then differentiate further to form the terminally differentiated secretory luminal layer [9]. The stages of the differentiation process are illustrated in Figure 3.
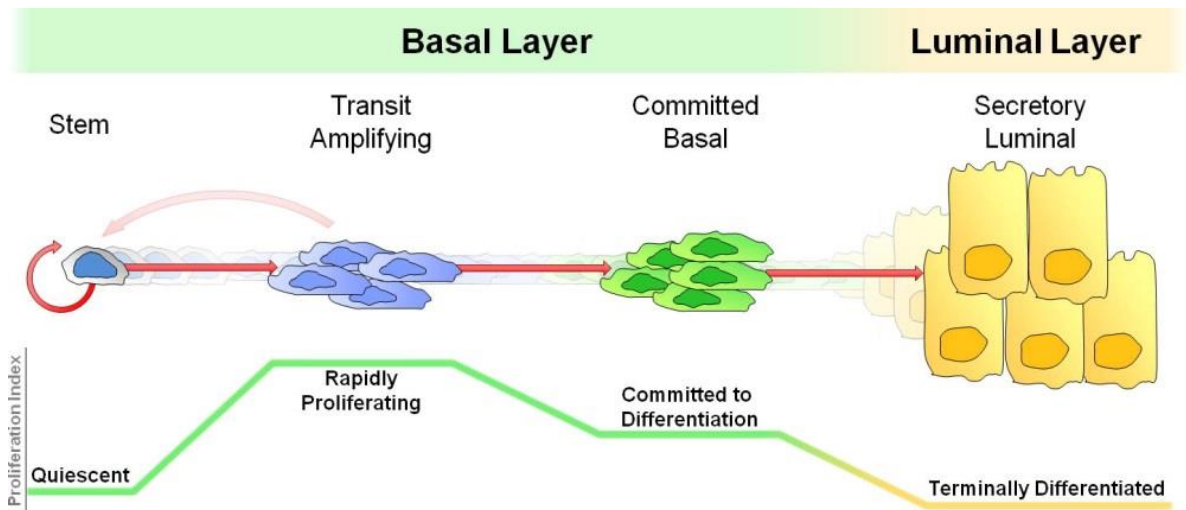
**Figure 3: Cellular hierarchy within the prostate epithelium.**

Quiescent stem cells give rise to a rapidly proliferating population of transit amplifying cells. These differentiate to form committed basal cells and ultimately the secretory cells of the luminal layer. Reprinted with permission from Oldridge et al[δ] [9]. *[δ]Reprinted from Mol Cell Endocrinol. 360(1-2), Oldridge E. E. et al., Prostate cancer stem cells: are they androgen responsive?, Pages 14-24, Copyright 2012, with permission from Elsevier.*

### 1.3  Diseases and disorders of the Prostate

### 1.3.1   Prostatitis

The term prostatitis can be used to describe a number of conditions of the prostate, namely: acute and chronic bacterial infections, pelvic pain, and inflammatory disorders [19]. It typically originates in the central zone and is the most common prostate disorder, with an incidence rate of 2-10% [20] and can occur in men of all ages. The condition can be treated successfully with antibiotic and anti-inflammatory drugs [21], however repeated or persistent inflammation of the prostate is thought to increase the risk of the development of benign prostatic hyperplasia (BPH) in later life [22, 23].

### 1.3.2. Benign Prostatic Hyperplasia

Benign enlargement of the prostate gland is a condition that is associated with aging men. It is estimated that over half of men over the age of 50 will have benign prostatic hyperplasia (BPH) [24], rising to ~75% in men aged 70 or older [25, 26]. BPH originates only in the transition zone, and arises from discrete regions of hyperplasia, which ultimately leads to considerable enlargement of the gland. As such, patients often experience the urge to urinate frequently due to increased pressure on the bladder, yet struggle to initiate and maintain a urine flow because of constriction of the urethra. First-line treatments include smooth muscle and steroid 5α-reductase inhibitors to improve urine flow and reduce prostate volume respectively [27]. BPH is ultimately alleviated using a procedure known as transurethral resection of the prostate (TURP), where tissue is surgically removed in order to clear the obstruction to the urethra, and reduce the volume of the gland; relieving pressure and discomfort.

### 1.3.3. Prostatic Intraepithelial Neoplasia

Prostatic intraepithelial neoplasia (PIN) usually occurs in the peripheral zone of the prostate, and denotes abnormal cellular proliferation that results in pre-invasive neoplasms in the bilayer of the epithelium [28]. Despite the potential for invasion and proliferation of secretory cells into the glandular lumen, the basal layer remains at least partially intact, and the basement membrane is not breached (see Figure 5). Considered as a precursor to carcinoma, studies suggest the majority of men with high-grade PIN will develop prostate cancer (PCa) within a decade [29].

### 1.3.4. Prostate Cancer

Cancer of the prostate is recognised as the most common non-cutaneous malignancy in men, accounting for around a quarter of all cases and over 10% of cancer related deaths [30]. In the UK, recent statistics indicate there are over 40,000 newly diagnosed cases and more than 10,000 deaths annually as a result of the disease [31]. The likelihood of diagnosis has risen in recent years, particularly in developed countries [32]. Prostate cancer (PCa) is often described as a disease of old age, with risk of development peaking in men aged 60 years or older. These values are represented in Figure 4. However, high incidence rates are also found in younger men [33], which may be influenced by hereditary factors such as inherited genetic defects, leading to elevated risk of aggressive cancer [34]. It has been suggested that as high as 42% of the risk of developing PCa may be attributed to heritable factors [35].
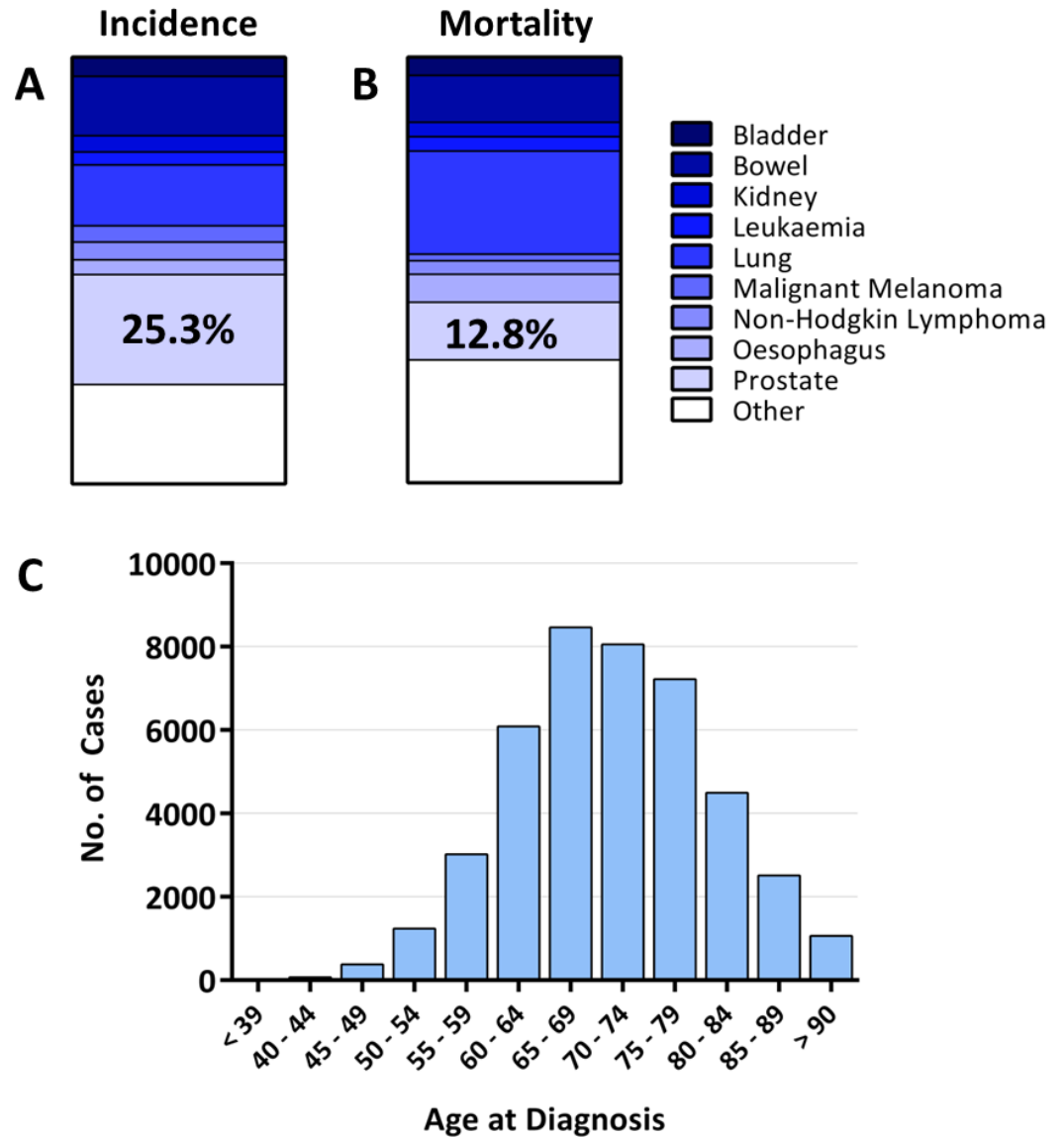
**Figure 4: Epidemiology of prostate cancer.**

Incidence rates show that prostate cancer accounts for a quarter of all diagnoses in men

(**A**), and over 10% of deaths (**B**). Risk of diagnosis significantly increases over the age

of 60 (**C**). Values obtained from freely available data from Cancer Research UK 2012 statistics:

*http://www.cancerresearchuk.org/content/cancer-statistics-for-the-uk,* accessed January 2016.

Cancer of the prostate is typically a slowly progressing disease which is believed to originate mostly in the peripheral zone. As the disease develops from PIN to adenocarcinoma, the organised glandular structure of the prostate is lost as cells begin to invade the glandular lumen, as seen in Figure 5. Reduced numbers of basal cells are noted in PIN, and prostate carcinogenesis is generally defined by the absence of basal cells, and thus is accepted to be of a predominantly luminal phenotype [36]. However, it is believed that cells within the basal population are the origin of carcinogenesis, and that there is a small population of basal cells within a tumour [37]. Differentiated, mutated luminal cells become highly proliferative [38], and as disease progression advances towards metastasis, the basement membrane is breached and mutated cells invade outwards into the surrounding stroma.

### 1.3.5. Metastatic Prostate Cancer

Prostate cancer typically metastasises into the lymph nodes and pelvic bones. For patients whose cancer has spread beyond the prostate gland, androgen deprivation therapy (ADT) is usually prescribed. As prostate tumours are largely dependent on androgens for growth, ADT removes circulating androgens and blocks their binding to the AR. This arrests cell proliferation, leading to apoptosis. Most patients initially respond well to ADT, showing tumour shrinkage and a reduction in their PSA levels [39]. However, invariably ADT eventually fails, leading to castrate-resistant prostate cancer (CRPC). At this stage, the treatment of the disease is palliative. Whilst the development of novel drugs such as abiraterone have shown modest overall survival improvements of a few months relative to placebo [40], life-expectancy following diagnosis of metastatic CRPC remains at around 18-24 months [39].

Normal epithelium

Prostatic intraepithelial neoplasia (PIN)

Adeno-carcinoma (latent)

Adeno-carcinoma (clinical)

Metastasis

Initiation

Progression

Treatment
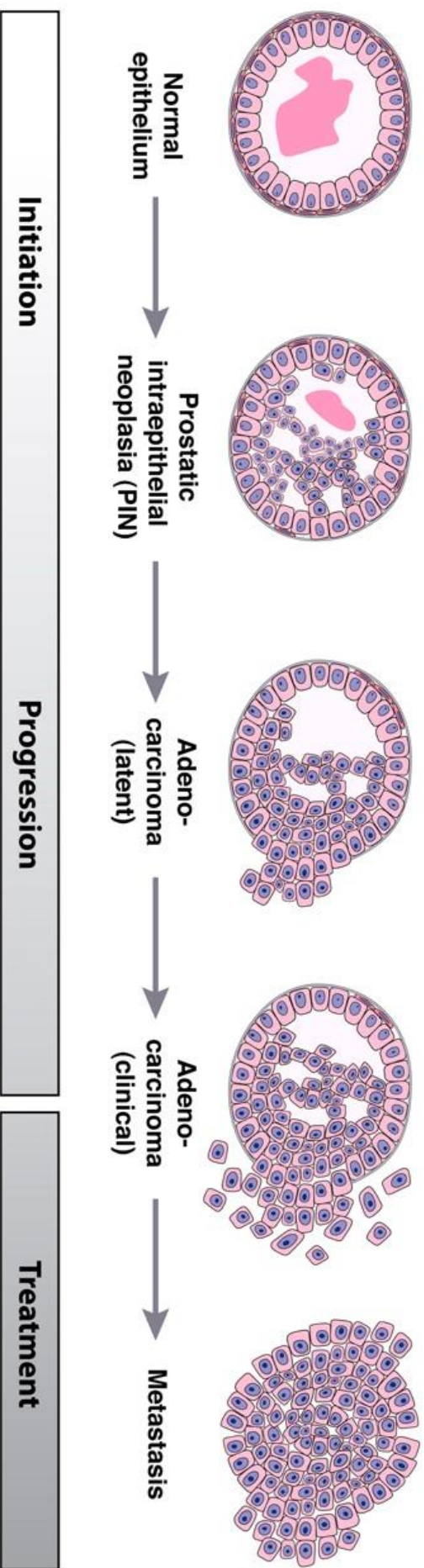
**Figure 5: Initiation and progression of prostate cancer.**

Clinical progression of prostate cancer is characterized by progressive loss of the basal layer, breakdown of the basement membrane and invasion into surrounding tissues. Reprinted from Shen and Abate-Shen [36], under a Creative Commons 4.0 Non-commercial license (*http://creativecommons.org/licenses/by-nc/4.0/*).

### 1.4 Diagnosis of Prostate Cancer

The PSA test is the most common means of screening, detecting, and monitoring PCa. PSA concentrations of higher than 4 ng/ml in patient blood samples are cause for concern and usually accompanied by digital rectal examination (DRE) for prostate abnormalities. As the PSA test has become more widespread, unsurprisingly higher numbers of men have been diagnosed with PCa [41], however the test can produce both false positives and negatives. For example, ~ 20% of test results could be false positives [42]. A healthy man without PCa can have elevated PSA levels, which may be indicative of other prostate conditions including BPH or prostatitis [43].

A more definitive means of diagnosis involves the use of trans-rectal ultrasound (TRUS) or magnetic resonance imaging (MRI). This allows direct visualisation of the prostate gland, zonal anatomy and areas of malignancy [44]. The enhanced resolution of MRI permits greater detection accuracy and the ability to stage the disease locally [45], i.e. whether the disease is confined to the prostate, uni- or multi-focal, or has metastasised. However, it lacks the portability of ultrasound detection and is considerably more expensive. Needle-core tissue biopsies are taken under TRUS guidance for subsequent analysis. A minimum of 10 cores is recommended to represent the overall morphology of the whole gland, although more cores may be taken from enlarged prostates [46]. These tissue sections are analysed by histopathology, and the disease is graded based on the tissue morphology and architecture, as shown in Figure 6. Removal of tissue affects the general morphology of the gland, and despite multiple cores being taken, it is still possible to miss areas of malignancy.
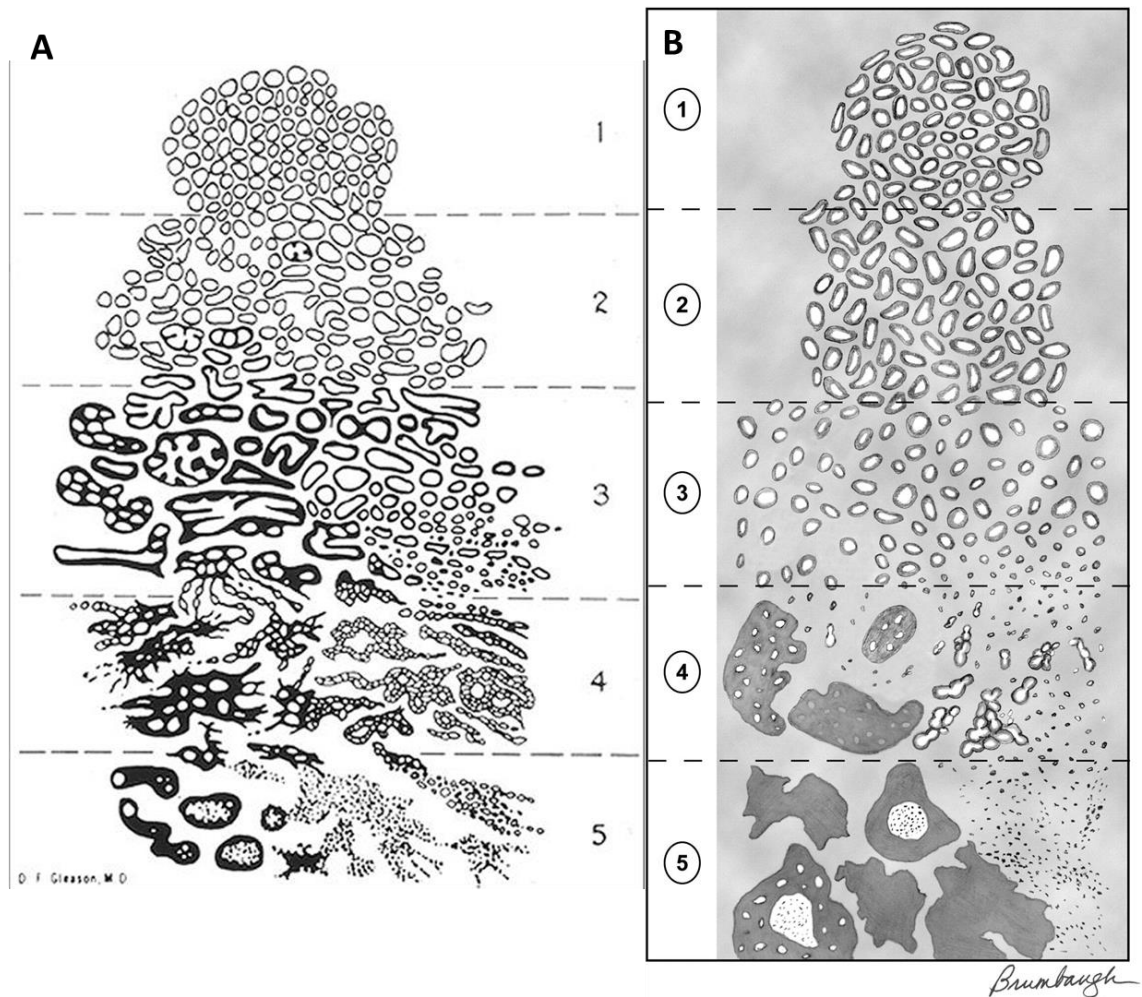
**Figure 6: The Gleason grading system of prostate cancer.**

The presently accepted system for defining the severity of prostate malignancy was devised by Gleason in 1966 [47] (**A**), and later updated by Epstein[ε] in 2010 [48] (**B**). A value is assigned from between 1 to 5 based on the morphological appearance of prostate tissue. [ε]*Reprinted and modified from The Journal of Urology, 183, Epstein J. I., An update of the Gleason Grading System, Pages 433-440, Copyright 2010, with permission from Elsevier.*

The disease scoring system adopted for PCa was developed in 1966 by Gleason [47] based on the architecture of benign tissue samples, and was updated by Epstein in 2010 [48]. The grading system indicates the progression from uniform glands representative of normal tissue (grade 1), to a decrease in cellular organisation and potentially invasive margins (grade 3), and ultimately to abstract morphological features devoid of glandular structure, indicative of aggressive disease (grade 5). The approach is routinely used by pathologists to describe the morphology of prostate tissue sections, who combine two separate graded scores to give an overall indication of disease stage and risk. One score is assigned for the most common pattern, and one for the second most common pattern as shown by Figure 6. When combined these values provide an overall grade out of ten, with Gleason grade 6-7 representing low risk disease (in the updated system, Gleason grade 6 is not considered cancer), and Gleason grade 8-10 indicative of high risk, potentially invasive PCa.

## 1.5  Models for Studying Prostate Cancer

Several models exist for the study of PCa in the laboratory. These are outlined below and illustrated in Figure 7.

### 1.5.1   Prostate Epithelial Cell Lines

The most commonly used method to studying PCa *in vitro* are cell lines. They are widely available, generally proliferate rapidly and can be cultured indefinitely [49]. Several commonly used prostate cell lines exist, such as those listed in Figure 7. However, extended culturing of cell lines over many years in the presence of serum has been shown to induce chromosomal changes [50]. Despite being the most frequently

used model system, prostate cell lines are not representative of the heterogeneity of tumours.

### 1.5.2   Primary Prostate Epithelial Cells

Derived directly from human prostate tumours, benign and healthy tissues, primary prostate epithelial cells serve as a far more accurate model of prostate disease, as they reflect the original properties of the tissue [49]. Needle core biopsies from the normal and tumour tissue of the same patient allow for direct comparison of the effect of treatments on normal and cancer cells. However, they are limited by a short lifespan in culture conditions and are not readily available. In addition, tumour samples may contain a proportion of normal prostate cells.

### 1.5.3   Three Dimensional Models of Prostate Cancer

Prostate cell lines and primary epithelial cells can be cultured to form three-dimensional structures known as aggregates and spheroids. These more accurately represent the morphology of tumours than cells cultured in monolayers. They are, however, labour intensive to produce, and large numbers are required to perform even simple assays.

### 1.5.4   In Vivo Mouse Models

Cell lines and primary cells cultured as mouse xenografts enable the study of tumours in a more realistic niche, whereby the cells interact with stroma and a blood supply. Nonetheless, compared to other models, they are expensive to maintain.

Immunocompromised mice do not accurately represent the functional immune system of a patient, and the infiltration and interaction of mouse cells with the human tumour is an issue.
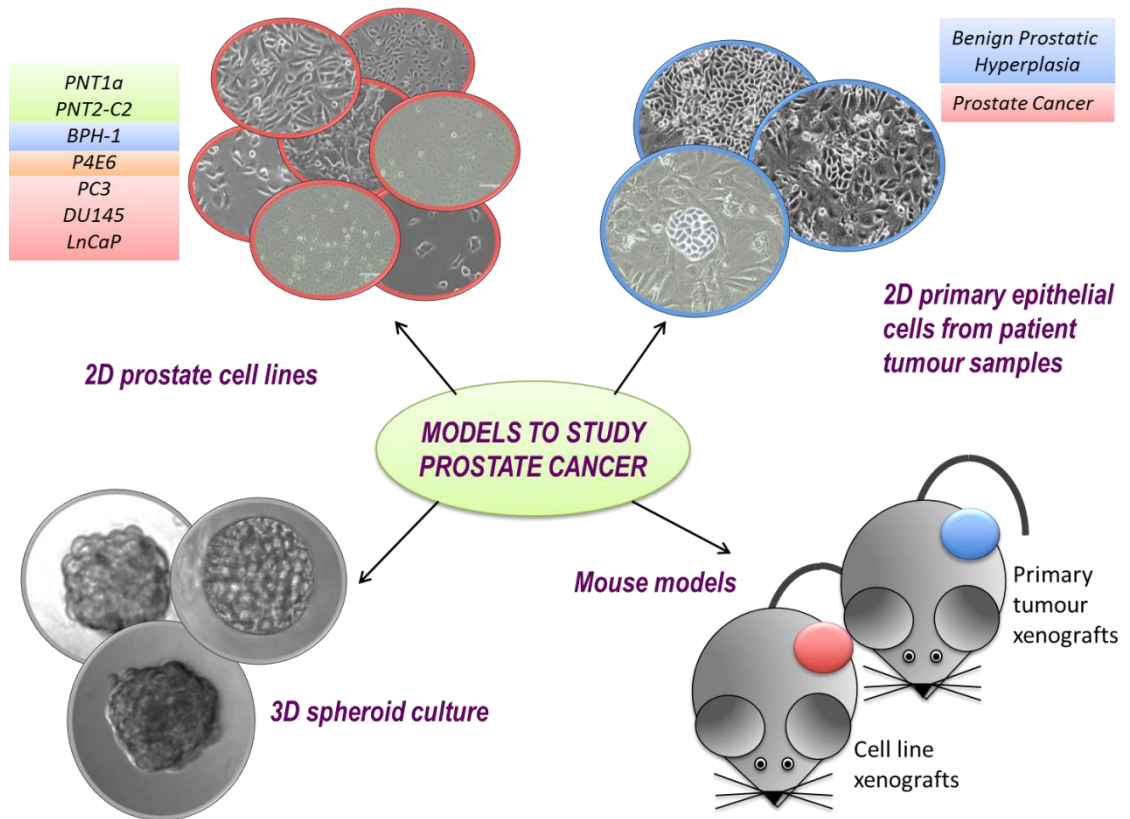
**Figure 7: Models to study prostate cancer.**

Several experimental models exist to study prostate cancer in the laboratory, ranging from cell lines grown as monolayers to mouse xenografts. Reprinted with permission from Frame et al$^\zeta$ [51]. $^\zeta$*Reprinted and modified from Human Cell Transformation, Chapter 9, Frame F. M. and Maitland N. J., Cancer Stem Cells, Models of Study and Implications of Therapy Resistance Mechanisms, Pages 105-118, Copyright 2011, with permission from Springer.*

## 1.6 Treatment of Organ Confined Prostate Cancer

When diagnosed with organ confined, or localised PCa, both the patient and clinician face a choice between a multitude of different treatment options, each with their own set of advantages and drawbacks. These range from monitoring of the disease, to radical surgery, and are outlined below.

### 1.6.1 Watchful Waiting

A 50 year old male has a lifetime risk of 42% of developing PCa, yet his risk of developing clinically significant disease is around 10%, and the risk of death as a direct result of PCa is only around 3% [52]. *Watchful waiting*, or *active surveillance* has become an increasingly accepted approach to the management of early-onset PCa, where PSA serum levels are typically monitored every 3-6 months. The rationale for watchful waiting is to only commence patient treatment when the disease shows evidence of clinical progression. This can be a particularly suitable option for elderly patients with shorter life-expectancies, to avoid invasive and risk-laden procedures. Clinical studies recorded over several decades have recorded rates of >80% disease specific survival 10-15 years after initial diagnosis [53, 54]. However, for many patients, the prospect of not taking direct intervention for their disease is an uncomfortable and uncertain option.

## 1.6.2   Radiotherapy

It has long been known that exposure to ionising radiation (IR) can lead to adverse effects on cells. DNA damage, cell cycle arrest, and ultimately cell death can be achieved through radiotherapy (RT) [55]. This is due to reactive oxygen species (ROS) formed from interactions with free radicals, produced as a result of multiple ionisations via the Compton effect [56]. Radical formation is believed to take place in discrete regions [55], with so-called 'clustered' DNA damage necessary in order to produce a lethal cellular effect [57, 58]. However, it has been shown that cancer stem cells (CSCs), which are thought to instigate cancerous growth [59], can be resistant to radiological techniques, as well as promoting cancer recurrence following treatment [60, 61]. Prostate stem-like cells in epithelial cultures derived from patient samples are more radio-resistant than more differentiated cells, due to increased levels of heterochromatin conferring a protective effect [62].

The dose of IR is measured in Grays (Gy), which are defined as the absorption of energy per unit mass (J/kg). Some studies have suggested that at least 74 Gy, and indeed upwards of 80 Gy [63], should be applied in the case of localised prostate cancer, as patients treated with less than 72 Gy have shown higher cancer recurrence rates [64]. The total dose is usually delivered in multiple smaller fractions of, for example, 2 Gy per day over 60 days, with weekend breaks [65]. Following treatment, patients may often experience side effects including, but not limited to, urinary incontinence, diarrhoea and rectal discomfort. Urinary problems can persist or present at longer time periods following initial treatment, as well as erectile dysfunction [66, 67]. In addition, and most worryingly, a third of patients experience radio-recurrent disease [68].

Another recent development, which seeks to improve localization of RT, is hypofractionated stereotactic body radiation therapy (SBRT) via the Cyberknife linear accelerator machine. During Cyberknife SBRT, movement of the prostate is detected and automatically corrected for during the procedure by the robotics [69], enabling delivery of the radiation to within 2 mm of the target area [70]. This enables the Cyberknife to deliver a hypofractionated radiation dose more accurately and non-invasively to the tumour [69] than conventional radiotherapy. Another major advantage is that treatments are usually delivered over a few days rather than weeks, rendering post-procedure hospitalization unnecessary [69]. However, rectal and urinary complications are still reported, in addition to erectile dysfunction [71], In addition, the cost of Cyberknife technology is more expensive than other radiological techniques, at least in terms of initial outlay [72], although this is yet to be thoroughly investigated. Only a handful of centres within the UK have access to a Cyberknife system.

### 1.6.3   Brachytherapy

An increasingly common approach for treating prostate cancer internally is brachytherapy, which uses radioisotopes such as $^{125}$I, $^{103}$Pd and $^{131}$Cs, and is typically applied in order to ablate the whole prostate gland [73]. The radioisotopes, with half-lives ranging from ~10-60 days [73], are delivered to the prostate as seeds through a matrix of narrow diameter needles, inserted transperineally. Brachytherapy can either be used as a stand-alone treatment, in conjunction with radiotherapy or prior to radical prostatectomy, or as a salvage treatment following radiotherapy [74].

### 1.6.4 Radical Prostatectomy

One of the most common treatment approaches for localised PCa is radical prostatectomy (RP). The rationale behind the procedure is simple: if the disease remains confined to the prostate, then removal of the whole gland should ensure a disease-free outcome for the patient. However, RP is an invasive surgical procedure that can lead to multiple side effects and complications post-treatment, including urinary incontinence and severely reduced sexual function [75]. Disease-control outcomes appear to be similar to radiotherapy [76]. Although modern robotic RP procedures and nerve-sparing techniques have reduced the length of hospital stay and improved post-treatment function [77], the approach is still perceived as a gross overtreatment of a large proportion of cases [78]. The majority of PCa cases are not immediately life-threatening, with 5 year survival rates >90% [79], however it is problematic to identify those that are at an early stage. As a result, more targeted, non-invasive techniques are required that provide satisfactory disease control.

## 1.7 Focal Therapy

The rationale for focal therapy is targeted destruction of the tumour site whilst sparing the surrounding healthy prostate tissue, resulting in preserved function and reduced side effects when compared to approaches that are more radical. For patients to be considered as candidates for focal therapy, their prostate cancer must be present in only one lobe, typically unifocal and contained within the prostate capsule [80]. It has been proposed that treatment directed to the index lesion only could still provide satisfactory disease control in multi-focal disease [81]. However, no absolute ideal patient selection criteria exist for focal prostate treatment [82]. In the following

subsections, some treatment approaches for localised prostate cancer are introduced, with their respective advantages and pitfalls outlined for comparison.

### 1.7.1   Photodynamic Therapy

Photodynamic therapy (PDT) damages tissues in a highly localised fashion by exciting photosensitizing drugs with light. The drugs are administered either orally or intravenously, absorb energy from light of a specific wavelength, and transfer it to molecular oxygen residing in the surrounding tissues in order to produce ROS [83]. It is believed that an activated form of molecular oxygen, known as singlet delta oxygen (SDO) is the predominant species produced following the excitation of the sensitizing agent by the light source [84]. SDO is highly toxic to cells, and can interfere with cell signalling as well as inducing cellular stress [85-87]. Theoretically, PDT has the advantage of greater selectivity relative to other cancer therapies, as only simultaneous exposure to the photosensitizing drug, light and oxygen will result in a cytotoxic effect on the treated cells [84]. It is necessary to protect the skin and eyes of the patient, even following treatment. Such protection may be required for a few hours up to several weeks, depending on the photosensitizer used [88], as the time each drug remains in the patient's bloodstream varies vastly. Transperineal application of the light source allows treatment of anterior prostate tumours [89], giving advantages over other treatment approaches such as HIFU. Disease-positive biopsies have been identified during treatment follow-up however [90]. PDT can also be applied as a salvage therapy following the failure of other techniques such as radiotherapy [91].

### 1.7.2 Cryotherapy

Rapid freezing and thawing cycles are employed by cryotherapy techniques in order to cause localised cellular destruction due to either: the extremely low temperature alone, the rapid rate of cooling, or the period of time for which the tissue stays frozen [92]. Either liquid nitrogen or argon gas is administered to the prostate transperineally via cryo-probes under TRUS guidance. Argon gas probes are now favoured over liquid nitrogen based approaches due their thinner diameters, permitting the insertion of additional probes (in a brachytherapy-like manner) to improve the efficacy of treatment [93]. Two cycles, reaching at least -40ºC are required for complete cell death, with cell shrinkage and protein denaturation occurring as the tissue temperature decreases beyond 0ºC [92]. A urethral warming catheter and multiple thermosensors are typically used to prevent freezing of unwanted regions [94, 95].

Cryotherapy can be applied as a salvage therapy, for example after the failure of, or recurrence following, radio- and brachytherapy [96, 97]. Common side effects following cryotherapy include rectal or perineal discomfort [98] and urinary infections [99]. Major complications can include recto-urethral fistula, although this is rare [94].

### 1.7.3 High-Intensity Focused Ultrasound

The concept of high-intensity focused ultrasound (HIFU) was first applied in the 1980s to BPH [100], with the first recorded application to localised PCa in 1995 [101]. If an ultrasonic beam is sufficiently focused and the intensity increased, high levels of energy can be delivered to very localised regions [90]. Energy delivered by the ultrasonic beam is absorbed by the treated area, leading to rapid heating effects, which can raise the temperature of the treated tissue to 80ºC in a few seconds [102]. This

instant heating leads to coagulative necrosis through protein denaturation [103, 104]. A recent study considered the treated area to have been successfully ablated once a minimum temperature of 65ºC had been reached [105].

The typical devices used for HIFU treatment of the prostate are applied transrectally and thus possess the advantage over other focal therapies in that an invasive surgical approach is not required. Treatment intensities of up to 2000 Wcm$^{-2}$ are achievable at focal lengths as short as 3 cm [106]. As a result, there is a need for accurate monitoring of the energy delivery to, and resulting temperature of, the target tissue. In recent years, the capability of real-time MRI has improved, allowing precise monitoring of the HIFU procedure [105, 107].

The difficulty with treating enlarged prostates with HIFU lies mainly in limitations on the focal length of the ultrasound probe [108, 109]. A TURP procedure is recommended prior to treatment to reduce organ volume, as post-HIFU swelling of the prostate is common [110, 111]. The effective treatment of anterior prostate tumours is also problematic using HIFU, as anterior perirectal fat tissue can prevent intended penetration depth of the ultrasound beam [112]. This occurs due to reflection of the signal, and is a particular problem if the patient is overweight [113].

| Treatment Approach | Summary of Pros | Summary of Cons |
|---|---|---|
| Watchful Waiting | - Majority of prostate cancers not immediately life-threatening. Avoids invasive procedures until necessary | - Uncomfortable and uncertain treatment option for many patients |
| Radiotherapy | - Minimally invasive approach as radiation is usually applied externally<br>- Cyberknife technology give hope of improved targeting with fewer side effects | - Many side effects as a result of radiation at unintended sites, causing urinary incontinence, rectal pain and erectile dysfunction<br>- A third of patients experience radio-recurrent disease |
| Brachytherapy | - Image guided seed placement allows effective treatment of localised areas | - Needle array application is a highly invasive process |
| Radical Prostatectomy | - Removal of entire gland should ensure disease-free survival from organ-confined tumours | - Highly invasive procedure, leading to many potential side-effects including infections and reduced sexual function |
| Photo-Dynamic Therapy | - More selective than other focal therapies due to conditions needed for SDO production<br>- Can be applied at the same treatment site multiple times | - Photosensitizing agent remains in patient's bloodstream following treatment, requiring protection of the eyes and skin for potentially weeks after the procedure |
| Cryotherapy | - Double freeze-thaw cycle effectively destroys cells in targeted region<br>- Can be applied as a salvage following radiotherapy techniques | - Urinary infections and perineal discomfort post-treatment are common<br>- Relatively invasive treatment, with added need for thermal protection of urethra, bladder and rectum |
| High-Intensity Focused Ultrasound | - Transrectal application negates the need for surgical approach<br>- Improvements in MRI technology allow real-time procedure monitoring and improved targeting | - Difficulty treating enlarged prostates, especially in overweight patients<br>- Effective treatment of anterior tumours is not achievable |

**Table 1. A summary of treatments for localised prostate cancer**.

### 1.8 Low Temperature Plasma: a Novel Focal Therapy for Prostate Cancer?

Despite improvements to existing techniques such as radio- and brachy-therapy, which have enabled enhanced targeting of tumours, side-effects and complications are still common. Emerging focal therapies have shown real promise for the treatment and control of prostatic disease, yet each comes with its own set of drawbacks [114].

This thesis represents an inter-disciplinary effort, between departments in physics and biology, to investigate a new treatment for localised prostate cancer, in the form of low temperature plasma.

# Chapter 2
## Fundamentals of Plasmas and Their use in Biomedicine

## 2. Fundamentals of Plasmas and Their Use in Biomedicine

### 2.1 Plasma Fundamentals

Plasmas are ionised gases and often referred to as the fourth state of matter. In the energetic progression of solids, liquids and gases, if sufficient energy is applied to a region of gas it will break down into the plasma state. A frequently cited definition of plasma by Chen is given as "a quasi-neutral gas of charged and neutral particles which exhibits collective behaviour" [115].

In an atmospheric pressure neutral gas, only collisions between particles within the gas will give rise to their motion. However, due to the presence of charged particles within a plasma, electromagnetic forces contribute strongly to the overall dynamics. This indicates that the movement of particles within a plasma can occur due to both collisions between particles on a local scale, and due to the interaction of long-range electromagnetic forces with charged species. This implies that each particle interacts with many other particles in its vicinity and not solely with the nearest one to it, leading to the concept of collective behaviour.

The interaction of charged species leads to another phenomenon exhibited by plasmas: their ability to shield out applied external charges. This screening effect essentially eliminates any large applied field. The length scale over which free charges are shielded within a plasma is defined by the Debye length ($\lambda_D$), and is given as:

$$\lambda_D = (\frac{\varepsilon_0 k_B T_e}{n e^2})^{\frac{1}{2}}$$

In this equation, $\varepsilon_0$ is the permittivity of free space, $k_B$ the Boltzmann constant, $T_e$ the electron temperature, $n$ the plasma density and $e$ the electronic charge.

Provided that the dimensions of the plasma, *L,* are much larger than the Debye length, then on a macroscopic scale, the shielding effect leads the plasma to be free of electrostatic potentials and is considered electrically neutral. This implies that the number density of positively and negatively charged particles roughly balance, i.e. $n_i \sim n_e \sim n$, where $n_i$ is the ion number density, $n_e$ the electron density, and $n$ the plasma density as outlined above. However, strong electric fields can still exist locally between neighbouring particles, leading to the system as a whole being referred to as quasi-neutral.

A final condition often imposed for an ionised gas to be defined as a plasma relates to the electrostatic oscillation frequency of electrons and ions in response to a small charge separation. The frequency of collisions between charged species and neutral gas atoms must be less than the plasma frequency, such that electrostatic interactions dominate over kinetic collisions.

$$\omega_p = \left( \frac{n_e e^2}{m_e \varepsilon_0} \right)^{\frac{1}{2}}$$

This is referred to as the plasma frequency, where $n_e$ is the electron number density, $m_e$ is the electron mass, and $\varepsilon_0$ is the permittivity of free space. An equivalent relationship exists for ions, however, as the relatively energetic electrons mostly govern the plasma dynamics, $\omega_p$ is often termed the electron plasma frequency, $\omega_{p,e}$. Energetic electron dynamics are of particular importance in low temperature plasmas, as outlined in a later section.

## 2.2 Gas Breakdown and Plasma Formation

One of the most common means of electrically igniting a plasma is to apply a voltage across one or more electrodes which are separated by a region of gas. The resulting electric field accelerates free electrons present in the background gas (e.g. from cosmic radiation). Provided that the mean free path of the electrons is adequately long, they can acquire sufficient energies to cause ionisation of atoms and molecules in the gas through electron impact ionisation. As a simple approximation, each ionisation event leads to the production of one new electron-ion pair. These secondary electrons are subsequently accelerated into other atoms and molecules by the applied field. This leads to an exponential increase in the number of free electrons, and the formation of an electron avalanche. This is often referred to as a Townsend discharge after its founder, who discovered the phenomenon in the late 1800s. The point at which this occurs for a given gas is referred to as the breakdown voltage ($V_B$), as coined by Paschen in 1889 [116], and varies with the product of pressure ($p$) and the electrode separation ($d$). At low values of $pd$, the electrons can attain high energies due to a lack of collisions. However, at high $pd$, the opposite is true, resulting in the requirement of higher voltages to cause gas breakdown at atmospheric pressure.

### 2.3 Low Temperature Atmospheric Pressure Plasmas

The defining characteristic of *low temperature*, or *non-thermal*, plasmas is that the ions and electrons within the plasma are not in thermal equilibrium with one another. Heavy ions cannot respond to rapidly varying applied electric fields with the same capacity as lower inertia electrons. This results in electrons being accelerated to temperatures of several eV, which drive the plasma chemistry through various collisional processes such as ionisation, excitation, dissociation, as depicted in Figure 8. The ions remain near ambient temperature at around ~ 300 K. Despite the increased collisionality present at atmospheric pressure, the global temperature of the gas does not increase due to the inefficient energy transfer between light electrons and heavy ions or molecules. In addition, only a very small proportion of the gas exists in an ionised state. This can be defined by the degree of ionisation α, where $n_e$ is the electron number density, and $n_n$ the number density of background neutral gas species.

$$\alpha = \frac{n_e}{n_e + n_n}$$

In thermal plasmas, such as those proposed for high temperature fusion technology, the degree of ionisation, $\alpha \approx 1$. However, in low temperature plasmas, $\alpha \ll 1$. This results in the majority of the environment consisting of background neutral gas molecules. This allows LTPs to create an otherwise impossible rich and complex chemistry without causing thermal defects to a sample. Until recently, atmospheric pressure plasmas have been unstable and low temperature plasmas have conventionally been operated under lower gas pressure conditions. While this approach has proven extremely beneficial, for example in the multi-billion dollar semiconductor industry, it is limiting with regards to broader exploitation of non-vacuum compatible materials. Through the use of gas flow it is now possible to sustain stable, controllable plasmas at atmospheric pressure. This

has led to their proposed usage in a wide-range of applications, including the treatment of surfaces to cause preferential modification of surface properties, such as wettability in the textiles industry [117, 118], or as etching technologies in the fabrication of semiconductor devices [119, 120]. The particle collisions that govern the physical and chemical processes involved in these applications are detailed in the following section.

.
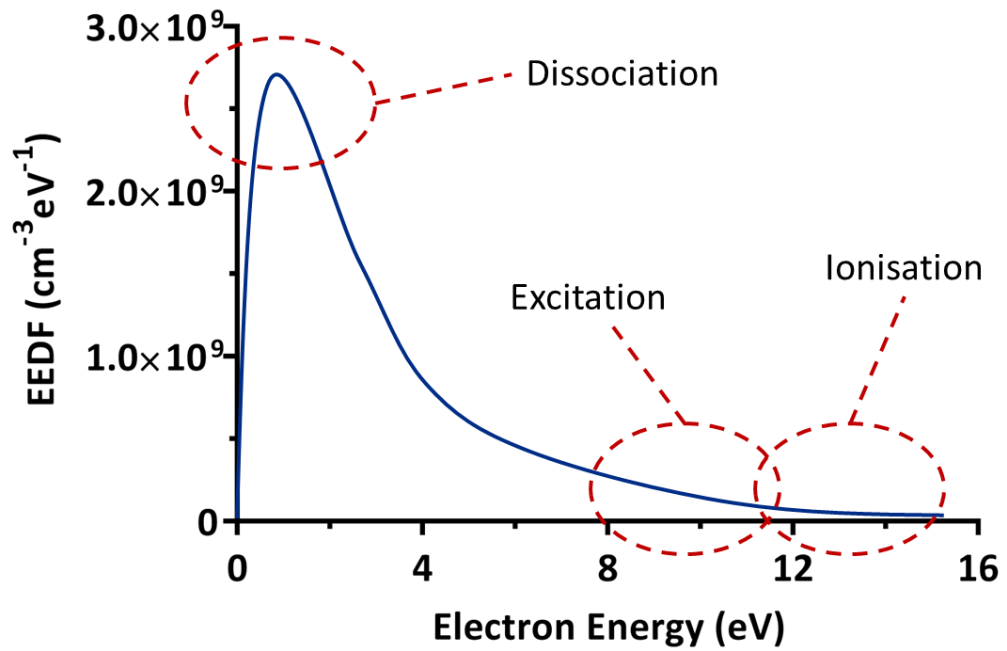


**Figure 8: An illustrative sketch of a typical electron energy distribution function.**

The associated energies are outlined for plasma processes including ionisation, excitation and dissociation.

## 2.4 Plasma Collisions

Collisions within a plasma can be either elastic or inelastic. During elastic collisions, the total kinetic energy of the particles is conserved, but the momentum (and direction) of the particles may change. For the case of inelastic collisions, energy may be transferred between particles, and the number of particles may change as a result. The probability of a collision event is proportional to the collision cross-section ($\sigma$), i.e. the target area that a particular species presents to an incoming particle. The mean free path ($\lambda$) gives the distance travelled through a gas of density $n_g$ by an incident particle between collisions:

$$\lambda = \frac{1}{n_g \sigma}$$

The average time between collisions ($\tau$) and associated collision frequency ($\nu$) are given by:

$$\tau = \frac{\lambda}{\upsilon}$$

$$\nu = \frac{1}{\tau} = n_g \sigma \upsilon$$

Where $\upsilon$ is the velocity of the incident particle. Finally, the rate constant ($K$), defined as the rate of interaction per atom of the background gas can be written as:

$$K = \sigma \upsilon$$

The rate constants for various multi-body reactions have been determined experimentally [121]. Elastic collisions between charged particles in a plasma are governed by electrostatic Coulomb scattering. However, in weakly ionised plasmas, which form the subject of this thesis, the majority of collisions are between electrons

and background neutral gas species. These collisional processes result in inelastic interactions including ionisation, excitation and dissociation, which are central to the rich and complex chemistry created by plasmas.

The transfer of energy through collisions can excite the electrons within atoms to higher energy states, which are usually extremely short-lived (i.e. $\sim \mu s - ns$). As an electron relaxes to the ground state, an energetic photon is emitted, which is specific to the transition between energy levels for a specific species. These photons can be detected by optical spectroscopic techniques to provide an understanding of the composition of species within the plasma [122, 123]. Electrons are very efficient at dissociating molecules in the background gas by overcoming the bond energy between atoms. They can undergo two- and three-body collisions with sufficient energy to ionise species by liberating electrons from their host atoms.

Another special case of collisional process is Penning ionisation, which governs collisions between metastable atoms in the plasma with other particles. These metastable species possess significantly longer lifetimes when compared to other excited species, as their decay to the ground state is optically forbidden by selection rules. Examples of atomic and molecular Penning ionisation reactions involving a metastable helium atom (He*) and a colliding partner such as oxygen (O) are given below.

$$He^* + O \rightarrow He + O^+ + e$$

$$He^* + O_2 \rightarrow He + O_2^+ + e$$
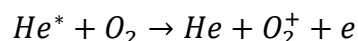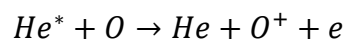
As these equations clearly show, Penning ionisation processes lead to the release of free electrons into the plasma, which was outlined earlier as a fundamental requirement for the sustainment of a discharge. One of the simplest metastable atoms is the lowest

triplet state of helium (He $2^3$S), which possesses an ionisation energy of ~ 20 eV, and a radiative lifetime of ~ 8000 s [124]. Penning ionisation plays a key role in driving the chemistry in low temperature atmospheric plasmas. The behaviour of colliding particles in two different low temperature plasma configurations are discussed in the following sections.

## 2.5 Capacitively Coupled Plasmas

Capacitively coupled plasmas (CCPs) are usually ignited between two parallel plate electrodes, one powered and one grounded. CCPs are often driven using radiofrequency (RF) sinusoidal voltages, namely 13.56 MHz and its higher harmonics. These frequencies are used as they are efficient at heating electrons, and these specific frequencies are permitted by international telecommunication laws. As the plasma ignites, the active electrode will initially absorb higher numbers of electrons than ions. This is owing to the comparatively higher mobility of the electrons, resulting in a higher electron flux. This leads to a region of positive space charge forming between the plasma and electrode. This region breaks the condition of quasi-neutrality locally and is known as the plasma sheath, which is illustrated in Figure 9. The sheath acts to accelerate ions towards the surface, and repel electrons back into the plasma bulk, satisfying the condition of zero-net charge flux at the electrode. This acceleration of high energy electrons in the sheath strongly influences the ionisation dynamics of the discharge, acting as a sustainment mechanism.
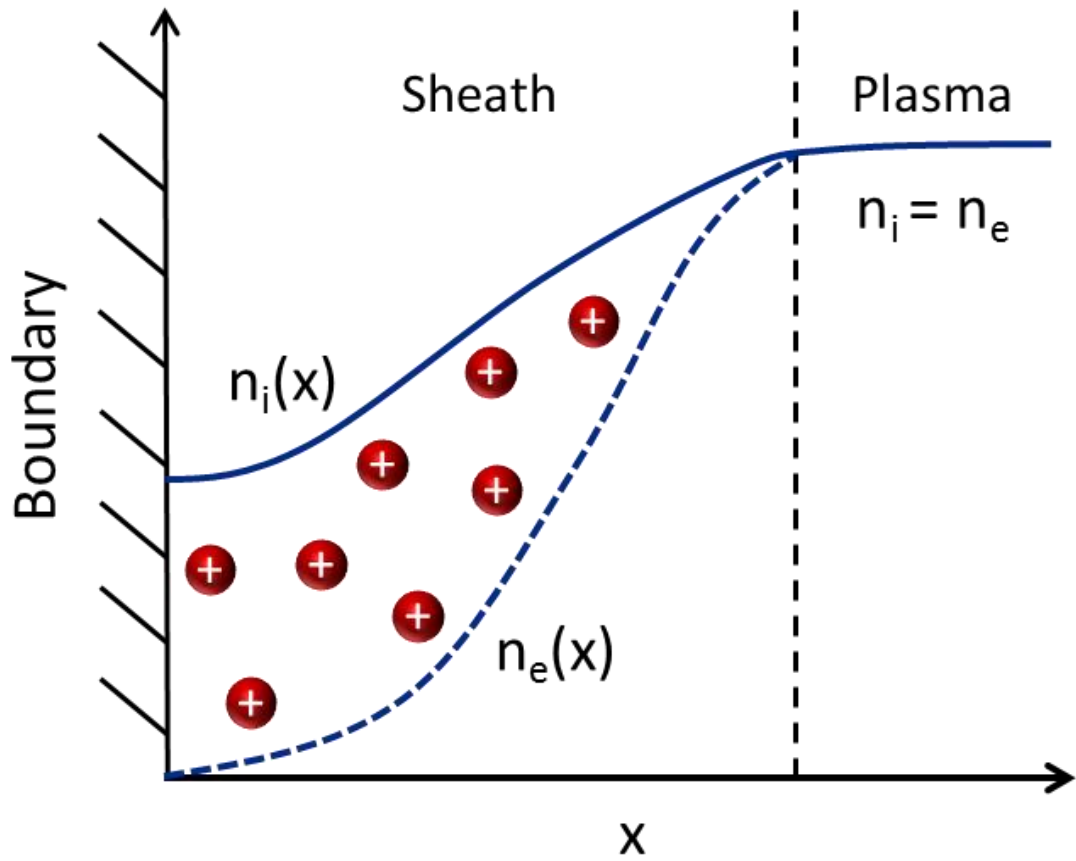
**Figure 9: Illustration of the plasma sheath.**

The formation of a positive space charge region is indicated between the bulk plasma and the boundary, with associated profiles for the ion and electron number densities.

## 2.6 Dielectric Barrier Discharges

Dielectric barrier discharges (DBDs) consist of a high breakdown-strength dielectric material inserted into a discharge gap between two electrodes, which are typically driven at kHz frequencies with continuous or pulsed AC. This limits the discharge current between the two electrodes, preventing sparking. It was found that Townsend's theory failed to satisfactorily describe gas breakdown at atmospheric pressure and larger gap widths, and thus the streamer mechanism was introduced [125, 126]. Unlike the relatively homogenous plasma production observed in CCPs, DBD plasma jets often ignite as a series of filaments. These take the form of a series of plasma channels, which ionise the gas immediately in front of the charged head (Figure 10), allowing the streamer to self-propagate. As the streamer forms and travels towards the cathode, the emission of photons from positive ions leads to the production of new free electrons through photoionisation events. These electrons are attracted back towards the positively charged plasma head, which leads to the neutralisation of ions, leaving behind a new positively charged ionisation front [127]. Photons are emitted from the new front and the process is perpetually repeated, driving the evolution of multiple fronts and the propagation of the plasma streamer, as shown by Figure 10. The areas of charge separation between successive ionisation fronts leads to instantaneous electric fields forming at the tip of the streamer (Figure 10). These strong, localised fields may have profound implications for biomedical applications, which is discussed later.

During the course of this study, two different plasma sources were used based on those illustrated in Figure 11. The first was a CCP plasma, ignited at RF, which was used to study reactive species formation in plasma-treated cell culture media (the results of this study are provided as an appendix). The second, which forms the main part of this thesis, was a DBD plasma jet, which was used to directly treat prostate cancer cells

and study their response, with a view to developing a novel cancer therapeutic. As the DBD jet directly contacts the cell culture media surface, it creates electrons at the treatment site, thereby enhancing the radical chemistry in the local cellular environment. This feature, combined with the potential for formation of strong electric fields, led to the selection of the DBD jet for the main body of this work.

**A**

Anode    Cathode

Channel    Head

Photon
*production*

🔴➕ Positive Ion
🔵➖ Electron
🟣 Photon

Photon
*ionisation*

Active Region

Neutralisation,
Photon production

**E** →

Electric Field

Applied Field

Instantaneous total
electric field

E = 0

**B**

**i**    **ii**    **iii**

Ionisation
Front

**E** →

**iv**    **v**    **vi**

52
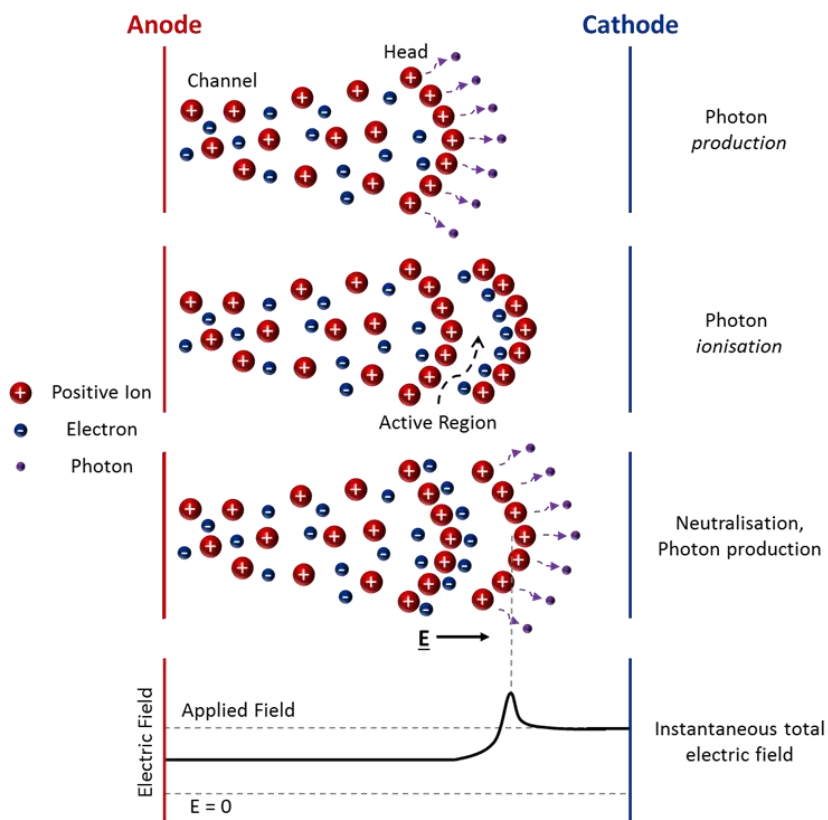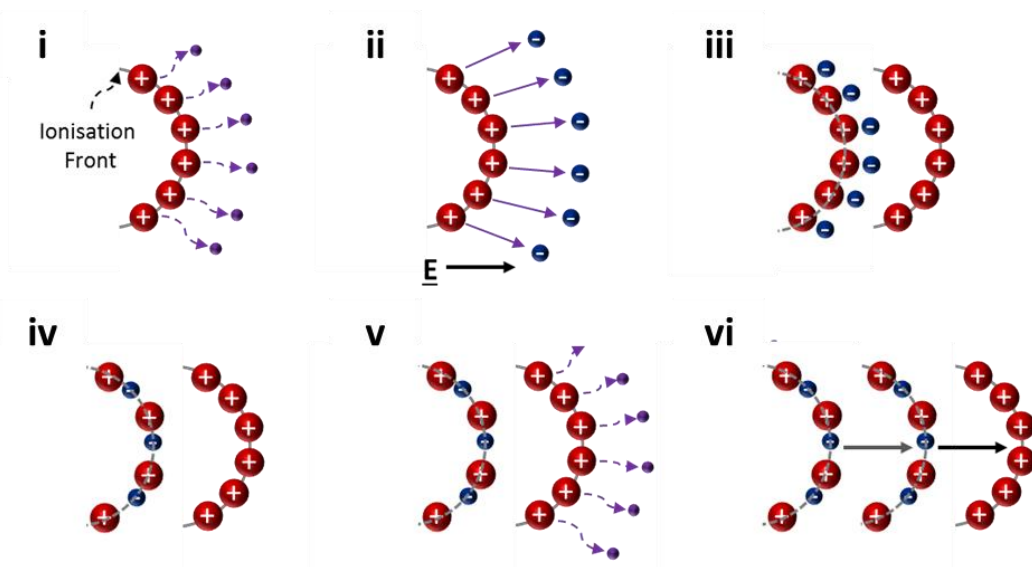
**Figure 10: Illustration of streamer propagation.**

The motion of an election electron avalanche through an electric field is depicted, with associated instantaneous electric field at the streamer head identified (**A**). This is expanded further in **B**: Positively charged ions emit photons (**i**), which leads to the production of electrons through photo-ionisation events and creates a strong electric field (**ii**). Newly produced photoelectrons are attracted towards the plasma head leading to neutralization of ions (**iii-iv**). This leads to the formation of a new ionisation front, which emits photons (**v**) and the process is repeated leading to the propagation of the plasma (**vi**).Elements of this figure are modified from Algwari, 2011 [128] and Walsh et al. 2010 [129].

## 2.7 Atmospheric Pressure Plasmas for Biomedical Applications

Low temperature plasmas are emerging as an exciting development for biomedical therapeutics. The unique properties of cold non-equilibrium plasmas have enormous potential in disease therapeutics and plasma pharmacology as drug alternatives. Applications of these plasmas range from surface sterilization and bacterial decontamination [130-135], biofilm inactivation [136-138], antimicrobial treatment in food preservation [139-141], wound healing [142, 143], to cancer treatment [144-147]. This rapidly growing field of *plasma medicine* has emerged over the last decade and offers great potential, bringing together multi-disciplinary branches of science and engineering.

Despite LTPs being earmarked as a technology for future healthcare, plasmas have been used for a range of surgical applications in the field of electrosurgery since as long ago as 1991 [148, 149]. Though not technically an LTP, the argon plasma coagulator has been employed in various surgical disciplines for the purposes of tissue removal and wound cauterization [148], and is perceived as an improvement on existing laser-based techniques [150]. Recently, plasma vaporization has been applied to benign prostatic hyperplasia (BPH), with the hope of reducing the common side effects of conventional transurethral resection of the prostate (TURP) procedures [151]. Early results show that the concept of plasma vaporization could prove to be a significant improvement over current TURP techniques for BPH [152]. Reduced bleeding and thermal lesions in surrounding tissues, a greater level of reduction of glandular volume, and shortened procedure times have all been recorded following plasma vaporization when compared to conventional TURP techniques [153].

### 2.7.1    Common Low Temperature Plasma Designs for Biomedical Applications

Various devices are available for the formation and delivery of plasma [154-158] which rely on broadly the same principles. Three such examples of commonly used designs are illustrated in Figure 11. DBD plasmas can either be ignited between two electrodes covered with dielectric material (Figure 11a), or between one active electrode and a grounded surface (Figure 11b). The resulting plasma plume self-propagates outwards, and as the dynamic high electric field is parallel to the direction of propagation, the effluent contains reactive neutrals, charged particles, electric fields and UV radiation. A variation of the DBD schematic is the floating electrode dielectric barrier discharge (FE-DBD) plasma (Figure 11b), which operates by using the surface to which it is applied as a floating counter electrode. A third example of a plasma source arrangement is the radio-frequency (RF), or cross-field, plasma source (Figure 11c) which uses an RF signal as a means of gas excitation. This device utilizes plane-parallel electrodes, with a gas flow passing through the core plasma volume. This particular source possesses a charge-free effluent since the applied electric field is perpendicular to the direction of gas-travel, thus confining charged species to the core plasma region. Due to the high collision frequency at atmospheric pressure, the effluent is devoid of charge carriers and its characteristics are dominated by energy carrying reactive neutrals. The RF plasma jet is the most comprehensively studied LTP set-up with respect to diagnostics and modelling [159-171]. Furthermore, a European reference RF jet is being developed and characterised, the designs of which will become freely available, in the hope that laboratories gain the capacity to make direct data comparisons [172].  In general, LTPs are ignited using a main feed gas of helium or argon, supplemented with small admixtures (< 1%) of molecular gases such as oxygen

or nitrogen. As shown earlier in Figure 8, plasmas are very efficient at dissociating molecular species, aiding the formation of a rich, chemically reactive environment.
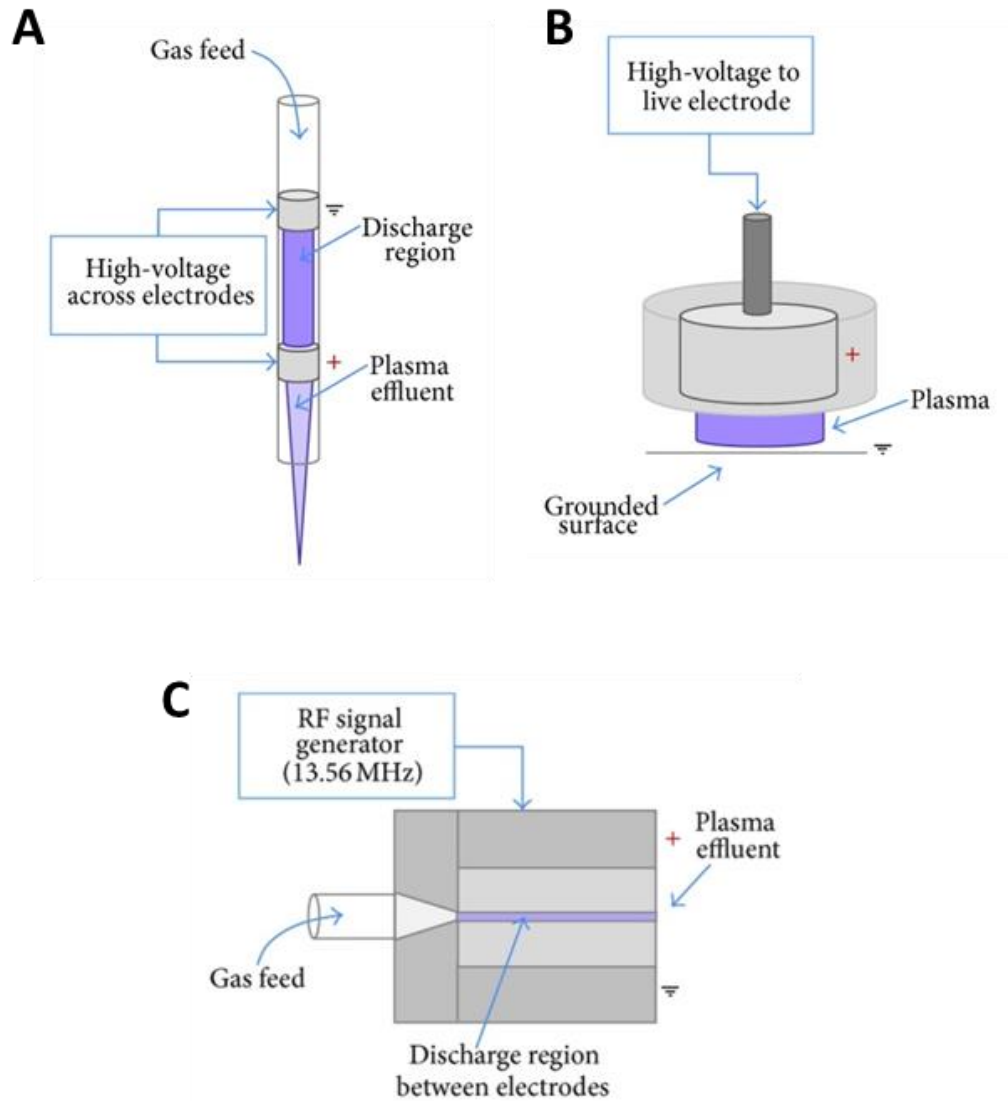
**Figure 11: Examples of different plasma devices for medical applications.**

Linear-field plasma jets: **A)** Dielectric barrier discharge (DBD), **B)** Floating-electrode DBD (FE-DBD), and cross-field plasma jets: **C)** Capacitively coupled at radio-frequency (RF). Reprinted from Hirst et al [114], under a Creative Commons 3.0 License (*http://creativecommons.org/licenses/by/3.0/*).

## 2.8 Low Temperature Plasmas for Cancer Treatment

Over the last decade, many research groups have studied the application of LTPs to different cancer models. It is becoming widely acknowledged within the field of plasma medicine that the principle mode of cellular interaction from LTPs is their ability to create large concentrations of various reactive oxygen species (ROS). The involvement of ROS in cancer initiation and progression [173], and their therapeutic potential [174] is now well documented. The cellular threat from low levels of ROS is well tolerated and neutralised through the action of enzymes including super oxide dismutase and catalase [175]. The inherent elevated metabolic activity in malignant cells (Warburg effect) may present a therapeutic window, as they are essentially already at their ROS-tolerance threshold or 'red-line' when compared with neighbouring normal cells [176, 177]. The creation of high levels of ROS is the mechanism by which long-established anti-tumour strategies, such as radio- [178] and some chemo-therapies [179, 180] operate to induce oxidative stress leading to cytopathic cellular responses. Given that LTPs can create and deliver a multitude of reactive oxygen *and* nitrogen species (RONS) simultaneously [154], they are an obvious candidate for cancer therapy. The role of these plasma components, even individually, is to date not fully known and is a topic of current research. It can be anticipated that, similar to low pressure plasma processes, in for example, plasma etching or plasma deposition, synergistic mechanisms govern the plasma surface interface rather than the individual species themselves.

Mounting evidence in the literature suggests that LTPs rely strongly on the formation of reactive species to facilitate cellular responses. Processes such as ionisation, dissociation, excitation and recombination of atoms and molecules within the plasma lead to a chemically rich environment of reactive oxygen species (ROS) including atomic oxygen (O) [121, 165], hydroxyl (OH) [181], superoxide ($O_2^-$)[82], singlet-delta

oxygen ($^1O_2$) [182], and hydrogen peroxide ($H_2O_2$)[183]. In addition, depending upon the gas composition and plasma geometry, reactive nitrogen species (RNS) may include atomic nitrogen (N) [160], nitric oxide (NO) [184], peryoxynitrite ($ONOO^-$) [185], and other members of the $NO_x$ family. The sheer multitude of RONS generated by LTPs could provide advantages over other cancer therapies, e.g. radiotherapy and photodynamic therapy, which generally produce only ROS. Indeed, high concentrations of NO has been shown to induce apoptosis in tumours, implying the action of nitrosative stress could also prove crucial to successful cancer therapy, [186].

The application of LTP to cells or tissues is a multi-phase process, which begins with an initial ignition and steady-state core plasma, followed by an afterglow plasma phase, leading to a diffusive interface with a liquid-like layer or environment. The liquid environment may relate to treatment of cell culture media in laboratory experiments, or the fluid within and surrounding a tumour in a clinical plasma application. This plasma-modified liquid environment then influences the cells and tissues around it. An illustrative overview of this process is depicted in Figure 12, along with approximate time-scales for various phenomena in the plasma and liquid phases and subsequent biological interaction. This different phases within this environment, and the interfaces between them, is extremely complex and only recently starting to be unravelled. Current research has suggested that $H_2O_2$ is created almost exclusively from species in the main plasma phase, whereas species such as OH and $O_2^-$ originate in the region between the plasma and the liquid environment [187]. OH and $O_2^-$ may also arise indirectly from $H_2O_2$, through Haber-Weiss or Fenton reactions [181].
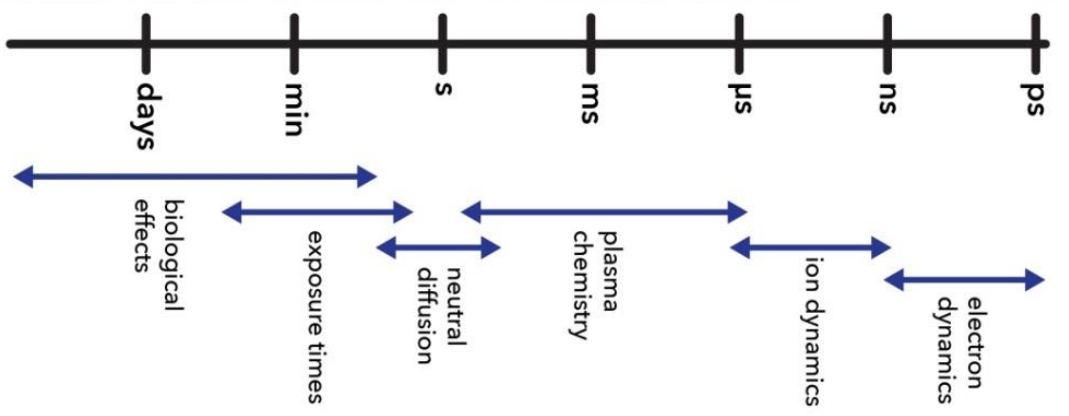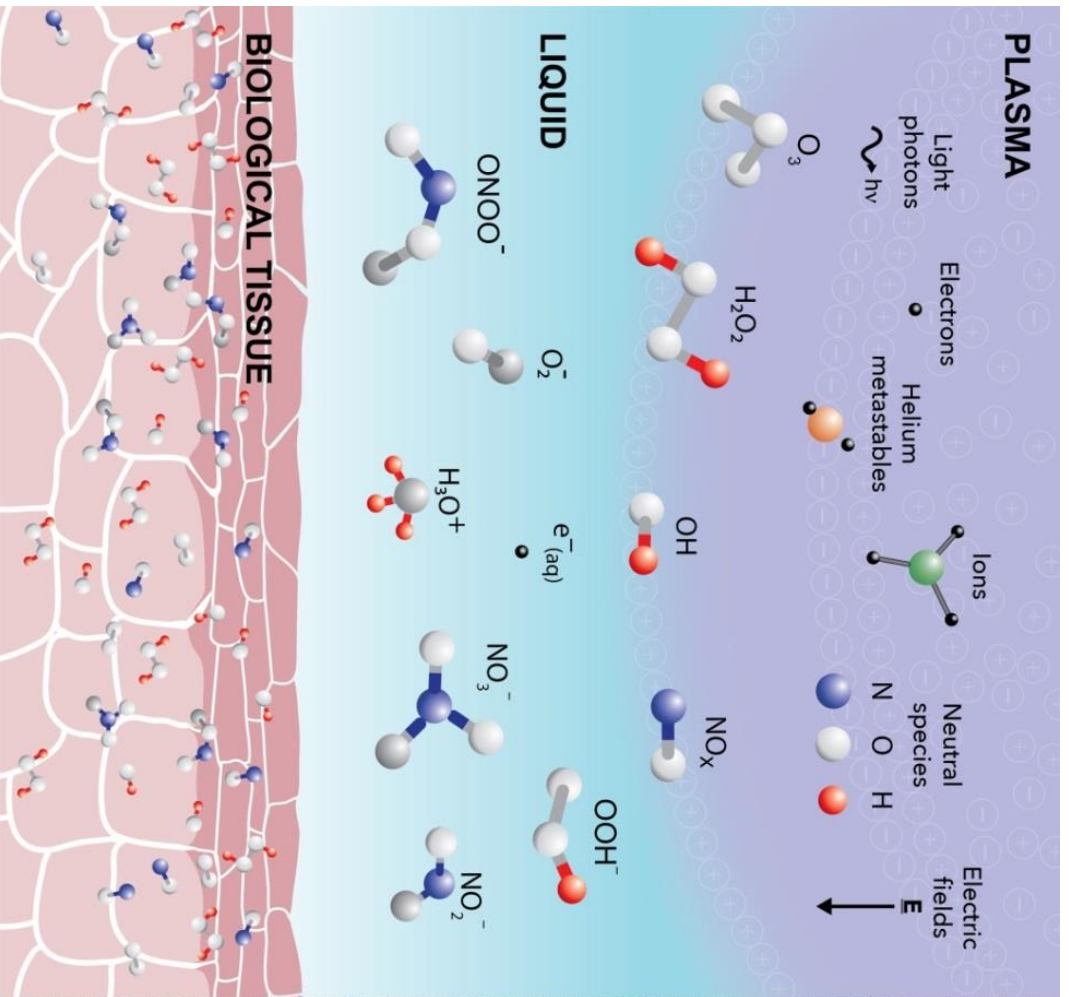
**Figure 12: An illustrative representation of the multi-phase transfer of plasma species towards a biological sample.**

The main components of the plasma phase, including ions, photons and neutral species are shown, leading to the creation of various RONS across the plasma-liquid interface and their propagation towards and diffusion through an arbitrary tissue layer. In addition, approximate timescales governing various phenomena across the plasma-liquid phases and biological interaction are outlined. Reprinted from Hirst et al [188], under a Creative Commons 4.0 License (*http://creativecommons.org/licenses/by/4.0/).*

The dynamics of the chemistry within the plasma core are extremely complex. To date, simulation studies have comprised in excess of 60 different species, involved in ~1000 different reactions [159]. Translation to the liquid environment and ultimately precise understanding of the specific extra- and intra-cellular RONS involved in both cellular effect and response, and their concentrations is vastly more so. Promising numerical models have attempted to resolve and understand this complexity, including both the variation in chemistry between gas-liquid-tissue phases [189], the fluxes of different reactive species at the tissue surface [190], and the influence of different molecular gas admixtures [191]. The mechanistic effects of LTPs on cells are presented in the following section.

## 2.9  Mechanisms of LTP Treatment

LTPs create and transfer numerous RONS to the cellular environment, as discussed earlier. Current evidence implies that the production of RONS is primarily responsible for cytopathic effects of the plasma, however other facets of LTPs may contribute to ultimate cell fate and treatment outcome, which are outlined below.

LTPs have been applied to a range of different malignant cell lines in culture with extremely promising results. A selection of these are presented in Table 2, along with a respective method of treatment. A range of common cellular responses have been documented including DNA damage [192, 193], decreased cell viability and clonogenicity [194, 195], reduced proliferation [196] and cell cycle arrest [197, 198]. From the growing literature, it would appear the cell death mechanism following LTP treatment varies with both the cell type and plasma source used (Table 2). Broadly speaking, after treatment with LTP cell death is likely to occur through apoptosis or

necrosis. Apoptosis is a tightly regulated chain of events involving specific proteins, resulting in cell shrinkage and fragmentation. Excessive oxidative stress triggers cytochrome c release from the mitochondria, leading to the activation of initiator and executioner caspases, and ultimately cell death. As the cell disintegrates, apoptotic bodies are formed which are engulfed and cleared by nearby phagocytic cells [199]. Necrotic cells are characterised by swelling, rounding up and sudden rupture of the cell membrane [200]. This has been likened to a balloon bursting, and leads to the spillage of the cell contents into the surrounding medium [201]. The vast majority of LTP studies report apoptosis [184, 196, 202-204], however senescence (loss of replicative capacity) [205] and non-apoptotic cell death [195] have also been presented.

Elevated RONS levels are continually cited as the likely perpetrators of plasma-induced effects, leading to the activation of apoptotic pathways including TNF-ASK1 [206], ATM/p53 [184] and MAPK [82]. Furthermore, LTP effects are (at least partially) alleviated by the use of various RONS scavengers [184, 207], further confirming the central role of reactive species produced by LTPs.

Although much of the focus of plasma oncology studies centre around elevated RONS levels and their effects, the formation of strong localised electric fields by LTPs can also occur (as highlighted earlier in Figure 10). These may interact directly with cell membranes and thus cause similar effects to those of emerging electroporative cancer therapies. Electroporation treatments utilise strong electric fields to irreversibly compromise cell membranes to provoke a cytocidal response. An example of this is Nanoknife technology, which has been proposed for focal treatment of pancreatic [208], prostate [209], and renal cancers [210]. Numerical modelling has suggested that LTPs may create electric fields in the hundreds of kV/cm range [211], capable of penetrating a few cell layers, and generating sufficiently high fields within individual cells for

electroporative effects [212]. Novel methods and diagnostic techniques have quantified average field strengths of around 10-20 kV/cm within LTPs, but locally these may rise towards 100 kV/cm [213, 214]. Electroporative effects have indeed been demonstrated biologically following plasma treatment [215], which may irreversibly damage cell membranes and aid the transfer of RONS into the cell, as well as permitting leakage of intra-cellular components.

LTP has also been applied *in vivo* to treat mice with tumours derived from glioma cell lines, where a preliminary study showed a reduction in tumour volume of over 50% at six days following initial plasma treatment [216]. Survival rates of plasma-treated mice increased by over half, compared with the control group who received no treatment [216]. In a follow-up study, ROS produced by the plasma were earmarked as the main anti-tumour agents, with evidence for cell cycle targeting [217] and apoptosis also presented [218-220]. LTP has also been recently applied to ablate tumours in mice subcutaneously injected with neuroblastoma cells, with a reduction in the rate of tumour growth observed versus control. In addition, survival time post-treatment almost doubled [221].

| Cancer Type | Method of Treatment | Treatment Duration | Cell Death Mechanism | Reference |
|---|---|---|---|---|
| Prostate cancer cell lines: *PC-3 and LNCaP* | In suspension, 500 µl volume | 10 s | Apoptosis | Weiss et al. [196] |
| Glioma cell lines: *U87, U373, A172* | Adherent cells, 96 well plates, ~40% confluence | Up to 180 s | Apoptosis/ Necrosis | Siu et al. [202] |
| Lymphoma cell line: *U937* | Adherent cells, 10 cm plates, 5 ml volume | Up to 480 s | Apoptosis | Kaushik et al. [204] |
| Malignant cell lines from various sites | Adherent cells, 35 mm plates | 30-60 s, up to 10 repeated exposures | Apoptosis | Ma et al. [184] |
| Colorectal cancer cell lines: *Caco2, HCT116, SW480 and HT29* | Adherent cells in various multi-well culture plates | Up to 30 s | Apoptosis | Ishaq et al. [203] |
| Glioma and colorectal cancer cell lines: *U87MG-Luc2 and HCT-116-Luc2.* Glioma xenografts: *U87MG-Luc2* | Adherent cells, 24-well plates, 500 µl volume  Subcutaneous tumours | Up to 30 s   6 mins daily for 5 consecutive days | Apoptosis   Apoptosis | Vandamme et al. [218] |
| Head and neck cancer cell lines: *FaDu, SNU1041, SNU899 and HN9* FaDu xenografts | In suspension, 6 cm plates, 3 ml volume  Subcutaneous tumours | 1 s at either 2 or 4 kV   20 s daily for 20 days | Apoptosis   Apoptosis | Kang et al. [82] |
| Various melanoma cell lines | Adherent cells, assorted culture plates, without culture medium | Up to 120 s | Senescence | Arndt et al. [205] |

**Table 2. LTP treatment induces different paths to cell death.**

Summary of assorted cell treatment methods and associated death mechanisms for a

range of malignancy models.

## 2.10 Aims of Research

Despite continual improvement and refinement, long-term treatment for prostate cancer remains inadequate. Interventions such as radical prostatectomy, which is a highly invasive procedure with many side effects, and radiotherapy, to which around a third of patients are resistant, are still commonplace. In the case of early onset, organ confined tumours, patients may be given the option of treatment from a range of emerging focal therapies. However, each of these treatments harbours its own set of drawbacks or inefficiencies. This thesis aims to determine the potential of low temperature plasma to become a novel approach to treat localised PCa.

The first part of this thesis contains preliminary data on the influence of different variables in the plasma-treatment of cells. Different models to study the effect of LTP on PCa are outlined, and the effect of treated cell number density on cellular response was explored. In addition, the contribution of the cell culture media components, including foetal calf serum, in the observed response was investigated.

The main part of this thesis presents the direct application of LTP to PCa cells from the perspective of a future therapeutic technique. Here, an initial study was first performed in order to validate the ability of LTP to induce cytopathic effects in two commonly utilised prostate cell lines, derived from benign and metastatic disease. Following this, experiments were repeated in primary cells cultured directly from tissue biopsies to ascertain if LTP treatment was cytotoxic to human cells. The effects of patient-to-patient variability were analysed through the treatment of three matched paired normal and cancer samples. This work represents the first study of its kind both on the application of LTP to PCa, and importantly, on the application of LTP to cells derived from human tissues.

# Chapter 3
## Materials and Methods

# 3. Materials and Methods

## 3.1 Low Temperature Plasma Design and Operating Conditions

Treatment of prostate cells was performed using a dielectric barrier discharge (DBD) plasma jet configuration similar to the one illustrated in Figure 11A, The DBD jet was powered (AC) in the kV/kHz regime. The details of the experimental setup are described in the following sub-sections.

### 3.1.1    Dielectric Barrier Discharge Plasma Jet

The DBD plasma jet consisted of a quartz glass tube of inner/outer diameter 4/6 mm, with two copper tape electrodes positioned 20 mm apart, as shown in Figure 13. Helium was used as a carrier gas at 2 SLM, fed with 0.3% molecular oxygen admixture (6 SCCM). Gas flow was mixed using two calibrated mass flow controllers (Analyt GFC17) and fed into the top of the quartz tube. The plasma was ignited using a PVM/DDR Plasma Driver power supply (Information Unlimited). One electrode was powered at ~ 6 kV (amplitude, sinusoidal) at a frequency of ~ 20 kHz measured using a high voltage probe (LeCroy PMK-14KVAC) connected directly across the electrodes, and an oscilloscope (LeCroy WaveJet 354A). The bottom electrode was grounded. These voltage and frequency parameters were found to produce the brightest plasma, without causing arcing between the copper tape electrodes.
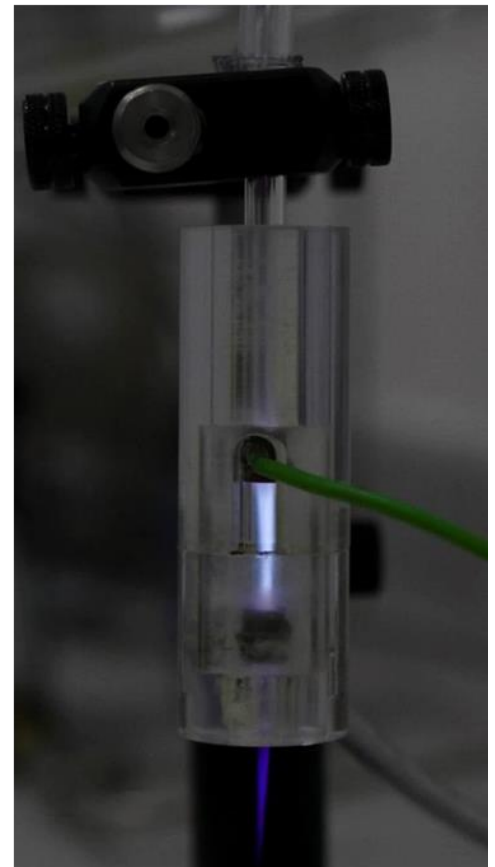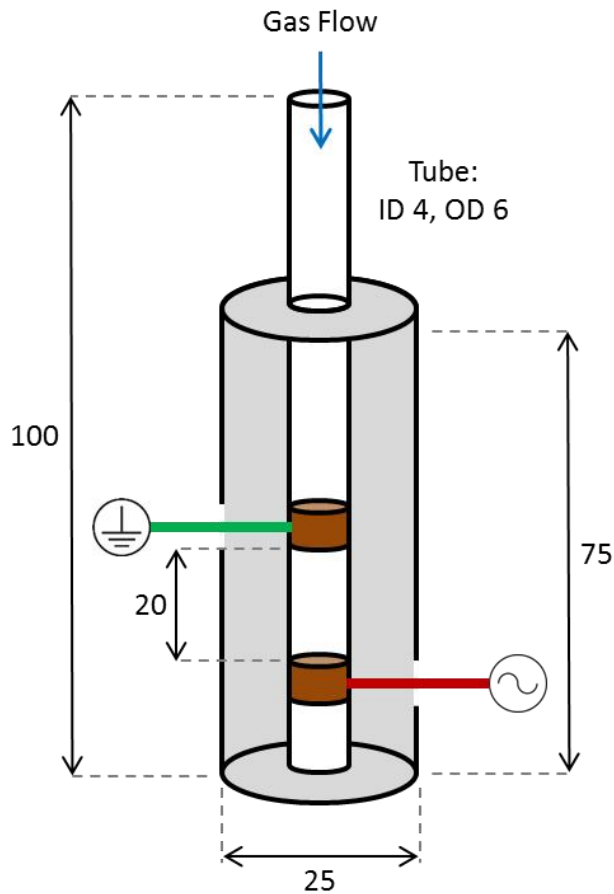
**Figure 13: Schematic of the DBD plasma jet.**

Illustration of the DBD plasma jet, with powered and grounded copper tape electrodes, and gas flow indicated. The physical dimensions of the tube and casing are given in mm. In the accompanying photograph, the core plasma is visible between the electrodes, with the plume propagating downwards from the nozzle.

### 3.2 Plasma Diagnostics

#### 3.2.1 Optical Emission Spectroscopy

Optical emission spectra were measured using an Ocean Optics HR4000CG-UV-NIR spectrometer (200 – 1100 nm range), and accompanying Spectra Suite analysis software. Integration time and scans-to-average were set at 6 s and 50 respectively. A background dark spectrum was first obtained and then subtracted from subsequent spectra. The optical fibre was aligned directly with the core plasma region and fixed at ~2 cm from the quartz tube.

### 3.3 Mammalian Cell Culture

#### 3.3.1 Culture and Maintenance of Prostate Cell Lines

Three prostate cell lines were used during the course of this study: BPH-1, P4E6 and PC-3 cells. BPH-1 cells were derived from benign prostatic hyperplasia (BPH) and immortalised with SV40 large T antigen [222]. P4E6 cells were derived in our own laboratory from a localised and well-differentiated prostate tumour, and immortalised with retrovirus HPV E6 gene [223]. PC-3 cells were established from a prostatic adenocarcinoma that had metastatised to bone [224]. BPH-1 cells were cultured in Roswell Park Memorial Institute-1640 (RPMI) medium (Invitrogen) supplemented with 5% foetal calf serum (FCS) (PAA) and 2 mM L-glutamine (Invitrogen), referred to as R5. P4E6 cells were cultured in keratinocyte serum-free media (KSFM), supplemented with 50 µg/ml bovine pituitary extract (BPE, Invitrogen), 5 ng/ml epidermal grown factor (EGF, Invitrogen), 2% FCS and 2 mM L-Glutamine, referred to as K2. Finally, PC-3 cells were cultured in Ham's F12 medium (Lonza), supplemented with 7% FCS and 2 mM L-glutamine, referred to as H7. No antibiotics or antimycotics were added to the cell culture medium. Cells were incubated at 37°C with 5% $CO_2$, and routinely

cultured in T-75 flasks (Corning). Cell lines were subcultured at a ratio of ~1:3-1:10 every 3-4 days depending on their growth characteristics, when they had achieved ~80% confluence.

### 3.3.2   Culture of Primary Prostate Epithelial Cells

Primary prostate tissue was obtained from patients undergoing transurethral resection of the prostate (TURP), or targeted biopsies from radical prostatectomy, with full ethical permission and patient consent. Needle core biopsies (14 g) were verified as normal or Gleason grade 7 cancer by subsequent pathology, with matched pairs (normal and cancer) obtained from the same patient immediately following radical prostatectomy. The site of each biopsy was determined by previous pathology, TRUS and MRI imaging, and palpation. Tissues were transported in RPMI-1640 with 5% FCS and 100 U/ml antibiotic/antimycotic solution (containing 100 IU/ml penicillin, 100 µg/ml streptomycin and 0.25 µg/ml fungizone (ABM, Invitrogen)) at 4°C, and processed within 6 hours as described previously [225]. Tissues were first dissected into $\sim 1 \text{ mm}^2$ sections, before overnight collagenase digestion (Worthington Biochemical Corporation) to release epithelial structures from the bulk tissue. Repeated centrifugation steps were used to separate out the stromal fraction. Epithelial structures were then further disaggregated through a 30 minute incubation in trypsin-EDTA (Invitrogen) at 37°C under agitation to form a single cell suspension. Primary cells were cultured in stem cell media (SCM), based on KSFM supplemented with 2 mM L-glutamine, 50 µg/ml bovine pituitary extract (BPE), 5 ng/ml epidermal growth factor (EGF), 2 ng/ml stem cell factor (SCF, Sigma,), 1 ng/ml granulocyte macrophage colony stimulating factor (GM-CSF, First Link UK Limited), 100 ng/ml cholera toxin (Sigma),

and 2 ng/ml leukaemia inhibitory factor (LIF, Millipore UK Limited) [225]. Cells were cultured on collagen-I coated 10 cm dishes (BD Biosciences) in the presence of irradiated STO feeder cells, and incubated at 37°C with 5% $CO_2$. No antibiotic or antimycotics were added to the cell culture medium. Primary cells were subcultured at a ratio of 1:2-1:4 once they had achieved 80-100% confluence. Information on the three patient samples used in this study is provided in Appendix A.

### 3.3.3    Preparation of Feeder Cells by Irradiation

Irradiated murine embryonic fibroblast feeder cells (STOs) were added to primary cultures and to primary clonogenic assays (due to very low seeding density). An RS2000 X-Ray biological irradiator containing a Comet MXR-165 X-Ray source (Rad-Source Technologies Inc.) was used to irradiate STO cells at 60 Gy in KSFM to inactivate replicative capacity. STOs were added to each culture dish such that a confluent layer was formed, through which epithelial cultures grew.

### 3.3.4    Determination of Live Cell Number

In order to ascertain the number of viable cells for use in different experiments, the number of live cells in a given culture was determined using a haemocytometer (Neubauer). Trypan Blue stain (0.4%, Sigma) was mixed equally with cells in culture media, 10 µl of which was added to a haemocytometer and visualised by microscopy. Non-viable, blue-stained cells were discounted.

### 3.3.5 Three-Dimensional Cell Culture

BPH-1 and PC-3 cell aggregates were formed by plating 10,000 cells in a volume of 100 µl into round-bottomed, non-adherent 96-well plates (Nalge Nunc International U96 #145399). Cell culture media was refreshed on alternate days, by the removal of 50 µl spent media and the addition of 50 µl fresh media. Aggregates were cultured for ~ seven days and were then treated with LTP.

To culture P4E6 spheroids, an equal mixture of matrigel (BD Biosciences #356231) and K2 media was added to each well of a 24 well plate (Corning) to form a 250 µl matrigel plug, which was allowed to set for 30 minutes at 37°C. Onto this, 6000 cells were added to each well in an equal matrigel/media mixture, and allowed to set at 37°C for a further 30 minutes. Cells and matrigel were supplemented with 2 ml of growth media, which was refreshed every other day by removal of 1 ml spent media and the addition of 1 ml fresh media. Cells formed spheroids after ~ seven days and were then treated with LTP.

## 3.4 Plasma-Treatment of Culture Media, Cells and Tissues

Cells in suspension were exposed to the DBD LTP jet at a distance of 15 mm from the end of the powered electrode for a range of treatment times from 0 to 600 s in micro-centrifuge tubes in a volume of 1.5 ml media. The distance between the end of the nozzle and the media surface was ~ 2 mm. Following measurements with a thermocouple (Hanna Instruments Ltd), treatment times of up to 600 s did not raise the surface temperature of culture media directly under the plasma jet above 36.5°C. The bulk of the media volume remained at room temperature, suggesting only localised heating effects occurred. It was found that ~300 µl of media evaporation occurred

following the longest plasma exposure of 600 s. The final volume in each tube was re-adjusted to 1.5 ml with fresh media in order to ensure cell number density for subsequent experiments was consistent. The level of evaporation from 180 s plasma exposure was found to be negligible.

For cells and spheroids cultured in multi-well plates (Corning), the distance between the DBD jet and the media surface was maintained at ~ 2 mm, in accordance with treatment of cells in suspension. Pieces of benign patient tissue were treated with the DBD plasma jet in 96-well plates (Corning) in 100 µl of culture media, at a distance of ~ 2 mm, such that the plasma effluent was in direct contact with the tissue surface.

### 3.4.1 Positive Cytotoxic Controls

Hydrogen peroxide ($H_2O_2$, Fisher Scientific, UK) was used throughout as a positive ROS control at a concentration of 1 mM [226]. Staurosporine (Cell Signalling Technology, #9953) was used as a positive control for apoptosis in cell death assays at a concentration of 1 µM. Staurosporine is an alkalyating agent, and has been shown to induce apoptosis in a range of cell lines [227-229] through protein kinase C inhibition.

## 3.5 Cytotoxicity Assays

### 3.5.1 Alkaline Comet Assay

LTP-induced DNA damage was quantified using the alkaline comet assay (adapted from Sturmey et al. [230]). Cells were treated with LTP in 1.5 ml centrifuge tubes at a density of 20,000 cells in 1.5 ml media suspension. Immediately after treatment, cells were resuspended in 30 µL PBS and mixed with 225 µl low melting point agarose (Sigma). This was then pipetted onto microscope slides pre-coated with high melting

point agarose (Invitrogen), allowed to set and placed into lysis buffer (2.5 M NaCl, 10 mM Tris, 1 mM EDTA, 10% v/v DMSO,  1% v/v Triton X-100), overnight at 4°C . The following day, cells were placed in alkaline buffer (0.3 M NaOH, 1mM EDTA, pH 13) on ice for 40 minutes, before being electrophoresed at 23-25 V, 300 mA in alkaline buffer for a further 40 minutes on ice. Slides were then placed into neutralising buffer (0.4 M Tris, pH 7.5) for two 10 minute periods, before DNA was stained using SYBRgold (1:10,000 in TE buffer: 10 mM Tris, 1mM EDTA, pH 7.5). Images were acquired by fluorescence microscopy (Nikon Eclipse TE300 microscope, 10x objective lens) using Volocity software (Volocity 6.3, PerkinElmer Inc, US). Autocomet software (Tritek Corp, US) was used to analyse cell images, with the median percentage DNA-in-tail values used to record DNA damage in a minimum of 100 cells per treatment group.

### 3.5.2   Cell Viability Assay

Cell viability was determined by use of the alamarBlue® assay. Cells were treated with LTP then plated into black-walled 96-well plates in triplicate at a density of 5000 cells per well in 100 µl of media. At 24, 48, 72 and 96 hours after treatment, 10 µl of alamarBlue® reagent (DAL1025, Invitrogen) was added to each well and incubated for 2 hours at 37°C. In the presence of actively proliferating cells, the weakly fluorescent blue resazurin solution is reduced to resorufin, which is pink-coloured and highly fluorescent. Fluorescence intensity was recorded at excitation/emission values of 544/590 nm using a microplate reader (Polarstar Optima, BMG Labtech, UK), with cell viability recorded against normalised untreated samples.

### 3.5.3   CellTox™ Necrosis Assay

LTP-induced necrosis was quantified using the CellTox™ green cytotoxicity assay (Cat. #G8741, Promega). Cells were treated with LTP and plated into black-walled 96-well plates at a density of 10,000 cells in 50 µl of media per well. In the case of primary cells, collagen coated plates were used. Contaminating STO cells were first removed from primary culture plates before plating by brief trypsinisation, to reduce the risk of overestimating cell death values. In addition to $H_2O_2$ (1 mM) and staurosporine (1 µM), 2 µl of lysis solution (supplied with assay) was added to necrotic positive control wells. Immediately after treatment with LTP, 50 µl of assay solution was added to all culture wells. The solution contains a cyanine dye which binds to the DNA released from cells with impaired membrane integrity, forming a proportional relationship between fluorescence activity and cytotoxicity. Fluorescence intensity was recorded using a plate reader (Polarstar Optima, BMG Labtech, UK), at excitation/emission wavelengths of 485/520 nm at 2, 4, 8, 12 and 24 hours after treatment. Fluorescence intensity values were normalised to untreated wells. Complementary fluorescence-brightfield merged microscopy images were also taken (Nikon Eclipse TE300 microscope, 10x objective lens) at the same post-treatment time intervals.

## 3.6  Detection of Reactive Oxygen Species

Intracellular reactive oxygen species (ROS) were detecting using the Cell Meter™ fluorimetric total ROS assay (Cat. #22900, AAT Bioquest). Cells were plated into black-walled 96-well plates at a density of 10,000 cells in 100 µl of media and allowed to adhere overnight. The following day, Amplite™ ROS green working stain solution was prepared and 100 µl added to each well prior to treatment. Amplite™ ROS green stain is cell permeable, and upon reaction with intracellular ROS fluoresces green. Cells

were then treated with LTP in darkness, and incubated for 30 minutes at 37°C. Fluorescence intensities were recorded using a microplate reader (Polarstar Optima, BMG Labtech, UK). Fluorescence images were also taken immediately after obtaining the plate read-out (Nikon Eclipse TE300 microscope, 10x objective lens).

Extracellular $H_2O_2$ formed in the culture media as a result of LTP treatment or $H_2O_2$ control was detected and quantified using the ROS-Glo™ $H_2O_2$ assay (Cat. #G8820, Promega). Cells were treated with LTP, before being plated into black-walled 96-well plates at a density of 10,000 cells in 80 µl of culture media. To this, 20 µl of $H_2O_2$ substrate solution was added, which produces a luciferin precursor upon reaction with $H_2O_2$. After incubation for 1 hour at 37°C, 100 µl of detection solution was added to all wells and incubated for a further 20 minutes at room temperature. This detection solution contains D-cysteine, which converts the luciferin precursor to luciferin, which then reacts with recombinant luciferase in the detection solution to produce a luminescence signal proportional to the level of $H_2O_2$ present in the treated media. Luminescence intensity was quantified using a microplate reader (Polarstar Optima, BMG Labtech, UK), and normalised to untreated wells.

### 3.7 Clonogenic Recovery Assay

Clonogenic recovery assays were used to measure cellular recovery post-treatment. Cells were treated in suspension and replated in 6-well plates in triplicate at a density of 200 disaggregated cells per well. Cells were supplemented with 2 ml of growth media, which was changed every other day. In the case of primary epithelial cell cultures, 200 µl of STO feeder cells were also added to each well on day one of the assay. At 12 days after treatment,  cells were stained with crystal violet (PBS, 1% crystal violet, 10%

Ethanol). Only colonies of greater than 50 cells (equating to more than 5 population doublings) were counted. Colonies of this size have been proposed to be self-sustaining [231].

## 3.8 Protein Expression Analysis

### 3.8.1 Caspase-Glo® 3/7 Assay

The activity of apoptotic proteins caspase-3 and -7 was analysed using the Caspase-glo® 3/7 assay (Cat. #G8090, Promega). Cells were treated with LTP and plated into collagen-coated 96-well plates at a density of 20,000 cells per well in 100 µl. A further 100 µl of caspase-glo® 3/7 detection reagent was immediately added to each well. Cells were incubated at 37°C, with luminescence intensity (Polarstar Optima, BMG Labtech, UK) recorded at 24 hours after treatment.

### 3.8.2 SDS-PAGE and Western Blotting

#### 3.8.2.1 Preparation of Whole Cell Lysates

Following treatment, adherent cells were trypsinised at 2, 4, 8, 12 and 24 hours after treatment, rinsed in PBS and stored as cell pellets at -80°C. If needed, cell scrapers were used to ensure complete cell collection. When required, cell pellets were thawed on ice and thoroughly resuspended in 50 µl of Cytobuster protein extraction reagent (71009, EMD Millipore, Germany) and 2 µl of 25x protease inhibitor (cOmplete, EDTA-free Protease Inhibitor Cocktail Tablets, Roche Applied Science, UK) per sample, and left on ice for 10 minutes. Samples were then centrifuged at 13,000 rpm for 2 minutes, and the supernatent transferred to fresh tubes and stored at -80°C.

### 3.8.2.2 BCA Assay

The protein concentration of whole cell lysates was determined using the bicinchoninic acid (BCA) assay (ThermoFisher Scientific, #23225). Bovine serum albumin (BSA) protein standards were prepared according to the manufacturer's protocol, 10 µl of which was pipetted in triplicate into a 96-well plate. 10 µl of treated sample was added to the plate, and 200 µl of working reagent was added to each well. The plate was incubated for 30 minutes at 37°C, and absorbance values recorded at 562 nm using a plate reader (Polarstar Optima, BMG Labtech, UK). The protein concentration of unknown samples was determined using the gradient of a standard curve derived from BSA standards.

### 3.8.2.3 SDS-PAGE

A total of 20 µg protein lysate was added to a solution of 4 x SDS loading buffer (1% w/v SDS, 10% v/v Glycerol, 62.5 mM Tris.HCL pH 6.8, 65 mM DTT, and bromophenol blue to colour) plus 10% ß-mercaptoethanol (Sigma), and briefly centrifuged to combine the elements. This mixture was then heated at 100°C for 5 minutes on a heating block, before being briefly centrifuged once more to collect the solution. Samples (10 – 30 µl) were loaded onto 12% acrylamide separating gels, which were constructed using the miniPROTEAN Tetra cell system (Bio-Rad).

Precision Plus Protein™ Kaleidoscope (Bio-Rad, 161-0375, 10 µl) and biotinylated (Cell Signalling Technology Inc. #7727, 1 µl) protein marker ladders were also loaded to a separate lane on each gel as approximate molecular weight references. Gels were ran at 100 V for ~1.5-2 hours in SDS running buffer (3.5 mM SDS, 25 mM Tris, 0.19 M Glycine).

### 3.8.2.4 Western Blotting

Wet transfer of proteins was performed immediately following electrophoresis. Immobilon-P transfer membranes (Millipore) were pre-soaked in methanol, rehydrated in ddH$_2$O and placed into transfer buffer (48 mM Tris, 39 mM Glycine, 10% (v/v) Methanol). Assembly of the membrane cassette consisted of: a pre-soaked ScotchBrite pad, three sheets of pre-soaked Western blotting paper, protein gel, membrane, three further sheets of Western blotting paper, and a second ScotchBrite pad. The stacked layers were gently rolled to remove air-bubbles, the cassette was firmly closed and placed into the transfer tank, and submerged in transfer buffer. The transfer was carried out 40 V overnight at 4°C.

After transfer, cassettes were dismantled and membranes placed immediately in TBS (50 mM Tris, 150 mM NaCl, pH 7.5) before transfer into blocking solution for 1 hour (Marvel powdered milk, 5% solution in TBS). Membranes were incubated in primary antibody overnight at 4°C in 1% blocking solution. Membranes were then washed three times for 5 minutes in TBS-T (0.1% v/v Tween-20 in TBS), before incubation in secondary antibody for 1 hour at room temperature in 1% blocking solution. A list of primary and secondary antibodies used for western blotting, and their associated concentrations, is given in Table 3. All blocking and antibody incubation steps were performed in vacuum sealed plastic pouches under gentle rocking. Membranes were washed for a further three times for 5 minutes in TBS-T, followed by chemiluminescent detection (BM Chemiluminescent Blotting Substrate (POD) kit, Roche). Blots were developed in darkness using Kodak® GBX developer and fixer solutions on ECL hyperfilm (GE Healthcare).

| Antibody | Primary/ Secondary | Manufacturer | Catalogue No. | Dilution |
|---|---|---|---|---|
| cleaved-PARP Asp214, rabbit polyclonal | Primary | Cell Signalling Technology Inc. | #9541S | 1:666 |
| anti-LC3B Rabbit polyclonal | Primary | abcam | Ab51520 | 1:3000 |
| β-actin mouse monoclonal | Primary | Sigma-Aldrich | A5316 *Clone AC-74* | 1:5000 |
| anti-rabbit IgG HRP-linked | Secondary | Cell Signalling Technology Inc. | #7074S | 1:5000 |
| anti-mouse IgG peroxidase | Secondary | Sigma-Aldrich | A5906 | 1:5000 |

**Table 3. Primary and secondary antibodies used in Western blotting experiments.**

3.8.2.5 Quantitation of Western Blotting Band Intensity

Band intensity quantitation was performed using ImageJ software (Mount Royal, Canada) to gain further insight into autophagic response. The ratio of LC3BII/I band intensity was determined, with all bands quantified against β-actin loading control lanes, and then normalised to untreated controls.

### 3.8.3    Immunofluorescence Staining

### 3.8.3.1 Fixation Techniques

For the treatment of monolayer cultures, cells were plated into chamber slides (Corning) and allowed to adhere overnight before treatment with LTP. At 20 minutes after treatment, cells were washed twice in PBS, before being fixed in paraformaldehyde (PBS, 4% Paraformaldehyde, 0.2% Triton X-100, pH 8.2) for 20 minutes. Cells were then rinsed twice in PBS and stained immediately, or stored at 4°C sealed in parafilm until use. This fixation approach was also used for spheroids cultured in matrigel.

### 3.8.3.2 Immunofluorescence Staining of Cells in Monolayer for $\gamma$H2AX Expression

After fixation cells were washed three times for 5 minutes in PBS before permeabilisation for 20 minutes (0.5% NP40 in PBS) at room temperature. Cells were washed for a further three times for 5 minutes in PBS before incubation in blocking solution for one hour (2% v/v BSA, 1% v/v NGS, PBS). After incubation overnight at 4°C in primary antibody (diluted in PBS, 3% BSA), cells were washed in PBS (0.5% BSA, 0.175% v/v Tween-20) three times for 5 minutes, before incubation in secondary antibody for 1 hour (diluted in PBS, 3% BSA) at room temperature. Cells were washed three times for 5 minutes (0.5% BSA, 0.175% v/v Tween-20 in PBS), before a final wash step in PBS to remove any remaining detergent. Nuclear staining was performed using Vectashield with DAPI (Vector Laboratories) and phalloidin (Sigma-Aldrich P1951) to stain the cytoskeleton. A coverslip was placed onto the surface of the slide and sealed with nail varnish. Cells were visualised under a fluorescence microscope (Nikon Eclipse TE300 microscope).

### 3.8.3.3 Immunofluorescence Staining of P4E6 Spheroids

Unless otherwise noted, all steps were carried out at room temperature under gentle agitation. Cells were incubated in PBS + 0.5% Triton X-100 for 20 minutes before three 10 minute washes (PBS + 0.3 M Glycine). A 1 hour blocking step was performed in IF buffer (0.1% w/v BSA. 0.2% v/v Triton X-100, 0.05% v/v Tween-20 in PBS, pH 7.4) + 10% normal goat serum (NGS) for 1 hour. The slides were then incubated overnight at 4°C in primary antibody in IF buffer + 10% NGS. The following day, three wash steps for 15 mins were performed in IF buffer, before a 1 hour incubation in secondary antibody in IF buffer + 10% NGS. Three final 10 minute rinse steps were performed in PBS, before counterstaining in either Hoechst 33342 (Molecular Probes H1399, 1 μg/ml) or Vectashield with DAPI (Vector Laboratories). A coverslip was placed onto the surface of the slide and sealed with nail varnish.

Propidium Iodide (PI) staining of P4E6 spheroids was conducted 15 minutes after treatment with LTP. Cells were incubated for 15 minutes in darkness in double staining solution (2 μg/ml PI, 100 μg/ml RNase A, 5 μg/ml Hoechst 33342 in PBS) before fluorescence imaging (Nikon Eclipse TE300 microscope).

### 3.8.3.4 Staining of Fixed Tissue Sections

Formalin fixed tissue sections were first baked for 20 minutes at 45°C, before being subjected to a series of washing steps: twice for 10 minutes in xylene, twice for 1 minute xylene, thrice for 1 minute 100% ethanol, once for 1 minute 70% ethanol, and finally for 5 minutes under running water. Mounted tissue sections were boiled in citrate buffer (10 mM trisodium citrate, pH 6.0, 0.05% v/v Tween-20) for three times for 10

minutes and allowed to cool, before being rehydrated in PBS for 15 minutes. Slides were blocked for 1 hour (10% v/v foetal calf serum in PBS) at room temperature. Primary antibody was diluted in the blocking solution and added to slides overnight at 4°C in the dark under rocking. The following day, slides were rinsed three time for 5 minutes in PBS, before adding secondary antibody in blocking solution and incubating for 1 hour at room temperature in darkness. The slides were then rinsed for a final three times for 5 minute washes in PBS, before being mounted using Vectashield with DAPI (Vector Laboratories) and sealed with nail varnish. A list of antibodies used for all immunofluorescence techniques is provided in Table 4.

| Antibody | Primary/ Secondary | Manufacturer | Catalogue No. | Dilution | Usage |
|---|---|---|---|---|---|
| γH2AX Ser139 Mouse monoclonal | Primary | Millipore | 05636 *Clone JBW301* | 1:1000 | Cells, Tissues |
| anti-LC3B Rabbit polyclonal | Primary | Abcam | Ab51520 | 1:2000 | Cells |
| Goat-anti mouse Alexa Fluor 568 | Secondary | Molecular probes | A11004 | 1:1000 | Cells |
| Goat-anti rabbit Alexa Fluor 568 | Secondary | Molecular probes | A11036 | 1:1000 | Cells, Tissues |

**Table 4. Primary and secondary antibodies used in immunofluorescence staining of cells and tissues.**

### 3.9 Statistical Analyses

All experiments were performed in triplicate and results expressed as the mean with associated standard error (SE), with the exception of comet assay data, which shows the median DNA damage value. Plots were constructed and statistical analyses performed using Prism 6 (GraphPad software, San Diego, USA). Statistical significance was determined using unpaired Mann-Whitney test (DNA damage results only, assumes non-Gaussian distribution), or unpaired t-test with Welch's correction (assumes non-equal standard deviation), and displayed on figure plots as $P<0.05$ (*), $P<0.01$ (**), $P<0.001$ (***), $P<0.0001$ (****).

# Chapter 4

## *Results I*

## Plasma Device Development and Cell Treatment Strategy

# 4. Plasma Device Development and Cell Treatment Strategy

In the initial stages of this study, several different approaches for the treatment of cells with LTP were investigated to determine the most reproducible and practical method. This chapter presents basic initial characterisation of the LTP jet, examines the effect of LTP on varying cell number densities, and the influence of different types of cell culture media on cellular response.

## 4.1 Optical Emission Spectroscopy of the Core Plasma

The core plasma of the LTP jet used during the course of this study was characterised by optical emission spectroscopy (OES), using the Ocean Optics system described in Section 3.2.1., across the 200-1100 nm wavelength range. The core plasma region refers to the discharge ignited between the copper ring electrodes, as visualised in Figure 11A and Figure 13. The positioning of the optical fibre with respect to the LTP jet is shown in Figure 14A. The fibre was aligned with the core plasma through a slot in the electrode casing, highlighted by a dashed line. This ensured a reproducible fibre position. The distance between the end of the fibre and the quartz tube was maintained at 2 cm. Figure 14B shows the emission spectrum acquired following LTP jet operation, which is typical of a helium/oxygen plasma jet. This was recorded for 2 SLM helium flow with 0.3% molecular oxygen admixture at 20% voltage output; the maximum achievable avoiding arcing between the electrodes. Photons emitted as a consequence of the relaxation of excited states were detected, with intensity plotted as a function of wavelength. Two peaks with high intensity corresponding to atomic oxygen (O) were detected at 777 nm and 844 nm, in addition to a peak corresponding to helium at 706 nm. The noise and small peaks visible between 500 and 650 nm are believed to be due to low levels of background light in the laboratory.
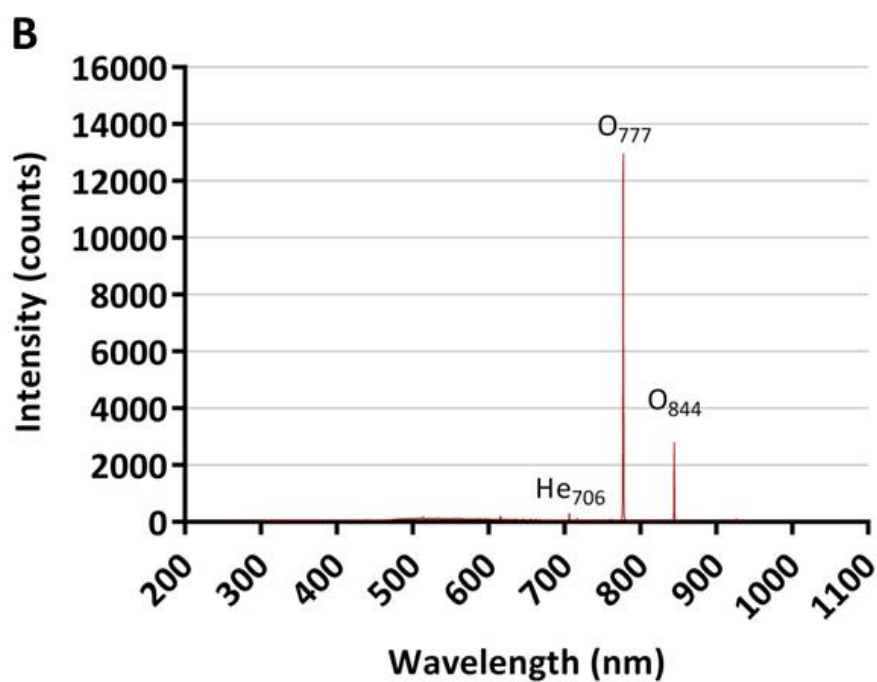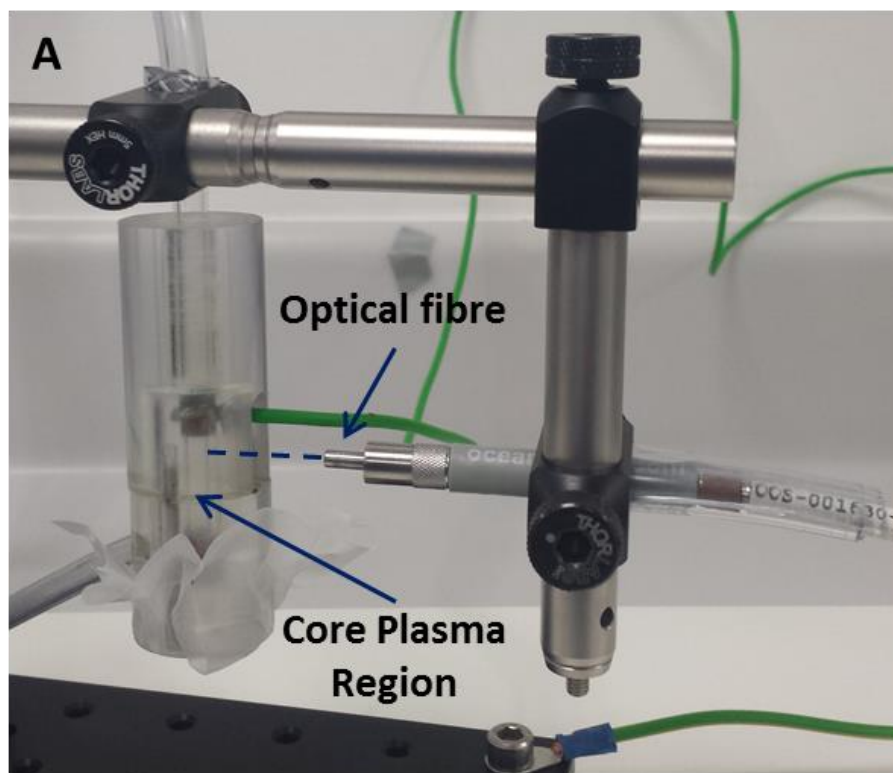
**Figure 14: Optical emission spectroscopy of the core plasma.**

The experimental setup is shown in (**A**), with the alignment of the optical fibre into the

core plasma indicated by the blue hashed line. The resulting optical emission spectra is

given in (**B**), with emission lines corresponding to key species identified.

## 4.2  Methods of LTP-Cellular Treatment

Several different approaches for the treatment of cells with LTP were analysed to determine the most suitable method to carry forward for the majority of this study. Similarly, different prostate cancer models were used to study LTP-effects, ranging from the treatment of cells in suspension to small pieces of tissue, and are presented in this and the following results chapters.
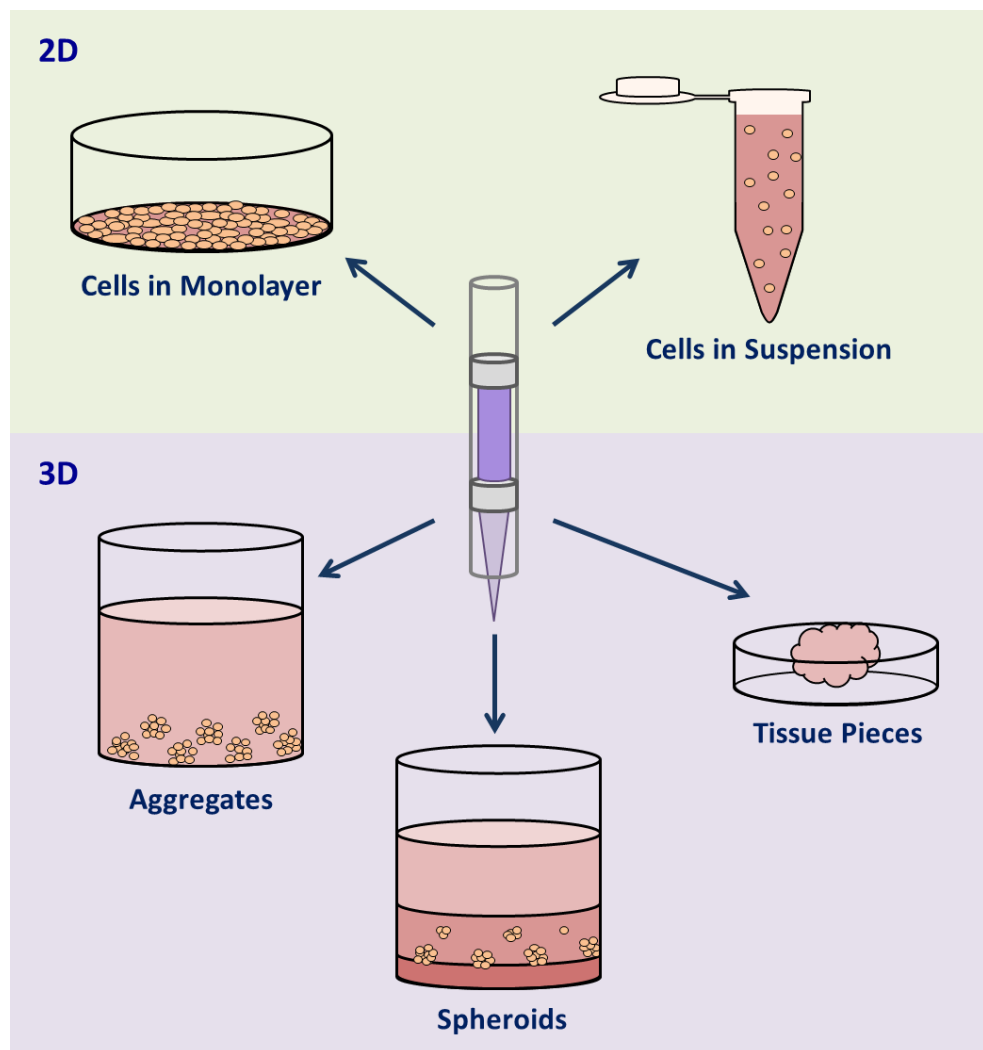


**Figure 15: Cell treatment models.**

Different cell models were used to compare the practicality of LTP treatment, comparing LTP effect in 2D (cells in monolayer and cells in suspension), and 3D (aggregates, spheroids and tissue pieces).

| Cell Treatment Model | Advantages | Disadvantages |
|---|---|---|
| Cells in monolayer | - Cells are actively growing before treatment | - Different media volumes required depending on culture vessel size <br> - Plasma arcs to vessel walls in 48/96 well plates |
| Cells in suspension | - Consistent media volume for treatment <br> - Allows for re-plating of desired cell number density following treatment | - Do all cells receive the same plasma 'dose'? <br> - Cells rapidly sediment at larger number densities |
| Aggregates | - Time-efficient means of creating 3D model | - Variability in aggregate morphology and size between different cell lines <br> - Problematic to transfer aggregates between culture plates for treatment |
| Spheroids | - Culture in matrigel mimics basement membrane environment <br> - Provides approximate model for tumour morphology and heterogeneity | - Not all cell lines form spheroids <br> - Assaying not straightforward <br> - Lengthy and expensive culture process |
| Tissue pieces | - Treatment of real patient tissue provides insight into clinical response | - Problematic to quantify penetrative effect of LTP <br> - Difficult to determine plasma-tissue contact point throughout fixation process |

**Table 5. Advantages and disadvantages of respective cell models used in this study.**

The illustrations in Figure 15 highlight the different models investigated in this work, including the treatment of cells in monolayer and suspension, and of aggregates, spheroids, and prostate tissue pieces. Table 5 serves to highlight some of the considerations and issues encountered with each model. Initially, cells were treated with LTP when growing in culture as a 2D monolayer. However, a few issues were quickly encountered. The cells directly beneath the LTP jet rapidly detached and fragmented after treatment, whereas cells at the outer edge of the culture dishes remained unaffected. The most problematic finding was that when treating cells in smaller wells, such as 48- and 96-well plates, the plasma effluent arced onto the side of the culture well and failed to make contact with the media surface. This was likely due to static build-up on the plastic, and meant that no cellular damage occurred. Another 2D model that was investigated was the treatment of cells in media suspension. This gave the advantage of a consistent 1.5 ml media volume for treatment, and allowed the re-plating of a desired cell number density following treatment, as required by different assays. One concern with this method was whether cells treated at high number densities would begin to collect at the bottom of the tube before the end of the treatment. This was investigated in section 4.3. in the context of DNA damage. Due to the flexibility it provided, the treatment of cells in micro-centrifuge tubes, in a volume of 1.5 ml media suspension, was adopted as the main method for LTP treatment over the course of this study.

Different 3D models were also trialled to more accurately represent 3D tumour morphology, including cell aggregates, spheroids, and direct treatment of prostate tissue pieces. The advantages and pitfalls of these treatments, as outlined in Table 5, are discussed in further detail in Chapter 6.

### 4.3 The Effect of Cell Number Density on DNA Damage Sustained

PC-3 cells were treated with 180 s LTP in 1.5 ml micro-centrifuge tubes at varying number densities, and analysed for DNA damage using the alkaline comet assay. For all future experiments, cells were treated in a volume of 1.5 ml media suspension, however different experiments and assays required varying numbers of cells per treatment. Therefore, a number of densities ranging from $10^4$ to $10^7$ cells per tube were treated with LTP to assess if the levels of DNA damage resulting from plasma treatment were dependent on cell number density. A control sample of untreated cells was also assayed, at a concentration of $10^4$ cells per tube. Figure 16 shows the results of the comet assay, and shows that treating $10^4$-$10^6$ cells per tube produces extremely comparable, high levels of DNA damage in PC-3 cells. However, treating $10^7$ cells in a 1.5 ml media volume leads to a statistically significant reduction of around 40% in the level of DNA damage following 180 s LTP exposure. The damage across the ~100 cells quantified for each treatment was uniformly distributed for the $10^7$ sample, compared to other treated groups, which were tightly grouped around the median damage value. This result shows that treatment of $10^4$-$10^6$ cells per tube with LTP produces consistent levels of DNA damage, and lead to an upper limit of $10^6$ cells per tube being imposed for future experiments.
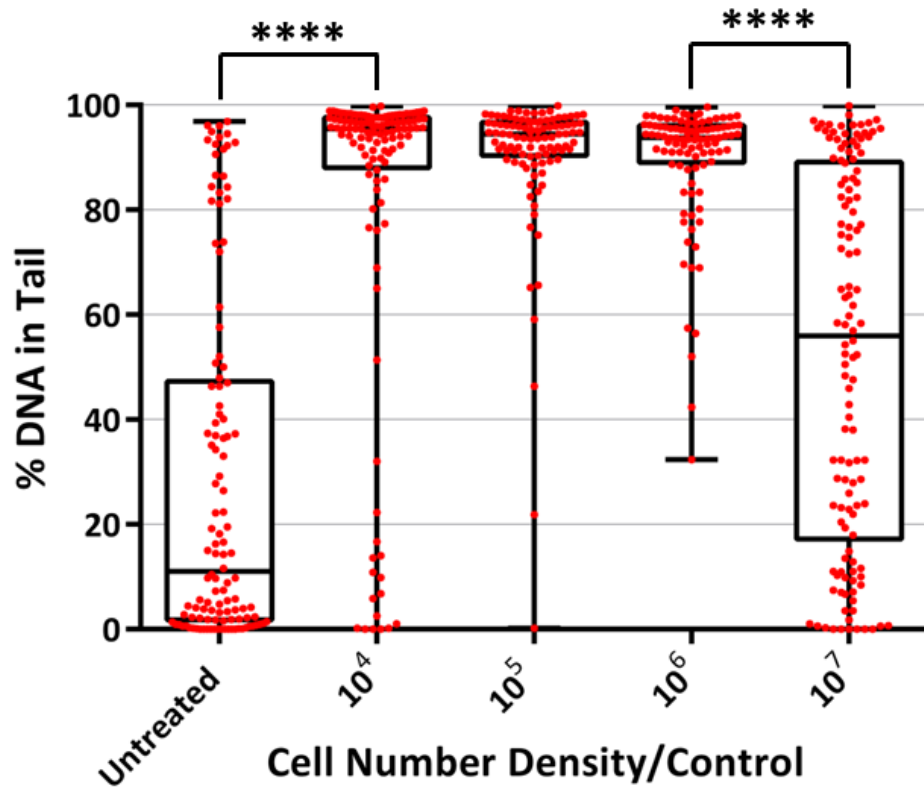
**Figure 16: DNA damage as a function of cell number density.**

PC-3 cells, ranging from $10^4 - 10^7$ cells per tube, were treated with 180 s LTP and analysed for DNA damage by the alkaline comet assay. Each dot represents a single cell, with a minimum of 100 cells counted for each treatment. Data are expressed as the median value, with the 25-75th percentile highlighted by boxes. Statistical significance (P<0.0001 = ****) was analysed by Mann-Whitney rank test, which assumes a non-Gaussian distribution.

## 4.4 Influence of Cell Culture Media on LTP-Cellular Effect

BPH-1 cells were exposed to LTP for 180 s or 1 mM $H_2O_2$ control to investigate if treatment in buffered saline solutions or cell culture media containing serum altered the observed cellular response. The reasoning for this was to examine if components in the media, such as the presence of serum, might quench reactive species produced by the plasma. Figure 18A examines changes in cell viability, 72 hours after treatment using the alamarBlue assay. BPH-1 cells were either treated in Hank's buffered saline solution (HBSS), or RPMI media with 5% serum content, with or without phenol red (R5 +/-). Phenol red is a colourant which is routinely added to cell culture media to serve as a pH indicator. However, it has been suggested that phenol red can become highly fluorescent when excited at specific wavelengths [232], and thus may influence plate reader based assays, such as alamarBlue. The effect of allowing cells to remain in treated culture media, versus pelleting the cells 15 minutes after treatment and re-suspending them in fresh culture media, was also investigated. Figure 17A clearly shows that the presence or absence of phenol red in the cell culture media has no influence on fluorescent cell viability readings. As such, all future experiments were performed using standard cell culture media with phenol red. The data from Figure 17A for cell treatments in media with phenol red are re-plotted in Figure 17B to simplify analysis between treatment groups. Leaving cells in the original LTP-treated media until the point of assay reduced the viability by 90%. Treatment of BPH-1 cells in HBSS with 180 s LTP, followed by removing the HBSS and adding fresh R5, reduced cell viability values by 50%. Removing the treated media following 180 s LTP treatment and adding fresh R5 appeared to lessen the reduction of cell viability to only 20% when compared to untreated control. However, replenishing cultures with fresh R5 media following treatment with $H_2O_2$ control did not induce significant differences in cell viability

readings when compared to leaving cells in treated media. LTP-treatment of cells in HBSS reduced cell viability by ~ 40% less than cells which were retained in treated R5 media. In all future experiments, cells remained in their original treated media. This provided a more physiologically realistic model with respect to the ultimate aim of treating a patient.

Given that different types of cell culture media contain different components and added serum levels, the levels of reactive species formed as a result of treatment may vary and thus contribute to the observed cellular response. The level of $H_2O_2$ formed in different cell culture media was analysed using the ROS-Glo $H_2O_2$ luminescence assay immediately after treatment with $H_2O_2$ control, and is shown in Figure 17C. Three different types of cell culture media were analysed, due to their future experimental use. These included: Hams F12 + 7% serum (PC-3 cells, H7), RPMI 1640 + 5% serum (BPH-1 cells, R5), and Keratinocyte serum free media (primary cells, KSFM). HBSS was used alongside for comparison purposes. Treatment of KSFM with $H_2O_2$ produced luminescence readings at least 6-fold lower than HBSS, H7 and R5. The highest $H_2O_2$ readings were recorded for both treated and untreated cells cultured in H7 or R5 media; however, R5 media produced over twice the intensity of any other media in the absence of cells (media blank). The implications of these results were considered when performing the ROS-Glo $H_2O_2$ luminescence assay in the context of LTP-treated cells. Given that the luminescence signals from H7, and particularly R5, were several-fold higher than for KSFM, the type of cell culture media could not be disregarded when comparing results between cell lines and primary cells.
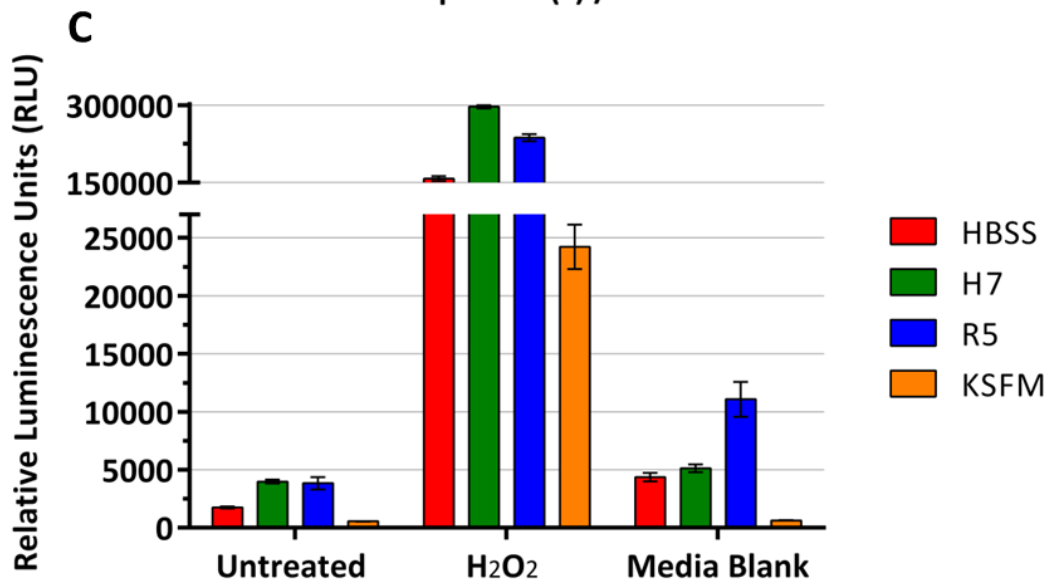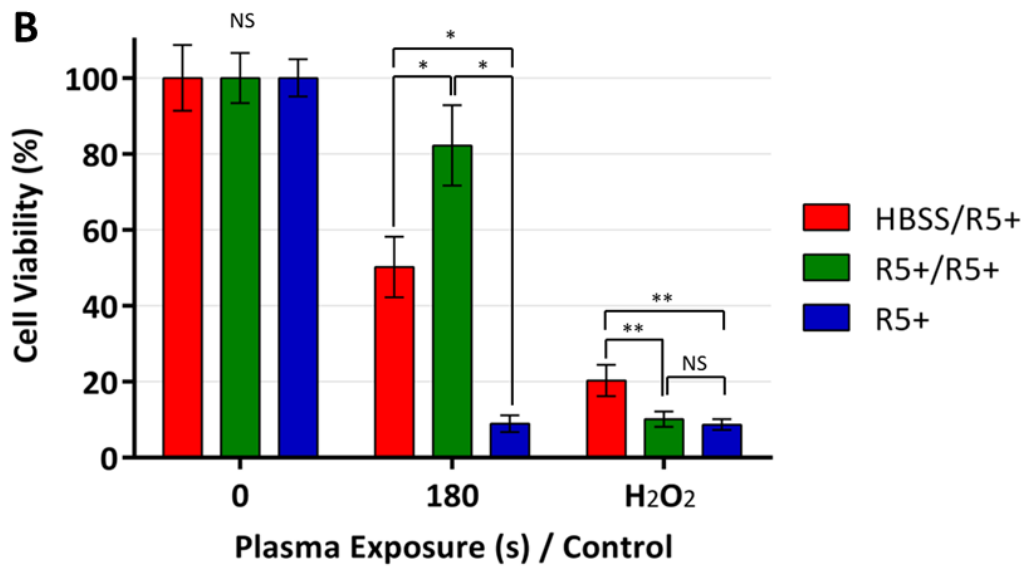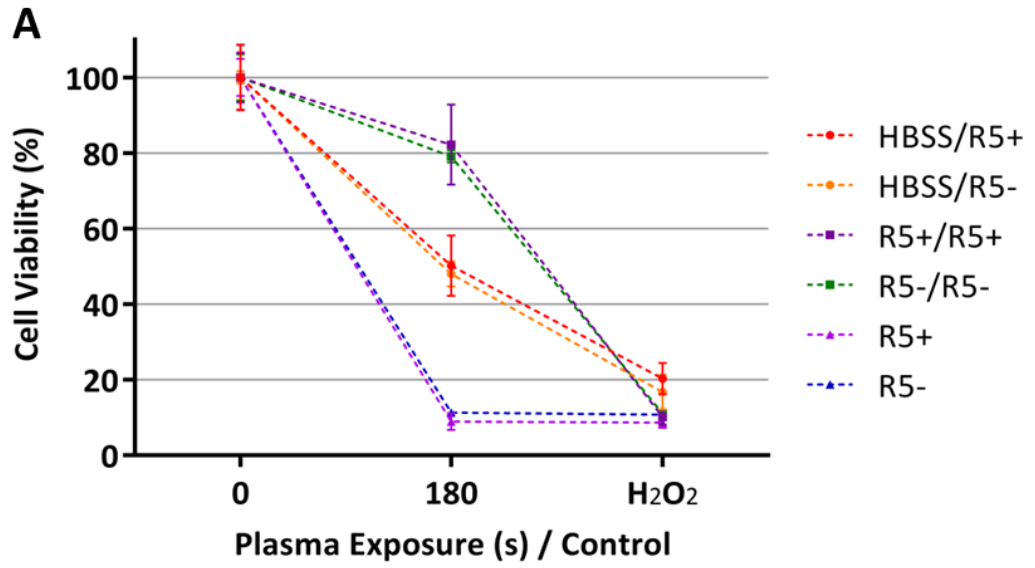
**Figure 17: Contribution of different types of cell culture media to changes in cell viability and reactive species formation.**

The viability of BPH-1 cells 72 hours after treatment with either 180 s LTP or 1 mM $H_2O_2$ control were analysed by alamar blue assay (**A**). Cells were treated in either HBSS, or RPMI 1640 + 5% serum (R5) with or without phenol red (R5+/R5-). Cells were either pelleted and re-suspended in fresh media, or remained in treated media. The readings for HBSS and R5+ were re-plotted to analyse differences between treatment groups (**B**). The levels of $H_2O_2$ in different cell culture media was determined by the ROS-Glo $H_2O_2$ luminescence assay immediately after treatment (**C**). BPH-1 cells were treated in either HBSS or RPMI 1640 media + 5% serum (R5), PC-3 cells in Hams F12 media + 7% serum (H7), and primary cells in KSFM. All cell types were treated with 1 mM $H_2O_2$ control. Data are expressed as the mean value ± standard error. Statistical analysis was conducted using unpaired t-test with Welch's correction, with significance recorded against untreated samples unless otherwise indicated.

# Chapter 5

## *Results II*

## Study of Plasma-Effects on Prostate Cell Lines

# 5.  Study of Plasma-Effects on Prostate Cell Lines

Following the initial optimisation of the plasma setup and cell treatment methods discussed in Chapter 4, this chapter focuses on an initial proof of principle study to examine the reproducibility of LTP treatment. This was performed on the metastatic prostate cell line PC-3. Further extended analysis was then conducted in both benign and malignant prostate cell lines to allow for comparison between different cell types. To give a point of reference for the effects of LTP treatment, PC-3 cells were treated with 2 Gy ionising radiation (IR), since radiotherapy has been a standard of care treatment for prostate cancer patients for many years. A daily dose of 2 Gy IR is also typically given to patients undergoing radiotherapy for PCa. PC-3 cells were derived from a metastatic tumour to bone marrow that was treated with cryotherapy [224], and have been shown to exhibit resistance to a wide range of cytotoxic agents *in vitro* [233-236]. In addition, IR and LTP both produce reactive species, and so cell death mechanisms may be predicted to overlap.

## 5.1  Treatment of PC-3 Cells with Ionising Radiation

The viability of PC-3 cells was analysed following treatment with ionising radiation (IR). Increasing doses of IR were applied, ranging from $2 - 75$ Gy, with cell response quantified by alamarBlue assay at 24-72 hours after treatment. The alamarBlue assay is a measure of metabolically active and thus proliferating cells, and is used as an indicator of cell viability following treatment compared to untreated cells. Figure 18A shows that no clear dose-dependent reduction was observed over the time-frame of the experiment; 75 Gy IR reduced cell viability by only 8% at 24 hours. By 72 hours after treatment, the viability of cells had recovered to that of untreated cells. This suggests that even the minimal reduction in viability following 75 Gy IR only resulted in temporary, rather

than permanent, arresting of cells. DNA damage immediately following treatment of PC-3 cells with either 2 Gy IR or $H_2O_2$ control was recorded using the alkaline comet assay. A modest, but statistically significant, increase in DNA damage was recorded following 2 Gy IR and is shown in Figure 18B. However, the $H_2O_2$ control induced DNA damage levels of ~ 90%. The clonogenic potential of PC-3 cells was determined at 12 days after treatment with either 2 Gy IR or $H_2O_2$ control (Figure 18C). Colonies of > 50 cells were counted by crystal violet staining, and expressed as surviving fraction (SF) relative to normalised untreated control wells. It was observed that 2 Gy IR reduced the surviving fraction to around 50%, whereas $H_2O_2$ control reduced the surviving fraction to around 25%.
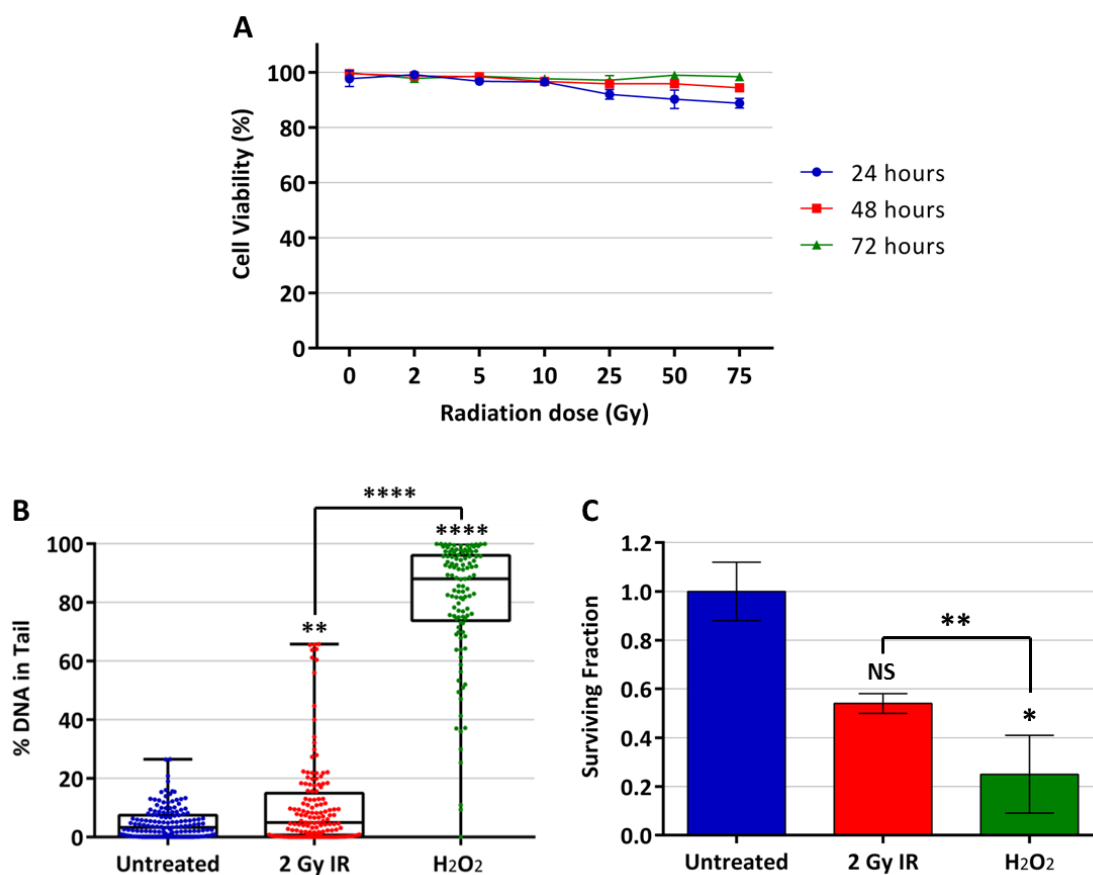
**Figure 18: Analysis of the effect of ionising radiation on PC-3 cells.**

Cells were treated with IR or with $H_2O_2$ control (1 mM). Cell viability was analysed following IR doses up to 75 Gy at 24-72 hours after treatment (**A**). DNA damage levels were recorded using the alkaline comet assay (**B**) immediately following treatment with 2 Gy IR or $H_2O_2$ control. Cell recovery at 12 days following treatment with either 2 Gy IR or $H_2O_2$ control was determined by clonogenic assay and expressed as surviving fraction (**C**). Data are expressed as the mean value ± standard error (**A, C**), or the median value with associated 25-75th percentiles, represented by boxes (**B**). Statistical analysis was conducted using unpaired t-test with Welch's correction, with significance recorded against untreated samples unless otherwise indicated. Note: Graph **A** was kindly provided by Dr Fiona Frame.

## 5.2 LTP Treatment Induces DNA Damage in PC-3 Cells

PC-3 cells were treated with LTP for a range of different exposures, or 1 mM $H_2O_2$ control, before being analysed immediately for DNA damage using the alkaline comet assay. The general principle of the comet assay is illustrated by Figure 19A, where increasing LTP exposure resulted in decreased size of the cell nucleus (comet head), and an increased migration of the electrophoresed fragmented DNA (comet tail). Defining the position of the cell nucleus can be problematic for heavily damaged cells whose nuclei appear either very small or almost non-existent. The alkaline comet assay predominantly detects single stranded DNA breaks, with the percentage of DNA in the comet tail used as a measure of the level of DNA damage to the cell. Figure 19B, C and D are examples of three individual experiments, and show a consistent pattern of increased DNA damage levels with extended LTP exposures, demonstrating the reproducibility of the plasma treatment. As little as 10 s LTP treatment induced statistically significant levels of DNA damage, with 600 s LTP treatment causing significantly higher damage than the $H_2O_2$ control (Figure 19B and D). Figure 19E represents an averaged plot of the three replicate experiments, and suggests that the maximum quantifiable level of DNA damage induced by LTP exposure plateaus at ≥ 180 s treatment duration. This is most likely due to a limit in sensitivity for detecting heavily damaged cells with the comet assay, as it would be assumed that the level of DNA damage would be proportional to plasma exposure, and presumably resultant ROS concentration.

A further experiment was conducted to determine if DNA damage was sustained or repaired following treatment. Cells were either re-plated for 24 hours following treatment before analysis using the comet assay, or analysed within 30 minutes as before. Figure 20A shows the same DNA damage trends immediately following

treatment as observed in Figure 19. However, Figure 20B shows that at 24 hours, DNA damage from LTP treatments returned to baseline untreated levels, indicative of DNA repair. Similarly, damage levels from $H_2O_2$ control fell from ~75% to ~6%. Only plasma exposure of 600 s resulted in sustained DNA damage, which was highly significant when compared to both 300 s LTP and $H_2O_2$ control. To more clearly illustrate the changes in DNA damage with time, Figure 20C shows the data obtained both immediately and at 24 hours after treatment, normalised to respective untreated samples. This shows that the level of DNA damage was reduced by around only 10% following 600 s LTP exposure.
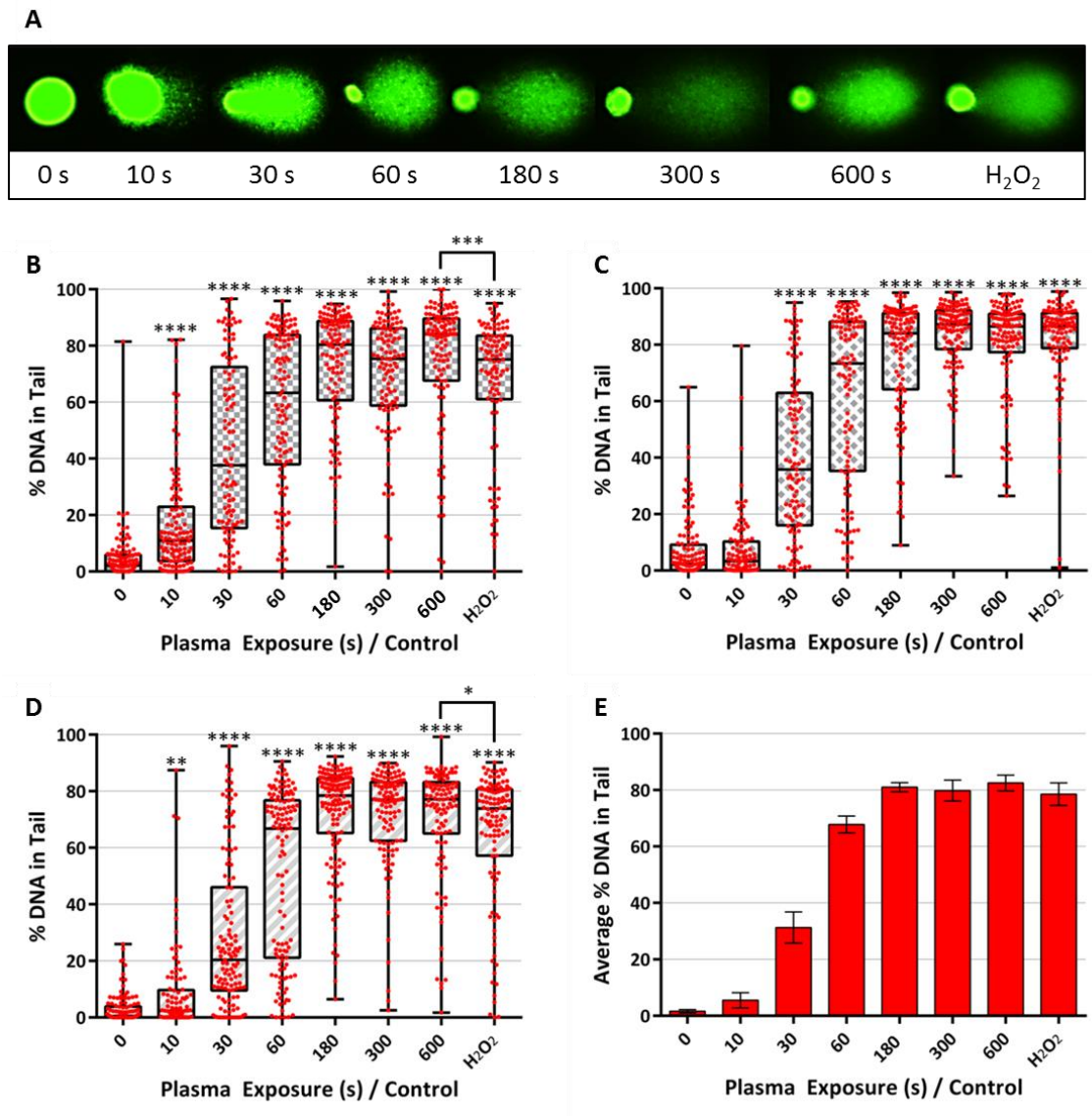
**Figure 19: LTP induces DNA damage in PC-3 cells.**

Cells were treated with LTP for a range of treatment times, or with $H_2O_2$ control (1 mM). DNA damage levels were recorded using the alkaline comet assay and represented as % DNA-in-tail. Representative photographs of cells and comet-like structures are given in **A**. Green represents fluorescent DNA in the nucleus and comet tail. Replicate experiments are shown in **B**, **C** and **D**, and are averaged in **E** (mean ± standard error). Each dot represents a single cell, with a minimum of 100 cells counted for each treatment. Data are expressed as the median value, with the 25-75th percentile highlighted by shaded boxes. Statistical significance was analysed by Mann-Whitney test, with significance recorded against untreated samples unless otherwise stated.
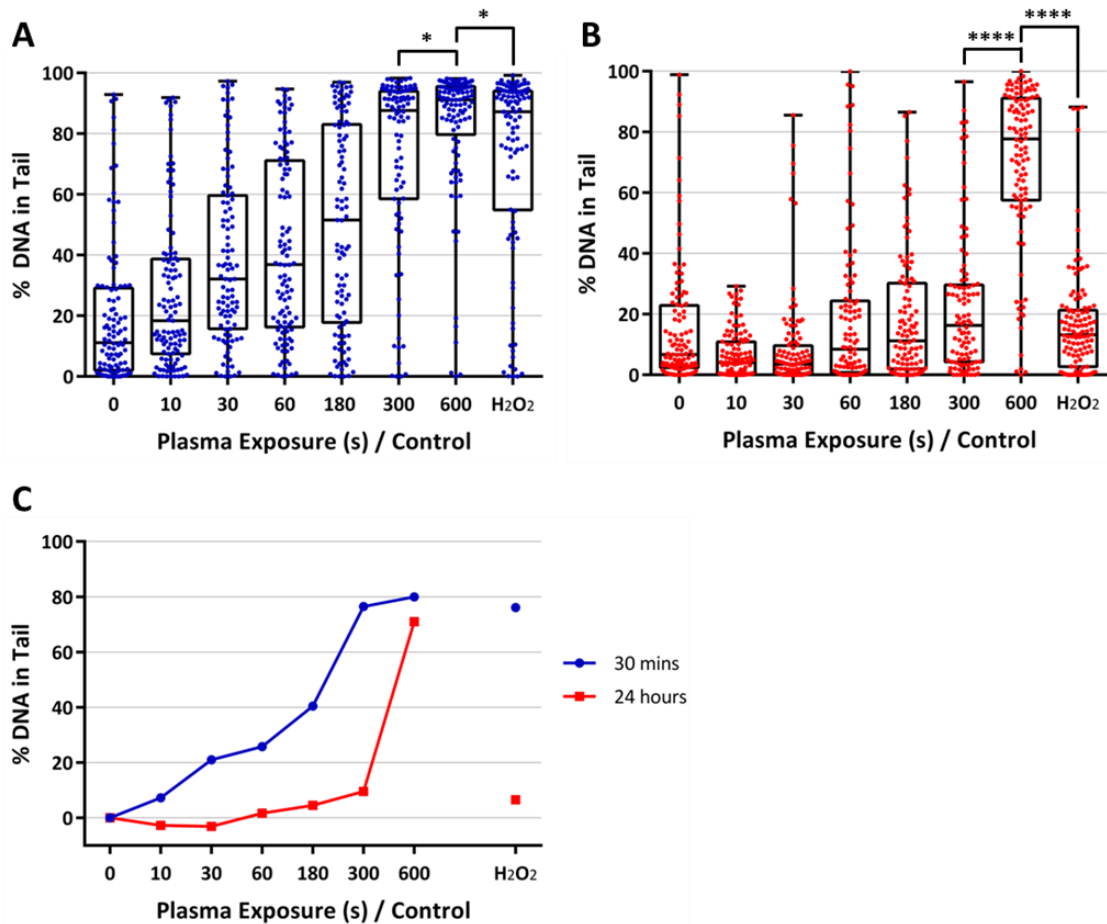
**Figure 20: Analysis of LTP-induced DNA damage levels in PC-3 cells at 24 hours post-treatment.**

Cells were treated with LTP for a range of treatment times or with $H_2O_2$ control (1 mM). DNA damage was quantified at either 30 minutes (**A**) or 24 hours (**B**) after treatment. DNA damage levels were recorded using the alkaline comet assay and represented as % DNA-in-tail. Each dot represents a single cell, with a minimum of 100 cells counted for each treatment. Data are expressed as the median value, with the 25-75th percentile highlighted by boxes (**A**, **B**). A direct comparison of median DNA damage is shown in **C**. Statistical significance was analysed by Mann-Whitney test.

## 5.3  Effect of LTP Treatment on Clonogenic Potential of PC-3 Cells

The clonogenic potential of PC-3 cells was analysed following treatment with a range of timed LTP exposures or 1 mM $H_2O_2$ control to assess cell recovery post-treatment, and is shown in Figure 21. Defined colonies of > 50 cells were quantified through crystal violet staining at 12 days after treatment. Figure 21A, B and C are examples of three individual experiments, the mean of which is shown in Figure 21D. Colony forming ability is expressed as the surviving fraction (SF) when compared against normalised untreated control wells. The three replicate experiments again show the consistency of response following LTP treatment. A statistically significant reduction in SF was observed following ≥ 180 s LTP treatment, and when comparing 600 s LTP directly to $H_2O_2$ control. Figure 21D shows that LTP exposures of 10 and 30 s led to a slight increase in SF, and that 60 s LTP produced no change in SF over untreated control. At LTP exposures of > 60 s, a dose dependent decrease in SF was recorded, with 300 and 600 s LTP treatment reducing SF below $H_2O_2$ control.

To further determine the long term clonogenic capacity of PC-3 cells following LTP treatment, a secondary colony forming assay was conducted. Cells were treated with either 600 s LTP or 1 mM $H_2O_2$ control for 12 days before colonies of > 50 cells were counted in the culture plates without staining. Primary colony forming efficiency was plotted as a fraction of the 200 single cells that were initially seeded into each culture well and is given in Figure 22A. It was found that treatment with 600 s LTP reduced the primary colony forming efficiency to < 10%; around half the reduction recorded from $H_2O_2$ control. Individual colonies were disaggregated and re-plated, and cultured for a further 12 days. Images of heterogeneous colony morphology were also recorded, with evidence of holoclones (tightly-packed colonies) and paraclones (diffuse, disordered colonies) presented in Figure 22B, C and D. Secondary colony forming efficiency was

plotted as a fraction of the cells re-seeded from harvested primary colonies. The secondary colony forming efficiency resulting from treatment with 600 s LTP was ~50%, and from $H_2O_2$ control ~ 60%. In the untreated control group, the majority (84%) of the secondary colonies formed were quantified as holoclones, as shown by Figure 22B. Only holoclones are thought to be capable of sustained passaging in culture [237]. However, in the treated groups, only 54% and 42% of colonies were quantified as holoclones following treatment with 600 s LTP or $H_2O_2$ control respectively. This suggests that LTP treatment reduces the proportion of cells with the capacity to repeatedly form colonies. Examples of paraclones formed following treatment are shown in Figure 22C for 600 s LTP and 22D for $H_2O_2$ control. These are much more disorganised, sparsely populated colonies compared to compact and regular holoclones. It could be viewed that the cells within the paraclone in Figure 22C appear more independent of their neighbours and potentially motile. This could be investigated through time-lapse microscopy to determine how far and how rapidly these cells migrate.
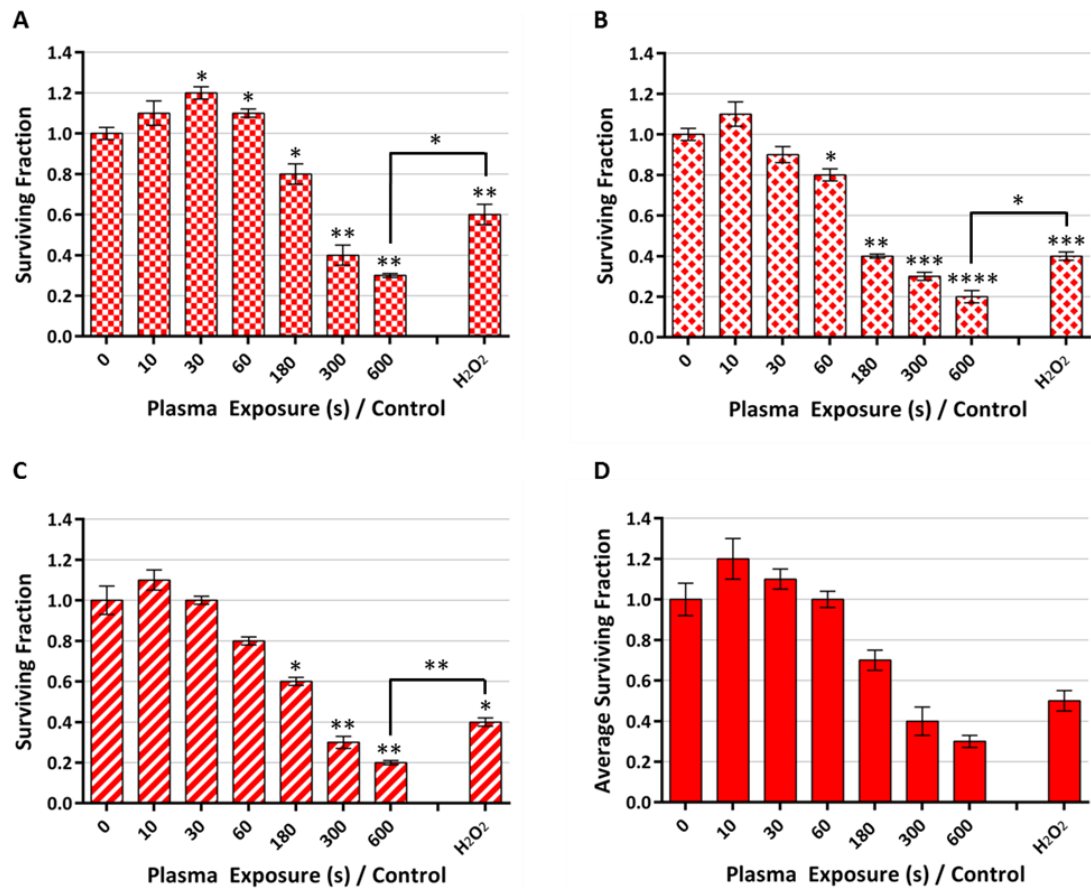
**Figure 21: LTP treatment reduces clonogenic recovery in PC-3 cells**.

Cells were treated with LTP for a range of treatment times, or with $H_2O_2$ control (1 mM). Colonies of > 50 cells were identified by crystal violet staining at 12 days following treatment, and expressed as surviving fraction against normalised untreated control wells. Replicate experiments are shown in **A**, **B** and **C**, and are averaged in **D**. Data are expressed as the mean value ± standard error. Statistical analysis was conducted using unpaired t-test with Welch's correction, with significance recorded against untreated samples unless otherwise stated.
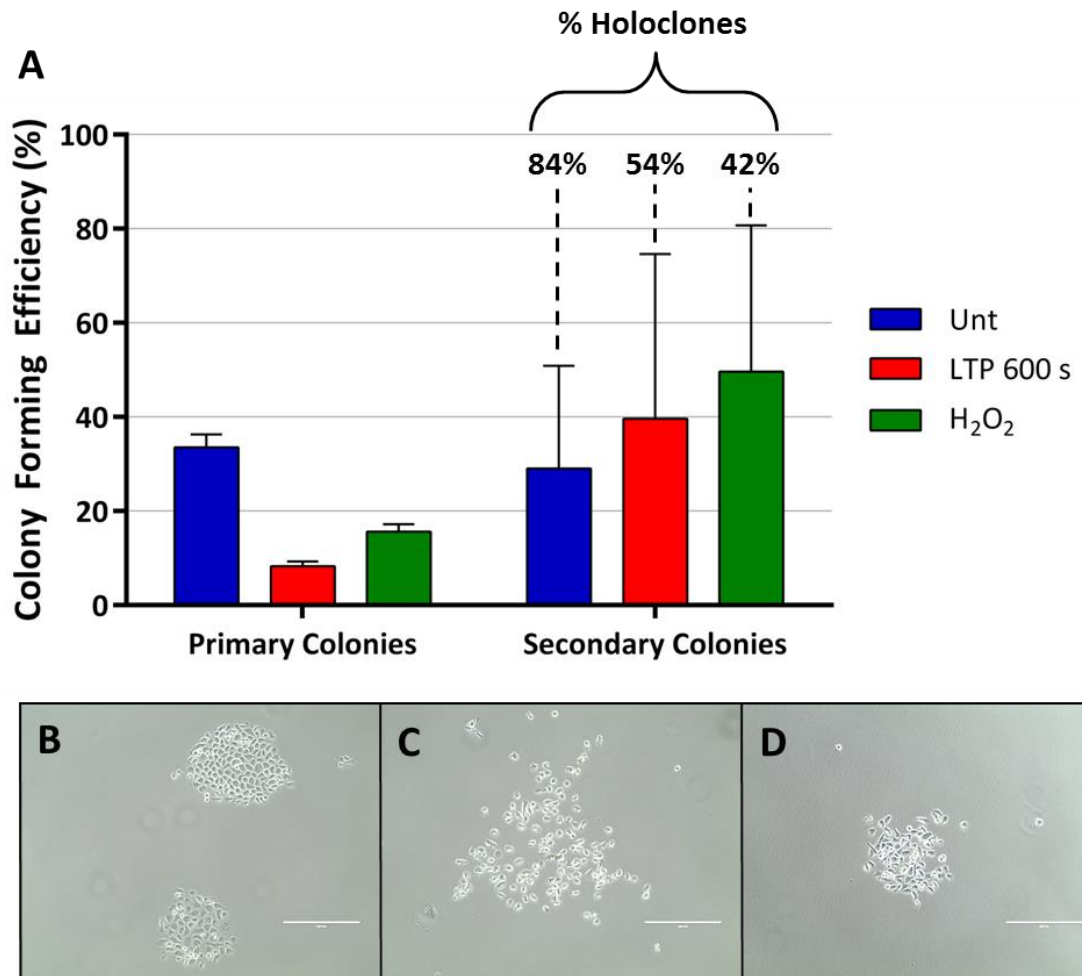
**Figure 22: PC-3 secondary colony formation following LTP treatment.**

Cells were treated with either 600 s LTP or with 1 mM $H_2O_2$ control. Colonies of $> 50$ cells were identified by crystal violet staining at 12 days following treatment, and expressed as colony forming efficiency as a proportion of total re-seeded cells (**A**). Three holoclones from each treatment group were selected and re-plated for a further 12 days before quantification of secondary colony forming efficiency. The percentage of holoclones are identified in **A**, along with representative images of untreated (**B**), 600 s LTP (**C**), and $H_2O_2$ (**D**) secondary colonies. Scale bar denotes 400 µm.

## 5.4 LTP-Treatment Induces Intracellular Reactive Oxygen Species

Intracellular reactive oxygen species (ROS) formation in PC-3 cells was quantified using the Cell Meter™ Intracellular Total ROS Activity assay. Cells were treated with either 300 s LTP or 1 mM $H_2O_2$ control. LTP treatment durations of longer than 300 s were not possible due to issues with evaporation of the assay detection reagent. It was found that treatment with 300 s LTP induced a > 2-fold increase in intracellular ROS formation, and is shown in Figure 23A. Exposure to 1 mM $H_2O_2$ control produced a very similar level of induction. Fluorescence microscopy photographs corresponding to untreated, 300 s LTP and $H_2O_2$ control are presented in Figure 23B, C and D respectively, and demonstrate a clear induction of intracellular ROS through the presence of fluorescent cells.
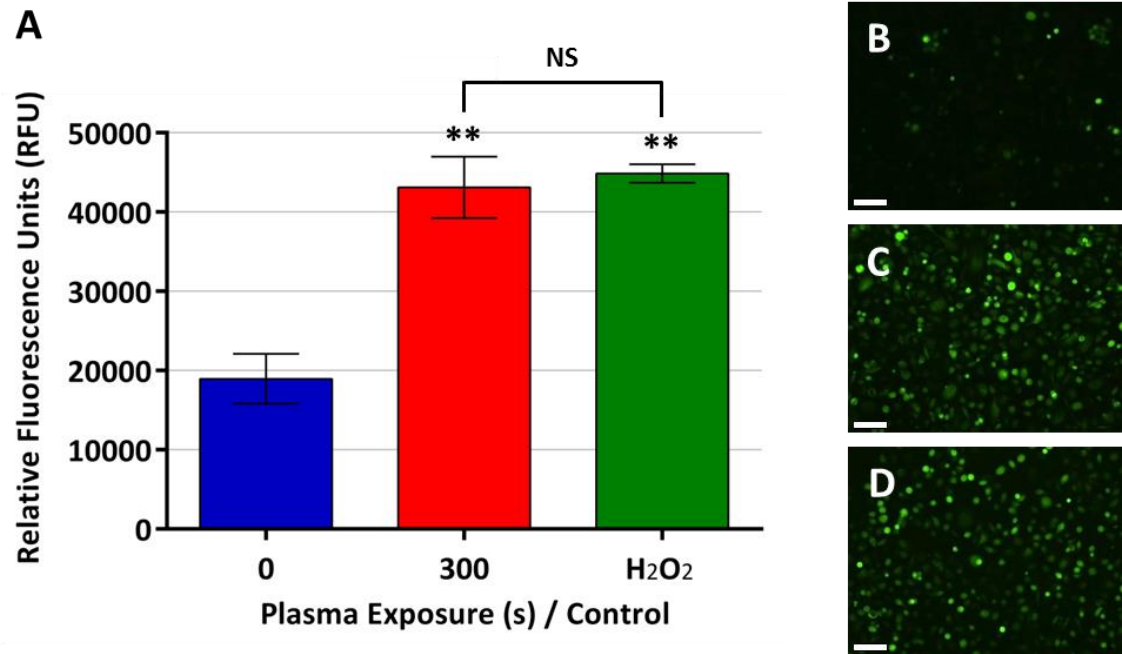
**Figure 23: Intracellular reactive oxygen species formation in PC-3 cells.**

Cells were treated with either 300 s LTP or with 1 mM $H_2O_2$ control. Intracellular reactive oxygen species formation was analysed by relative fluorescence intensity using the Cell Meter™ Intracellular Total ROS Activity assay immediately after treatment (**A**). Representative fluorescence images are shown for untreated (**B**), 300 s LTP (**C**) and $H_2O_2$ control (**D**). Scale bar denotes 100 μm.

### 5.5 Cytotoxic Effects of LTP in Benign and Malignant Prostate Cell Lines

Following the consistency of plasma effect in PC-3 cells, the benign cell line BPH-1 was introduced as a non-malignant comparison. Cells were treated and analysed as discussed in section 5.2., with the results shown in Figure 24. Based on the consistency and reproducibility of the results obtained from comet and clonogenic assays, a reduced set of plasma exposures were used for experiments henceforth. Figure 24B has been reproduced from Figure 19B, in order to serve as a comparison between the levels of DNA damage recorded in BPH-1 and PC-3 cells. It was found that BPH-1 cells show higher levels of DNA damage across the range of LTP exposures when compared to PC-3 cells. For example, 30 s LTP treatment of BPH-1 cells led to a > 40% increase in average DNA damage compared to PC-3 cells. BPH-1 cells also appear more susceptible to the $H_2O_2$ control treatment. Furthermore, very few BPH-1 cells remained undamaged following 600 s LTP, with the vast majority of treated cells grouped close to 100% DNA damage. The population of PC-3 cells that fell below the 25th percentile were more uniformly distributed, and around one-fifth of the total cell number sustained < 50% DNA damage.
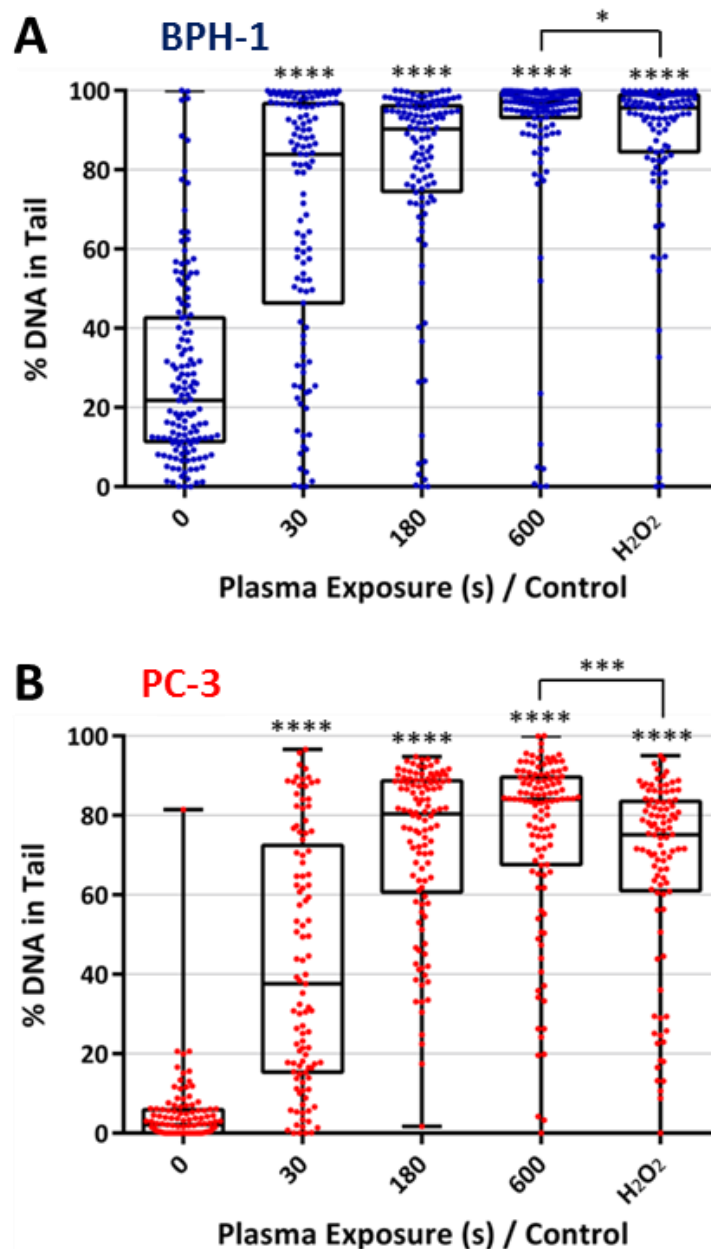
**Figure 24: DNA damage following LTP treatment in BPH-1 and PC-3 cells.**

Cells were treated with LTP for a range of treatment times, or with $H_2O_2$ control (1 mM). DNA damage levels were recorded in BPH-1 (**A**) and PC-3 (**B**) cells using the alkaline comet assay, and represented as % DNA-in-tail. Each dot represents a single cell, with a minimum of 100 cells counted for each treatment. Data are expressed as the median value, with the 25-75th percentile highlighted by boxes. Statistical significance was analysed by Mann-Whitney test against untreated samples unless otherwise indicated.

### 5.5.1 LTP Reduces Cell Viability in Benign and Malignant Prostate Cell Lines

Following treatment with LTP, changes in cell viability were determined for BPH-1 and PC-3 cells using the alamarBlue assay and plotted in Figure 25. Cell viability was quantified at 24, 48, 72 and 96 hours after treatment against normalised untreated samples. In BPH-1 cells, the viability was reduced to around 10% following both 180 and 600 s LTP, and $H_2O_2$ control at 24 hours following treatment. No further quantifiable reduction in viability was recorded beyond 24 hours after treatment. Conversely in PC-3 cells, a more progressive decline in cell viability was observed in the days following treatment. At 96 hours after treatment, 600 s LTP exposure reduced PC-3 cell viability by ~90%, whereas 180 s treatment only reduced cell viability by ~50%. Nonlinear regression analysis was performed on the data, and displayed in Figures 25C and D for BPH-1 and PC-3 cells respectively. This was conducted in order to determine $IC_{50}$ values at 72 hours after treatment for both cell lines, as is commonplace in pharmacological drug development. The logarithmic value of the inhibitor (LTP treatment) was plotted against normalized cell viability to calculate the minimum plasma exposure required to reduce cell viability by 50%. For BPH-1 cells this was calculated as 34 s, whereas for PC-3 cells the $IC_{50}$ was found to 220 s, implying the latter are far more resistant to LTP treatment.
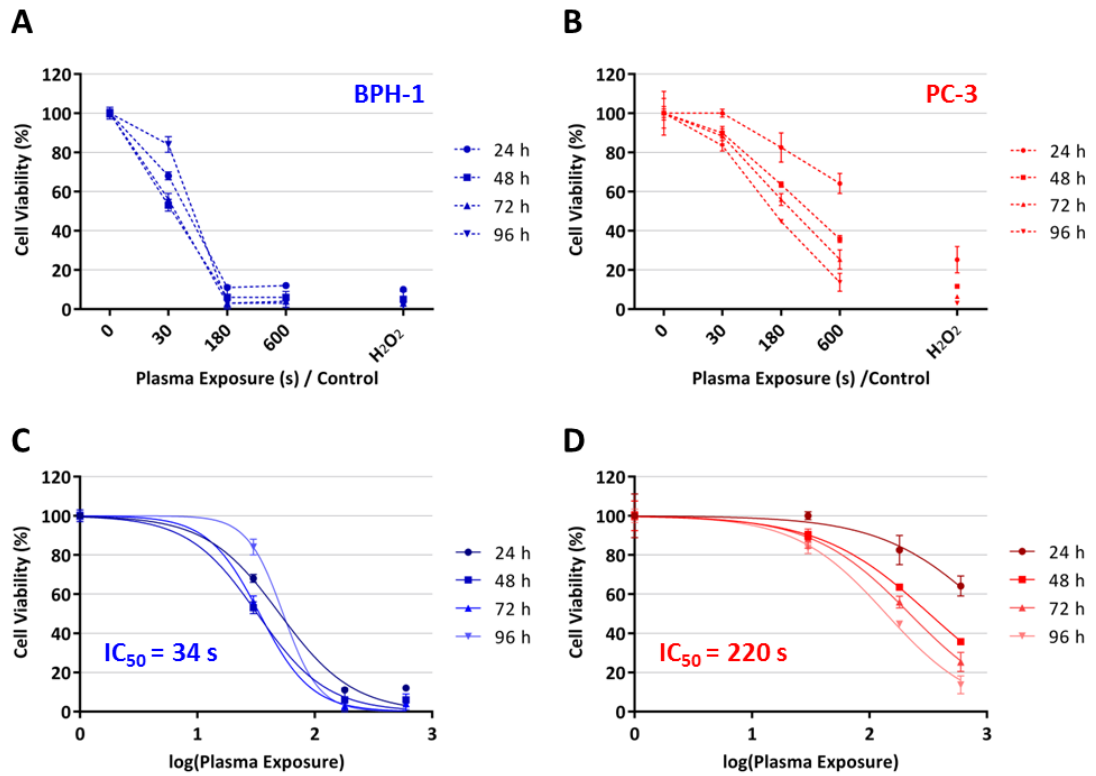
**Figure 25: Cell viability following LTP treatment of BPH-1 and PC-3 cells.**

Cells were treated with LTP for a range of treatment times, or with $H_2O_2$ control (1 mM). Cell viability was analysed using the alamarBlue assay at $24 - 96$ hours after treatment (**A, B**). Graphs **C** and **D** display non-linear regression analysis of LTP treated cells, with representative $IC_{50}$ values given for readings taken 72 hours following treatment. Viability levels are normalised to untreated control samples, and data are expressed as mean ± standard error.

### 5.5.2 Cell Line Clonogenic Potential is Reduced Following LTP Treatment

Treatment with LTP showed a dose dependent inhibition of cell recovery of both BPH-1 and PC-3 cells. Figure 26B has been reproduced from Figure 21A, in order to serve as a comparison between surviving fraction of both benign and malignant cell lines. Figure 26 shows that treatment with 1 mM $H_2O_2$ eliminated the colony forming ability in BPH-1 cells, whereas in PC-3 cells the surviving fraction was more than 50%. A similar trend was found for treatment with 600 s LTP; the surviving fraction was reduced to ~10% for BPH-1's, but to only ~40% for PC-3s. However, treatment with either 30 or 180 s LTP produced almost identical survival results for both cell lines.

LTPs are known to create a plethora of RONS [154]; one of the most stable and long-lived of these species is $H_2O_2$ [238], which is also a by-product of other ROS-enzyme reactions [239, 240]. The ROS-Glo $H_2O_2$ luminescence assay was performed immediately following treatment to detect relative levels of this species in the cell culture media. Figure 26 shows a general trend of increased levels of extracellular $H_2O_2$ following increased LTP exposure for both BPH-1 (**C**) and PC-3 cells (**D**). In BPH-1 cells, a 180 s LTP treatment produced a luminescence signal equivalent to $H_2O_2$ control, whereas 600 s LTP yielded higher readings. The level of $H_2O_2$ detected in PC-3 culture media following LTP treatment was far lower than that for BPH-1 cells; over three-fold less for 180 and 600 s treatments. Conversely, the luminescence signal from $H_2O_2$ treatment was slightly higher for PC-3 cells than BPH-1 cells. All LTP treatments produced statistically significant increases in extracellular $H_2O_2$ levels over untreated samples for both cell lines.
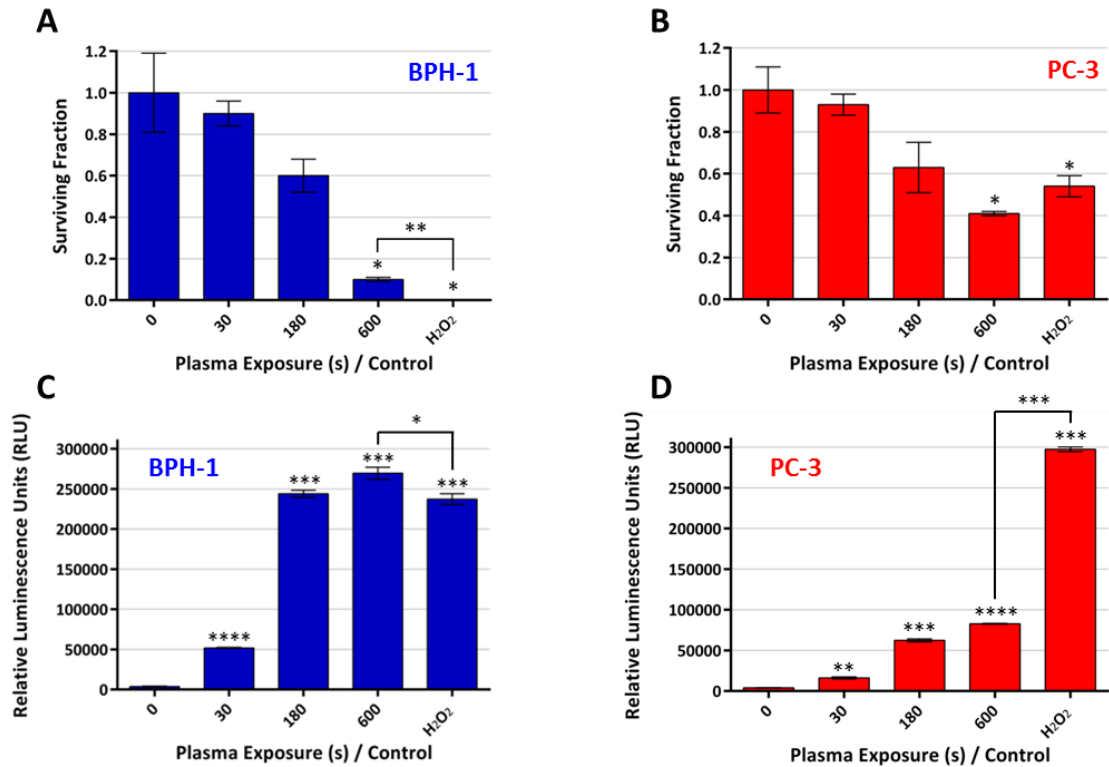
**Figure 26: Analysis of colony formation and $H_2O_2$ formation following LTP treatment of BPH-1 and PC-3 cells.**

Cells were treated with LTP for a range of treatment times, or with $H_2O_2$ control (1 mM). Colonies of > 50 cells were identified by crystal violet staining at 12 days following treatment, and expressed as surviving fraction against normalised untreated control wells in BPH-1 (**A**) and PC-3 (**B**) cells. Immediately after treatment, the ROS-Glo $H_2O_2$ luminescence assay was performed to ascertain the levels of extracellular $H_2O_2$ formed in the cell culture media, with luminescence readings quantified against normalised untreated samples for BPH-1 (**C**) and PC-3 (**D**) cells. Data are expressed as the median value ± standard error. Statistical analysis was conducted using unpaired t-test with Welch's correction, with significance recorded against untreated samples unless otherwise indicated.

### 5.5.3 Mechanism of Cell Death Following LTP Treatment in Prostate Cell Lines

The results of initial experiments on prostate cell lines revealed the immediate effects of LTP exposure included high levels of DNA damage and significant reductions in cell viability. These were predicted to be a pre-cursor for, and associated with, cell death. As such, cells were analysed to determine the cell fate following LTP treatment.

### 5.5.3.1 Analysis of Apoptotic Cell Death in BPH-1 and PC-3 Cells

Analysis of apoptotic cell death was conducted through western blotting for C-PARP protein expression from 2 to 24 hours after treatment. PARP protein is involved in DNA repair, and its cleavage usually occurs following extensive cellular DNA damage, thus inhibiting repair mechanisms and leading to apoptotic cell death. BPH-1 and PC-3 cells were treated with either a range of LTP exposures, 1 mM $H_2O_2$, or 1 μM staurosporine. Staurosporine was included as a known positive control for apoptosis [227, 229], and ß-actin was used as a loading control. It can be seen in Figure 27 that apoptosis is induced at 8 hours in BPH-1 cells following treatment with $H_2O_2$ and staurosporine controls, but not until 12 hours following 600 s LTP. Exposures of less than 600 s LTP did not cause apoptosis in BPH-1 cells. In PC-3 cells, only the staurosporine control treatment induced apoptosis from 8 hours onwards, although the response was considerably less than recorded for BPH-1 cells. Both $H_2O_2$ control, and all LTP exposures failed to induce apoptosis in PC-3 cells. Sample cell morphology photographs, taken at 12 hours following treatment, are provided for BPH-1 and PC-3 cells in Figures 28 and 29 respectively. These photographs were taken immediately before adherent cells were harvested for western blotting. This time-point was chosen as the earliest apoptotic response following LTP treatment occurred at 12 hours (Figure 30) in BPH-1 cells. It can be seen that far fewer adherent BPH-1 cells are present following treatment with

either 600 s LTP of $H_2O_2$ (Figure 28), when compared to untreated control. Figure 29 shows that same response for PC-3 cells although this is less pronounced than observed for BPH-1 cells. The staurosporine control treatment produces a quite distinctly different morphological response when compared to both LTP and $H_2O_2$ treatment in both BPH-1 and PC-3 cells, with cell membrane blebbing evident.
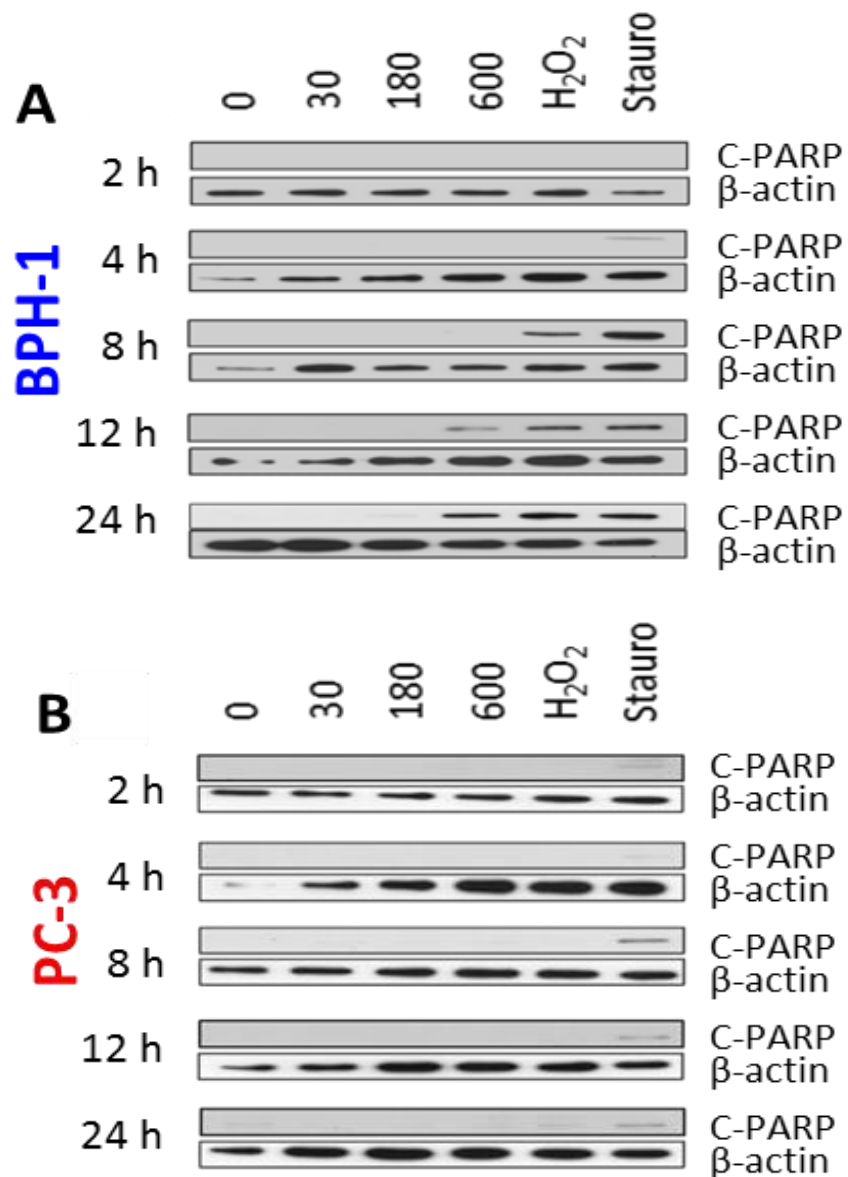
**Figure 27: LTP treatment induces apoptosis in BPH-1, but not PC-3, cells.**

Cells were treated with a range of timed LTP exposures, 1 mM $H_2O_2$ or 1 µM staurosporine, and harvested between 2 and 24 hours after treatment. BPH-1 (**A**) and PC-3 (**B**) cell lysates were probed for apoptosis (C-PARP) following LTP treatment, which was detected following 600 s LTP exposure in BPH-1 cells, but not in PC-3 cells. ß-actin was used as a loading control.
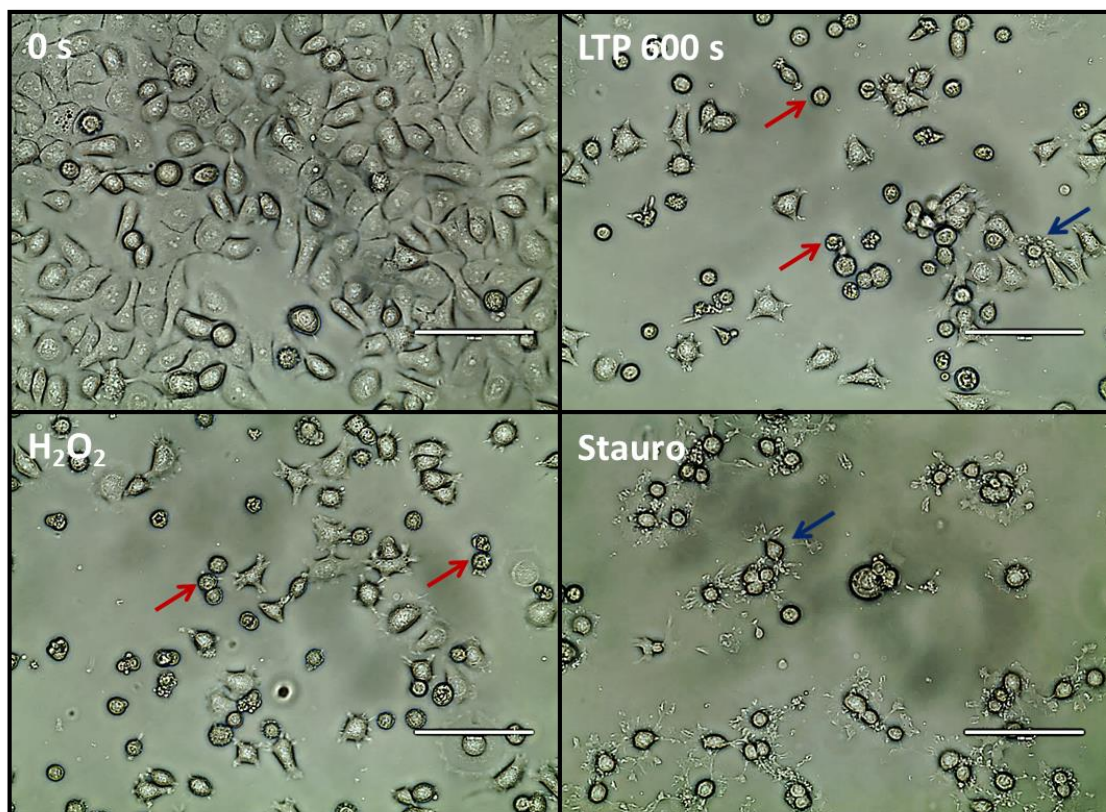
**Figure 28: BPH-1 cell morphology following treatment.**

Photographs of BPH-1 cells were taken at 12 hours following treatment, prior to Western blotting. Representative images are shown for cells treated with either 600 s LTP, 1 mM $H_2O_2$, or 1 µM staurosporine. Images of all treated groups show a high reduction in cell density, with cells treated with LTP and $H_2O_2$ appearing small and rounded (red arrows). A small number of cells treated with LTP share the same morphological features as those treated with staurosporine (blue arrows), as verified by Western blotting results. Scale bar denotes 400 µm**.**
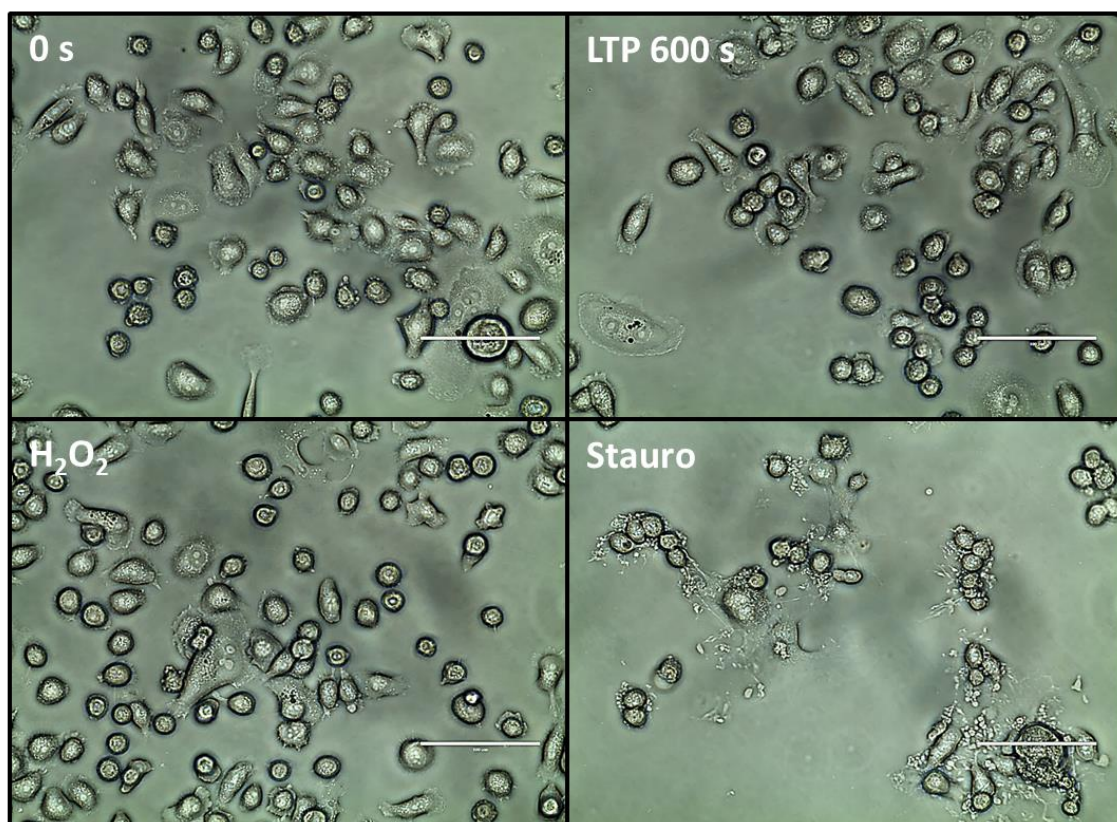
**Figure 29: PC-3 cell morphology following treatment**.

Photographs of PC-3 cells were taken at 12 hours following treatment, prior to Western blotting. Representative images are shown for cells treated with either 600 s LTP, 1 mM $H_2O_2$, or 1 μM staurosporine. Cells treated with LTP and $H_2O_2$ appear small and rounded, and morphologically distinct from those treated with staurosporine, which is in agreement with Western blotting results. Scale bar denotes 400 μm.

5.5.3.2 Analysis of Necrotic Cell Death in BPH-1 and PC-3 Cells

Cell death resulting from LTP-induced necrosis was determined using the CellTox Green cytotoxicity assay. Cells were treated with either 0, 30, 180 or 600 s LTP, 1 mM $H_2O_2$, 1 μM staurosporine, or lysing agent (toxicity control). Immediately following treatment, the CellTox dye was added to the cultures, which fluoresces green when bound to the DNA of membrane-compromised cells, which are characteristic of necrosis. Representative images of treated BPH-1 and PC-3 cells, taken at 4 hours after treatment, are shown in Figures 30 and 31. The highest proportion of positive green cells are found as a result of 600 s LTP treatment. Both $H_2O_2$ and staurosporine controls contained very few, if any, necrotic cells at 4 hours after treatment.

Quantitative fluorescent readings were obtained at 2, 4, 8, 12 and 24 hours following treatment and are shown in Figure 32 for BPH-1 (**A**) and PC-3 cells (**B**). The toxicity control produced consistently high fluorescence readings across all data collection points from 2-24 hours suggesting total cell lysis, which was confirmed by fluorescence microscopy (data not shown). Dose dependent increases in necrosis were observed following LTP treatment of both BPH-1 and PC-3 cells. In general, the levels of necrosis induced from all treatments were considerably higher for BPH-1 cells than PC-3 cells. The fluorescence values steadily increased up to 8 hours after treatment of both cell lines. At 12 hours and onwards after treatment of BPH-1 cells, a large increase in the fluorescence intensity was recorded from 600 s LTP and $H_2O_2$ exposure. However, staurosporine control readings remained substantially lower, due to cells undergoing apoptosis, and therefore their cell membrane remained intact. At 24 hours after treatment, the readings from staurosporine cells increased several-fold in both cell lines, suggesting late-stage apoptosis.

**BPH-1**
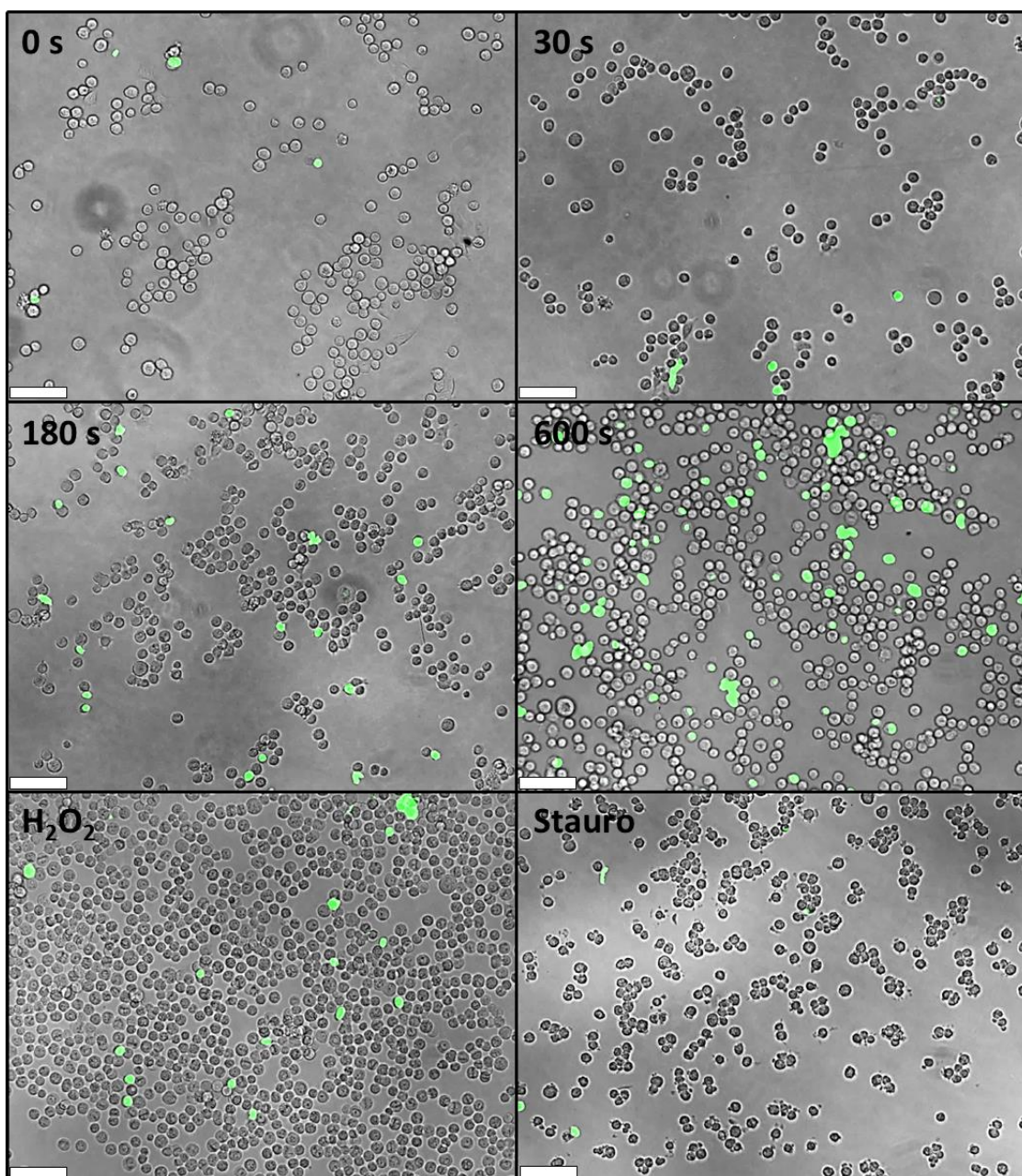
**Figure 30: Evidence of necrotic cells following LTP treatment of BPH-1 cells.**

Cells were treated with a range of LTP exposures, 1 mM $H_2O_2$, or 1 μM staurosporine. Merged fluorescence/bright-field images (10x magnification) were captured 4 hours after treatment. Green cells possess compromised membrane integrity, indicative of necrosis. Scale bar denotes 100 μm.

**PC-3**
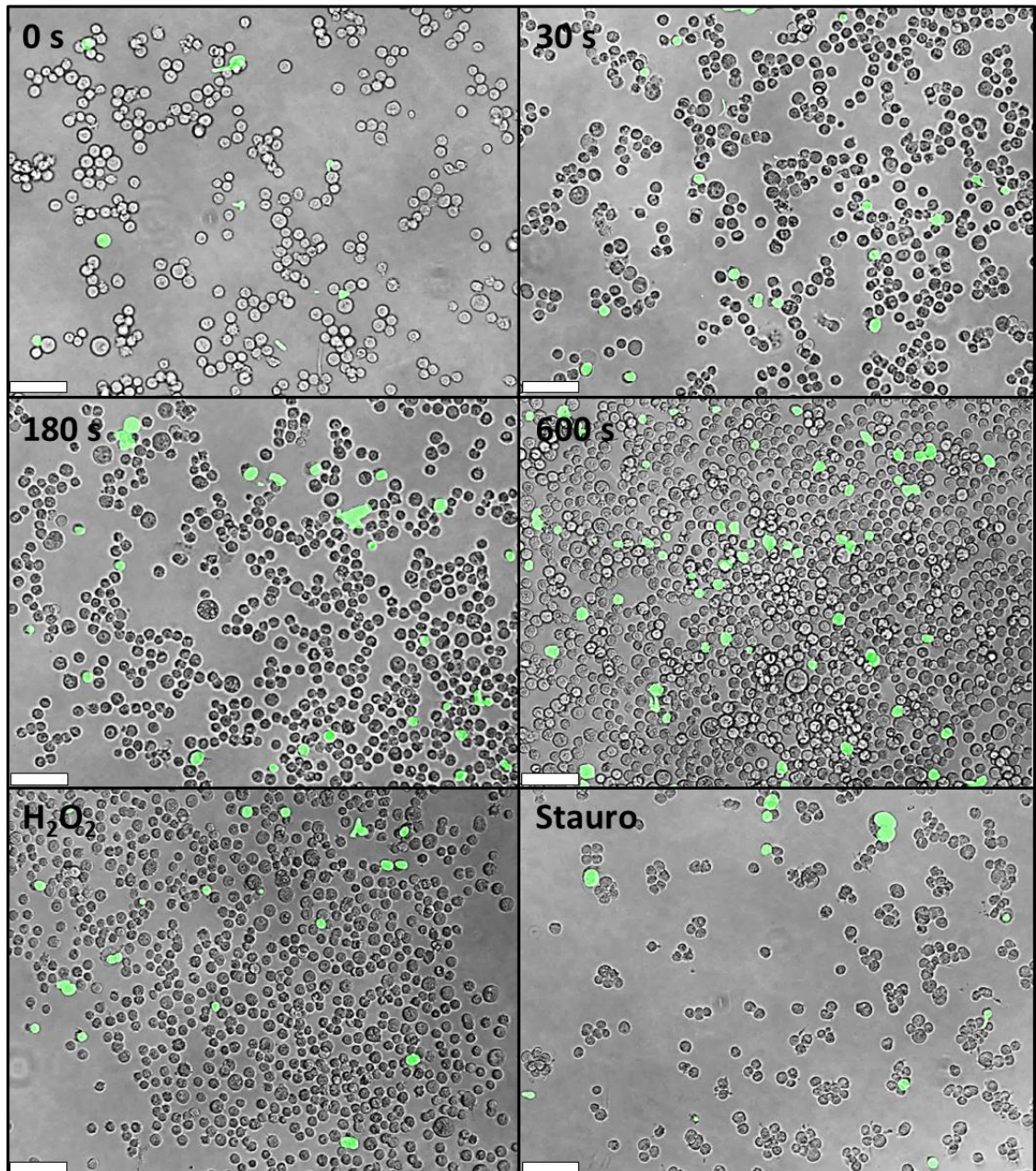


**Figure 31: Evidence of necrotic cells following LTP treatment of PC-3 cells.**

Cells were treated with a range of LTP exposures, 1 mM $H_2O_2$, or 1 μM staurosporine. Merged fluorescence/bright-field images (10x magnification) were captured 4 hours after treatment. Green cells possess compromised membrane integrity, indicative of necrosis. Scale bar denotes 100 μm.
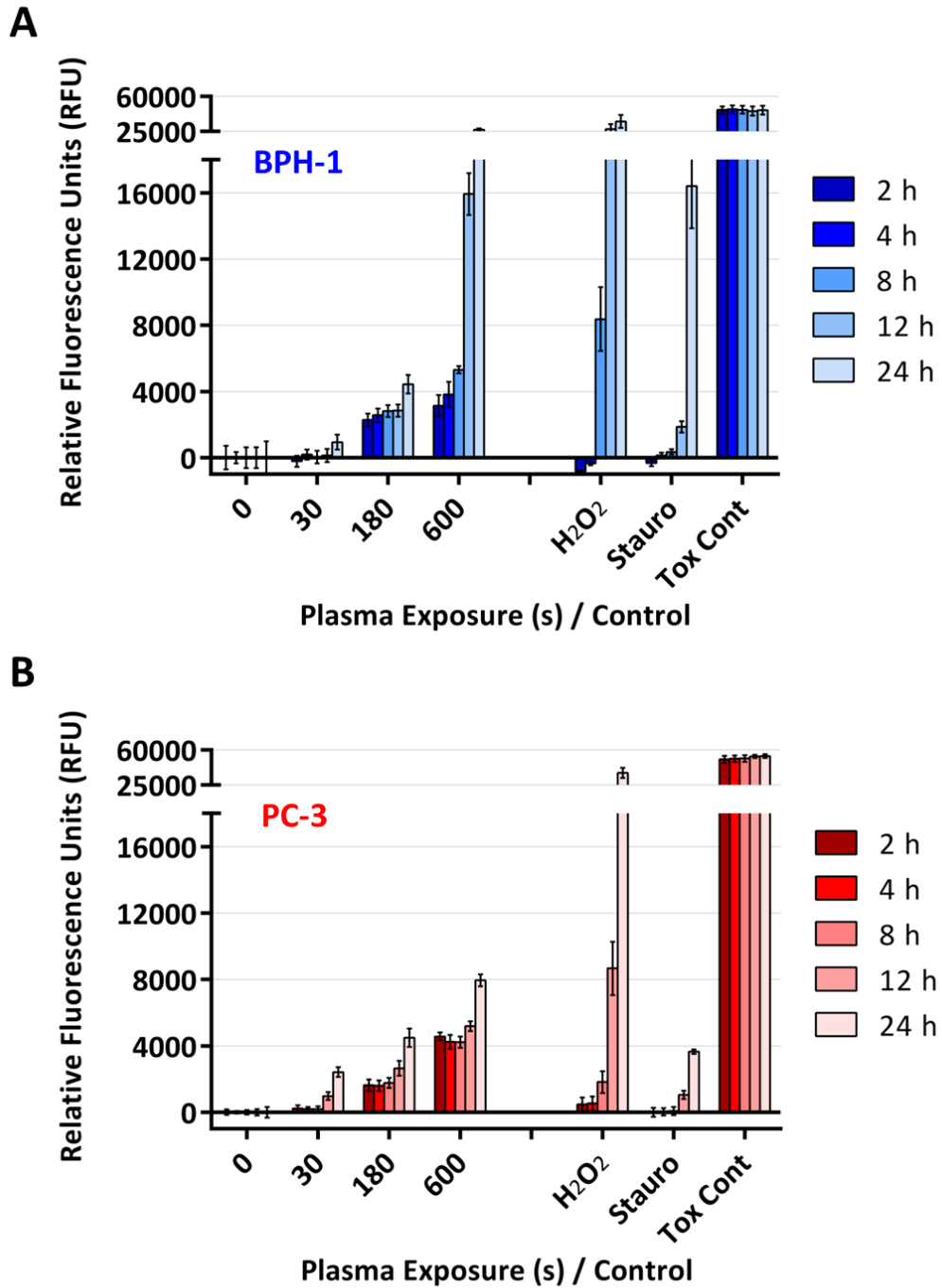
**Figure 32: Quantification of LTP-induced necrosis in BPH-1 and PC-3 cells.**

Cells were treated with a range of LTP exposures, 1 mM $H_2O_2$, 1 μM staurosporine, or lysis toxicity control. At 2 − 24 hours after treatment, LTP induced necrosis was assessed using the CellTox green assay, with fluorescence values normalised to untreated control wells. Data are expressed as mean ± standard error.

To summarise this chapter, it was deduced that LTP treatment induced high levels of DNA damage in both benign and malignant prostate cell lines, leading to a reduction of cell viability and clonogenicity. It was found that LTP exposure was more cytotoxic to PC-3 cells than 2 Gy IR treatment; the vast differences in DNA damage and cell viability levels between both treatments suggesting they interact with cells through different mechanisms. Interestingly, differential cell death modalities were recorded following LTP treatment, with benign BPH-1 cells showing evidence of both apoptosis and necrosis, whereas malignant PC-3 cells were positive for necrosis only. This implies that PC-3 cells may resist the initiation of programmed cell death, and only excessive oxidative stress levels may induce cytopathic effects. The next chapter introduces the effects of LTP on prostate models with increased clinical relevance.

# Chapter 6

## *Results III*

## The Effect of Low Temperature Plasma in Clinically Relevant Prostate Models

# 6. Effect of LTP Treatment in Clinically Relevant Prostate Models

An initial study examining LTP treatment of benign and malignant prostate cell lines was presented in the previous chapter. The rapid and indefinite growth of cell lines makes them a useful preliminary model to investigate the response of prostate cells to LTP. However, they are not wholly representative of the heterogeneity and complexity of real prostate tumours. In order to assess the potential for future translation into clinical practice, the study was expanded to ascertain the effect of LTP in clinically relevant models. These included primary prostate epithelial cells derived directly from patient tissue samples, 3D aggregates and spheroids formed from cell lines, and direct treatment of pieces of patient tissue.

## 6.1 LTP Induces DNA Damage in Primary Prostate Epithelial Cells

Primary cells from three different patients were treated with LTP at a range of different exposure times, or 1 mM $H_2O_2$ control, before being examined immediately for DNA damage using the comet assay. Matched normal and cancer (Gleason grade 7; indicative of localised, early-onset disease) paired samples originating from the same patient were analysed. This enabled direct comparisons to be made between the normal and malignant cells of the same patient, which has not been reported previously in the literature. These three patient sample pairs were chosen as the tumours were localised, and would have been viable candidates for treatment with focal therapy. Figure 33 shows the results obtained for the normal and cancer cells of three patients in Figure 33A, B and C. As little as 30 s LTP treatment induced highly significant levels of DNA damage in all samples, with significantly higher damage recorded from $H_2O_2$ control than from 600 s LTP exposure in the Patient 1 sample (Figure 33A). There was no significant difference between 600 s LTP exposure and $H_2O_2$ control in Patient 2 and 3

samples (Figure 33B, C). Similar to the observations with cell lines in Figure 23, the level of DNA damage induced by LTP exposure appeared to plateau at ≥ 180 s treatment duration. The spread of the data for Patient 1 and Patient 3 samples appear very similar, however the level of DNA damage for Patient 2 is at least 20% (and as much as 50%) lower than the other two samples. The damage quantified from individual cells also appears to be more evenly distributed for Patient 2 (Figure 33B), whereas in the other two samples the data points are more closely distributed around the median value. The average DNA damage induced in normal and tumour cells is presented in Figure 33D, which showed up to 10% higher levels of damage to the tumour cells across all treatments. However, standard error analysis also revealed a high degree of patient-patient variability. As the error values of the averaged data overlap, the differences in DNA damage between normal and tumour cells are unlikely to be clinically significant.
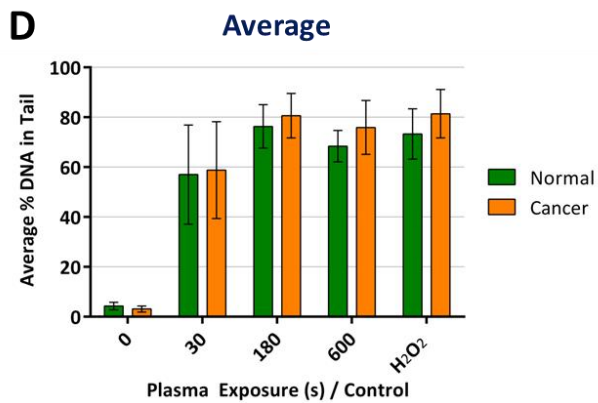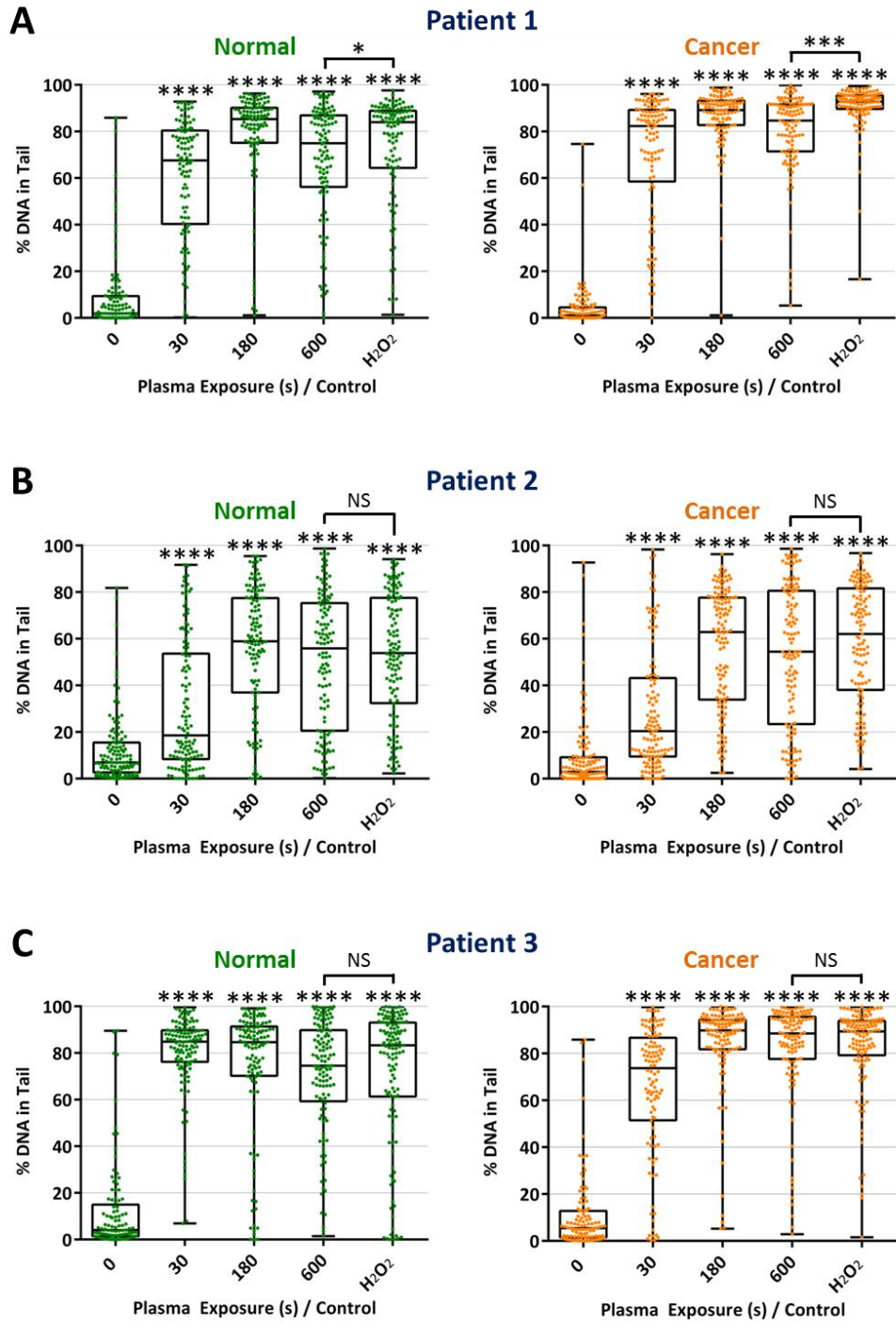
**Figure 33: LTP induces DNA damage in primary prostate epithelial cells.**

Cells were treated with LTP for a range of treatment times, or with $H_2O_2$ control (1 mM). DNA damage levels were recorded using the alkaline comet assay and represented as % DNA-in-tail. Paired normal and cancer samples from three different patients are shown, in addition to an averaged comparison of normal and tumour cells across all three patients. Each dot represents a single cell, with a minimum of 100 cells counted for each treatment. Data are expressed as the median value, with the 25-75th percentile highlighted by shaded boxes. Statistical significance was analysed by Mann-Whitney rank test (which assumes a non-Gaussian distribution), with significance recorded against untreated samples unless otherwise indicated.

DNA damage was also investigated through immunofluorescence imaging. Immediately following treatment with LTP, cells were fixed and stained for γH2AX foci to detect DNA double strand breaks, which are particularly lethal to cells [241]. Phosphorylated protein H2AX, (referred to as γH2AX) is a rapid response marker following double strand breaks, and is implicated in the recruitment of DNA repair proteins [242, 243]. Figure 34 shows representative images of untreated cells (A) and cells treated with 300 s LTP (B). The cells treated in this experiment originated from a separate Gleason grade 7 patient sample to the three normal and cancer paired samples presented throughout this chapter. Both needle cores originating from this patient were disease-positive and as such no normal comparison was available for this sample. Nuclear staining was performed using DAPI (blue), cell cytoskeleton staining using phalloidin (green), and double strand break DNA damage through γH2AX foci (red). Figure 34B shows abundant, clearly defined DNA damage foci located in the nucleus of cells treated with 300 s LTP, whereas untreated cells (Figure 34A) were devoid of foci. Although there was a degree of heterogeneity across treated cells, Figure 34B is representative of the treated population. This result implies that LTP treatment induces lethal DNA damage in primary prostate cancer cells.
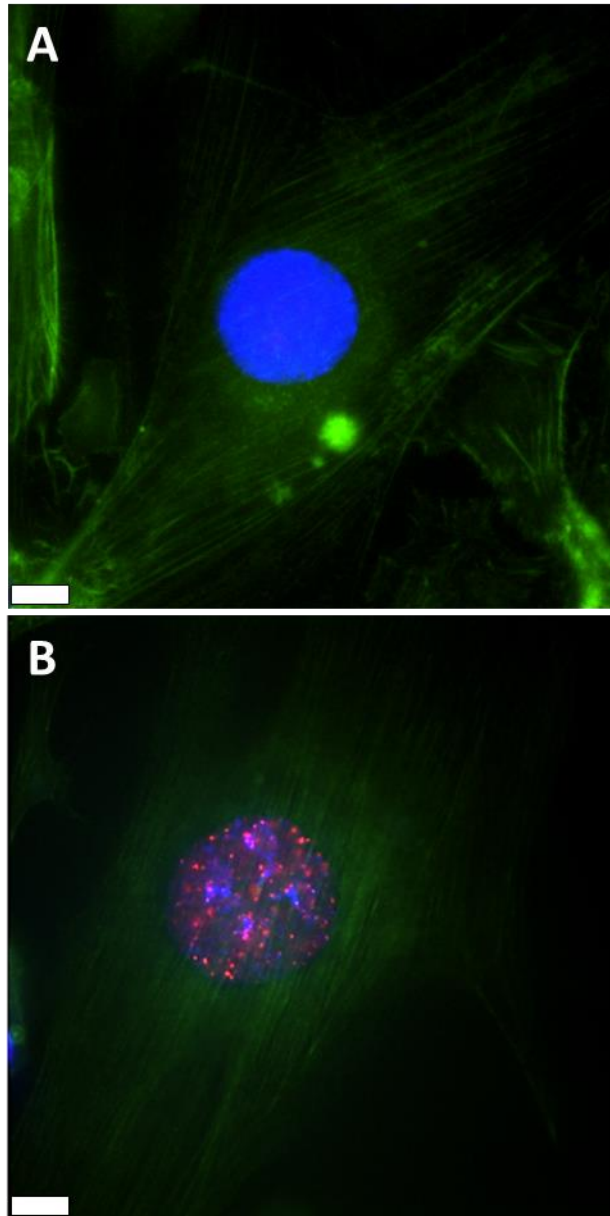
**Figure 34: LTP induces double strand break DNA damage in primary prostate epithelial cells.**

Gleason grade 7 patient cancer cells were either left untreated (**A**) or treated with LTP for 300 s (**B**). Double strand break DNA damage foci were identified by γH2AX straining (red dots). DAPI (blue) and phalloidin (green) were used as nuclear and cytoskeleton stains respectively. Scale bar denotes 10 µm.

## 6.2  LTP Reduces Cell Viability in Primary Prostate Epithelial Cells

Following treatment with LTP or $H_2O_2$ control, changes in cell viability were determined for three matched patient primary cell samples using the alamarBlue assay and plotted in Figure 35. Cell viability was quantified at 24, 48, 72 and 96 hours after treatment against normalised untreated samples. The results obtained for all three samples show the same trend; increasing LTP exposure progressively reduces cell viability in both normal and cancer cells. This reduction also progresses from 24 to 96 hours following treatment with 30 and 180 s LTP treatment, although little difference was found for 600 s LTP and $H_2O_2$ control. In general, Patient 1 cancer sample (Figure 35A) shows no further decrease in viability from post-exposure 24 hours onwards from any treatment. In all patient samples, 600 s LTP exposure reduced cell viability to <20% at 96 hours after treatment. The normal and cancer cells of Patient 1 appeared more sensitive to $H_2O_2$ control treatment than those of Patient 3, with the reduction in viability comparable between normal and tumour cells (Figure 35A and C). However, the viability of cancer cells from Patient 2 was reduced ~ 60% further than normal cells (Figure 35B). Plotting the average response across all time-points from 24-96 hours and across all patients (Figure 35D) revealed no differences between normal and tumour cells following 30 or 600 s LTP treatment. However, normal cells appeared more susceptible to 180 s LTP treatment, but less so to $H_2O_2$ control, than tumour cells on average. Nonlinear regression analysis was performed on the cell viability data and displayed in Figure 38. This was conducted to determine $IC_{50}$ values at 72 hours after treatment for both cell lines, which is the standard time delay used in industry for pharmacological drug development. These values serve as an indication of the LTP treatment duration required to reduce the cell viability by 50%. For the normal and cancer cells of Patients 2 and 3, this was found to be 153 / 76 s and 115 / 94 s

respectively (Figure 38B and C), indicating the cancer cells were more susceptible. However, in Patient 1 (Figure 38A), the opposite trend was observed, with the $IC_{50}$ value calculated for the cancer cells being roughly double that for the normal cells; 163s compared to 88 s.
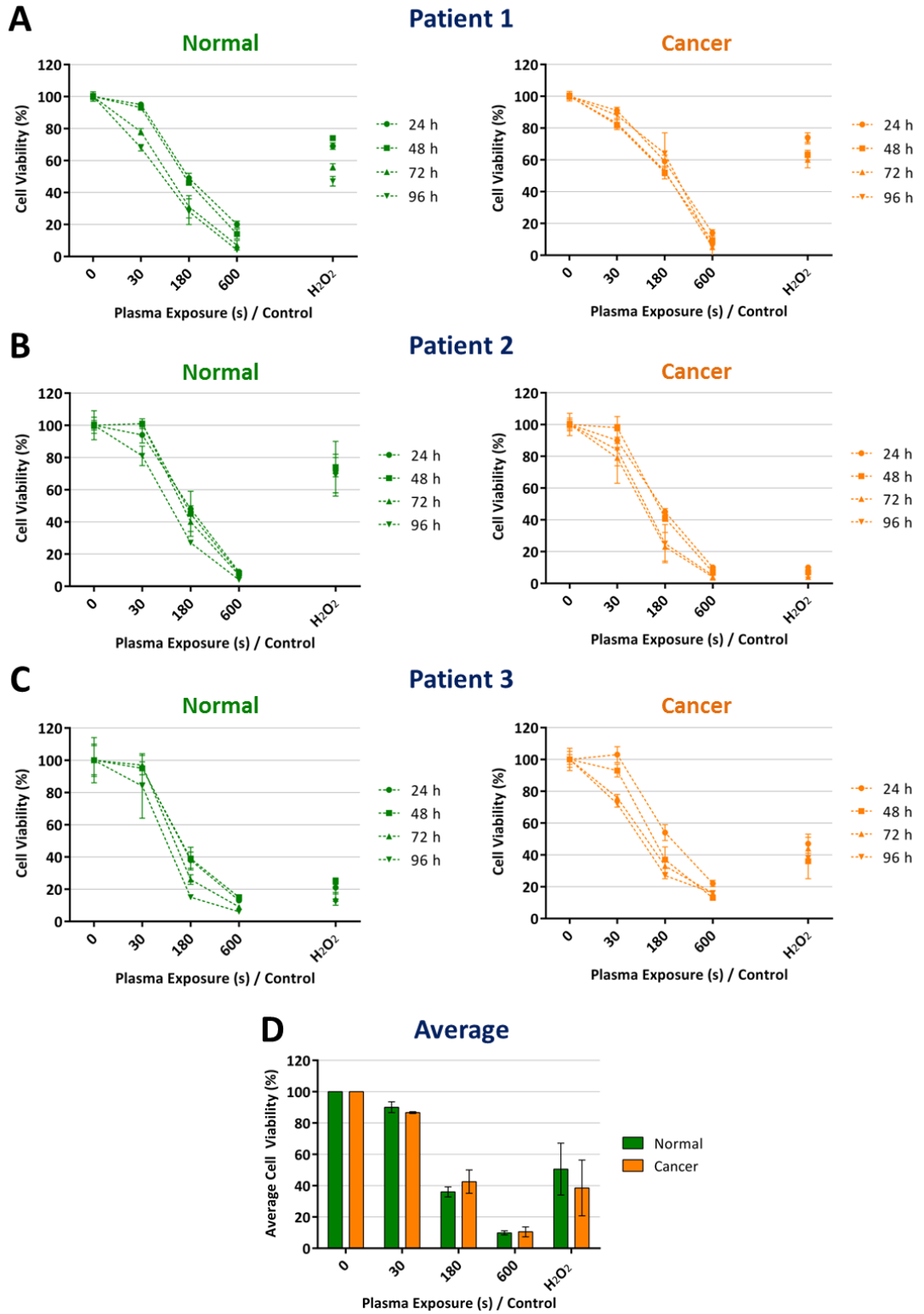
**Figure 35: Cell viability following LTP treatment of primary prostate epithelial cells.**

Three normal and cancer-paired samples were treated with LTP for a range of treatment times or with $H_2O_2$ control (1 mM). Cell viability was analysed using the alamarBlue assay at 24 − 96 hours after treatment. Viability levels are normalised to untreated control samples, and data are expressed as mean ± standard error. The averaged data for the three patient samples across all time-points is also presented as the mean ± standard error between samples.
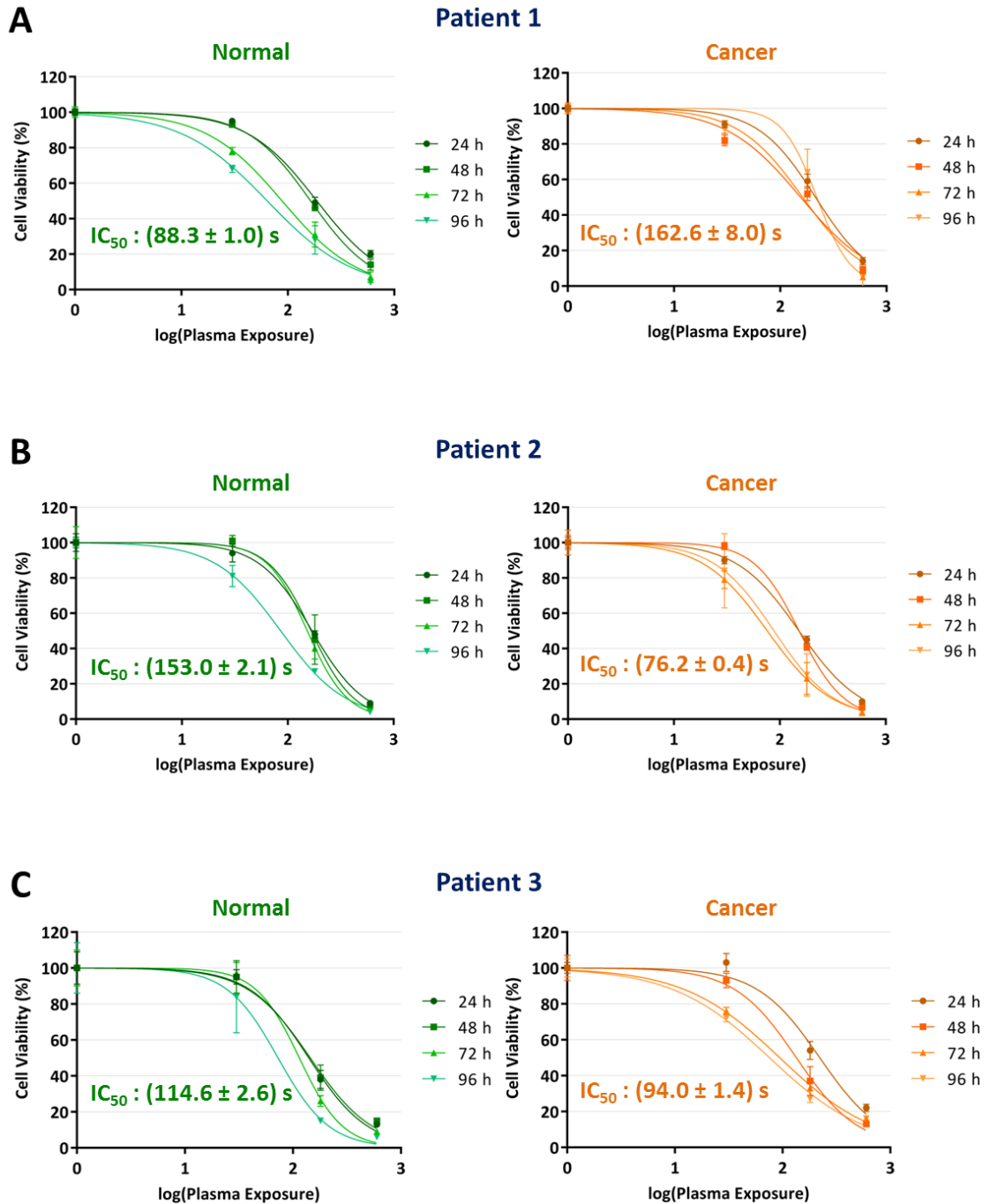
**Figure 36: Determination of IC$_{50}$ values for primary prostate epithelial cells following LTP treatment.**

Non-linear regression analysis was applied to the data in Figure 38 for three matched normal and cancer patient samples. Representative IC$_{50}$ values calculated at 72 hours following LTP treatment are displayed. Viability levels are normalised to untreated control samples, and data are expressed as mean ± standard error.

## 6.3 Primary Cell Clonogenic Potential is Reduced Following LTP Treatment

The clonogenic potential of primary cells (Patient 1 only due to time-constraints and availability of samples) was analysed following treatment with a range of timed LTP exposures or 1 mM $H_2O_2$ control to assess cell recovery post-treatment. Defined colonies of > 50 cells were quantified through crystal violet staining at 10-14 days after treatment. Figure 37 shows a dose dependent inhibition of cell recovery of both normal (A) and tumour (B) cells from Patient 1. Treatment with 600 s LTP reduced the surviving fraction to 20% in both normal and tumour cells, whereas the tumour cells appeared approximately twice as resistant as normal cells to 180 s LTP treatment. This differential resistance agrees with the $IC_{50}$ values obtained for the Patient 1 sample in Figure 36. The same pattern was recorded for the $H_2O_2$ control sample. LTP exposure of 600 s produced statistically significant reductions in survival fraction when compared to $H_2O_2$ control.

The levels of extracellular $H_2O_2$ following treatment with either LTP or $H_2O_2$ control were quantified using the ROS-Glo $H_2O_2$ luminescence assay. Figure 37C and D show the results obtained for normal and cancer cells from the Patient 1 sample respectively. Treatment with 30, 180 and 600 s LTP led to higher levels of $H_2O_2$ in the cell culture media of normal cells than the same exposures in cancer cells. The same result was found for the $H_2O_2$ control. Treatment with 600 s LTP produced statistically higher luminescence readings than $H_2O_2$ control in both normal and cancer cells. The ROS-Glo $H_2O_2$ luminescence assay was also performed to study the accumulation of extracellular $H_2O_2$ levels over time. Figure 38 shows the results of the assay performed either immediately, or at a delayed set of time-points of up to 8 hours following treatment with either 600 s LTP or $H_2O_2$ control. The same pattern was recorded for both normal (A) and cancer (B) cells, where initially high luminescence readings taken immediately after

treatment decayed with increasing time. By 4 hours after treatment, the signal recorded following $H_2O_2$ control had returned to untreated baseline levels in both normal and cancer cells, indicative of cells actively quenching $H_2O_2$ in the surrounding media. However, exposure to 600 s LTP produced sustained levels of $H_2O_2$ in the cell culture media which remained $\geq$ 3-fold that of untreated control cells at 8 hours after treatment.
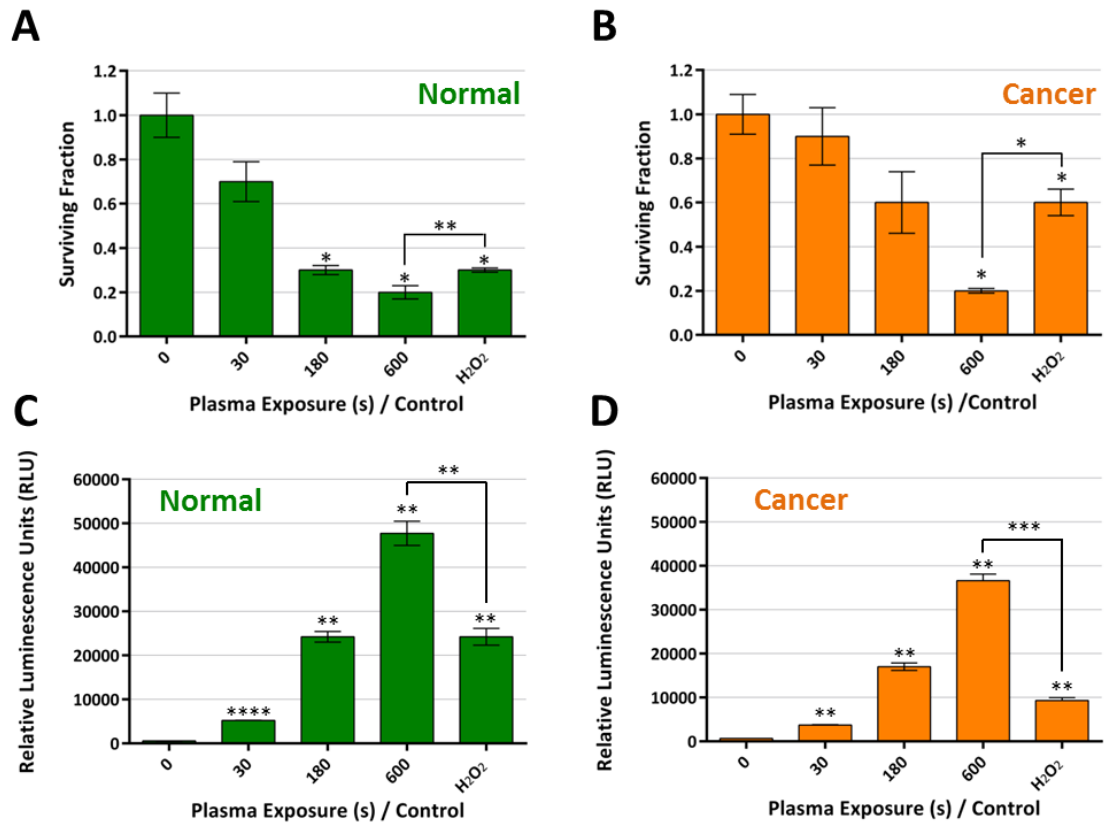
**Figure 37: Analysis of colony formation and induction of $H_2O_2$ following LTP treatment of primary prostate epithelial cells.**

Cells from the Patient 1 sample were treated with LTP for a range of treatment times, or with $H_2O_2$ control (1 mM). Colonies of > 50 cells were identified by crystal violet staining at 10-14 days following treatment, and expressed as surviving fraction against normalised untreated control wells in normal (**A**) and tumour cells (**B**) originating from the same patient. Immediately after treatment, the ROS-Glo $H_2O_2$ luminescence assay was performed to ascertain the levels of extracellular $H_2O_2$ formed in the cell culture media, with luminescence readings quantified against normalised untreated samples for normal (**C**) and tumour (**D**) cells. Data are expressed as the mean value ± standard error. Statistical analysis was conducted using unpaired t-test with Welch's correction, with significance recorded against untreated samples unless otherwise indicated.
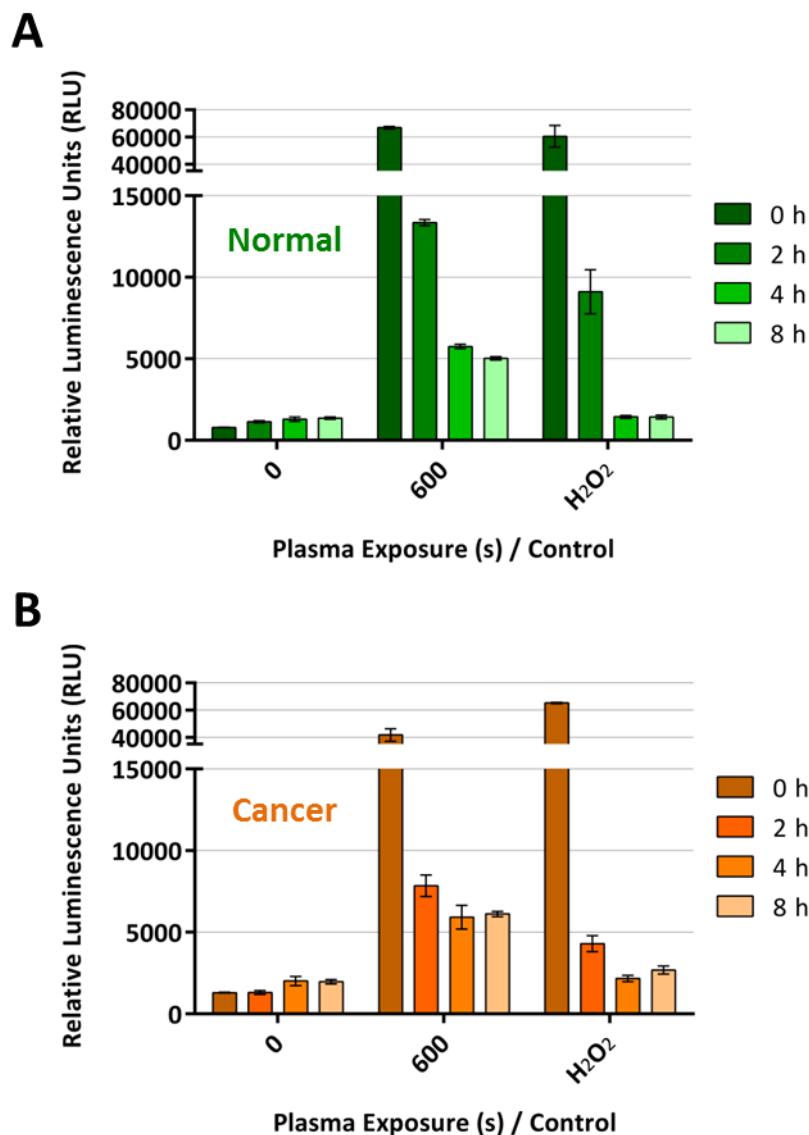
**Figure 38: Time-dependency of $H_2O_2$ levels induced following LTP treatment of primary prostate epithelial cells.**

Cells from the Patient 1 sample were treated with either 600 s LTP or $H_2O_2$ control (1 mM). The ROS-Glo $H_2O_2$ luminescence assay was performed at a range of timed intervals up to 8 hours after treatment to ascertain the evolution of extracellular $H_2O_2$ levels formed in the cell culture media. Data are expressed as the mean value ± standard error.

**6.4 Cell Death Following LTP Treatment in Primary Prostate Cells**

The results for prostate cell lines presented in Chapter 5 demonstrated that cells may undergo apoptosis or necrosis following treatment with LTP. The cell death assays conducted on cell lines were repeated for LTP-treated primary prostate epithelial cells. In addition, analysis of autophagy was also conducted on primary cells by Western blotting.

6.4.1    Analysis of Apoptosis and Autophagy in Primary Prostate Cells

Analysis of apoptotic and autophagic responses were conducted through Western blotting for C-PARP and LC3B protein expression respectively from 2 to 24 hours after treatment. Normal and cancer primary cells from the Patient 1 sample were treated with either a range of LTP exposures, 1 mM $H_2O_2$, or 1 μM staurosporine. Staurosporine was again included as a known positive control for apoptosis [227, 229], and ß-actin was used as a loading control. Figure 39 shows that expression of C-PARP occurred at 8 – 24 hours after treatment with staurosporine only. There is no evidence of an apoptotic response in either normal or cancer primary cells following 1 mM $H_2O_2$ control, or LTP treatment of any duration. LC3B expression levels suggested the induction of an autophagic response at around 24 hours following treatment with 600 s LTP (Figure 39). The intensity ratio of LC3BI and II bands was normalised against respective ß-actin control lanes, and compared to untreated control samples. In the normal cells, treatment with 180 and 600 s LTP induced a 3- and 4-fold increase in LC3B expression over untreated cells respectively. In the cancer cells, the same plasma treatments induced an ~ 2-fold increase in LC3B expression compared to untreated control cells. No clear evidence of increased LC3B expression was recorded at less than 24 hours after treatment with LTP. $H_2O_2$ control treatment induced an ~ 3-fold increase in LC3B

expression in both normal and cancer cells at 24 hours after treatment. Treatment with staurosporine control induced the largest autophagic response of all treatment groups; 21- and 14-fold increase in LC3B expression compared to untreated samples in the normal and cancer cells respectively.

Bright-field primary cell images were taken at 72 hours after treatment and are presented in Figures 40 and 41 for normal and cancer cells from the Patient 1 sample respectively. Morphologically, there are no obvious discernible variations between the normal and cancer cells across the different treatment groups. By 72 hours, untreated samples had formed a confluent layer of cells, whereas increasing levels of exposure to LTP progressively decreased the density of adherent cells. The images of 600 s LTP-treated and $H_2O_2$ control treated cells are morphologically comparable, with both rounded cells and cells exhibiting cytoplasmic swelling common. The most obvious feature of Figures 40 and 41 are the clear morphological distinction between cells treated with staurosporine, and cells treated with either LTP or $H_2O_2$, which verifies the Western blotting results shown in Figure 39.
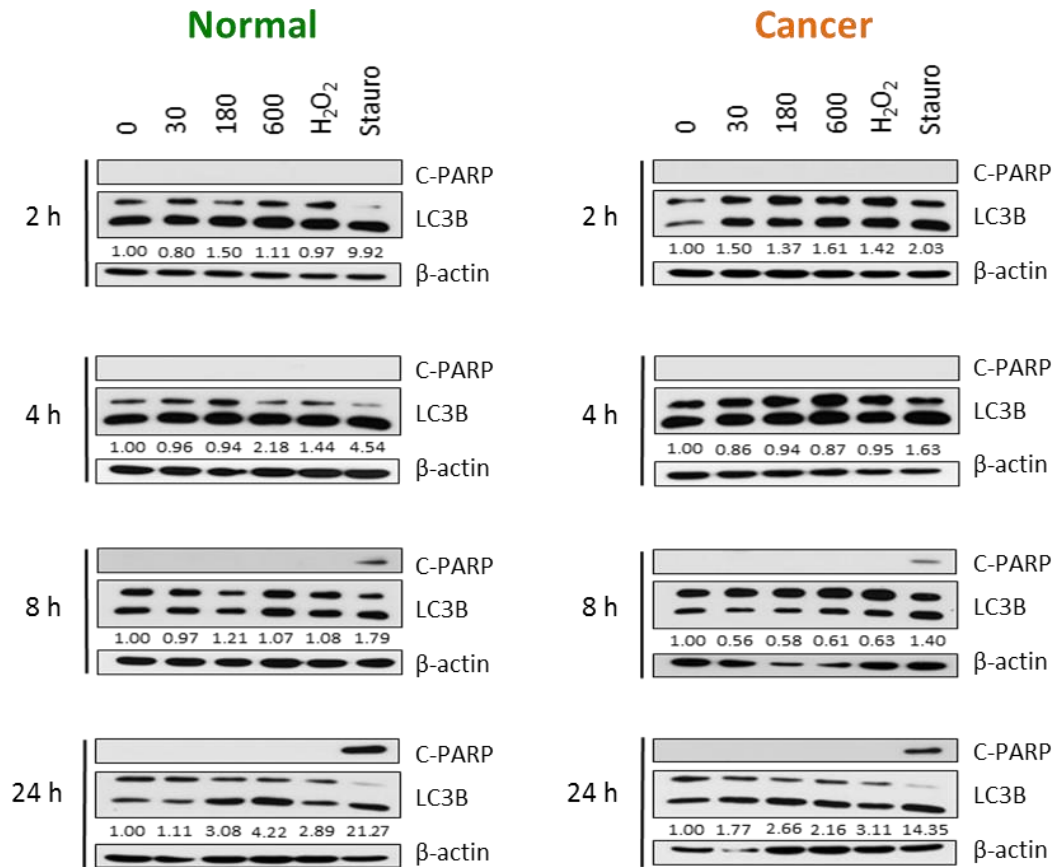
**Figure 39: Western blotting analysis of LTP-treated primary cells.**

Cells were treated with a range of timed LTP exposures, 1 mM $H_2O_2$ or 1 μM staurosporine, and harvested between 2 and 24 hours after treatment. Normal and primary cell lysates from the Patient 1 sample were probed for apoptosis (C-PARP) and autophagy (LC3B) following treatment. ß-actin was used as a loading control.
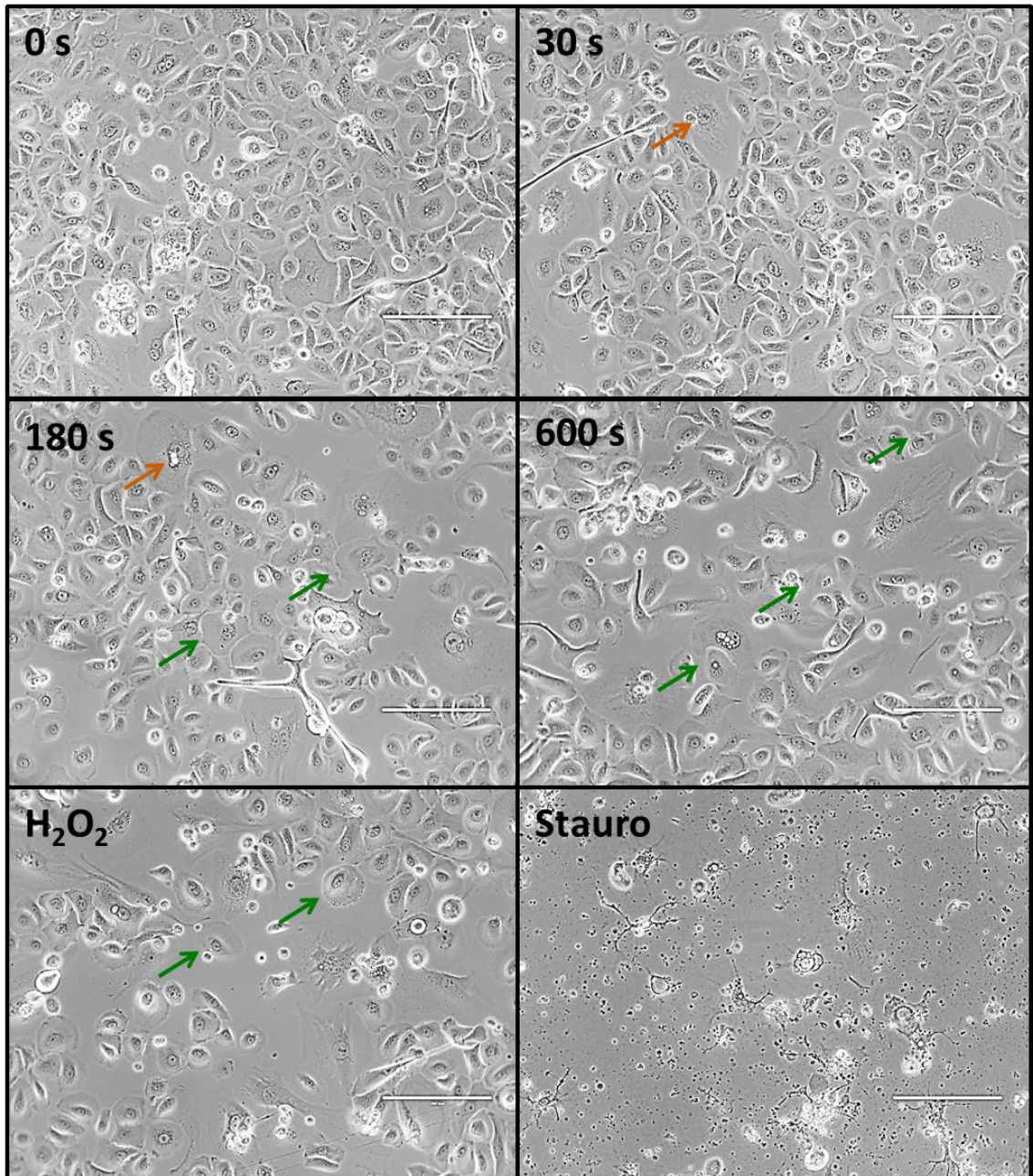
**Figure 40: Morphology of primary normal cells following treatment**.

Photographs of Patient 1 normal cells were taken 72 hours after treatment with either LTP, 1 mM $H_2O_2$ or 1 µM staurosporine. Green arrows indicate cells exhibiting cytoplasmic swelling indicative of necrosis. Orange arrows indicate cells exhibiting vacuolation indicative of autophagy. Scale bar denotes 400 µm**.**
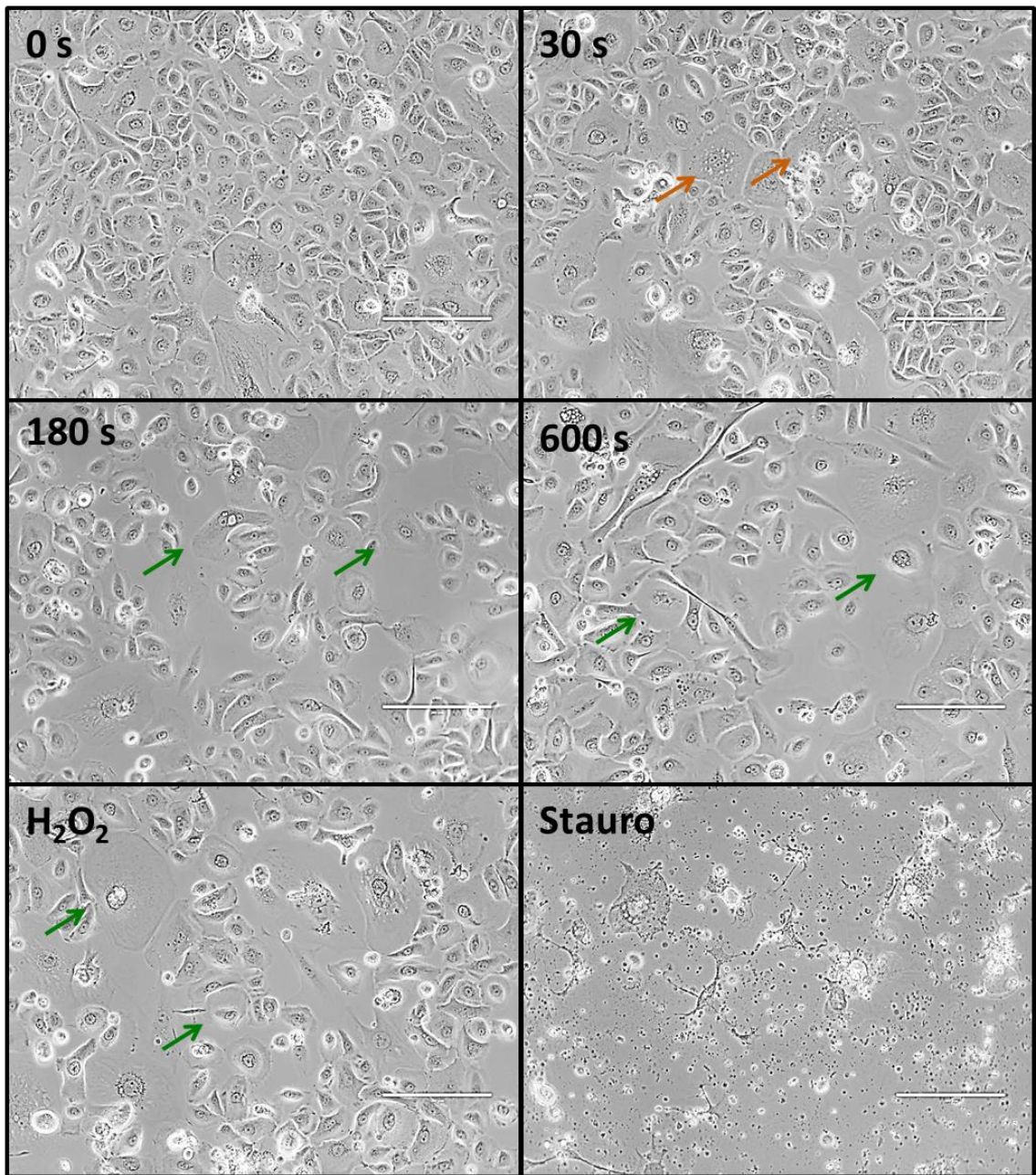
**Figure 41: Morphology of primary cancer cells following treatment**.

Photographs of Patient 1 cancer cells were taken 72 hours after treatment with either LTP, 1 mM $H_2O_2$ or 1 μM staurosporine. Green arrows indicate cells exhibiting cytoplasmic swelling indicative of necrosis. Orange arrows indicate cells exhibiting vacuolation indicative of autophagy. Scale bar denotes 400 μm.

In addition to Western blotting, the induction of apoptosis following treatment was also investigated using the Caspase-Glo 3/7 luminescence assay. Normal and cancer primary cells from all three patient samples were treated with either 180 or 600 s LTP, or 1 μM staurosporine control. At 24 hours after treatment the assay was performed, with luminescence values normalised against untreated control samples. Figure 42 shows that the relative levels of apoptosis induced by 180 and 600 s LTP exposures were below those recorded in untreated control cells for all three patient samples. Treatment with staurosporine induced higher levels of apoptosis in the normal cells of Patients 1 and 3 (A, C), which is in good agreement with the relative band intensities recorded from Western blotting of Patient 1 cells (Figure 39). The level of staurosporine-induced apoptosis for Patient 2 was roughly equivalent for normal and cancer cells (B). The averaged data across all three patient samples is also presented in Figure 42D, which showed that treatment with LTP induced almost identical responses in normal and tumour cells, and that staurosporine led to ~ 2-fold higher levels of apoptosis in normal cells. Combined, the results shown in Figures 39 - 42 show that treatment with LTP did not induce apoptosis in any of the three paired primary prostate patient samples.

**A**

Patient 1

**B**

Patient 2

**C**

Patient 3

**D**

Average
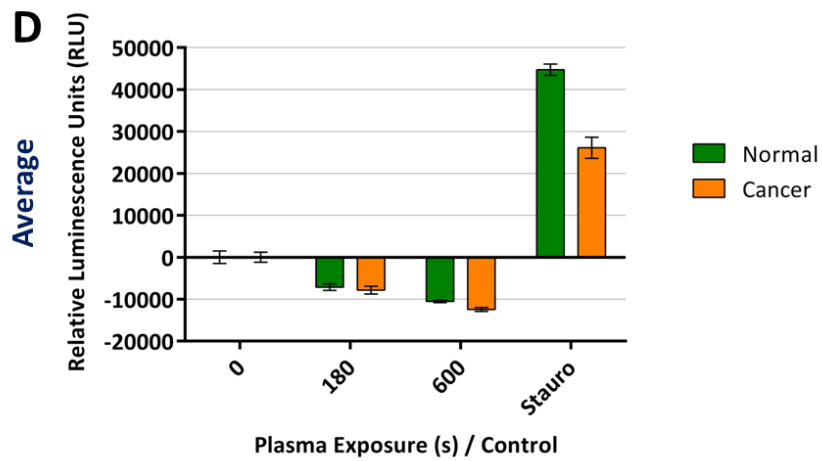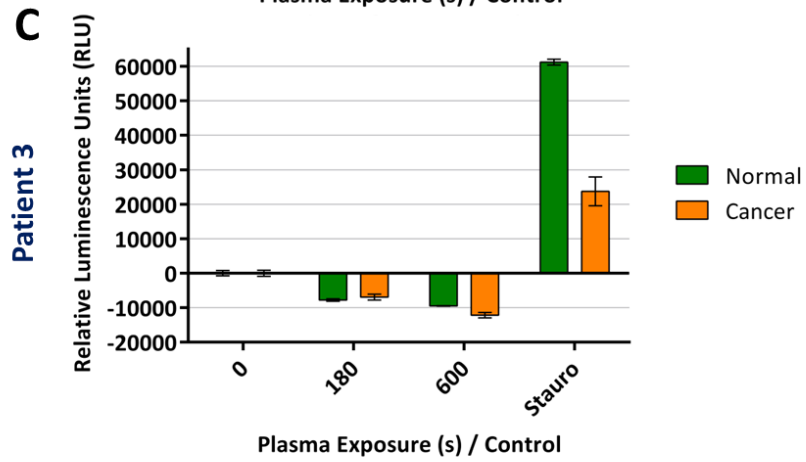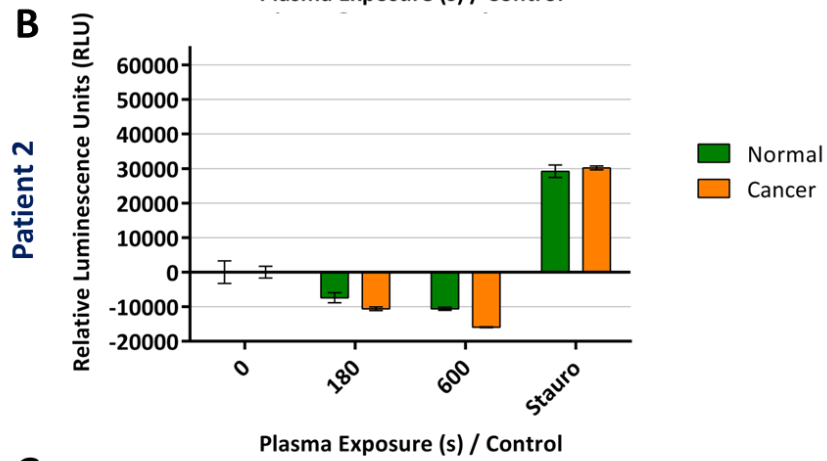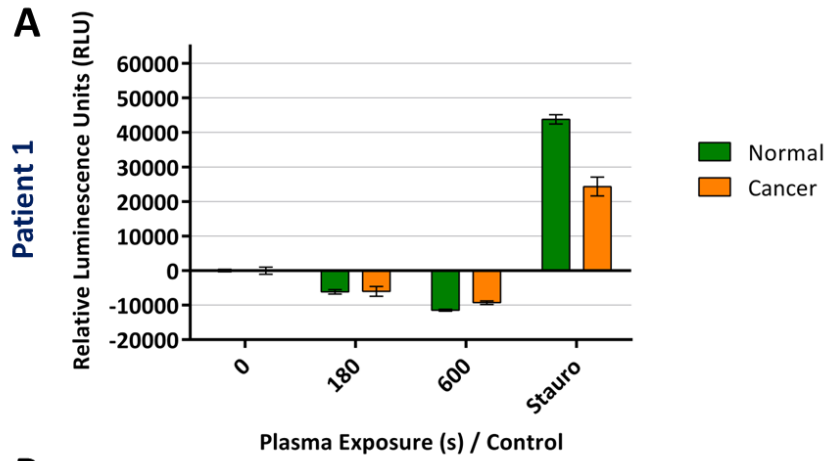
**Figure 42: Analysis of apoptotic response following LTP treatment in primary patient cells.**

Cells were treated with either 180 or 600 s LTP, or 1 μM staurosporine. At 24 hours after treatment, the Caspase-Glo 3/7 assay was performed to analyse apoptotic responses following treatment in three patient samples. Luminescence values were normalised to untreated control samples, with the data expressed as the mean value ± standard error.

### 6.4.2 Analysis of Necrotic Cell Death in Primary Prostate Cells

Cell death resulting from LTP-induced necrosis in patient samples was determined using the CellTox Green cytotoxicity assay. Cells were treated with either 0, 30, 180 or 600 s LTP, 1 mM $H_2O_2$, 1 µM staurosporine, or lysing agent (toxicity control). Immediately following treatment, the CellTox dye was added to the cultures, which fluoresces green when bound to the DNA of membrane-compromised cells, which are characteristic of necrosis. Representative images of the treated normal and cancer cells originating from the Patient 1 sample (due to time-constraints and availability of samples only Patient 1 data are shown) in Figures 43 and 45. These images were taken at 4 hours after treatment. The majority of positive green cells are found as the result of 600 s LTP treatment, where the cells exhibit a rounded appearance and are sparsely distributed. Both $H_2O_2$ and staurosporine controls showed little evidence of necrosis (non-fluorescent) at 4 hours after treatment.

Quantitative fluorescence readings were obtained at 2, 4, 8 and 24 hours following treatment of all three patient samples, and are shown in Figure 44 for normal cells and in Figure 46 for cancer cells. The toxicity control produced consistently high fluorescence readings across all time points (note: split y-axis scale), indicative of total cell lysis, which was confirmed by fluorescence microscopy (images not shown). A dose dependent increase in necrosis was observed following LTP treatment of all patient samples. The only slight exception to this trend was the cancer cell sample of Patient 3 (Figure 46C), where there was little difference between cells treated with 180 or 600 s LTP. There was no clear distinction between the levels of necrosis recorded for normal and cancer cells, however a few subtle differences were observed. For instance, higher necrotic readings were noted in the cancer cells of Patient 1, when compared to the paired normal cells (Figure 44A and Figure 46A). For patients 2 and 3 the opposite

was found, where higher levels of necrotic cell death occurred in the normal cells (Figure 44B/C and Figure 46B/C). However, staurosporine control treatments resulted in substantially less necrosis, due to cells undergoing apoptosis, and therefore their cell membrane remained intact. However, between 8 and 24 hours after treatment, the fluorescence readings from staurosporine-treated cells increased up to several-thousand-fold in all patient samples, often becoming comparable with LTP-treated values. It may be difficult to differentiate between late-stage apoptosis and necrosis with this particular assay, especially given that Figure 39 verifies that staurosporine treatment induced apoptosis at 24 hours, but LTP did not.

**Normal**
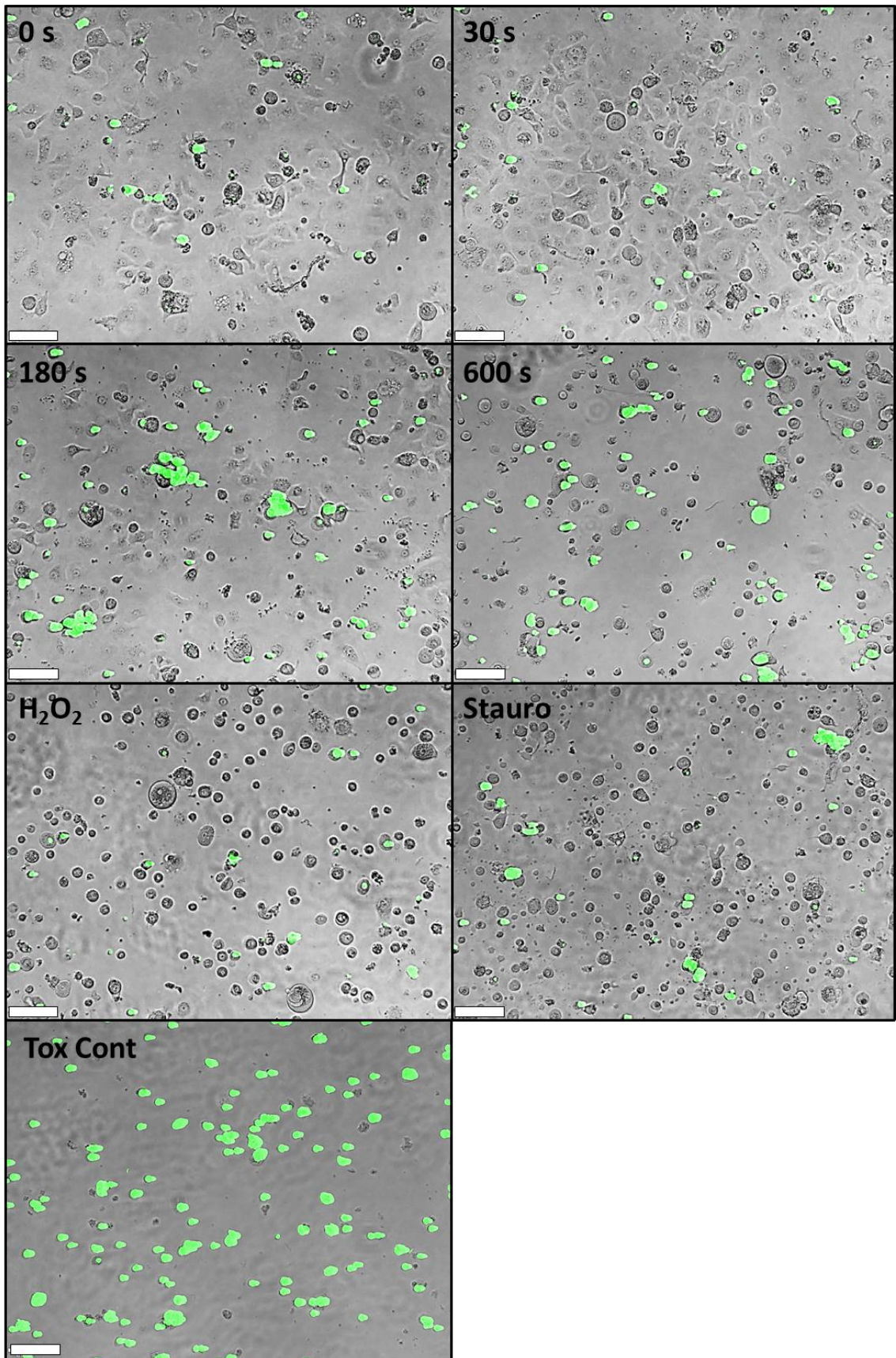
**Figure 43: Evidence of necrotic cells following LTP treatment of primary prostate normal cells.**

Cells were treated with a range of LTP exposures, 1 mM $H_2O_2$, 1 μM staurosporine or lysing agent (toxicity control). Merged fluorescence/bright-field images (10x magnification) were captured 4 hours after treatment. Green cells possess compromised membrane integrity, indicative of necrosis. Scale bar denotes 100 μm.

A



B



C
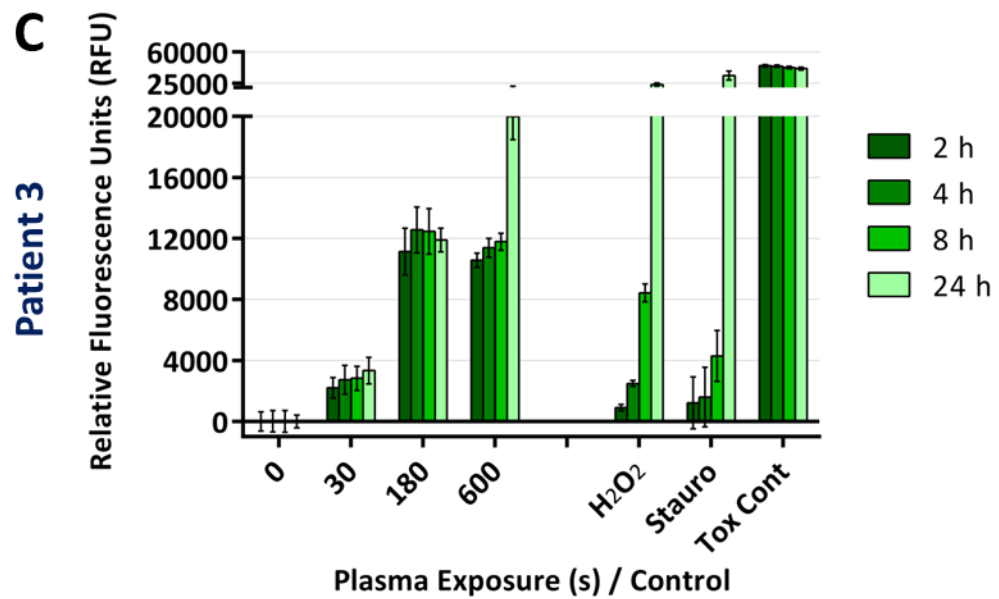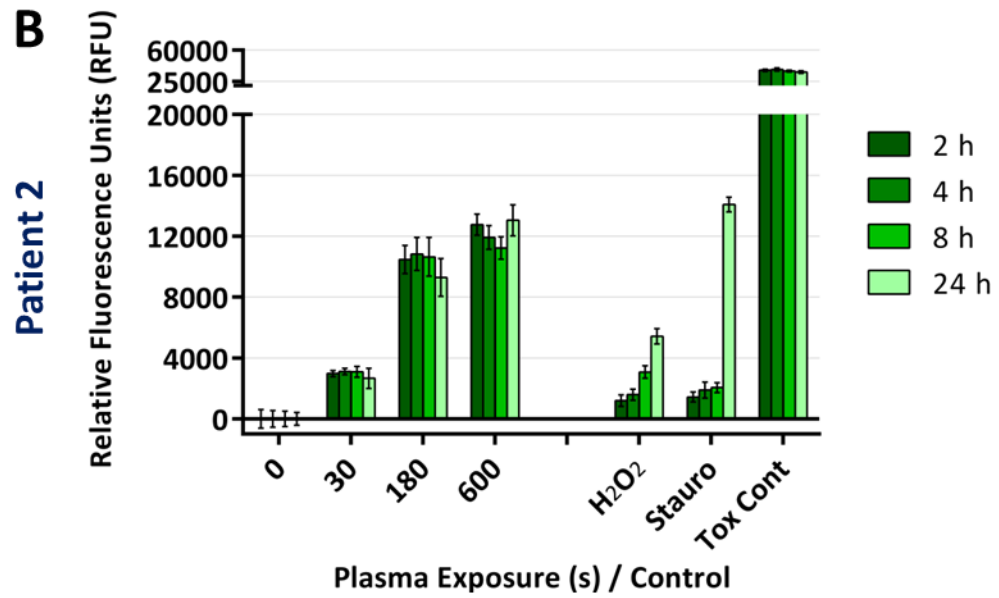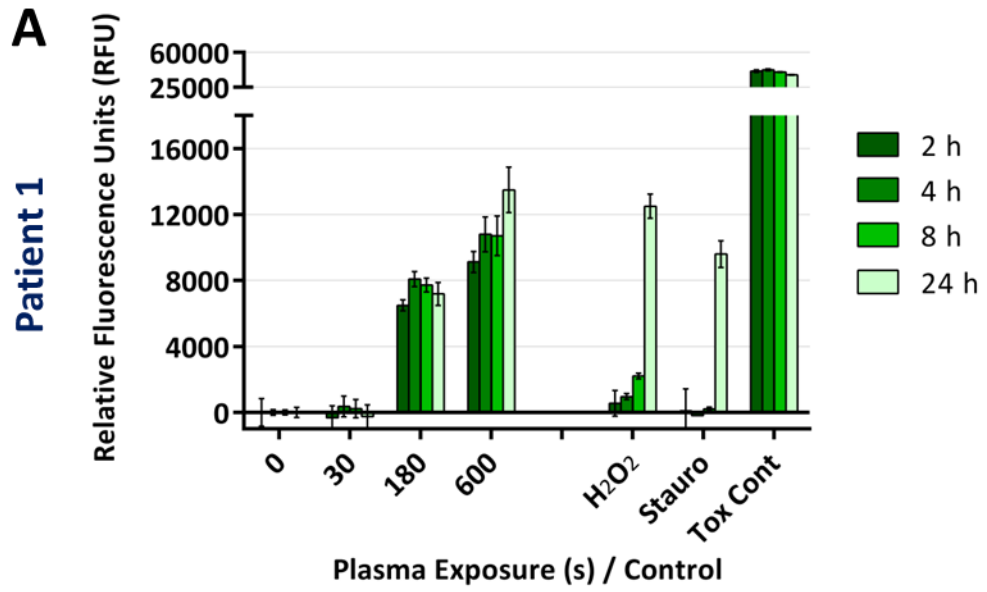
**Figure 44: Quantification of LTP-induced necrosis in primary prostate normal cells**.

Cells were treated with a range of LTP exposures, 1 mM $H_2O_2$, 1 µM staurosporine or lysis toxicity control. At 2 – 24 hours after treatment, LTP induced necrosis was assessed using the CellTox green assay, with fluorescence values normalised to untreated control wells. Data are expressed as mean ± standard error.

**Cancer**
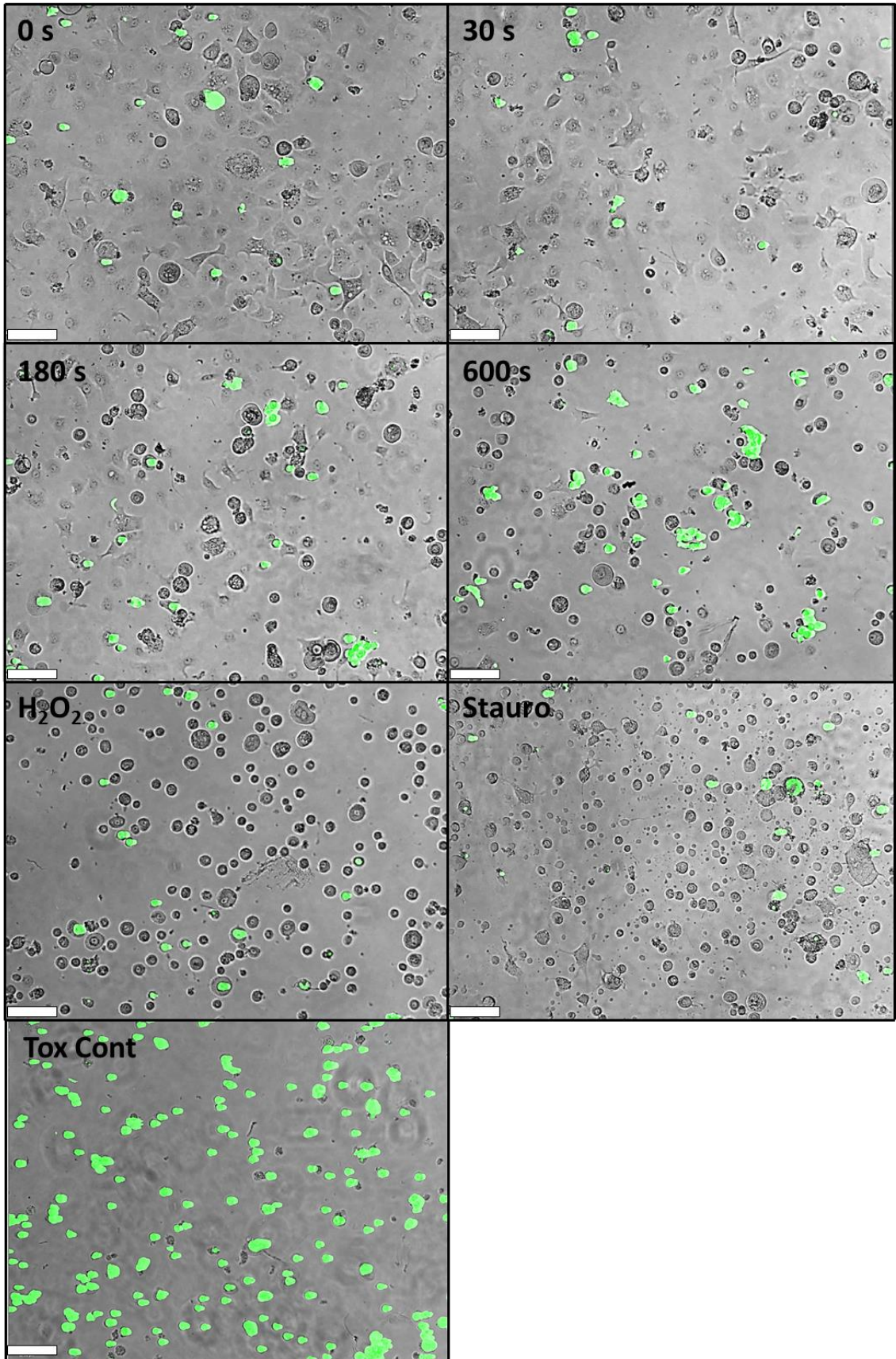
**Figure 45: Evidence of necrotic cells following LTP treatment of primary prostate cancer cells.**

Cells were treated with a range of LTP exposures, 1 mM $H_2O_2$, 1 μM staurosporine, or lysing agent (toxicity control). Merged fluorescence/bright-field images (10x magnification) were captured 4 hours after treatment. Green cells possess compromised membrane integrity, indicative of necrosis. Scale bar denotes 100 μm.

**A** — Patient 1

**B** — Patient 2

**C** — Patient 3
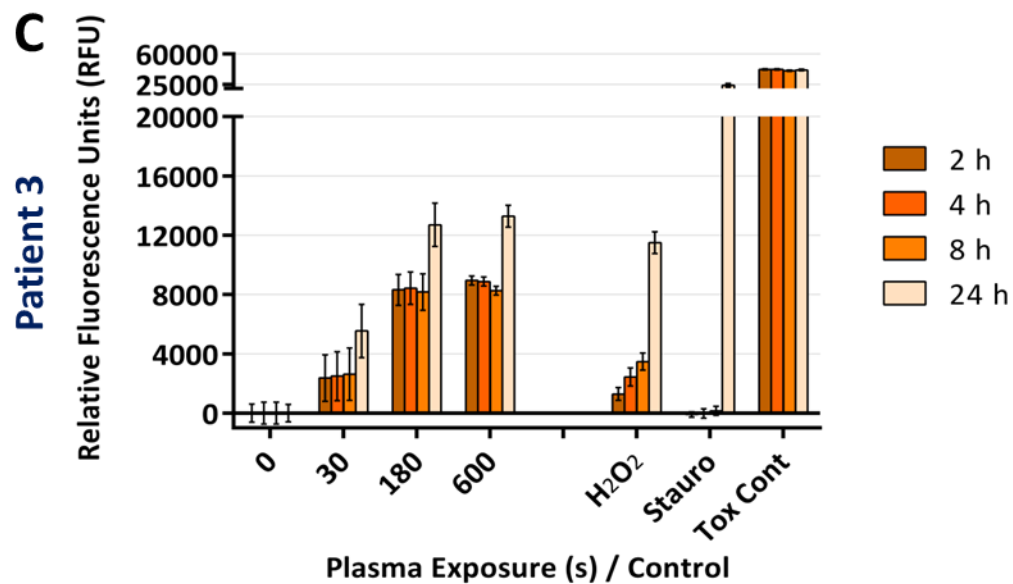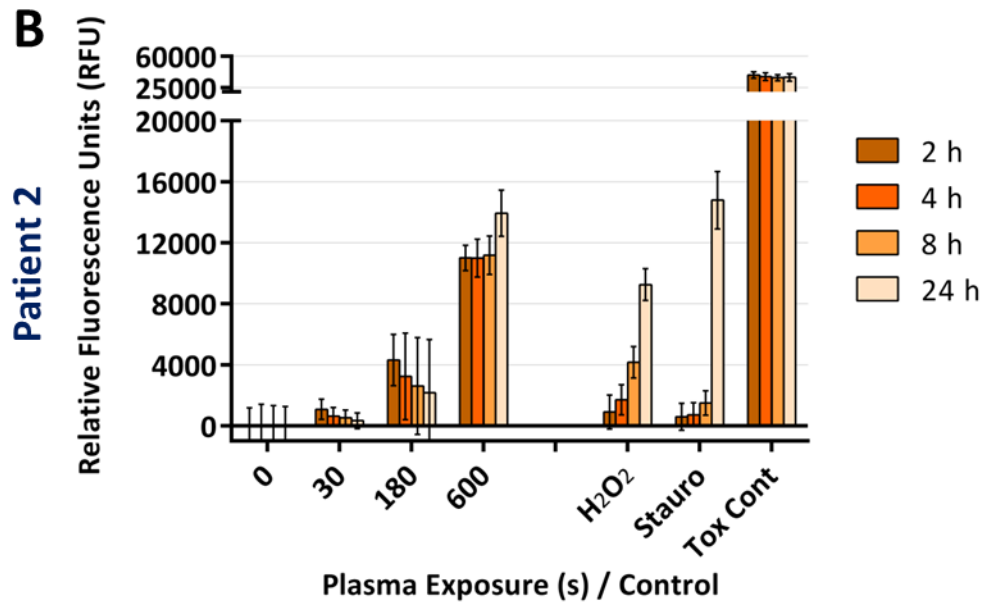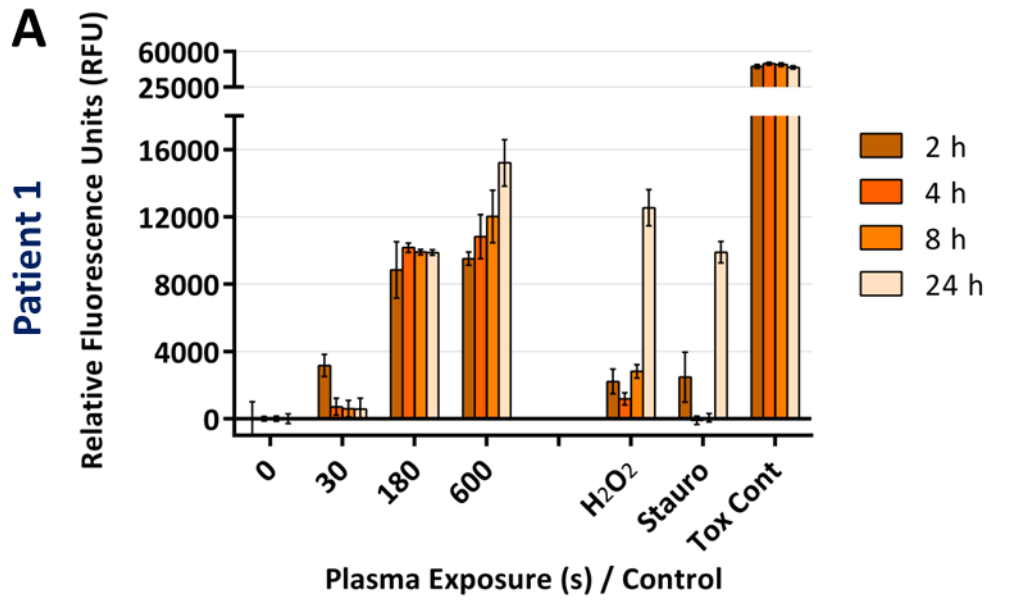
**Figure 46: Quantification of LTP-induced necrosis in primary prostate cancer cells**.

Cells were treated with a range of LTP exposures, 1 mM $H_2O_2$, 1 μM staurosporine, or lysis toxicity control. At 2 − 24 hours after treatment, LTP induced necrosis was assessed using the CellTox green assay, with fluorescence values normalised to untreated control wells. Data are expressed as mean ± standard error.

## 6.5  Application of LTP to Three-Dimensional Prostate Models

To extend the scope of this study beyond the treatment of cells in suspension, LTP was applied to clinically relevant, three-dimensional prostate models including aggregates, spheroids and tissue pieces.

### 6.5.1  Treatment of BPH-1 Cell Aggregates with LTP

BPH-1 cells were plated into non-adherent 96-well plates and cultured for 7 days to form aggregates of ~ 0.5 mm diameter. These were then carefully transferred to 24-well plates for treatment with either 180 or 600 s LTP, or 1 mM $H_2O_2$ control. Immediately after treatment, cell aggregates were pipetted back into 96-well plates in a 100 µl media volume. A minimum of 6 aggregates were recovered for each treatment group. At 72 hours after treatment, the CellTiter-Glo® 3D viability assay was performed to give an indication of metabolic activity. Images showing the morphology of cell aggregates following treatment are presented in Figure 47A for each treatment group. Exposure to either 600 s LTP or $H_2O_2$ control appeared to result in a number of cells sloughing away from the aggregate, however the core size of the treated aggregates did not differ from untreated controls. Despite this, a significant reduction in cell viability was recorded following treatment with LTP or $H_2O_2$ control, as shown in Figure 47B. LTP exposure of 600 s reduced BPH-1 aggregate cell viability to 20%, and $H_2O_2$ control to 10%. These results are in good agreement with those obtained for BPH-1 cells treated in suspension in Figure 25A. This suggests that although treatment with LTP did not cause the aggregates to disintegrate, the proliferative capacity of cells within the aggregate was strongly reduced.
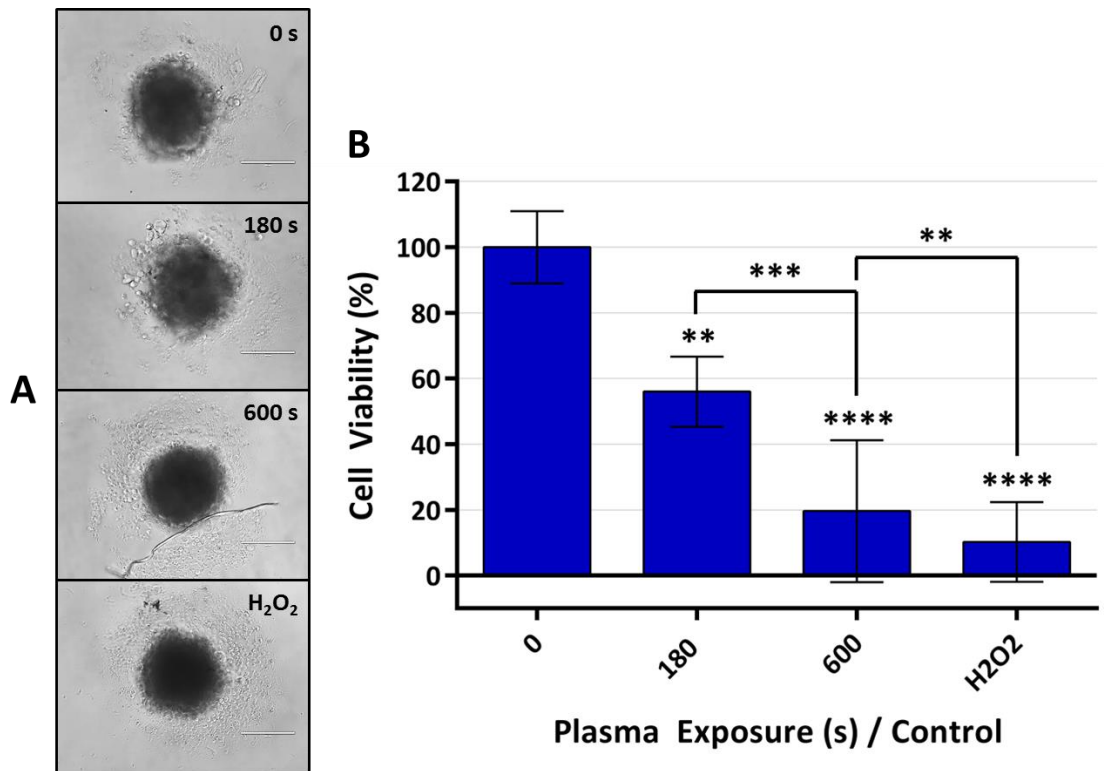
**Figure 47: LTP-treatment of BPH-1 cell aggregates.**

Cell viability of BPH-1 aggregates was recorded at 72 hours following treatment with either 180 or 600 s LTP, or 1 mM $H_2O_2$. Representative bright-field images were captured at 72 hours for each treatment group (**A**). Scale bars denote 400 μm. Cell viability results are plotted in (**B**), with data expressed as the mean value ± standard error. Statistical analysis was conducted using unpaired t-test with Welch's correction, with significance recorded against untreated samples unless otherwise indicated.

### 6.5.2 Treatment of P4E6 Spheroids with LTP

To further investigate the effects of LTP in 3D models, P4E6 cells were cultured as spheroids in matrigel. P4E6 cells were originally derived from a localised Gleason grade 7 tumour [223], and thus serve as a realistic model given the envisaged application of LTP as a focal treatment. As shown by Figure 48, P4E6 cells form well-rounded and tightly packed spheroids. Cells were suspended in a media/matrigel solution overlaid with media, and cultured for 6 days before treatment with 180 s LTP or 1 mM $H_2O_2$ control.
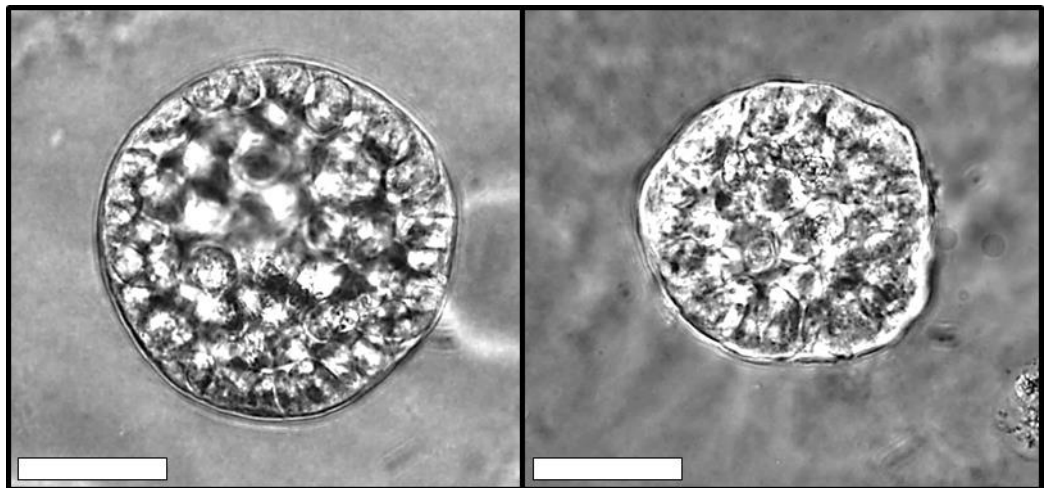


**Figure 48: P4E6 spheroid morphology.**

Representative untreated images of P4E6 spheroid morphology after 6 days in culture in matrigel. Scale bar denotes 50 µm.

Spheroids were fixed and stained to determine necrosis (propidium iodide, PI), or apoptosis (C-PARP) following treatment, with representative fluorescence images shown in Figure 49. Live-cell PI staining was performed immediately after treatment, whereas spheroids stained with C-PARP were fixed 4 hours after exposure to LTP or $H_2O_2$ control. P4E6 spheroids treated with 180 s LTP or $H_2O_2$ control show evidence of PI-positive cells (Figure 49B and C) indicative of necrosis. However, it was evident that necrotic cell death is not extensive, with PI-positive cells only accounting for a small proportion (<10%) of the total population. In addition, by the virtue of taking a 2D image snapshot of a 3D structure, it is difficult to identify the location of the positive cells within the spheroid, i.e. whether positively-stained cells are present only at the surface, or in the centre of, the spheroid.

It is clear from Figure 49E that treatment with LTP does not induce apoptosis in P4E6 spheroids. This result is in agreement with the findings in primary prostate cells (Figures 39 and 42). Treatment with $H_2O_2$ control induced apoptosis in a small number of cells (Figure 49F); yet as alluded to above in the context of necrosis, the level of apoptotic cell death was not extensive.
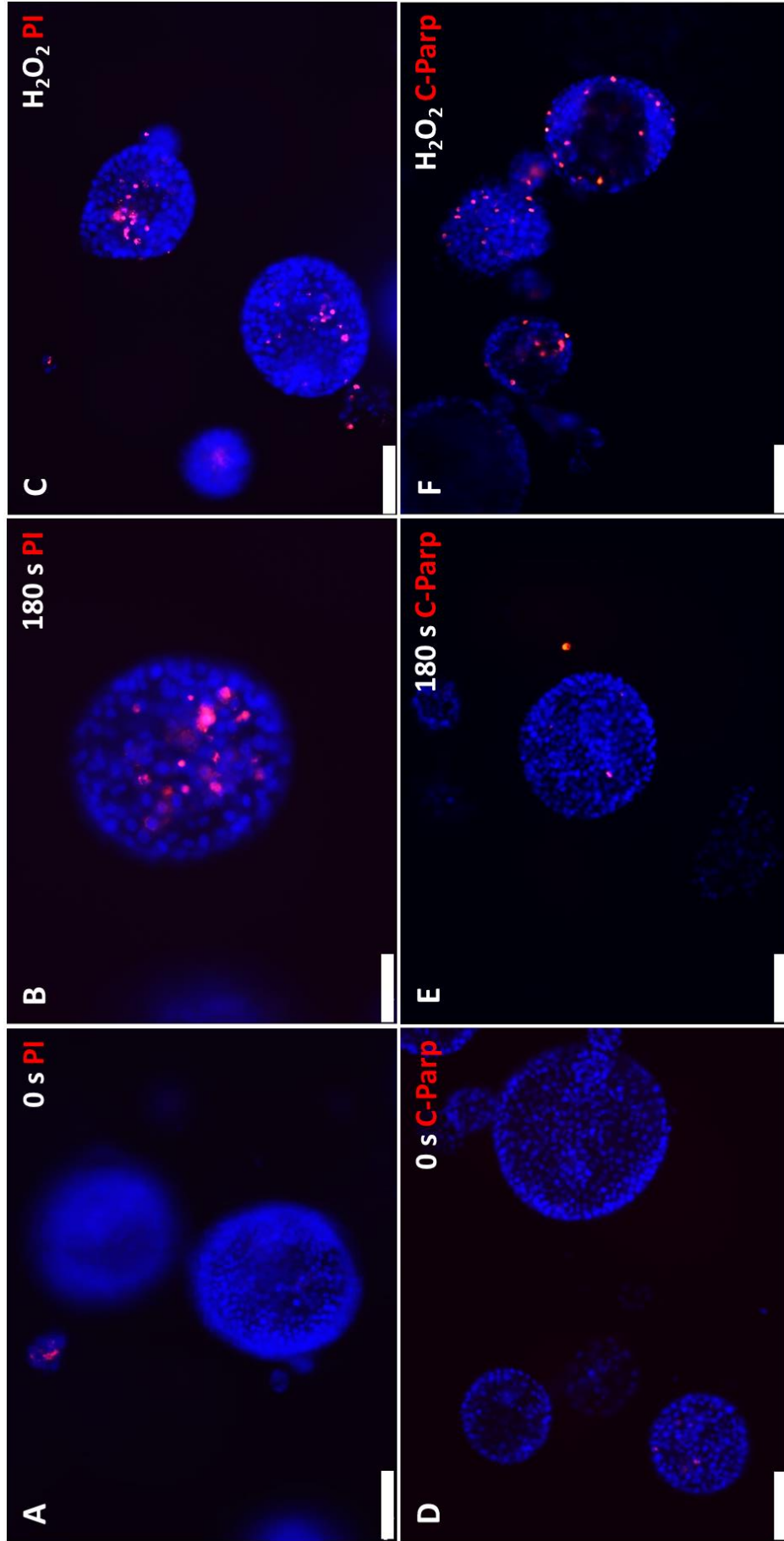
**Figure 49: LTP-treatment of P4E6 spheroids.**

Cell death mechanisms in LTP-treated spheroids was investigated through immunofluorescence staining. P4E6 Spheroids were either stained for necrosis (PI, **A** – **C**) or apoptosis (C-PARP, **D** - **F**). Staining of spheroids was carried out either immediately (**A** - **C**), or at 4 hours after treatment (**D** - **F**). Scale bars denote 100 μm.

### 6.5.3 Treatment of Prostate Tissue with LTP

Prostate tumour tissue originating from an excised xenograft was treated with LTP to analyse the effects of LTP on solid tissue structures in 3D. Tissue pieces were $\leq 1$ cm$^2$ in size, and fixed in formalin immediately following treatment. The distance between the end of the nozzle and the tissue was ~ 5 mm, such that the LTP jet was in contact with the tissue surface as shown in Figure 50A. This is highlighted in the magnified section of the image. A stitch of surgical thread was tied into the tissue piece to provide a directional reference point to identify the region of LTP-tissue contact after the tissue was sectioned. However, following processing to paraffin-embed the tissue, the stitch resulted in tearing of the tissue, and the plasma-tissue interacting surface could not be identified.

In a revised attempt to study the effects of LTP in patient tissue, pieces of benign prostate originating from TURP procedures were exposed to LTP. In this instance, the tissue was treated in 100 μl of PBS, thus allowing active species to interact with the entire surface area of the tissue. Tissue pieces $\leq 0.5$ cm$^2$ were treated with LTP for 300 s, fixed immediately and stained for γH2AX foci to identify DNA double strand breaks. Figure 50 shows images of untreated (B) and LTP-treated (C) benign tissue sections. Extensive DNA damage can be observed in Figure 50C, with the majority of cells positive for γH2AX staining. However, due to the treatment of the tissue in a liquid volume, it was not possible to determine how the location of the image shown in Figure 50C corresponds to the position of the LTP jet. Through the treatment of the tissue in a small liquid volume, it is likely that reactive species generated as a result of treatment would be able to interact with the tissue surface as a whole, causing cell damage uniformly around the tissue. However, the ability of reactive species to penetrate through the tissue sections is doubtful due to their inherently short lifetimes,

and the resulting high probability of interaction with cells primarily at the tissue surface. It is therefore most likely that the damage recorded in Figure 50C is surface-limited to a few ($\leq 5$) cell-layers, which would agree with other findings for plasma-treated multi-cellular structures in the literature [244]. Nevertheless, this result shows that DNA damage caused by LTP treatment does occur in both cells in suspension and solid patient tissue.
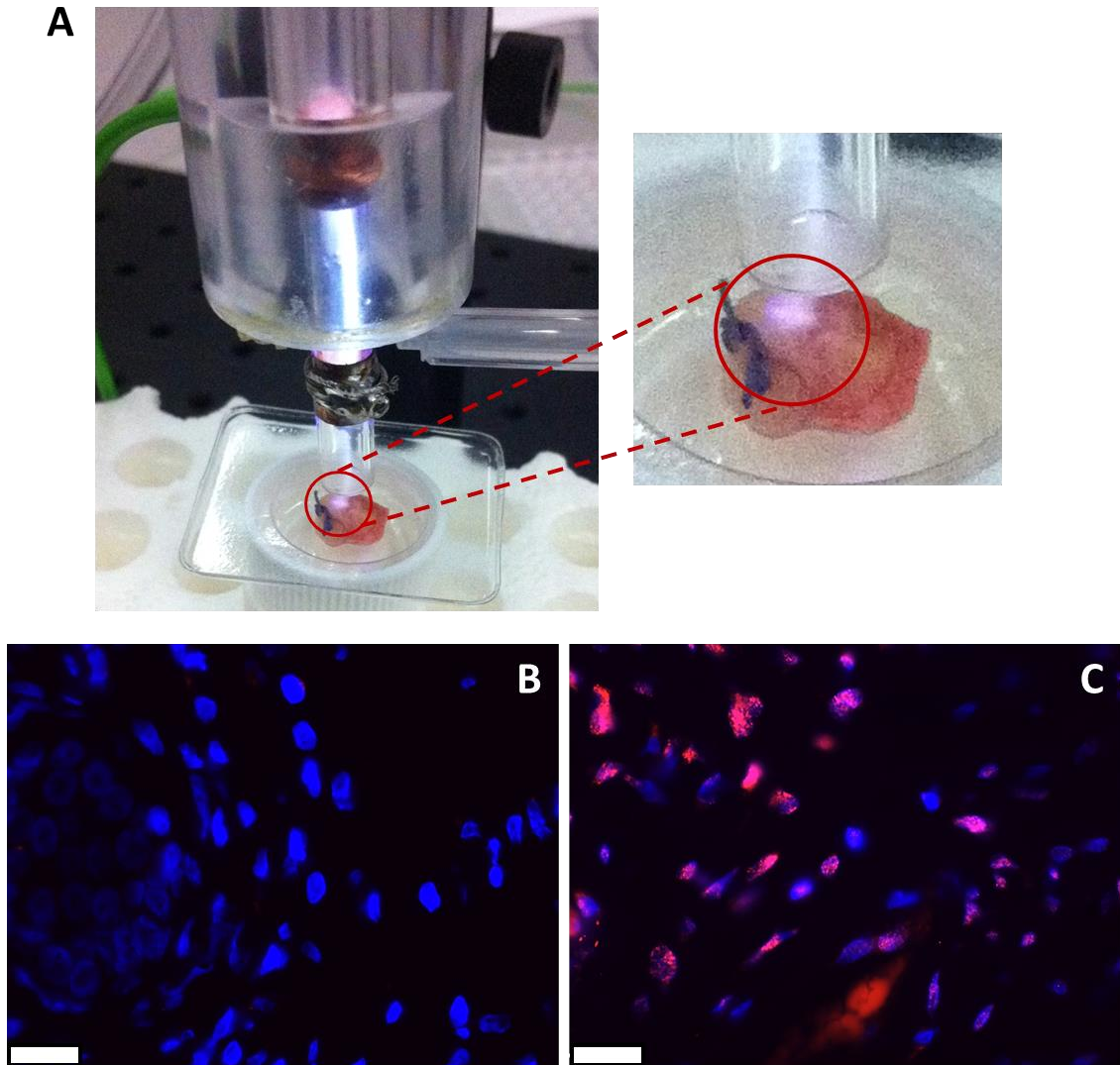
**Figure 50: LTP treatment of prostate tissue.**

Pieces of tissue were treated with LTP for 300 s before immediate fixation. The distance between the end of the nozzle and the tissue was ~ 5 mm, such that the LTP jet was in contact with the tissue surface (**A**). This is highlighted in the magnified image. Immediately after treatment, tissue pieces were fixed and stained for γH2AX foci. Immunofluorescence images of untreated tissue (**B**) and tissue treated with 300 s LTP (**C**) are presented. Scale bar denotes 100 μm.

# Chapter 7

## *Results IV*

## Development Towards a Clinically Applicable Plasma Device

# 7. Development Towards a Clinically Applicable Plasma Device

In order to progress the study onwards from the LTP source shown in Figure 13 towards a clinically applicable setup, some preliminary experiments were conducted to test the ability of a plasma to propagate down a thin needle. The device used in these studies was a DBD plasma ignited in a glass laboratory pasteur pipette, with the same electrode spacing shown in Figure 13. The plasma was ignited at the thicker end of the pipette in 1 SLM helium flow, and fed into the tapered end of the pipette. The outer and inner diameters of the two ends of the pipette were 7/6 mm and 1.5/1 mm respectively. The plasma was driven by a high-voltage pulsed power supply at 20 kV/1 kHz, with a pulse width and rise-time of 5 μs and 1 μs respectively. The power supply was designed and operated by Dr. Jérôme Bredin.

Initially, the plasma was ignited into open air, where it clearly propagated to the end of the glass tube (Figure 51A). The next step was to determine whether the plasma would ignite within a tissue-like substance. As a first attempt to investigate this, a 1% agarose gel was used to mimic a solid, but largely aqueous, environment. A spare glass pipette was used to forge channels into the gel, in order to prevent the plasma pipette becoming obstructed with pieces of gel. The pipette was inserted into a closed channel, i.e. the gas flow could not escape straight through the opposite end of the gel, as this is physiologically relevant when treating a tumour within a prostate (or in reality, an internal tumour). When inserted into the gel, the plasma still ignited (Figure 51B), however it no longer propagated to the end of the pipette.

The effect of only the gas flow into the gel was also investigated. The pipette was inserted into a new pre-made channel and the gas flow turned on. Almost instantly, a ballooning effect was observed as the gas permeated through the gel. This stabilised after a few seconds, forming the structure highlighted by the dashed lines in Figure

52A. When the gas flow was switched off, the structure seen in Figure 52A rapidly shrank, up to a point at which a permanently deformed region was observed in the gel (Figure 52B). The images in this section have clear implications with regard to the clinical application of LTP, which are addressed in the following discussion chapter.
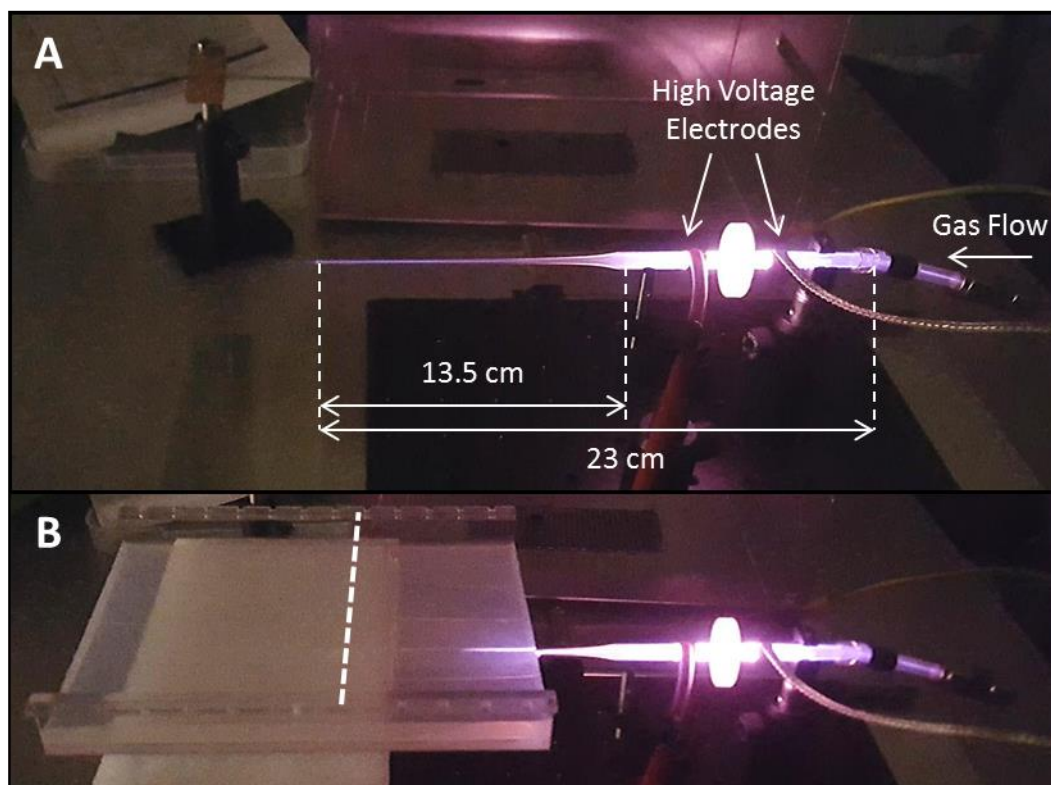


**Figure 51: Propagation of LTP in a thin needle.**

The plasma was ignited between two copper tape electrodes and propagated along a glass aspirator pipette. When propagated into open air, the plasma is clearly visible at the end of the tube (**A**). When the needle was inserted into an agarose gel (**B**), the visible plasma no longer reached the end of the tube, which is marked by the white hashed line.
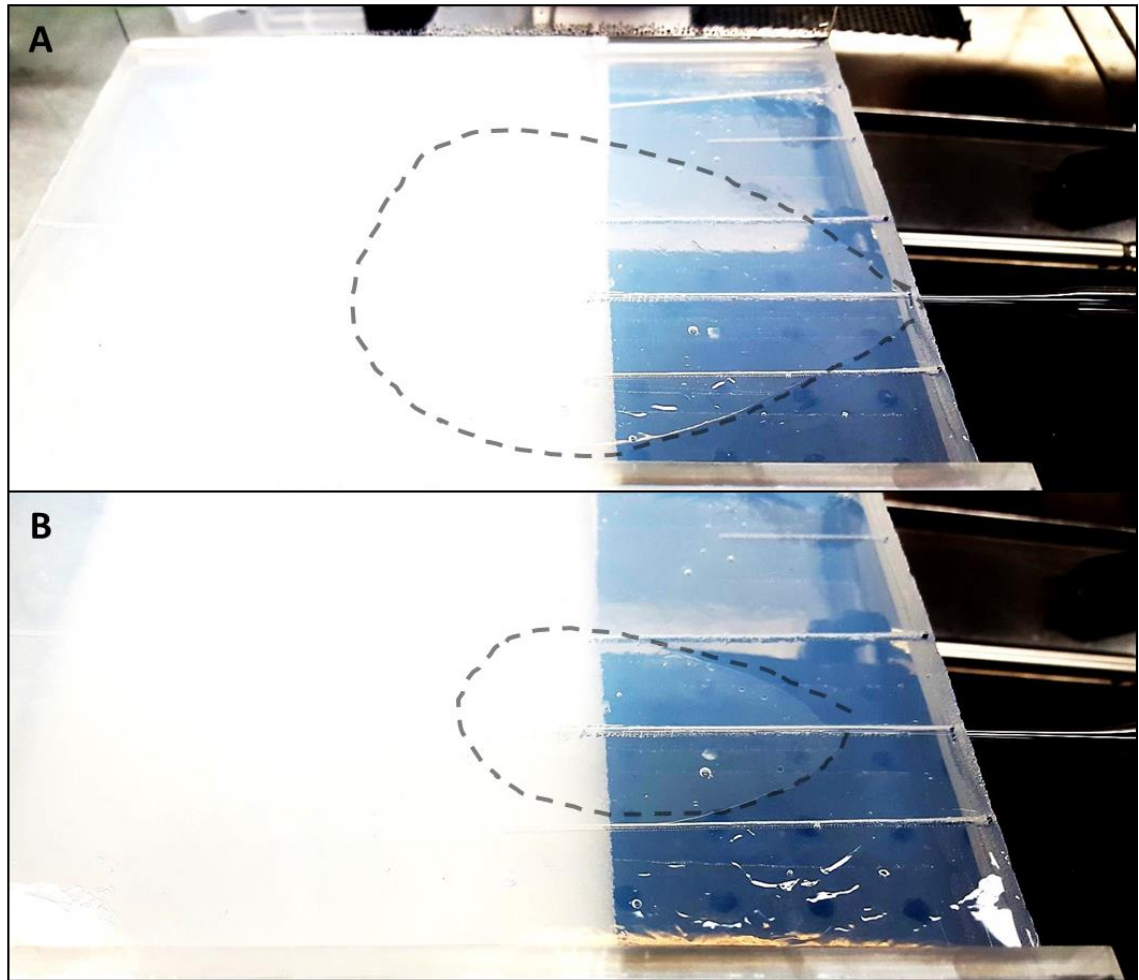
**Figure 52: Effect of gas flow in an agarose gel.**

Without the plasma ignited, gas flow of 1 SLM helium was fed into the glass tube. Almost instantaneous balloon-shaped deformation occurred in the gel (**A**), marked by grey dashed lines. After the gas flow was turned off, the size of the deformation gradually decreased, until a region of permanent deformation in the gel was visible (**B**). NB: The contrast in this image has been considerably increased to demonstrate the effect on the gel.

# Chapter 8
## Discussion

# 8. Discussion

Despite continual treatment refinements, prostate cancer still accounts for over 10% of cancer-related deaths in men. Patients with localised disease are often treated with radical surgery, which is highly invasive and can lead to a reduced quality of life [75]. It is also deemed a gross-overtreatment in a large number of cases [245]. Another common option is radiotherapy, which has been associated with off-target toxicity and incomplete tumour eradication [66, 68]. A range of relatively new treatments known as focal therapies are being developed, which aim to eliminate the tumour whilst minimising damage to normal tissues and side effects to the patient. Whilst promising, each of these has its own limitations, as outlined earlier in Table 1. The aim of this study was to analyse the potential of using low temperature plasma (LTP) as a novel focal therapy for prostate cancer. This was assessed by first conducting an initial study in prostate cell lines, before progressing to a more in-depth study in clinically relevant models.

## 8.1 Mechanisms of Plasma-Cell Interaction and Response

The first study examining the effect of LTPs on cancer cell lines was published in 2004 by Stoffels et al [246]. Since then, a growing number of papers have been published year-on-year investigating the effects of LTP on a wide range of different malignant cell lines. Common responses include DNA damage [183, 193, 198], reduced cell viability and clonogenicity [194, 195], and cell cycle arrest [196]. A handful of *in vivo* studies on subcutaneous tumours derived from cell lines have also been performed, which all concluded a significant reduction in tumour volume following LTP treatment [82, 218, 247]. In addition, internal plasma application has already been evaluated as

effective and well-tolerated in a pancreatic *in vivo* model [247]. Despite the documentation of multiple different cellular responses, two clear trends have emerged from the literature: LTP treatment appears to exhibit selective cytoxicity towards malignant cell lines [195, 202, 248-252], and LTP treatment induces apoptotic cell death [144, 184, 196, 198, 203, 204, 206, 253-256].

Perhaps the simplest explanation for the selective effects recorded elsewhere may be the comparison of different cell types, for example normal fibroblasts from one organ with the epithelial cancer cells of another, which may possess quite different response profiles. For example, Iseki et al. compared the effects of LTP on ovarian carcinoma epithelial cells with normal lung fibroblast cell lines, and concluded cancer-selective apoptotic effects [257]. In another study, Conway et al. directly compared cervical cancer cells with glioblastoma cells [258]. To make legitimate conclusions on the proposed selective effect of LTP, the treated cells should ideally originate from the same site.

Despite the rapidly growing literature, no data had yet been published studying the effects of LTP on prostate cancer models at the beginning of this project. Due to there being no direct point of reference, this study began by examining the effects of LTP in prostate cell lines. Crucially, where this study differs from many others is the use of malignant and non-malignant cell lines from the same organ. The effects of LTP were first investigated on BPH-1 (benign) and PC-3 (malignant) prostate cell lines. In contrast to the perceptions in the literature relating to plasma-selectivity, BPH-1 cells were more susceptible to LTP than PC-3 cells in all experiments. After treatment, BPH-1 cells had higher levels of DNA damage, reduced clonogenicity, and an $IC_{50}$ value ~ 6-fold lower than PC-3 cells (Chapter 5). It is worth re-iterating that PC-3 cells exhibit resistance to a range of cytotoxic agents *in vitro* [233-236], and thus the fact that they

exhibit elevated resistance to LTP compared to BPH-1 cells was not unexpected. However, this also highlights that the cytotoxicity recorded from single LTP treatments are particularly promising, especially when compared to initial experiments involving PC-3 cells treated with ionising radiation (IR). Following the single standard dose of 2 Gy IR, the viability of PC-3 cells fell by only ~ 10%, and only a modest increase in DNA damage was recorded over untreated controls. Conversely, following 600 s LTP treatment PC-3 cell viability fell by ~ 90%, and DNA damage values increased by 80% (Figures 18 and 25). In addition, LTP treatment of PC-3 cells resulted in very consistent and reproducible outcomes, verified through three independent assay repeats for DNA damage and clonogenicity. The surviving fraction of PC-3 cells from 2 Gy IR and 600 s LTP were found to be 54% and 41% respectively, which are in comparatively closer agreement than the findings for cell viability and DNA damage. This implies that IR and LTP may induce different cell death mechanisms; treatment with IR was recently shown to induce senescence in primary prostate cells [259]. This would explain the reduced clonogenicity of PC-3 cells following treatment with IR, yet the cells could remain viable despite losing their replicative potential. The results for LTP-treated PC-3 cells showed quite clearly that non-surviving cells died through necrosis.

The mechanism of cell death provided further differential responses in BPH-1 and PC-3 cells. BPH-1 cells underwent apoptosis, whereas PC-3 cells did not. As mentioned earlier, the induction of apoptosis following LTP treatment has been shown by many studies. However, both cell lines were found to undergo necrotic cell death as a result of exposure to LTP. Although a few studies appear to have identified necrosis following LTP treatment, it was referred to as 'non-apoptotic' [195] or 'caspase-independent' [258, 260] cell death. The emphasis on apoptosis suggests that necrosis is perceived as an unfavourable cell death modality following LTP treatment when compared to the

tightly regulated and controlled cell execution involved in apoptosis. For example, in a review publication, it was directly stated that an advantage of LTP over existing cancer treatment modalities is "no necrosis nor inflammation" [261]. In addition, there appears to be a bias towards demonstrating apoptosis in the literature based on the assays applied to analyse cell death. Many studies cite evidence of apoptosis through C-PARP and/or cleaved-caspase-3 protein expression [82, 206, 256, 257, 262, 263]. Apoptotic activity is also commonly shown by annexin V and propidium iodide (PI) fluorescence activated cell sorting (FACS) [262, 264]. However, in some cases only a very modest (< 5%) induction of apoptosis was recorded [254], or there was no quantitation of the PI-positive (potentially necrotic) cell population [82, 198, 263]. Another study by Panngom et al. showed upregulation of genes specifically related to apoptosis only [250]. In the majority of these works, cell death assays were conducted at extended time intervals following LTP treatment. Necrosis appears to be a comparatively rapid response, as the results both in this study and others have shown [265]. As such, had the studies only citing apoptosis performed early cytotoxicity assays similar to those applied here, they may have also observed a proportion of cells undergoing necrosis following LTP treatment.

Despite the fact that this study showed no evidence of apoptotic activity in PC-3 cells, a different approach by Gibson et al. showed that PC-3 cells did undergo apoptosis 24 hours following LTP treatment of 600 s [253]. The device used was a different geometry to the one used in this study (a CCP similar to that described in Appendix B), producing an effluent devoid of charged species which was directed into the nozzle of a cell culture flask. The authors recorded elevated levels of nitrate in the cell culture media, which may have been formed from reactions between the plasma-effluent and nitrogen in the ambient air inside the culture flask. It has been proposed

that NO could be a key factor in both overcoming resistance and promoting apoptosis in tumour cells [266], through secondary reactions to form $ONOO^-$ [267, 268], and by inhibition of DNA repair mechanisms [269]. In this work however, no nitrogen peaks were recorded in the optical spectra, and the distance between the nozzle and the media was probably too small to permit the formation of RNS from the ambient air. Induction of NO could be achieved by the direct addition of molecular nitrogen into the gas feed, either alone or in combination with the oxygen admixture used in this work. It would be interesting to determine if the presence of $NO_x$ species sensitised PC-3 cells to apoptotic cell death.

To summarise this section, the results presented in this work for LTP-treated prostate cell lines appear to contradict the findings of the research field highlighted at the beginning of this chapter. Many investigators report that LTP treatment preferentially targets tumour cells, whilst leaving non-malignant cells relatively unscathed [195, 251]. This is without doubt a highly desirable, 'gold standard' outcome, but may relate to the comparisons of different cell types outlined before. Nevertheless, there are many potential explanations and contributing factors for this concept. One explanation may be the rapidly dividing nature of tumour cells (in cell culture), increasing their vulnerability to DNA damage in M-phase [270]. Volotskova et al. showed induction of $\gamma$H2AX in both G2/M and S-phases of various keratinocyte cell lines treated with LTP [217]. In addition, LTP has also been shown to interfere with other stages of the cell cycle. Chang et al. showed that oral squamous cell carcinoma cells underwent G1 arrest, leading to apoptosis, following exposure to LTP [198]. However, not all cells within a tumour population are actively cycling and undergoing DNA replication. Cancer stem cells are often quiescent and as a result may be more protected from sustaining DNA lethal damage. This could be crucial in the context of treating primary cells (and thus patient

tumours), and could be tested through cell cycle analysis using stem cell markers such as CD133.

Another theory revolves around the different tolerance levels of normal and tumour cells to increased RONS levels [176]. The vast majority of studies in the field cite LTP-induced RONS as the main facilitators of cellular stress and death [82, 181, 184, 187, 194, 203, 206, 207, 218, 249]. The inherent elevated metabolic activity in malignant cells (Warburg effect) may present a therapeutic window, as these cells are essentially already at their ROS-tolerance threshold or 'red-line' when compared with their neighbouring normal counterparts [177]. Any further increase in the RONS concentration in the local environment may be sufficient to tip the balance and sentence tumour cells to death. This latter theory is most frequently used to explain the discrepancies presented in LTP-cancer studies, and may well influence the cytotoxic and cytopathic profiles of different cells. However, whilst normal cells may possess an extended capacity to withstand elevated RONS levels in the short term, this is unlikely to render them invulnerable to cytotoxic agents. Off-target toxicity to normal tissues is a concern in both radio- and chemo-therapies [66, 67, 271] (which, like LTP, may generate RONS), so it would seem unlikely to expect LTP to be different in this respect, especially when considering the apparent potency of the plasma used in this work. Gene expression analysis on markers of oxidative stress response could allow further quantitative clarification on the role of reactive species and plasma selectivity.

## 8.2 The Influence of Cell Culture Media on Experimental Assays

Different types of culture media may play a contributing role in the formation of RONS in the cellular environment following LTP treatment. As the growth of different

cell lines has been optimised in different types of culture media, it is logical to treat and retain them in their standard conditions. However, the reactive species produced by the plasma will interact not only with cells, but also with all organic components within the culture media. Even in the absence of cells, RPMI-based media is known to yield high $H_2O_2$ readings by the manufacturer of the ROS-Glo assay [272], which was confirmed in this study. In the presence of cells, the level of $H_2O_2$ was comparable to other media types, indicating that cells actively quench exogenous levels of $H_2O_2$ (and other ROS) in the culture media. One option to eliminate the influence of treating cells in different types of cell culture media would be to treat all cells in buffered saline solutions. A counter argument to this would be that this is non-physiological with respect to ultimately treating a patient, given that the plasma would react with numerous proteins and organic molecules when ignited inside the body.

Although the constituents of most commonly used base media types may be similar, the concentration of added serum may vary from 2-10% of the total volume. Hypothetically, the interaction of RONS with the serum may play one of two opposing roles. Either the serum could quench RONS produced by the plasma, therefore providing a false-negative result with regard to LTP-cytotoxicity, or the serum could be degraded and form other secondary RONS, adding to the cumulative toxicity of the environment and thus producing false-positive results. This could be tested by performing a direct comparison of plasma-treated water with cell culture media (containing serum) and analysing the effects on cells, for instance using the ROS-Glo $H_2O_2$ assay used in this thesis. It was noted that $H_2O_2$ levels recorded in KSFM (serum-free) media were an order of magnitude lower than those for serum-containing media. This suggests that serum can amplify the levels of ROS, which does not occur in

KSFM. Thus, concerns regarding the contribution of KSFM culture media in later studies with patient cells could be allayed.

The availability, ease-of-use, and relative inexpense of various cell lines make them a versatile starting point to model the response of multiple different malignancies to cytotoxic agents. However, they are not representative of real tumours. Through many years of extended passaging in laboratory culture, in media containing high levels of serum, aberrations including the loss or gain of chromosome numbers have been documented in many different cell types [50, 273-275]. Primary prostate epithelial cells provide a far more accurate representation of both the original disease, and the heterogeneous nature of prostate tumours [49]. However, they are expensive to culture and maintain, grow slowly, and cannot be indefinitely passaged. These factors, when combined with the ethical approval required to acquire and store patient tissues, results in their usage being rare. The value of such a resource cannot be underestimated. This thesis represents the first study applying LTP to normal and tumour cells derived directly from human tissues, and thus marks the main contribution of this work to the field of plasma oncology.

## 8.3  LTP Treatment of Clinically Relevant Prostate Models

During the course of this study, paired normal and tumour primary cells originating from three different patients were treated with LTP. The tumour cells were cultured form Gleason grade 7 tumours, with the corresponding normal cells obtained from the opposite, normal side of the prostate to the tumour-bearing region. This allowed the first truly direct comparisons between normal and cancer cells to be made. In addition, as normal and tumour cells were cultured in identical media, the issues alluded to earlier

regarding the influence of different media types in cell lines no longer needed to be considered.

The effects of LTP in primary cells were similar to those recorded in prostate cell lines; high levels of DNA damage, reduced cell viability and clonogenicity, and elevated levels of $H_2O_2$ in the culture media of treated cells. Indeed, the results showing an increase in extracellular $H_2O_2$ formation with LTP treatment almost perfectly overlay those showing the progressive reduction in clonogenic survival. However, a degree of patient-to-patient variability was observed. For example, the levels of DNA damage recorded for the Patient 2 sample were at least 20% lower across all treatment durations than for Patients 1 and 3, which were very comparable. When examining cell viability, the data for Patient 2 and 3 were in close agreement: the cancer cells appeared more susceptible to LTP treatment than their matched normal cells. The cells from the Patient 1 sample showed the opposite trend, and also seemed more resistant to $H_2O_2$ control treatment. Averaged data showing the response across all patients revealed no differences in the cell viability of normal and tumour cells following 30 or 600 s LTP exposure. However, normal cells appeared comparably more susceptible to 180 s LTP treatment than tumour cells, but the opposite trend was seen following $H_2O_2$ control. These data show that the relative levels of DNA damage immediately following treatment do not necessarily correlate to the relative reduction in cell viability at extended periods after LTP exposure, and that LTP-effect is not solely due to $H_2O_2$ production.

Interestingly, evidence of an autophagic response was recorded in primary cells treated with LTP, which has not been documented before in the literature. Autophagy involves the degradation of cytoplasmic contents to provide sustenance during periods of cellular stress [276], which may act as either a cell-survival mechanism or as a pre-

cursor to apoptosis [277]. Quantitation of band intensity in Western blotting experiments revealed that induction in the normal cells of Patient 1 was approximately double that of the tumour cells. The differential autophagic expression in normal and cancer cells may be attributed to their ROS imbalance alluded to earlier [176, 177], whereby normal cells possess an additional capacity to tolerate the effects of ROS compared to tumour cells. Nevertheless, further investigation of these findings is required, through measuring evidence of autophagy and autophagic flux in multiple patient samples.

Despite the subtleties recorded across the three different patient samples, three findings were plainly clear; the effects of LTP cannot be solely due to $H_2O_2$ production, there is no strong selective effect of LTP between normal and tumour cells, and primary cells do not undergo apoptosis following LTP treatment. In all three primary samples, high levels of necrosis were recorded, yet with variability again recorded in induction between patients.

The results also highlight the differences between cell line and primary cell models. An illustration summarising the findings in cell lines and primary cells is shown by Figure 53. Prostate cell lines were observed to undergo both apoptosis and necrosis (BPH-1 cells, red arrows), whereas primary prostate cells were only found to undergo necrosis (thick green arrow). In addition, primary cells were also found to exhibit autophagy, which may act as a cell-survival mechanism or as a pre-cursor to apoptosis [277] (black arrows with question marks). These factors imply that primary cells respond quite differently to LTP treatment than the broadly apoptotic response found in various cell lines across the literature. Differences between prostate cell lines and primary cell models in the context of response mechanisms to treatment has also been previously recorded in our laboratory following exposure to chemotherapeutic agents

[236, 278]. The data also show that selective plasma effects may be less pronounced and particularly patient-specific if LTP was applied as a treatment. These findings may have important implications when progressing LTP therapies towards the clinic, which is discussed in a later section.

Treatment

Cell

■ Primary cells
■ Cell lines

?

Autophagy

?

Apoptosis
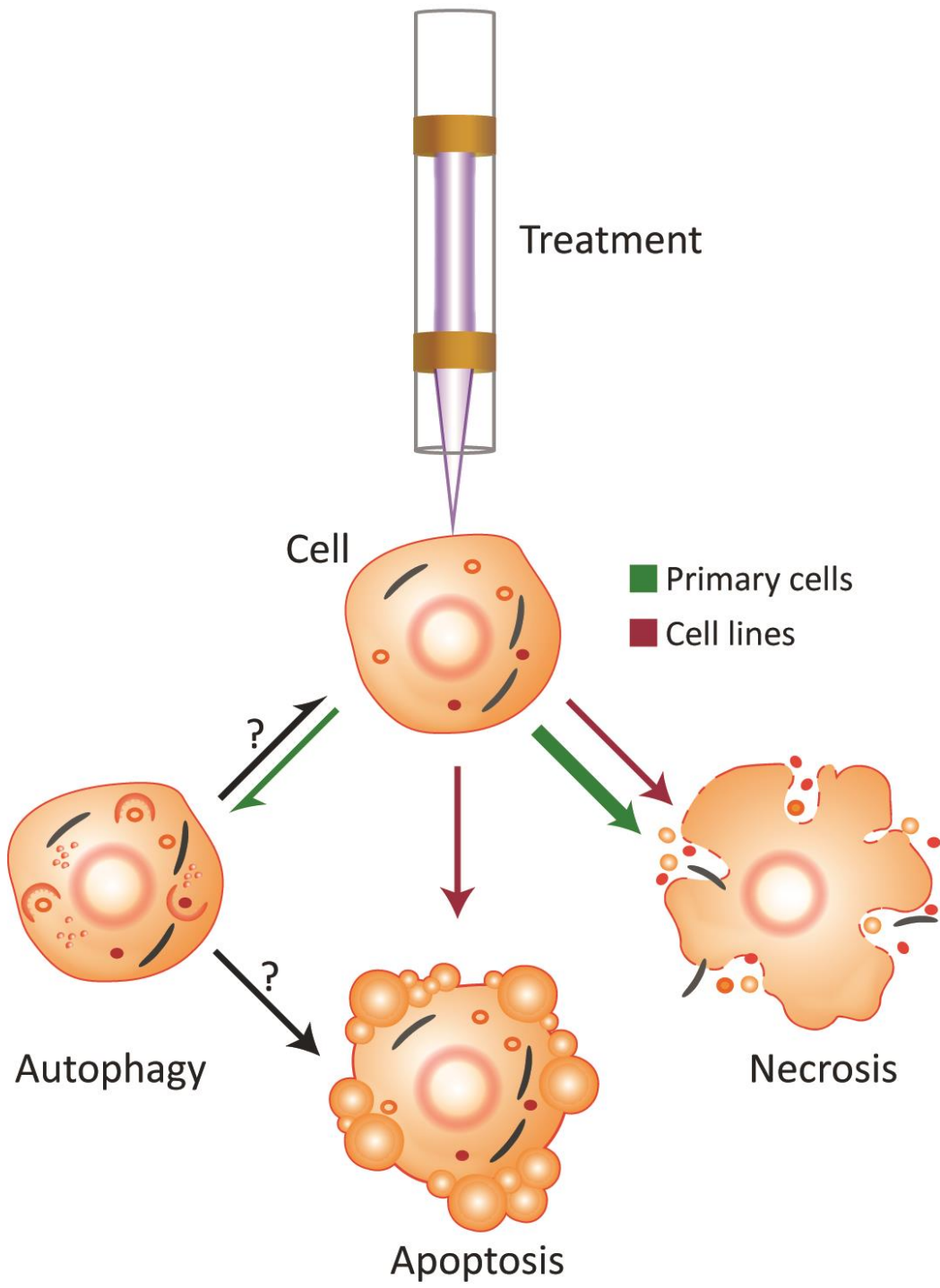
Necrosis

**Figure 53. Overview of cellular response mechanisms following low temperature plasma treatment.**

As a result of exposure to low temperature plasma, cells were observed to undergo either (or a combination of) autophagy, apoptosis or necrosis. The relative proportions of, and differences between, cell lines (red arrows) and primary epithelial cells (green arrows) that exhibit these phenomena is emphasised. Reprinted from Hirst et al [183] under a Creative Commons 4.0 License (*http://creativecommons.org/licenses/by/4.0/),* and originally adapted from Kepp et al. [279].

### 8.3.1 The Treatment of 3D Structures with LTP

To further progress the clinical relevance of this work, a number of 3D prostate models were treated to evaluate the effectiveness of LTP beyond the responses observed from cells in suspension. Cell aggregates were used as an initial model, by plating BPH-1 and PC-3 cells into non-adherent, round bottomed well plates, such that the cells sink and clump together to form rough spheres. Unfortunately, PC-3 cells did not form aggregates; the cells failed to clump together and instead formed a disorganised hollow and diffuse mass of cells, well over a millimetre in diameter. Conversely, BPH-1 cells formed smaller, rounded and tightly packed structures of ~ 500 μm.

The viability of LTP-treated BPH-1 aggregates reduced significantly, with the data in close agreement with results obtained for BPH-1 cells in suspension analysed by alamarBlue assay. The morphology of the treated aggregates appeared overall very comparable to untreated controls, albeit with evidence of a halo of cells surrounding the aggregate, suggesting these cells had sloughed away. The strongly reduced metabolic activity of the cells, combined with the relatively intact appearance of the aggregates might imply that the cells had simply growth arrested following treatment. However, the assay applied specifically quantifies the level of intracellular ATP, as an indicator of actively proliferating cells. As reduced ATP levels are associated with necrosis [280-283], this again would be in agreement with the response of BPH-1 cells of earlier 2D studies.

To examine further the effect of LTP in 3D models, P4E6 cells were cultured as spheroids in matrigel. P4E6 cells form regular, tightly packed spheroids [284]. Originally derived from a localised and well-differentiated (Gleason grade 2+2 = 4) tumour, they provide a representative model for patients who would be suitable for

focal therapy. In addition, matrigel mimics the basement membrane, further replicating the tumour environment, and providing a barrier that plasma produced reactive species would have to traverse.

Evidence of necrosis was determined following LTP treatment, but no induction of apoptotic activity was recorded. Further evidence that the LTP-effect is not solely based on $H_2O_2$ production was also found, since treatment with $H_2O_2$ led to some C-PARP positive cells, whereas LTP did not. From the images generated, it is difficult to precisely determine the location of positively stained cells within the spheroid volume. This could be achieved in future through the use of confocal microscopy to analyse staining within the spheroid layer-by-layer. It would appear that cell death occurred mainly in cells on the surface of the spheroid, which would agree with the findings of Plewa et al. and Judee et al. [244, 285], who showed that the cytotoxic effect of LTP was surface-limited in a cell aggregate model. The results of γH2AX staining of prostate tissue would also suggest this. Although the DNA damage appeared widespread following LTP treatment, with virtually every cell staining positively, the sections most likely originated from the surface of the tissue. For the clinical eradication of tumours, LTP treatment would need to induce cytopathic effects to cells in the core of the tumour.

The fact that cell death was recorded in P4E6 spheroids following LTP treatment suggested that RONS produced by the plasma were able to pass through a relatively large media volume, diffuse into the matrigel, and ultimately deeply into the spheroids. This is a promising finding in the context of clinical application, and is reinforced by Szili et al., who showed that plasma produced RONS could pass through an agarose gel [286]. Nevertheless, the treatment application used here is not representative of how LTP might be applied clinically, as the plasma effluent was not in contact with the

spheroids themselves. In addition, spheroids are physically too small to be used to model clinical plasma application, based on the approach proposed in the next subsection.

## 8.4 Future Perspectives

The models presented in this study have shown the potential of LTP treatment of both primary patient cells, and of multi-cellular, tumour-like structures. However, to ultimately realise a clinical application, LTP would need to be applied locally into the prostate. This chapter concludes the study by outlining how this may be achieved in the future, and speculating on how LTP treatment may compare against other currently applied technologies.

### 8.4.1   The Clinical Application of LTP

Following discussions with Professor Mark Emberton and Mr. Manit Arya, urological clinicians at University College Hospital London, it was decided that the most efficient means of LTP treatment application would be to follow the approaches of cryotherapy and brachytherapy by inserting the plasma transperineally to provide focal treatment of organ confined tumours. The preliminary studies in Chapter 7 showed that in principle it is possible to propagate a plasma along a thin tube. The images showed that the length of the narrow section of the tube was ~ 13 cm, with a diameter of 1.5 mm. These dimensions are approximately equal to those of freezing needles used in cryotherapy procedures. An illustration of such a potential treatment delivery of LTP is outlined in Figure 54. The plasma is delivered transperineally down a thin needle or tube, and into a localised prostate tumour under TRUS guidance. The high-voltage electrodes are encased and distanced from the patient's body for safety.

It would be logical to anticipate that similar criteria for patients to be considered for current focal therapies would be applied for LTP treatment [287]. Patients with low risk cancer (Gleason 6) are likely to opt for active surveillance to avoid unnecessary

invasive procedures [288]. Patients with metastatic or locally advanced prostate cancer (typically Gleason 8-10) are not generally considered for focal therapy. Therefore, the final group with intermediate risk prostate cancer would be the most probable candidates for LTP therapy. These patients are likely to have a predicted life expectancy of more than five years, with no detection of locally advanced disease using imaging technologies (clinical stage T2a or lower) [91, 289]. Their cancer is likely to be Gleason 7 (although some localised cancer could be Gleason grade 8) and their PSA should be low (less than 10-20 ng/ml). The other consideration for treatment is whether the tumour is unifocal or multifocal. 3D mapping of biopsies should assist in identification of the location, number and size of tumour foci [290]. Ultimately, such a focal therapy treatment is a good option for patients who do not like the uncertainty of watchful waiting but do not want to suffer the side effects of aggressive overtreatment for a low risk cancer. If radical prostatectomy was unavoidable, LTP could conceivably also be applied to destroy any tumour cells released during surgery, or to treat potentially positive surgical margins.

Gas cylinder

Gas Massflow controller

0.200

HV power supply

Gas flow

Monitor for TRUS probe

LTP device

High voltage electrodes

Direction of plasma propagation
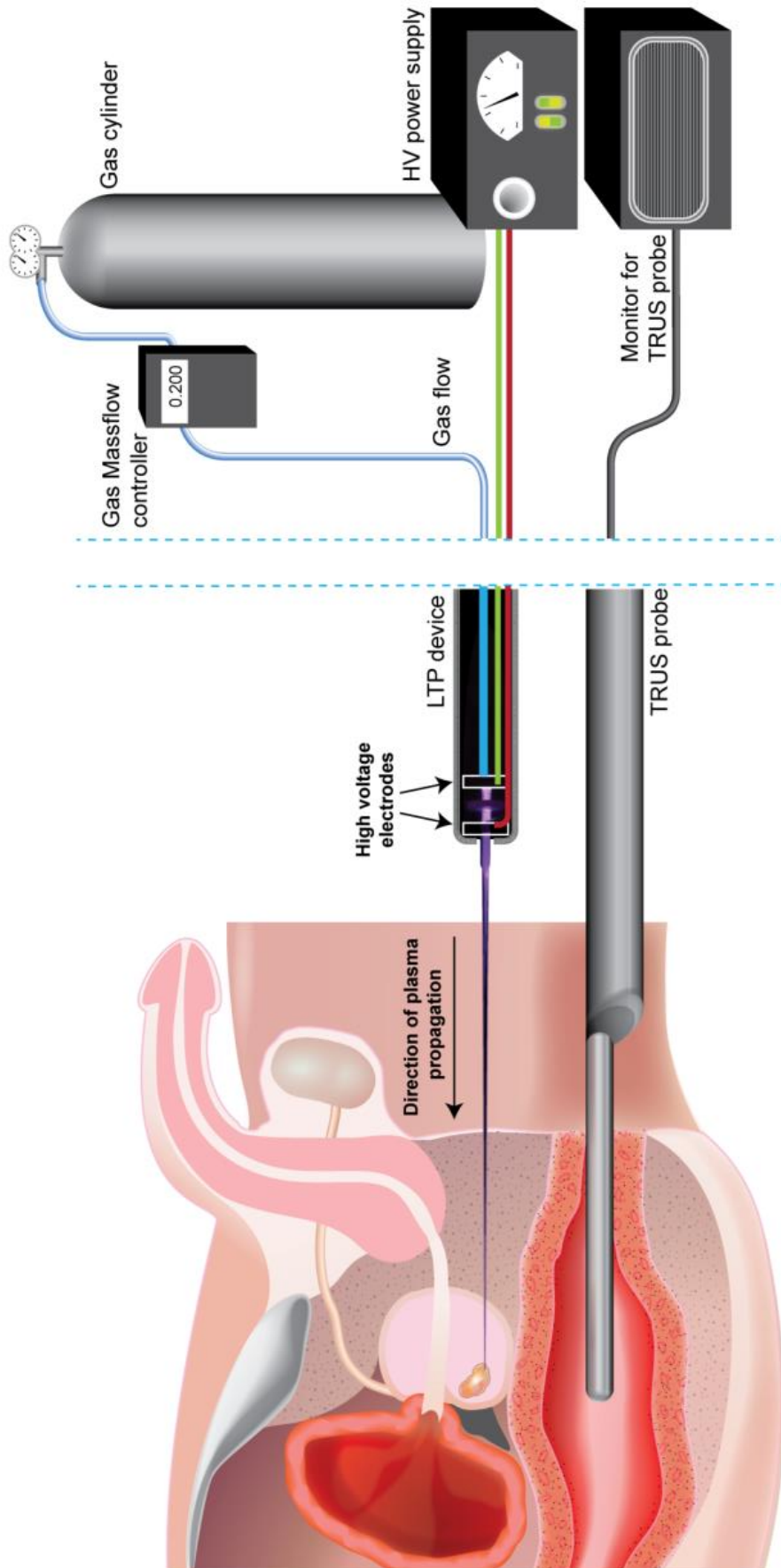
TRUS probe

**Figure 54: Proposed treatment approach for LTP treatment of localised prostate cancer.**

The LTP device is administered transperineally to an organ confined prostate tumour. Supporting image guidance from a TRUS probe, along with high-voltage (HV) power supply and gas flow-rate control are shown. This figure is reproduced from Hirst et al. 2014 [114], under a Creative Commons 3.0 License (*http://creativecommons.org/licenses/by/3.0/*).

Much of the current literature concerns the propagation of the plasma effluent in air before contact with a liquid interface; however, the treatment of a tumour within a tissue would require the sustainment of an active plasma within a relatively liquid environment. Clearly, the degree of relative moisture within the tumour environment will play a defining role in the plasma propagation and chemistry, and is likely to vary from tumour to tumour. Martini et al. showed that OH radical production varied by up to a factor-of-two when water admixtures up to ~ 0.5% were fed directly through a DBD plasma [291]. This shows how sensitive the plasma chemistry is even to small deviations in the liquid environment. Concentrations of other reactive oxygen species, including $H_2O_2$ and $O_2^-$, have been shown to be strongly dependent on the humidity of the feed gas [187]. Delivery of the plasma to areas that are potentially difficult to access, and penetration inside the tumour are two of the main technical hurdles with the proposition of internal LTP treatment; nevertheless evidence within the literature, and also this thesis, suggests both could be overcome. As mentioned previously, the preliminary findings presented in Chapter 7 demonstrated that DBD plasma could be sustained and propagated in a thin glass tube. A biocompatible plastic would ultimately need to be used for patient application. It is possible to propagate plasmas along tubes which are metres in length [292], thus precise LTP-delivery even to tumours deep within the body should be possible in principle. If necessary, LTPs can be propagated in narrower tubes than that shown in Figure 54. In shorter tubes, plasmas have been sustained in tubes as small as ~ 10 μm in diameter [146].

Given the length of tubing required for internal treatment of the prostate, the inherently short lifetimes of the most reactive (and thus likely most damaging) species may curtail their journey from source to target. However, provided an active plasma emerges from the end of the tube where electrons are present, as shown in this study,

short-lived species will be created locally at the application site. Regardless, a rigorous knowledge of the RONS densities emerging from the specific aperture used for application is essential. It has recently been suggested that control and selectivity towards different reactive species may be achievable by using different feed gases [293]. Combinations of molecular oxygen and nitrogen could create a chemistry containing ROS and RNS to which tumours may be indefensible. This should provide advantages over radiotherapy and PDT, which only induce ROS production [55, 84]. Maximal lethality of treatment is likely to be found by tuning combinations of the plasma operating conditions including voltage waveform parameters, gas composition, and treatment duration [62]. Owing to time-limitations, an optimal parameter range for plasma-operation was not identified during this study.

The most successful method of realising an effective, focal and minimally invasive surgical approach is likely to be penetration of the plasma into the tumour core, to destroy the cancer radially outwards. This is illustrated in Figure 55, which also highlights the potentially multi-faceted action of LTP treatment of a bulk tumour. Short-lived reactive species (red dots) interact with cells in the centre of the tumour, or may recombine to form longer-lived species (blue dots) which diffuse towards the tumour periphery. Cells in the immediate vicinity of the plasma effluent are likely to rapidly undergo necrosis, and may experience strong electroporative effects due to the strong instantaneous fields produced by plasma streamers. Cell death mechanisms may be dependent on the plasma composition (related to the different experimental parameters outlined in the previous paragraph), in addition to potential synergies with local electric fields.

Electroporation

DNA damage

Cell to cell communication

Apoptosis

Necrosis

Autophagy
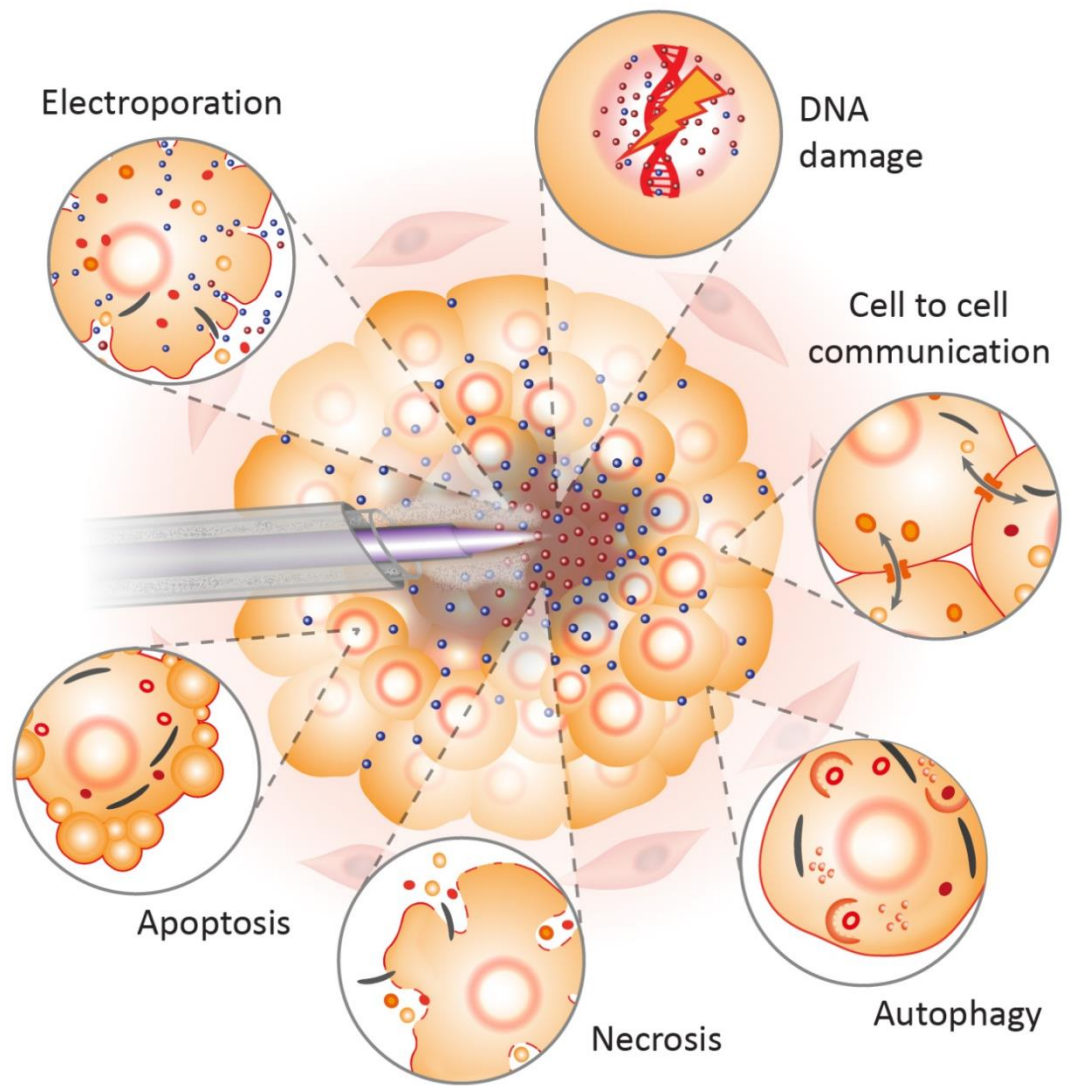
**Figure 55: Illustration of LTP treatment of a tumour.**

In the proposed approach, the LTP probe is inserted under needle guidance into the core of the tumour. The plasma is then ignited, creating short-lived reactive species (red dots) that induce DNA damage, necrosis and potentially electroporative effects to cells in the immediate vicinity. The diffusion of longer-lived species (blue dots) to the periphery tumour is shown, contributing to apoptotic and plasma-induced bystander effects. Proposed cellular effects and responses are estimated based on their proximity to the plasma source. Gas extraction is also indicated through a co-axial configuration in the LTP probe. This figure is re-produced from Hirst et al. 2016 [183] under a Creative Commons 4.0 License (*http://creativecommons.org/licenses/by/4.0/*).

Direct insertion of LTP into the core of a tumour may have implications in the context of tumour hypoxia, which has been identified as a key factor in radio- and chemo-therapeutic resistance and tumour invasiveness [294-296]. Whilst direct DNA damage is inflicted by energetic particles, secondary damage following radiotherapy is caused by the production of oxygen radicals from the interaction of ionising X-rays and molecular $O_2$ in tissues and the local environment. As a result, in oxygen-deficient regions of the tumour, lethal DNA damage may not be achieved [297]. The majority of LTP-cancer studies feed small admixtures of molecular oxygen (or nitrogen) into the main gas flow to aid the production of oxidative (and nitrosative) radicals. As such, LTP treatment could provide oxygen radicals directly to the treatment site, circumventing the need for endogenous $O_2$ in the tissue (as with radiotherapy), which may help to surmount the issue of hypoxic resistance.

Cancer stem cells (CSCs) have been proposed to be the root of both disease initiation [6] and recurrence [298]. They have been widely implicated in both radio- and chemo-resistance [299-302]. One reason for this may be higher levels of heterochromatin in CSCs compared to the bulk population; affording added protection against DNA damaging treatments [303]. It is also thought that CSCs have higher levels of ROS-quenching enzymes in order to alleviate toxicity effects from reactive species formation [304] more effectively than their differentiated counterparts. Overloading the CSC population with an abundance of RONS generated by LTPs may overcome this protective shield. Data showing that LTP-treatment of primary prostate CSCs induces high levels of DNA damage is presented in Appendix C.

Direct and uniform exposure of all cells within a bulk tumour population to LTP treatment would be extremely technically challenging. However, it is conceivable that cell-to-cell communication will play a role in LTP treatment of a tumour. Radiation-

induced bystander effects (RIBEs) are well documented following DNA damage events and elevation of ROS levels in irradiated cells. These lead to extracellular stress-signalling through cytokines to neighbouring non-irradiated cells, which can trigger increases in ROS production and cell death [305]. Given that LTPs are known to inflict comparable initial cytotoxic effects on tumour cells, it would therefore seem logical to anticipate a similar plasma-induced bystander effect following LTP treatment [306]. Cells located towards the outer edge of a tumour may undergo apoptosis via the bystander effect through cell-cell communication mechanisms, as indicated in Figure 55. Although many tumours are multi-focal, it has been argued that targeted treatment to only the index lesion of a localised tumour is sufficient to provide satisfactory disease control [81]. This would also limit treatment invasiveness, as only one LTP probe would need to be inserted. Assuming the effects of LTP could propagate beyond a few cell layers (be it directly or via bystander effects); precisely monitored plasma ablation should also enable a satisfactory clearance zone to be achieved. This implies that damage to normal cells is not necessarily a negative feature, as a degree of collateral damage is a more favourable consequence than incomplete tumour ablation. It is unclear at this stage how plasma treatment of a tumour would be precisely monitored, but could involve a combination of TRUS and MRI.

The exact mechanism of plasma-induced cytopathic effects could prove crucial to the long-term success of any prospective anti-cancer treatment. Apoptotic cell death is potentially immunosuppressive and thus can assist immune system evasion of the tumour [307, 308]. However, in several pre-clinical studies addressing the combination of radio- and immuno-therapies to improve therapeutic potential [309], it has been shown that necrotic cell death can increase tumour immunogenicity through induction of heat shock protein expression [310]. As already discussed, necrosis is induced by

thermally ablative treatments such as cryotherapy [311] and HIFU [312], and is known to cause local inflammation at the treatment site. This study has conclusively demonstrated that LTP treatment of primary prostate cells results in high levels of necrosis. This speculatively raises the question of immune activation against the tumour following plasma application, and the possibility of spontaneous regression of metastatic tumours, as has been occasionally recorded following radiotherapy [313], radiofrequency ablation [314, 315] and cryotherapy [316]. Direct combination with immunotherapy may present further synergistic prospects, as has been shown for ionising radiation [317]. As a result, it may be argued that plasma-induced cell death via necrosis may provide the most effective long-term treatment outcome. Should this be the case, immune checkpoint inhibitors (such as nivolumab, which has very recently demonstrated efficacy in the treatment of advanced nonsquamous non-small-cell lung cancer and metastatic melanoma [318, 319]) could be combined with LTP treatment. These inhibitors restore immune targeting of tumour cells by preventing them from binding to and inactivating T-cells. Agents such as these may present an interesting prospect for future use in conjunction with LTP to boost tumour immunogenicity.

Finally, some form of gas flow extraction would almost certainly be necessary during treatment with LTP to minimise the risk of embolisms, and could be combined with cyclic LTP application. This is highlighted in Figure 55 where the plasma is inserted under needle guidance, and the gas extracted through co-axial configuration of the LTP probe. If it were possible to accurately monitor the increase in prostate volume during treatment, be it through ultrasound or MRI, then it would be plausible to apply LTP safely into the tumour. This would allow the clinician to apply LTP for extended time-periods, until the entire tumour volume had been successfully ablated.

## 8.5 Summary

This work has provided the first evidence showing the potential of LTPs as a novel prostate cancer therapy. High levels of DNA damage were recorded in both benign and malignant prostate cell lines, leading to reduced clonogenicity and both apoptotic and necrotic cell death. Elevated levels of $H_2O_2$ in the cell culture media following exposure to LTP was identified as a likely facilitator of cell response, and is also a strong indicator that plasma treatment resulted in the production of a range of short-lived radical species (for example OH and $O_2^-$) in the cellular environment. Use of specific reactive species scavengers would further cement these findings.

This study also presented the first data showing the effects of LTP on tumour cells derived directly from patient samples. Primary cells have been previously shown in our laboratory to display increased resistance to cytotoxic treatments when compared to prostate cell lines. However, LTP treatment resulted in highly comparable results in terms of DNA damage, cell viability reduction, and inhibition of colony forming capacity between cell lines and primary cells. However, unlike cell lines, only necrotic cell death was recorded following LTP treatment of primary cells. This highlights the importance of studying clinically relevant cell models in order to gain insight into potential patient response. It would be crucial to understand how and why a proportion of cells survive LTP treatment, and if these cells could be sensitised through pre-treatment with drugs or inhibitors. In addition, the first evidence of an autophagic response following LTP treatment of primary cells was documented, which may act as a stress-induced survival mechanism for those cells that do not immediately undergo cell death.

Finally, evidence that LTP induces cytotoxic and cytopathic effects in 3D prostate model structures was presented, along with a potential LTP-treatment patient delivery

strategy. Further investigation is now required to develop and characterise the clinically applicable plasma device presented at the end of this study, and to test its effectiveness in 3D cell, tissue and *in vivo* models. The mechanism of cell death in 3D structures needs to be identified, in addition to the radial distance that reactive species produced at the plasma source can cause cellular effects. The behaviour of the gas flow within a solid mass needs to be understood and controlled or a method for extracting it devised. This would truly verify the potential of LTP as a future focal therapy for localised prostate cancer.

# Appendix A
## Reference Table of Primary Cells Used in This Study

| | Age at Diagnosis | PSA (ng/ml) | Gleason Grade | Cores Positive for PCa | | Tumour Palpable? |
|---|---|---|---|---|---|---|
| **Patient 1** | 52 | 5.0 | 3 + 4 = 7 | Normal | 0/5 | Yes |
| | | | | PCa | 3/5 | |
| **Patient 2** | 68 | 6.9 | 4 + 3 = 7 | Normal | 0/6 | Yes |
| | | | | PCa | 4/4 | |
| **Patient 3** | 64 | 8.2 | 4 + 3 = 7 | Normal | 0/5 | Yes |
| | | | | PCa | 4/5 | |

**Table 6. Patient information for the primary cell samples used in this study.**

# Appendix B
## Preliminary Study to Unravel the Multiphase Action of LTP

# B. Preliminary Study to Unravel the Multiphase Action of LTP

The data included in this appendix chapter form the beginning of a fundamental study to unravel and correlate the cellular effects of different reactive species produced by a reference plasma jet through indirect treatment of cell culture media. The source used was a capacitively coupled plasma (CCP) excited at radiofrequency (RF), and as such these results fall outside of the main study presented in this thesis.

## B.1. The Radiofrequency Plasma Jet

The micro-scaled atmospheric pressure plasma jet (μ-APPJ) used in these experiments is an iterative development of an earlier design by Schultz von-der Gathen et al. [320, 321], for biological applications and diagnostic purposes. This μ-APPJ forms part of an EU COST action, which is in progress to produce a standardised reference source, such that direct data comparisons are possible across institutions. The μ-APPJ consisted of two stainless steel parallel electrodes, separated by a 1 mm$^2$ channel. One electrode was powered at a frequency of 13.56 MHz, and the other grounded as shown in Figure 56 [172]. The plasma was ignited using an RF power generator and matching unit (Coaxial Power). The outer ends of the two electrodes are chamfered to permit easier access to cell culture plates for biological treatments. Voltage measurements were obtained using a high voltage probe (LeCroy PMK-14KVAC) and an oscilloscope (LeCroy Teledyne HDO6054), connected to the output socket of the matching unit. Helium was used as a carrier gas at 1 standard litre per minute (SLM), fed with an incremental range of molecular oxygen admixtures from 0-10 standard cubic centimetres per minute (SCCM), i.e. 0-10% of the total gas flow.

Using two calibrated mass flow controllers (Analyt GFC17), the gas admixture was fed into the top of the discharge channel.
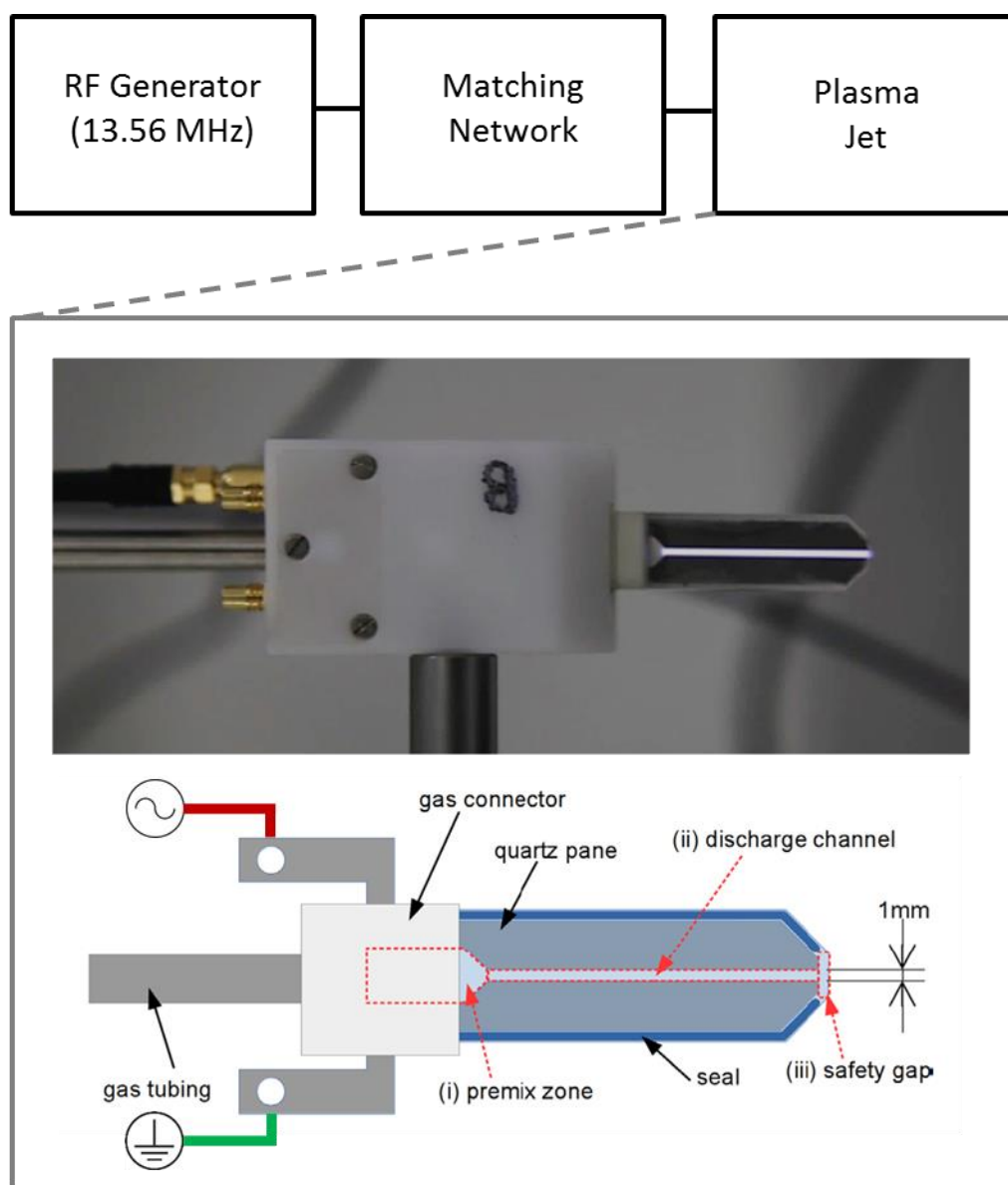


**Figure 56: Schematic of the μ-APPJ.**

Illustration of the μ-APPJ including RF generator and matching network. The powered and grounded electrodes are indicated, and gas flows from left-to-right. In the accompanying photograph, plasma is visible in the discharge channel between the electrodes. Elements of this figure are adapted from Golda et al. [172], under a Creative Commons 3.0 License (*http://creativecommons.org/licenses/by/3.0/*).

## B.2. Indirect Treatment of Cells Following Treatment of Cell Culture Media

The μ-APPJ was used to treat cell-free culture media (henceforth referred to as plasma treated media, PTM), which was subsequently added to adherent cells. P4E6 Cells were plated in 96-well plates at a density of 5000 cells in 100 μl of media the day before treatment. A 5 ml volume of culture media was added to a 6 cm dish (Corning) and treated under the μ-APPJ for 6 minutes under gentle mixing using an orbital mixer. The distance between the media surface and the discharge nozzle was maintained at 3 mm. Evaporation of the media was found to be negligible.

Figure 57 shows the plate layout used in PTM experiments. Following 6 minutes treatment with μ-APPJ, 150 μl of neat PTM was added directly to cells in column 3 of the plate, referred to in Figure 60 as PTM 1:0. Into column 4 of the plate, 150 μl of PTM was added to the 150 μl of existing cell culture media, resulting in a 1:1 dilution, and a total well volume of 300 μl. This was the subsequently serially diluted across the plate, until column 10 contained only a 1:32 dilution of PTM. Columns 2 and 11 contained untreated P4E6 cells, and 250 μM $H_2O_2$ was added to column 3 as a positive cytotoxic control. The outer wells of the plate contained 150 μl of untreated media as a control. At 72 hours after treatment, the cell viability was assessed by alamarBlue assay against normalised untreated control wells, and plotted in Figure 58.
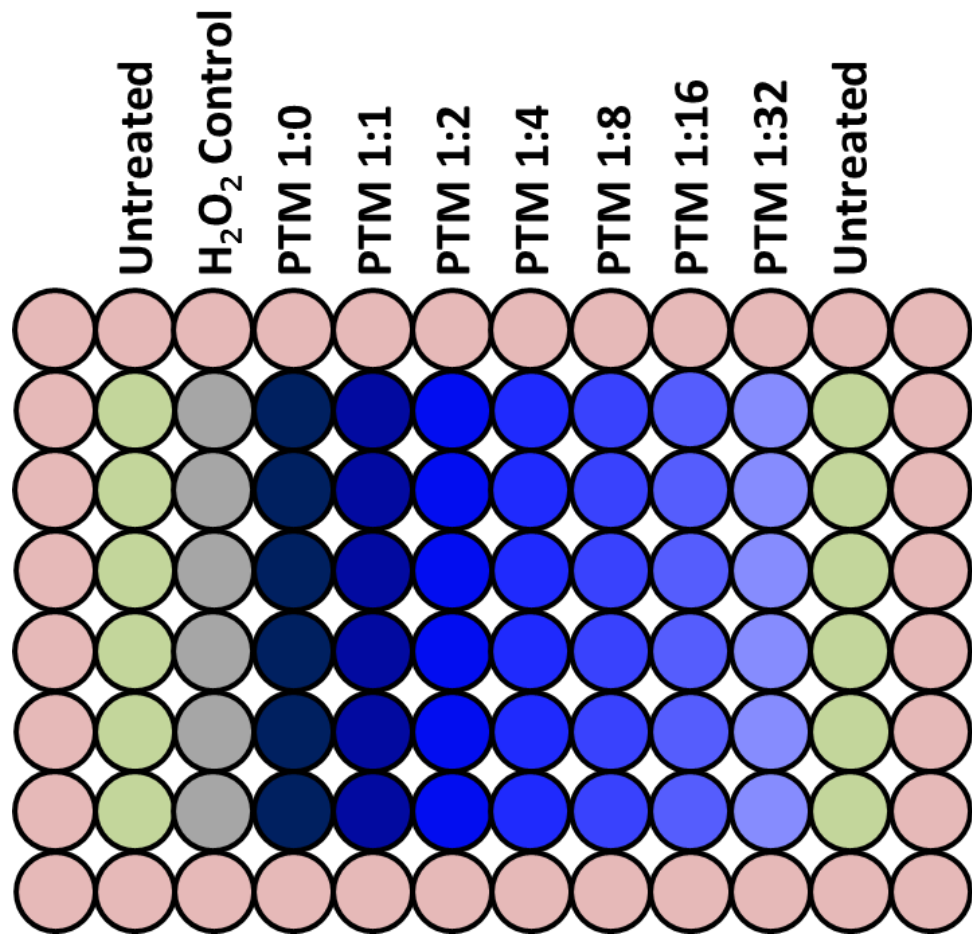
**Figure 57: Layout of 96-well plate for PTM serial dilution**.

Following treatment with μ-APPJ, PTM was added to column 4 of the culture plate and serially diluted. Columns 2 and 11 were untreated control wells, and 250 μM $H_2O_2$ was added to column 3 as a positive control. The outer wells were filled with culture media only, as a blank control.
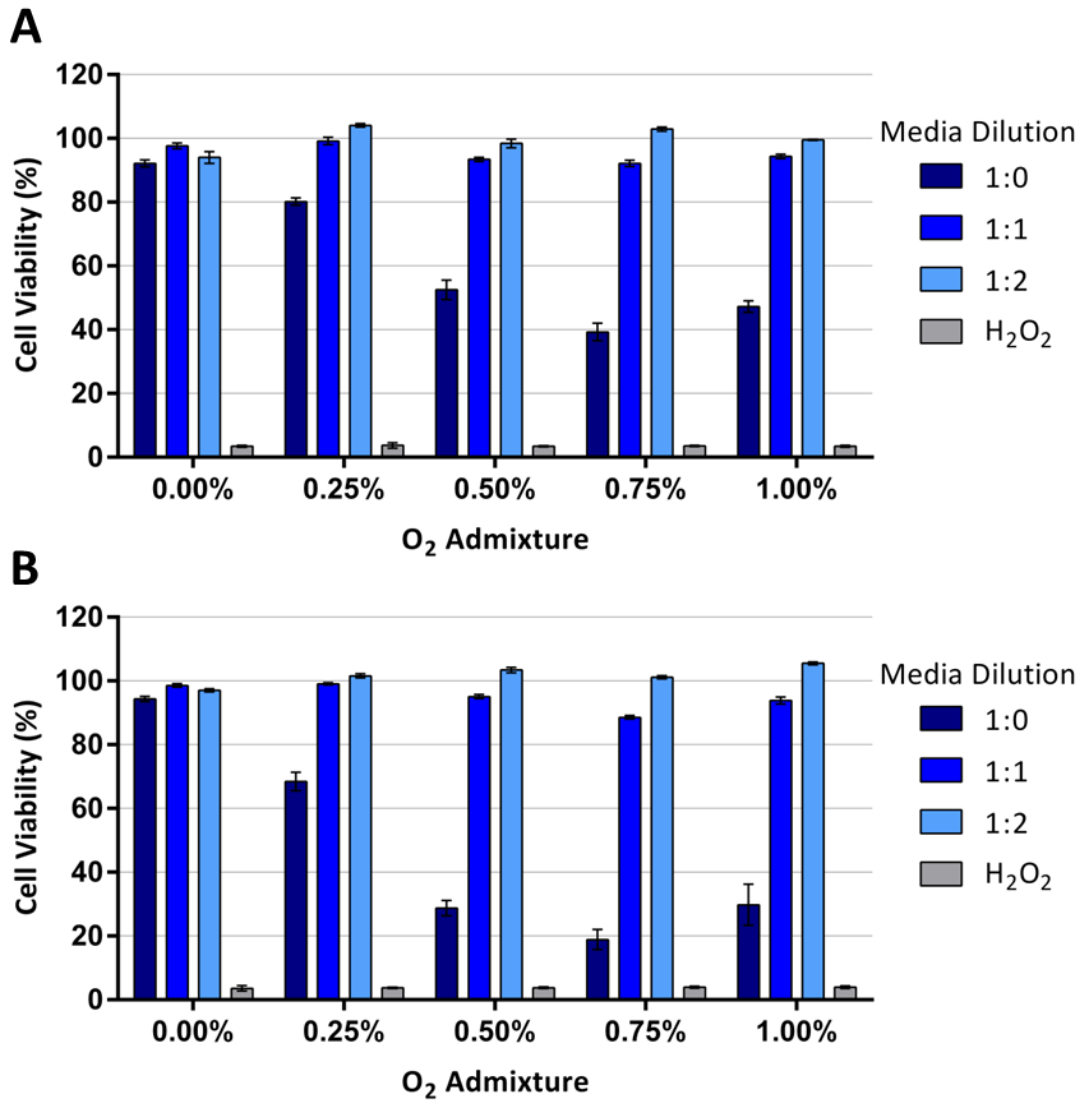
**Figure 58: Viability of P4E6 cells following PTM treatment.**

Culture media was treated with µ-APPJ for 6 minutes, added to cells and serially diluted. $H_2O_2$ (250 µM) was used as a positive control. At 72 hours after treatment, cell viability was analysed using the alamarBlue assay. Viability levels are normalised to untreated control samples, and data are expressed as mean ± standard error. **A** and **B** represent two independent experiments.

### B.3. Reduction in Cell Viability is Dependent upon Oxygen Admixture

Two independent experiments were performed to assess P4E6 cell viability following exposure to PTM, which are shown in Figure 58A and B. This project aims to ultimately investigate the role different plasma-produced reactive species play in cell response. As such, P4E6 cells were selected for these experiments based on the low serum content of their culture media, the significance of which was discussed earlier.

In both experiments, it became clear that diluting the PTM by more than 1:2 had no effect on cell viability, and as such these values are not plotted in Figure 58. It was found that a pure helium treatment did not reduce cell viability in either experiment. However, adding increasing levels of $O_2$ into the gas flow progressively reduced cell viability up to 0.75% $O_2$ admixture. At higher admixtures, the viability increased, with 0.5% and 1% $O_2$ producing similar reductions in viability. Figure 58B shows an overall greater reduction in viability than Figure 58A, and thus a third experiment is required in order to produce an averaged result. However, both graphs show an identical trend with respect to $O_2$ admixture. The results correlate with laser spectroscopy data by Knake et al. [322], who showed a maximum in atomic oxygen density at 0.5 - 0.75% $O_2$ admixtures for the same plasma source.

Future work could include narrowing the $O_2$ range to between $0.5 - 1.0\%$, with 0.1% increments, to determine the most effective admixture. The Celltox green and Caspase-glo 3/7 assays already presented in this thesis could be multiplexed to gain insight into the mechanism of cell death following exposure to PTM. Once an optimal $O_2$ admixture had been determined, liquid phase chemistry analysis would provide detailed information on the concentrations of different reactive species created in the cell culture media. Finally, the experimental data could be combined with numerical simulations of

the RF plasma core. This would help to correlate the different interfaces illustrated in Figure 12; the species created in the core plasma at different $O_2$ admixtures could be compared to those that are present in the culture media, and are responsible for cytopathic cellular effects.

# Appendix C
**Publications Relating to This Work**

*Review Article*

# Low Temperature Plasma: A Novel Focal Therapy for Localized Prostate Cancer?

## Adam M. Hirst,[1] Fiona M. Frame,[2] Norman J. Maitland,[2] and Deborah O'Connell[1]

[1] *Department of Physics, York Plasma Institute, University of York, Heslington, York YO10 5DD, UK*
[2] *YCR Cancer Research Unit, Department of Biology, University of York, Heslington, York YO10 5DD, UK*

Correspondence should be addressed to Norman J. Maitland; njm9@york.ac.uk

Despite considerable advances in recent years for the focal treatment of localized prostate cancer, high recurrence rates and detrimental side effects are still a cause for concern. In this review, we compare current focal therapies to a potentially novel approach for the treatment of early onset prostate cancer: low temperature plasma. The rapidly evolving plasma technology has the potential to deliver a wide range of promising medical applications via the delivery of plasma-induced reactive oxygen and nitrogen species. Studies assessing the effect of low temperature plasma on cell lines and xenografts have demonstrated DNA damage leading to apoptosis and reduction in cell viability. However, there have been no studies on prostate cancer, which is an obvious candidate for this novel therapy. We present here the potential of low temperature plasma as a focal therapy for prostate cancer.

## 1. Introduction

Prostate cancer is now recognised as the second most diagnosed cancer overall and accounts for around a quarter of all cancers in males [1]. The risk of prostate cancer peaks in men over 60 years of age, yet high incidence rates are also found in younger aged groups [2]. In addition, benign enlargement of the prostate becomes increasingly common in men over the age of 40 and particularly so beyond 60 years of age [3].

Treatment for advanced prostate cancer is still unsatisfactory, with an almost inevitable development of hormone resistance [4]. Even new generation androgen ablation drugs fail to deliver a life extension beyond several months [5]. In addition, there is poor response to chemotherapy, alongside unpleasant side effects, and reduced quality of life [6]. Therefore, the emphasis remains to detect and treat prostate cancer at an early stage to have most hope of a cure. Indeed, early diagnosis has become more common with increased uptake of PSA testing [7, 8].

Once prostate cancer is diagnosed, the clinician is presented with a series of dilemmas; firstly, is the tumour localized or has it spread [9]; second, if localized is it potentially aggressive or indolent [10]; and the third, should the patient undergo active surveillance or be treated immediately [11]. If the latter is chosen in the context of a localized tumour, then the next decision is between radical surgery with the risk of incontinence and impotence, radiotherapy, or treatment with a focal therapy [12]. Radical surgery has the potential to be an overtreatment in early-onset or low-risk disease [13], where active surveillance or treatment with a focal therapy may be more suitable [14]. Ideally, focal therapy is targeted to maximize elimination of the tumour foci without treating the whole gland, while minimizing side effects [15, 16]. This review aims to evaluate several currently available focal therapies for prostate cancer and introduces a potential focal treatment in the form of low temperature plasma (LTP). Application of LTPs to internal organs such as the prostate may seem technically difficult but could offer many advantages over current treatments.

## 2. Approaches to Focal Therapy of Localized Prostate Cancer

For patients to be considered as candidates for focal therapy, their prostate cancer must be present in only one lobe, typically unifocal, and contained within the prostate capsule [17]. However, no absolute ideal patient selection criteria exist

for focal prostate treatment [18]. In the following subsections, some focal therapies for localized prostate cancer are briefly analyzed, with their respective advantages and pitfalls outlined for comparison. In addition, the importance of imaging techniques in the context of focal therapy treatments is also discussed.

### 2.1. High-Intensity Focused Ultrasound.

The concept of high-intensity focused ultrasound (HIFU) was first applied in the 1980s to benign prostate hyperplasia (BPH) [19], with the first recorded application to localized prostate cancer in 1995 [20]. The physical mechanism of HIFU follows the same principles as diagnostic ultrasound, whereby ultrasonic waves pass through healthy tissues without causing harm. However, if the ultrasonic beam is sufficiently focused and the intensity increased, high levels of energy can be delivered to very localized regions [7]. These high levels of energy are capable of causing irreversible damage to the targeted tissue via hyperthermia mechanisms, either by heating or inertial cavitation [7, 21, 22]. In the case of thermal effects, energy delivered by the ultrasonic beam is absorbed by the treated area, leading to rapid heating effects, which can raise the temperature of the treated tissue to 80°C in a few seconds [23]. This instant heating leads to coagulative necrosis through protein denaturation [15, 24]. A recent study considered the treated area to have been successfully ablated once a minimum temperature of 65°C had been reached [25].

The typical devices used for HIFU treatment of the prostate are applied transrectally and so possess the advantage over other focal therapies in that an invasive surgical approach is not required. There are two devices currently available for HIFU: Sonablate and Ablatherm. Taking Sonablate as an example, the device utilizes a 4 MHz transducer which is capable of both treatment and imaging depending upon the intensity applied, with intensities of up to 2000 W cm$^{-2}$ achievable at focal lengths as short as 3 cm [26]. Due to the extremely high intensities involved in the procedure, there is a need for accurate monitoring of the energy delivery to, and resulting temperature of, the target tissue. In recent years, the effectiveness of real-time magnetic resonance imaging (MRI) has improved, such that it constitutes an invaluable tool for the monitoring of the HIFU procedure [25, 27].

The difficulty with treating enlarged prostates lies mainly in limitations on the focal length of the ultrasound probe [22, 28]. A transurethral resection of the prostate (TURP) procedure is recommended prior to treatment to reduce organ volume, as post-HIFU swelling of the prostate is common [8, 29]. The effective treatment of anterior prostate tumours is also problematic using HIFU, as anterior perirectal fat tissue can prevent intended penetration depth of the ultrasound beam [30]. This occurs due to reflection of the signal and is a particular problem if the patient is overweight [31].

### 2.2. Photo-Dynamic Therapy.

Photodynamic therapy (PDT) damages tissues in a highly localized fashion by exciting photosensitizing drugs with light. The drugs are administered either orally or intravenously, absorb energy from a light source, for example a laser, and transfer it to molecular oxygen residing in the surrounding tissues [32]. This in turn produces an activated form of molecular oxygen [33] known as singlet delta oxygen ($^1O_2$, SDO). It is believed that SDO is predominantly produced following the excitation of the sensitizing agent from its triplet ground state, upon irradiation from the light source [34]. SDO is highly toxic to cells and can interfere with cell signalling as well as inducing cellular stress [35–37]. Importantly, the photosensitizing process is recurrent, eliminating the need for repeated applications during delivery as a stream of SDO is produced [33]. In addition, PDT has the advantage of greater selectivity versus other cancer therapies, as only simultaneous exposure to the photosensitizing drug, light, and oxygen will result in a cytotoxic effect on the treated cells [34]. This selectivity can be further improved by the use of an antibody, applied in conjunction with the photosensitizer, which is specific to the tumour [38, 39].

PDT predominantly utilizes two approaches to damage cancerous tissue. Either tumour hypoxia can be induced following laser targeting of the blood supply to the tumour or an apoptotic/necrotic response can be initiated following direct targeting of the tumour surface itself [40]. It is necessary to protect the skin and eyes of the patient, even following treatment. Such protection may be required for a few hours up to several weeks, depending on the photosensitizer used [41], as the time each drug remains in the patient's bloodstream varies vastly. A transperineal approach allows treatment of tumours localized to anterior prostate [42], giving advantages over other treatment approaches such as HIFU (see Table 1), although this can still be problematic [7]. However, PDT has the advantage of being potentially applicable at the same treatment site multiple times [42], unlike for instance surgery or radiotherapy, in addition to being a potential salvage therapy following failure of these techniques [43].

### 2.3. Cryotherapy.

Rapid freezing and thawing cycles are employed by cryotherapy techniques in order to cause localized cellular destruction due to either the extremely low temperature alone, the rapid rate of cooling, or the period of time for which the tissue stays frozen [21]. Either liquid nitrogen or argon gas is administered to the prostate transperineally via cryoprobes under transrectal ultrasound (TRUS) guidance. Argon gas probes are now favoured over liquid nitrogen based approaches due their thinner diameters, permitting the insertion of additional probes (in a brachytherapy-like manner) to improve the efficacy of treatment [44]. In addition, the use of argon gas dramatically improves the freeze-thaw effect by reducing the probe tip to a temperature of −187°C, before 67°C helium gas rapidly thaws the treated region [44, 45], causing rupturing and bursting of the cells. Two cycles, reaching at least −40°C are required for complete cell death, with cell shrinkage and protein denaturation occurring as the tissue temperature decreases beyond 0°C [21]. A urethral warming catheter and multiple thermosensors are typically used to prevent freezing of unwanted regions [45, 46].

Cryotherapy can be applied as a salvage therapy, for example, after the failure of or recurrence following radio- and

TABLE 1: Pros and cons of focal therapies currently available for prostate cancer.

| Treatment | Summary of Pros | Summary of Cons |
| --- | --- | --- |
| High-intensity focused ultrasound | (i) Transrectal application negates the need for surgical approach<br>(ii) Improvements in MRI technology allow real-time procedure monitoring and improved targeting | (i) Difficulty treating enlarged prostates, especially in overweight patients<br>(ii) Effective treatment of anterior tumours is not achievable |
| Photodynamic therapy | (i) More selective than other focal therapies due to conditions needed for SDO production<br>(ii) Can be applied at the same treatment site multiple times | Photosensitizing agent remains in patient's bloodstream following treatment, requiring protection of the eyes and skin for potentially weeks after the procedure |
| Cryotherapy | (i) Double freeze-thaw cycle effectively destroys cells in targeted region<br>(ii) Can be applied as a salvage following radiotherapy techniques | (i) Urinary infections and perineal discomfort posttreatment are common<br>(ii) Relatively invasive treatment, with added needed for thermal protection of urethra, bladder and rectum |
| Radiotherapy | (i) Minimally invasive approach as radiation is usually applied externally<br>(ii) Proton beam therapy and Cyberknife technologies give hope of improved targeting with fewer side effects | (i) Many side effects as a result of radiation at unintended sites, causing urinary incontinence, rectal pain, and erectile dysfunction<br>(ii) A third of patients experience radiorecurrent disease |
| Brachytherapy | Image guided seed placement allows effective treatment of localized areas | Needle array application is a highly invasive process |

brachytherapy [47, 48]. Common side effects following cryotherapy include rectal or perineal discomfort [49] and urinary infections [50]. Major complications can include rectourethral fistula, although this is rare [45].

*2.4. Radiotherapy.* Whilst radiotherapy is not considered a focal therapy, variants such as Cyberknife and brachytherapy have the potential to be applied to more localized cancers and are discussed later in this section. It has long been known that ionizing radiation (IR) can lead to adverse effects on cells. Using this principle, effects include, but are not limited to DNA damage, cell cycle arrest, and ultimately cell death can be achieved through radiotherapy [51]. This is due to reactive oxygen species (ROS) formed from interactions with free radicals, produced as a result of multiple ionizations via the Compton effect [52]. Radical formation is believed to take place in discrete regions [51], with so-called "clustered" DNA damage necessary in order to produce a potentially lethal cellular effect [53, 54]. However, it has been shown that cancer stem cells (CSCs), which are thought to instigate cancerous growth [55], can be resistant to radiological techniques, as well as promoting cancer recurrence following treatment [56, 57]. Indeed, prostate stem-like cells in epithelial cultures derived from patient samples are more radioresistant than more differentiated cells, due to increased levels of heterochromatin conferring a protective effect [58].

Some studies have suggested that at least 74 Gy, and indeed upwards of 80 Gy [59], should be applied in the case of localized prostate cancer, as patients treated with less than 72 Gy have shown higher cancer recurrence rates [60]. The total dose is usually delivered in multiple smaller fractions of, for example, 2 Gy per day for 60 days, not including weekends [61]. Following treatment, patients may often experience side effects including but not limited to urinary incontinence, diarrhoea, and rectal discomfort. Urinary problems can persist or present at longer time periods following initial treatment, as well as erectile dysfunction [62, 63]. In addition, and most worryingly, a third of patients experience radiorecurrent disease [64].

Different techniques are available, whereby the radiation is either deposited externally or internally. For the external treatment of tumours, the most applied therapy is external beam radiotherapy (EBRT), where the cancerous area is treated by a focused beam of IR. This relies on precise beam alignment with the targeted area, in order to maximize treatment efficacy and minimize collateral damage to surrounding healthy tissue. Several variants of EBRT are being pursued and constantly developed, including three-dimensional conformal radiotherapy (3D-CRT) and intensity-modulated radiation therapy (IMRT), which aim to utilize improvements in imaging technology to satisfy the aforementioned criteria for most effective treatment [65].

Other approaches for the radiological treatment of prostate cancer exist, which rely on the underlying principles of IR, including proton beam therapy. Proton beam therapy has the advantage that protons deliver their energy at the end of the particle's path in the tissue compared to photons which deliver radiation along their path in the tissue [66]. The focal nature of the energy delivery in proton beam therapy could in theory mean that untargeted areas are left unharmed [67]. However, a recent study indicated that damage to irradiated tissues outside of the target area is less severe following IMRT [68], in addition to being of lower cost than proton beam therapy. As such, questions still remain as to the efficacy and effectiveness of proton beam therapy as a focal technique.

Another recent development, which seeks to improve localization of radiotherapy compared to EBRT, is hypofractionated stereotactic body radiation therapy (SBRT) via the Cyberknife linear accelerator machine. A unique feature of prostate cancer is its low "$\alpha/\beta$ ratio," which represents nonrepairable versus repairable cellular damage,respectively, with the $\alpha$-term linearly dependent on administered dose and the $\beta$-term to its square [69]. For this reason several studies have suggested that hypofractionated radiation doses may result in more effective treatment of localized tumours [69–72]. During Cyberknife SBRT movement of the prostate is detected and automatically corrected for during the procedure by the robotic arm [73], enabling delivery of the radiation to be directed within 2 mm of the target area [74]. This enables the Cyberknife to deliver a hypofractionated radiation dose more accurately and noninvasively to the tumour [73] than conventional EBRT. Another major advantage of SBRT over EBRT is that treatments are usually delivered over a few days rather than weeks, rendering posttreatment hospitalization unnecessary [73]. However, SBRT treatment results in similar side-effects to those experienced following conventional radiotherapy. Rectal and urinary complications have been reported, in addition to erectile dysfunction [70], although the levels of these have been proposed as within acceptable limits [75]. In addition, the cost of Cyberknife technology is more expensive than other radiological techniques, at least in terms of initial outlay [72], although this is yet to be thoroughly investigated.

An increasingly common approach for treating prostate cancer internally is brachytherapy, which uses radioisotopes such as ^{125}I, [103]Pd, and [131]Cs and is typically applied in order to ablate the whole prostate gland [76]. The radioisotopes, with half-lives ranging from ~10–60 days [76] are delivered to the prostate as seeds through a matrix of narrow diameter needles inserted transperineally. Brachytherapy can either be used as a stand-alone treatment, in conjunction with radiotherapy or radical prostatectomy, or as a salvage treatment following EBRT [77].

A more recent development of brachytherapy is known as high dose rate (HDR) brachytherapy with [192]Ir [76], which provides a boosted dose of radiation following EBRT [78]. If administered in conjunction with utilizing imaging tools such as MRI or TRUS, radioactive seeds may be delivered to the targeted area more accurately, providing a case for HDR brachytherapy as a focal therapy [79].

*2.5. Imaging: An Integral Part of Focal Therapy.* All focal therapies for prostate cancer rely on accurate imaging to have maximum effect [79]. Imaging techniques are constantly advancing and are used for initial detection, determination of tumour location, staging of tumour, assessment of tumour aggressiveness, and detection of recurrences as well as identifying metastases [80, 81]. In the context of administration of focal therapies, early detection is most critical. Since the widespread uptake of the PSA test, early detection has become more common [79].

The kinds of imaging used in prostate cancer detection, diagnosis, and treatment are TRUS to enable targeted biopsies; MRI for accurate imaging of soft tissue; positron emission tomography (PET) for detecting lymph node metastasis and bone scans; and X-rays and computerized tomography (CT) scans to assess bone metastases. To detect localized prostate cancer, TRUS and MRI are by far the most used and most useful scans.

TRUS was traditionally used to allow biopsies from predetermined sites in the prostate, following an abnormal digital rectal examination (DRE) and increased PSA, and not as a method to identify precise locations of tumour foci [82]. However, improvements to the technique, including contrast-enhanced ultrasound using microbubble contrast media, elastography to measure tissue stiffness, and Doppler ultrasound to measure blood flow, can result in more targeted biopsies, leading to improved detection and diagnosis [83, 84]. TRUS can distinguish between an outer and inner gland encompassing the central, peripheral, and transition zones, though not at the same resolution as MRI [82].

MRI is highly sensitive and is the dominant imaging modality used for focal treatment [85, 86]. To undertake standard MRI, endorectal and pelvic phase-arrayed coils are used in conjunction to improve positioning of the prostate and to receive MR signals, respectively, resulting in clearer images with optimal signal-to-noise ratio [79]. The prostate zones are clearly visualized using MRI [87]. However, standard MRI is not accurate enough to determine precise location and diagnosis, where multiparametric MRI is required [88]. This includes diffusion-weighted imaging (DWI-MRI) that measures water diffusivity, dynamic contrast enhanced (DCE-MRI), making use of a contrast agent, and proton magnetic resonance spectroscopic imaging (H MRSI) that measures metabolites (citrate, choline, creatine, and polyamines), the ratios of which change between normal and cancerous prostate [89]. The technology to allow real-time MRI-guided biopsy has also advanced, and it is conceivable that this would be the ultimate method used when administering any focal therapy, including low temperature plasma-based treatment [88, 90–92].

In order for the more sophisticated imaging procedures to become routine, there has to be access to specialized equipment and personnel (e.g., magnetic resonance physicists), which both contribute to the potentially prohibitive expense [93]. To confidently choose focal therapy as a treatment option, patients and clinicians alike have to be convinced of its effectiveness. Imaging technology and both present and future focal therapy procedures therefore need to evolve in tandem to assure focal tumour ablation.

# 3. Low-Temperature Plasmas and Their Use in Biomedicine

Low temperature plasmas are emerging as an exciting development for therapeutics. The unique properties of cold nonequilibrium plasmas have enormous potential in disease therapeutics and plasma pharmacology as drug alternatives. Applications of these plasmas range from surface sterilization and bacterial decontamination [94–99], biofilm inactivation [100–102], antimicrobial treatment in food preservation
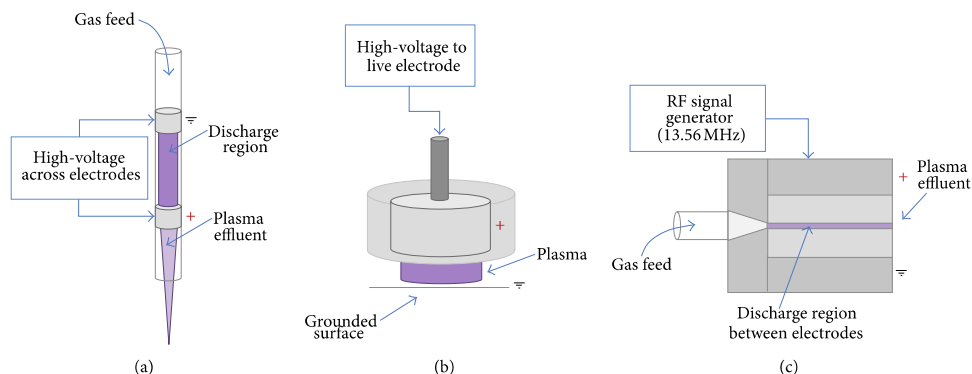
Figure 1: Examples of different plasma devices for medical applications. Linear-field plasma jets: (a) dielectric barrier discharge jet configuration (DBD), (b) floating-electrode DBD (FE-DBD), and cross-field plasma jets (c) radiofrequency (RF).

[103–105], and wound healing [106, 107], to cancer treatment [108–111]. This rapidly growing field of "plasma medicine" has emerged over the last 5–10 years and offers great potential, bringing together multidisciplinary branches of science and engineering.

Nonequilibrium plasmas, operated at ambient atmospheric pressure and temperature, are very efficient sources for the production of highly reactive neutral particles, for example, reactive oxygen and nitrogen species (RONS) (such as atomic oxygen [112–114], atomic nitrogen [115], hydroxyl radical, superoxide, singlet delta oxygen, and nitrogen oxides), charged particles, UV-radiation, and electromagnetic fields. Individually, many of these components have been implicated in therapeutics. RONS are known to play a crucial role in biological systems, such as signalling and generating oxidative damage to a variety of cellular components, which can ultimately lead to cell death [116–119]. Graves presents a comprehensive review summary on the role of RONS of relevance for plasma applications in biology [120]. Plasmas have the advantage of delivering these *simultaneously*, providing potentially superior processes. The role of these plasma components, even individually, is to date not fully known and is a topic of current research. It can be anticipated that, similar to low pressure plasma processes, in for example, plasma etching or plasma deposition, synergistic mechanisms govern the plasma surface interface rather than the individual species themselves.

*3.1. Methods of Plasma Formation and Production of Reactive Species.* The low temperature plasma environment is actually quite remarkable. Plasmas are formed by applying a sufficiently high electric field across a region of gas such that electrons are stripped off atoms and breakdown of the gas occurs. These free electrons in the background gas are accelerated by the applied field and collide with ions and neutral gas molecules through various processes, which are discussed below. An important feature is that the electrons are not in thermodynamic equilibrium with the background

gas due to the largely different masses (light electrons, heavy atoms, and molecules). The background gas is the dominating constituent and is at room temperature, while the electrons are hotter and can drive a unique reactive environment. Ions and electrons can be created through ionization, and processes such as excitation and dissociation of the background gas result in, for example, formation of metastable particles, reactive species, radicals, and also radiation. These plasmas essentially create an otherwise impossible dry, chemically reactive environment at room temperature. Until recently, atmospheric pressure plasmas have been unstable and low temperature plasmas have conventionally been operated under lower gas pressure conditions. While this approach has proven extremely beneficial, for example, in the multibillion dollar semiconductor industry, it is limiting with regard to broader exploitation of nonvacuum compatible materials. Through the use of gas flow it is now possible to sustain stable, controllable plasmas at atmospheric pressure. Reactive species can be brought from the main plasma production region, transporting energy to a surface. Here, two distinctly different plasma sources, with varying degrees of reactivity will be discussed.

Various devices are available for the formation and delivery of plasma [120–124] which rely on broadly the same principles. One variant is the dielectric barrier discharge (DBD) configuration plasma jet (Figure 1(a)). Such plasmas are produced by feeding carrier gas (e.g., helium or argon) with small oxygen admixtures (around 0.5% is typical), across a high voltage kHz operated supply, typically 5–30 kV, generating a discharge between two electrodes of dielectric material. Using helium as a buffer gas provides a flexible parameter space for stable homogenous operation at cold gas temperatures. The resulting plasma plume self-propagates outwards, and as the dynamic high electric field is parallel to the direction of propagation, the jet contains reactive neutrals, charged particles, electric fields, and UV radiation (Figure 2). A variation of the DBD schematic is the floating electrode dielectric barrier discharge (FE-DBD) plasma (Figure 1(b)), which operates by using the surface
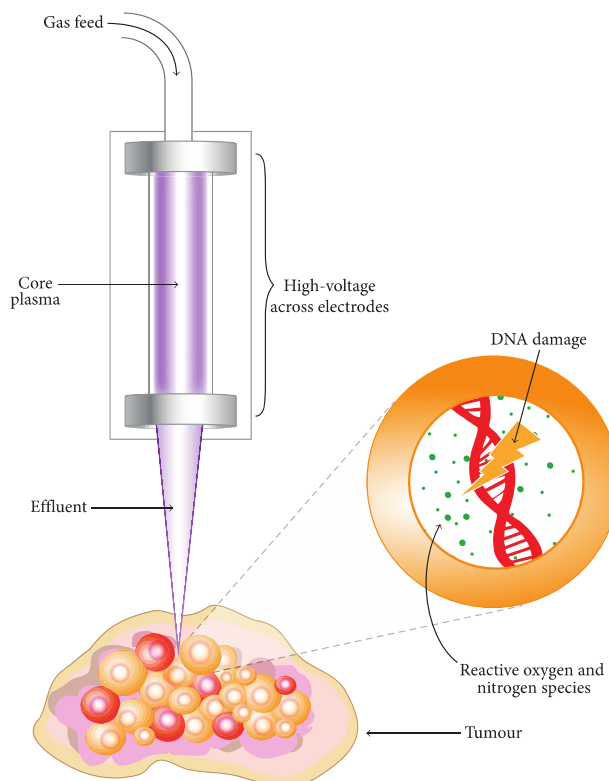
Figure 2: Illustrative diagram conveying the interaction of a DBD plasma jet with a cancerous tumour, leading to the induction of intracellular RONS, DNA damage, and resultant effects such as cell cycle arrest, cell death, and decreased viability.

to which it is applied as a floating counter electrode. This is possible provided that the surface has sufficient "charge storage" [94]. FE-DBD has even been applied to human skin without causing thermal damage or unwanted effects [125].

A third example of a plasma source arrangement is the radiofrequency (RF), or cross-field, plasma source (Figure 1(c)) which uses a 13.56 MHz RF signal as a means of gas excitation. This device utilizes plane-parallel electrodes, with a gas flow passing through the core plasma volume. This particular source, unlike the DBD plasma jet, possesses a charge-free effluent since the applied electric field is perpendicular to the direction of gas-travel, thus confining charged species to the core plasma region. Due to the high collision frequency at atmospheric pressure, the effluent is devoid of charge carriers and its characteristics are dominated by energy carrying reactive neutrals. The RF plasma jet is the most comprehensively studied LTP with respect to diagnostics and modelling [112, 115, 126–136] and is currently being developed into a reference source.

The transport of the plasma components to the targeted area is complex. In the core plasma region a large, but defined, number of species can be created (including O, N, NO, and $O_2^-$). As the plasma crosses the interface with ambient air, new reactions and components are formed. Upon interaction with either humidity or liquid layers on biological samples (Figure 2) new species with varying lifetimes can be created (OH, H, $H_2O_2$, and $ONOO^-$). Energy dissipation at these interfaces is important and to date unclear. Measurements and simulations under this atmospheric pressure environment are challenging, primarily due to the multiphase (solid, liquid, gas, and plasma), strongly nonequilibrium environment with large gradients (e.g., in electric field), high collisionality thus short-lived species and micron length scales. This requires the development of many new techniques for both measurements and models. The plasma chemistry can be deliberately manipulated or optimized for a desired result by fine alterations to gas admixtures or the electron energy distribution function (EEDF) [129, 137]. Despite the multitude of work that has been conducted to diagnose and characterize the RONS produced [126–128] in addition to the ionization processes and mechanisms that occur in LTPs, these are not yet comprehensively understood.

*3.2. Supporting Evidence for LTP as a Therapeutic Medical Device.* As already mentioned, the potential of LTPs has been explored in many different medical areas. One highly

active division of research is in the area of bacterial inactivation and surface sterilization. It has been shown that LTPs can damage the membranes of bacterial cells, through the interaction of reactive species, leading to the bactericidal effect [138]. Survival has been shown to be greatly reduced following LTP treatment, with a clearly defined voided region forming on the irradiated surface [139], suggesting that the interaction is mediated by short-lived reactive species [140, 141]. LTPs do not cause thermal or chemical damage to the treated surface, presenting an advantage over conventional sterilization techniques [140, 142]. Furthermore, LTPs have also been shown to be effective in the treatment of biofilms, minimizing bacterial formation posttreatment [101, 143] and greatly reducing cell viability even at short plasma-exposures [144]. These attributes give potential for applications in dentistry [145, 146].

Plasma-based bacterial inactivation has also been applied to the sterilization of chronic wounds in order to improve the rate of healing. This was shown in a recent phase II trial, which reported a significant reduction of bacterial load in the plasma treated area versus control [147, 148]. Crucially, plasma effects were localized, with no side effects (such as pain due to plasma application) reported. Another trial provided further agreement that LTP does not damage the surface of skin nor lead to dryness through exposure, with a view to antimicrobial applications [149]. It has also been found that when LTP was applied to surface wounds on the skin of mice, vastly improved blood coagulation and consequential accelerated healing resulted versus untreated wounds [106]. It was perceived that plasma-produced NO may be responsible for the improved wound response, which is in agreement with other work on NO as the key RONS in cell proliferation and wound healing [150–154]. Another study showed improved clotting of wounds on the surface of pig skin, in addition to establishing safe operating parameters for LTP exposure [107].

Despite LTPs being earmarked as a technology for future healthcare, plasmas have been used for a range of surgical applications in the field of electrosurgery since as long ago as 1991 [155, 156]. Though not technically a LTP, the argon plasma coagulator (APC) has been employed in various surgical disciplines for the purposes of tissue removal and wound cauterization [155] and is perceived as an improvement on existing laser-based techniques [157]. Recently, plasma vaporization has been applied to benign prostate hyperplasia (BPH), with the hope of reducing the common side effects of conventional transurethral resection of the prostate (TURP) procedures [158]. Early results show that the concept of plasma vaporization could prove to be a significant improvement over current TURP techniques [159] for BPH, with reduced complications [160].

In recent years, investigations have been performed into the interaction of LTPs with different types of cancer cells, including melanoma [161–163], ovarian [164], colorectal [165], liver [166], lung [110], breast [167], and brain [168] amongst others. The gold standard for LTP as a cancer therapy has to be the selective cytocidal targeting of cancerous tissue, whilst leaving healthy tissues unaffected. The effect of reactive species produced by plasma treatment has been extensively studied *in vitro*, with plasma induced DNA damage and apoptosis has been investigated [108, 169]. Another investigation showed the same response due to cellular detachment [170]. A considerable reduction in cell viability has been demonstrated using the MTT assay, as a result of high nitric NO and ROS concentrations [109]. It has also been suggested that immediate cell death can be caused by sufficiently high plasma doses, following minimal cell survival after extended plasma exposure [171]. LTP has also been applied *in vivo* to treat mice with tumours derived from glioma cell lines, where a preliminary study showed a reduction in tumour volume of over 50% at six days following initial plasma treatment [172]. Survival rates of plasma-treated mice increased by over half, compared with the control group who received no treatment [172]. In a follow-up study, ROS produced by the plasma were earmarked as the main antitumour agents, with evidence for cell cycle targeting [173] and apoptosis also presented [174–176]. LTP has also been recently applied to ablate tumours in mice subcutaneously injected with neuroblastoma cells, with a reduction in the rate of tumour growth observed versus control. In addition, survival time posttreatment almost doubled [177]. Another means of LTP-cellular interaction is the electric field that is generated at the effluent tip of DBD jet devices. This may lead to the phenomenon of irreversible cellular electroporation, which has been shown to cause tumour regression and cell death in its own right [178–180] and may aid the transport of RONS to the cell nucleus.

Despite LTP-based approaches demonstrating considerable promise in cancer treatment, further focussed work on the exact mechanisms of plasma-cellular interaction is required before such a technique could be used therapeutically. This includes primarily the quantification of which reactive species are causing adverse cellular effects, tailoring the plasma to deliver maximum damage to the cancer, before developing practical apparatus for patient treatment in the operating theatre. This process may be aided by the use of plasma in combination with radiological and chemotherapeutic techniques [181], in order to increase efficacy.

## 4. Low-Temperature Plasma as a Focal Therapy for Prostate Cancer

At the time of writing, no published study exists on the application of LTP to prostate cancer. The following section outlines how LTPs could be utilized as a focal therapy in practice, how LTPs might compare to other conventional focal therapies for prostate cancer in terms of efficacy, and what might be the upper limit of disease stage for treatment of localized cancer with LTP.

*4.1. Methods of Treatment Delivery and Plasma "Dose".* Application of LTP to a patient has been successfully applied clinically by treatment of the skin with the FE-DBD system mentioned earlier [125]. Clearly, delivery to the prostate represents a more complex technical challenge. Probably the most efficient means of application would be to follow the approach of PDT and brachytherapy by inserting the
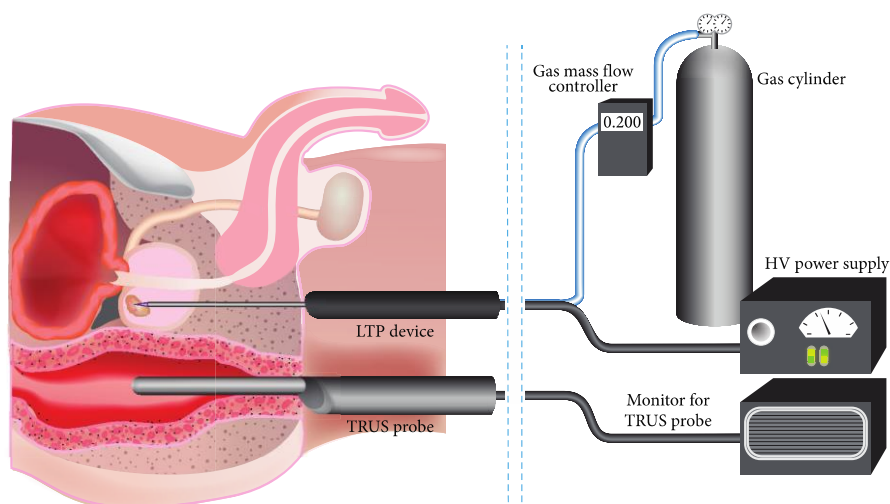
FIGURE 3: Proposed treatment approach for LTP treatment of localized prostate cancer. The LTP device is administered transperineally to an organ confined prostate cancer. Supporting image guidance from a TRUS probe, along with high-voltage (HV) power supply and gas flow-rate control are shown.

plasma transperineally to provide a focal treatment of organ confined cancers. In reality, whichever way LTP is applied, there is an obvious common dependence on accurate imaging techniques, as discussed in Section 2.5. With simultaneous image guidance by means of TRUS, following prior MRI scan, it is conceivable that LTP could be applied to localized tumours. A representation of one potential treatment delivery system is outlined in Figure 3.

DBD configuration plasma jet devices have already been fabricated and delivered via flexible optical fibres for the treatment of carcinoma, with outer diameters as fine as 60 $\mu$m [110].

One of the most important factors for LTP as a cancer therapy is a thorough understanding of the species produced and their concentration for each particular type of device. Correlating the concentration of produced species to a known plasma "dose" is crucial, as lower doses and exposures can stimulate a proliferative response in cells [182, 183]. For LTP therapy to be accepted clinically, there first needs to be agreement on what constitutes the units of plasma "dose." At present, independent research groups use different devices with different operating parameters (such as those outlined in Figure 1, amongst others), with varying exposure times. Such an agreement would lead to directly comparable data across institutions, which may accelerate the route to the clinic, and thus the patient.

*4.2. Proposed Efficacy as Compared to Other Therapies.* Given that plasma induces ROS, one obvious comparison to current cancer therapies is with radiotherapy, in that both are forms of ionizing radiation that produce reactive species. Besides the lack of a need for radioactive materials, another advantage that LTP possesses over radiotherapy is the production of

reactive nitrogen species (RNS) in addition to ROS. As mentioned in Section 3.2, high concentrations of NO have been shown to have a considerable detrimental effect on cell viability, induce apoptosis [184], and have the potential to cause cytostasis in tumour cells [185]. In addition, the production of peroxynitrite ($ONOO^-$) formed as a result of reactions between superoxide ($O_2^-$) and NO has been shown to cause DNA damage and oxidation of proteins [186, 187]. Some recent diagnostic studies have demonstrated the production of the radical singlet-delta oxygen by LTPs [188–190], which suggests similarities between LTP treatment and PDT. LTP, however, has the advantage of SDO production in addition to a range of other reactive species with cytotoxic effects.

There is some evidence to suggest that LTP may offer a selective kill of cancerous cells [164, 191–193], which offers a potential advantage over conventional radiological techniques, where unwanted damage to surrounding tissues is the main concern. However, this selectivity is yet to be definitively proven. Furthermore, due to the ambient temperature of the plasma, there should be no requirement for the probes employed by cryoablation (which monitor and regulate the temperature of the urethra and bladder), as thermal effects to the neighbouring tissues should not be of concern. This could offer a more simplified treatment procedure, targeting the tumour bed preferentially.

*4.3. When to Treat with LTP?* In terms of patient selection for treatment with LTP, similar criteria to current focal therapies would be applied [194]. Patients with low risk cancer (Gleason 6) are likely to opt for active surveillance to avoid unnecessary invasive procedures [195]. Patients with metastatic or locally advanced prostate cancer (typically Gleason 8–10) are not generally considered for focal therapy, as stated in Section 2.

Therefore, the final group with intermediate risk prostate cancer would be candidates for LTP therapy. These patients are likely to have a predicted life expectancy of more than five years, with no detection of locally advanced disease using imaging technologies (clinical stage T2a or lower) [43, 196]. Their cancer is likely to be Gleason 7 (although some localized cancer could be Gleason 8) and their PSA should be low (less than 10–20 ng/mL). The other consideration for treatment is whether the tumour is unifocal or multifocal, thereby perhaps necessitating more than one treatment probe. 3D mapping of biopsies should assist in identification of the location, number, and size of tumour foci [197]. Fewer well-defined tumour foci would be logistically easier to treat than multiple foci. Ultimately, such focal therapy treatment is a good option for patients who do not like the uncertainty of watchful waiting but do not want to suffer the side effects of aggressive overtreatment for a low risk cancer.

## 5. Conclusions

In this review we have analysed some of the currently available focal therapies for localized prostate cancer and where their advantages and limitations lie. We propose that the emerging field of low temperature plasmas may offer an alternative and viable solution to the effective treatment of prostate cancer, with minimal side effects and improved treatment efficacy versus other focal therapies. However, for this promising concept to become a reality, further study must be undertaken in order to fully diagnose the cellular interaction mechanisms of the plasma, and also how surgical administration would occur, a means of which has been suggested here. In addition, there is a need for continued development of imaging diagnostics, upon which a plasma-based approach would rely for precise application.

## Conflict of Interests

The authors declare that there is no conflict of interests regarding the publication of this paper.

## Authors' Contribution

Norman J. Maitland and Deborah O'Connell contributed equally to this work.

## References

[1] A. Jemal, F. Bray, M. M. Center, J. Ferlay, E. Ward, and D. Forman, "Global cancer statistics," *CA Cancer Journal for Clinicians*, vol. 61, no. 2, pp. 69–90, 2011.

[2] J. Li, J. A. Djenaba, A. Soman et al., "Recent trends in prostate cancer incidence by age, cancer stage, and grade, the United States, 2001–2007," *Prostate Cancer*, vol. 2012, Article ID 691380, 8 pages, 2012.

[3] H. Lepor, "Pathophysiology, epidemiology, and natural history of benign prostatic hyperplasia," *Reviews in Urology*, vol. 6, supplement 9, pp. S3–S10, 2004.

[4] J. Ansari, S. A. Hussain, A. Zarkar, J. S. Tanguay, J. Bliss, and J. Glaholm, "Docetaxel chemotherapy for metastatic hormone refractory prostate cancer as first-line palliative chemotherapy and subsequent re-treatment: birmingham experience," *Oncology Reports*, vol. 20, no. 4, pp. 891–896, 2008.

[5] P. Chris and O. Sartor, "Abiraterone and increased survival in metastatic prostate cancer," *The New England Journal of Medicine*, vol. 364, pp. 1995–2005, 2011.

[6] D. L. Berry, C. M. Moinpour, C. S. Jiang et al., "Quality of life and pain in advanced stage prostate cancer: results of a Southwest Oncology Group randomized trial comparing docetaxel and estramustine to mitoxantrone and prednisone," *Journal of Clinical Oncology*, vol. 24, no. 18, pp. 2828–2835, 2006.

[7] G. Bozzini, P. Colin, P. Nevoux et al., "Focal therapy of prostate cancer: energies and procedures," *Urologic Oncology*, vol. 31, no. 2, pp. 155–167, 2013.

[8] L. Mearini and M. Porena, "Transrectal high-intensity focused ultrasound for the treatment of prostate cancer: past, present, and future," *Indian Journal of Urology*, vol. 26, no. 1, pp. 4–11, 2010.

[9] G. Duchesne, "Localised prostate cancer: current treatment options," *Australian Family Physician*, vol. 40, no. 10, pp. 768–771, 2011.

[10] L. Klotz, "Active surveillance versus radical treatment for favorable-risk localized prostate cancer," *Current Treatment Options in Oncology*, vol. 7, no. 5, pp. 355–362, 2006.

[11] M. A. Kollmeier and M. J. Zelefsky, "How to select the optimal therapy for early-stage prostate cancer," *Critical Reviews in Oncology/Hematology*, vol. 83, no. 2, pp. 225–234, 2012.

[12] J. L. Stanford, Z. Feng, A. S. Hamilton et al., "Urinary and sexual function after radical prostatectomy for clinically localized prostate cancer: the prostate cancer outcomes study," *Journal of the American Medical Association*, vol. 283, no. 3, pp. 354–360, 2000.

[13] M. Bul, R. C. van den Bergh, X. Zhu et al., "Outcomes of initially expectantly managed patients with low or intermediate risk screen-detected localized prostate cancer," *BJU International*, vol. 110, no. 11, pp. 1672–1677, 2012.

[14] M. Bul, X. Zhu, R. Valdagni et al., "Active surveillance for low-risk prostate cancer worldwide: the PRIAS study," *European Urology*, vol. 63, no. 4, pp. 597–603, 2013.

[15] U. Lindner, J. Trachtenberg, and N. Lawrentschuk, "Focal therapy in prostate cancer: modalities, findings and future considerations," *Nature Reviews Urology*, vol. 7, no. 10, pp. 562–571, 2010.

[16] V. Kasivisvanathan, M. Emberton, and H. U. Ahmed, "Focal therapy for prostate cancer: rationale and treatment opportunities," *Clinical Oncology*, vol. 25, no. 8, pp. 461–473, 2013.

[17] S. Eggener, G. Salomon, P. T. Scardino, J. De la Rosette, T. J. Polascik, and S. Brewster, "Focal therapy for prostate cancer: possibilities and limitations," *European Urology*, vol. 58, no. 1, pp. 57–64, 2010.

[18] M. Valerio, H. U. Ahmed, M. Emberton et al., "The role of focal therapy in the management of localised prostate cancer: a systematic review," *European Urology*, 2013.

[19] R. Bihrle, R. S. Foster, N. T. Sanghvi, J. P. Donohue, and P. J. Hood, "High intensity focused ultrasound for the treatment of benign prostatic hyperplasia: early United States clinical experience," *Journal of Urology*, vol. 151, no. 5, pp. 1271–1275, 1994.

[20] S. Madersbacher, M. Pedevilla, L. Vingers, M. Susani, and M. Marberger, "Effect of high-intensity focused ultrasound on human prostate cancer in vivo," *Cancer Research*, vol. 55, no. 15, pp. 3346–3351, 1995.

[21] T. Nomura and H. Mimata, "Focal therapy in the management of prostate cancer: an emerging approach for localized prostate cancer," *Advances in Urology*, vol. 2012, Article ID 391437, 8 pages, 2012.

[22] E. R. Cordeiro, X. Cathelineau, S. Thüroff et al., "High-intensity focused ultrasound (HIFU) for definitive treatment of prostate cancer," *BJU International*, vol. 110, no. 9, pp. 1228–1242, 2012.

[23] G. R. Ter Haar, R. L. Clarke, M. G. Vaughan, and C. R. Hill, "Trackless surgery using focused ultrasound: technique and case report," *Minimally Invasive Therapy*, vol. 1, no. 1, pp. 13–19, 1991.

[24] F. Orsi, P. Arnone, W. Chen, and L. Zhang, "High intensity focused ultrasound ablation: a new therapeutic option for solid tumors," *Journal of Cancer Research and Therapeutics*, vol. 6, no. 4, pp. 414–420, 2010.

[25] A. Napoli, M. Anzidei, C. De Nunzio et al., "Real-time magnetic resonance-guided high-intensity focused ultrasound focal therapy for localised prostate cancer: preliminary experience," *European Urology*, vol. 63, no. 2, pp. 395–398, 2013.

[26] S. Madersbacher, C. Kratzik, N. Szabo, M. Susani, L. Vingers, and M. Marberger, "Tissue ablation in benign prostatic hyperplasia with high-intensity focused ultrasound," *European Urology*, vol. 23, no. 1, pp. 39–43, 1993.

[27] J. G. Bomers, J. P. Sedelaar, J. O. Barentsz et al., "MRI-guided interventions for the treatment of prostate cancer," *American Journal of Roentgenology*, vol. 199, no. 4, pp. 714–720, 2012.

[28] A. B. El Fegoun, E. Barret, D. Prapotnich et al., "Focal therapy with high-intensity focused ultrasound for prostate cancer in the elderly. A feasibility study with 10 years follow-up," *International Brazilian Journal of Urology*, vol. 37, no. 2, pp. 213–222, 2011.

[29] C. Chaussy and S. Thüroff, "The status of high-intensity focused ultrasound in the treatment of localized prostate cancer and the impact of a combined resection," *Current Urology Reports*, vol. 4, no. 3, pp. 248–252, 2003.

[30] G. M. Spencer, D. J. Rubens, and D. J. Roach, "Hypoechoic fat: a sonographic pitfall," *American Journal of Roentgenology*, vol. 164, no. 5, pp. 1277–1280, 1995.

[31] M. Sumitomo, J. Asakuma, H. Yoshii et al., "Anterior perirectal fat tissue thickness is a strong predictor of recurrence after high-intensity focused ultrasound for prostate cancer," *International Journal of Urology*, vol. 17, no. 9, pp. 776–782, 2010.

[32] T. Liu, L. Y. Wu, J. K. Choi, and C. E. Berkman, "Targeted photodynamic therapy for prostate cancer: inducing apoptosis via activation of the caspase-8/-3 cascade pathway," *International Journal of Oncology*, vol. 36, no. 4, pp. 777–784, 2010.

[33] S. B. Brown, E. A. Brown, and I. Walker, "The present and future role of photodynamic therapy in cancer treatment," *The Lancet Oncology*, vol. 5, no. 8, pp. 497–508, 2004.

[34] W. M. Sharman, C. M. Allen, and J. E. Van Lier, "Photodynamic therapeutics: basic principles and clinical applications," *Drug Discovery Today*, vol. 4, no. 11, pp. 507–517, 1999.

[35] L.-O. Klotz, K.-D. Kröncke, and H. Sies, "Singlet oxygen-induced signaling effects in mammalian cells," *Photochemical and Photobiological Sciences*, vol. 2, no. 2, pp. 88–94, 2003.

[36] L. J. Schiff, W. C. Eisenberg, J. Dziuba, K. Taylor, and S. J. Moore, "Cytotoxic effects of singlet oxygen," *Environmental Health Perspectives*, vol. 76, pp. 199–203, 1987.

[37] K. Briviba, L.-O. Klotz, and H. Sies, "Toxic and signaling effects of photochemically or chemically generated singlet oxygen in biological systems," *Biological Chemistry*, vol. 378, no. 11, pp. 1259–1265, 1997.

[38] W. M. Sharman, J. E. Van Lier, and C. M. Allen, "Targeted photodynamic therapy via receptor mediated delivery systems," *Advanced Drug Delivery Reviews*, vol. 56, no. 1, pp. 53–76, 2004.

[39] A. J. Bullous, C. M. A. Alonso, and R. W. Boyle, "Photosensitiser-antibody conjugates for photodynamic therapy," *Photochemical and Photobiological Sciences*, vol. 10, no. 5, pp. 721–750, 2011.

[40] N. L. Oleinick, R. L. Morris, and I. Belichenko, "The role of apoptosis in response to photodynamic therapy: what, where, why, and how," *Photochemical and Photobiological Sciences*, vol. 1, no. 1, pp. 1–21, 2002.

[41] C. M. Moore, M. Emberton, and S. G. Bown, "Photodynamic therapy for prostate cancer—an emerging approach for organ-confined disease," *Lasers in Surgery and Medicine*, vol. 43, no. 7, pp. 768–775, 2011.

[42] N. Arumainayagam, C. M. Moore, H. U. Ahmed, and M. Emberton, "Photodynamic therapy for focal ablation of the prostate," *World Journal of Urology*, vol. 28, no. 5, pp. 571–576, 2010.

[43] H. Lepor, "Vascular targeted photodynamic therapy for localized prostate cancer," *Reviews in Urology*, vol. 10, no. 4, pp. 254–261, 2008.

[44] A. Zisman, A. J. Pantuck, J. K. Cohen, and A. S. Belldegrun, "Prostate cryoablation using direct transperineal placement of ultrathin probes through a 17-gauge brachytherapy template—technique and preliminary results," *Urology*, vol. 58, no. 6, pp. 988–993, 2001.

[45] A. De La Taille, M. C. Benson, E. Bagiella et al., "Cryoablation for clinically localized prostate cancer using an argon-based system: complication rates and biochemical recurrence," *BJU International*, vol. 85, no. 3, pp. 281–286, 2000.

[46] J. K. Cohen and R. J. Miller, "Thermal protection of urethra during cryosurgery of prostate," *Cryobiology*, vol. 31, no. 3, pp. 313–316, 1994.

[47] P. Derakhshani, S. Neubauer, M. Braun, J. Zumbe, A. Heidenreich, and U. Engelmann, "Cryoablation of localized prostate cancer. Experience in 48 cases, PSA and biopsy results," *European Urology*, vol. 34, no. 3, pp. 181–187, 1998.

[48] J. L. Chin, D. Lim, and M. Abdelhady, "Review of primary and salvage cryoablation for prostate cancer," *Cancer Control*, vol. 14, no. 3, pp. 231–237, 2007.

[49] J. I. Izawa, K. Ajam, E. McGuire et al., "Major surgery to manage definitively severe complications of salvage cryotherapy for prostate cancer," *Journal of Urology*, vol. 164, no. 6, pp. 1978–1981, 2000.

[50] A. Gangi, G. Tsoumakidou, O. Abdelli et al., "Percutaneous MR-guided cryoablation of prostate cancer: initial experience," *European Radiology*, vol. 22, no. 8, pp. 1829–1835, 2012.

[51] D. A. Palacios, M. Miyake, and C. J. Rosser, "Radiosensitization in prostate cancer: mechanisms and targets," *BMC Urology*, vol. 13, no. 1, article 4, 2013.

[52] H. E. Johns, "The physicist in cancer treatment and detection," *International Journal of Radiation Oncology Biology Physics*, vol. 7, no. 6, pp. 801–808, 1981.

[53] I. R. Radford, "Evidence for a general relationship between the induced level of DNA double-strand breakage and cell-killing after X-irradiation of mammalian cells," *International Journal of Radiation Biology*, vol. 49, no. 4, pp. 611–620, 1986.

[54] J. F. Ward, "Biochemistry of DNA lesions," *Radiation Research. Supplement*, vol. 8, pp. S103–S111, 1985.

[55] Y. M. Cho, Y. S. Kim, M. J. Kang, W. L. Farrar, and E. M. Hurt, "Long-term recovery of irradiated prostate cancer increases cancer stem cells," *Prostate*, vol. 72, no. 16, pp. 1746–1756, 2012.

[56] K. Ogawa, Y. Yoshioka, F. Isohashi et al., "Radiotherapy targeting cancer stem cells: current views and future perspectives," *Anticancer Research*, vol. 33, no. 3, pp. 747–754, 2013.

[57] C. Chargari, C. Moncharmont, A. Lévy et al., "Cancer stem cells, cornerstone of radioresistance and perspectives for radiosensitization: glioblastoma as an example," *Bulletin du Cancerr*, vol. 99, no. 12, pp. 1153–1160, 2012.

[58] F. M. Frame, D. Pellacani, A. T. Collins et al., "HDAC inhibitor confers radiosensitivity to prostate stem-like cells," *British Journal of Cancer*, vol. 109, pp. 3023–3033, 2013.

[59] S. Hummel, E. Simpson, P. Hemingway, M. D. Stevenson, and A. Rees, "Intensity-modulated radiotherapy for the treatment of prostate cancer: a systematic review and economic evaluation," *Health Technology Assessment*, vol. 14, no. 47, pp. 1–108, 2010.

[60] P. Kupelian, D. Kuban, H. Thames et al., "Improved biochemical relapse-free survival with increased external radiation doses in patients with localized prostate cancer: the combined experience of nine institutions in patients treated in 1994 and 1995," *International Journal of Radiation Oncology Biology Physics*, vol. 61, no. 2, pp. 415–419, 2005.

[61] Y. Trada, A. Plank, and J. Martin, "Defining a dose-response relationship for prostate external beam radiotherapy," *Journal of Medical Imaging and Radiation Oncology*, vol. 57, no. 2, pp. 237–246, 2013.

[62] M. J. Chen, E. Weltman, R. M. Hanriot et al., "Intensity modulated radiotherapy for localized prostate cancer: rigid compliance to dose-volume constraints as a warranty of acceptable toxicity?" *Radiation Oncology*, vol. 2, no. 1, article 6, 2007.

[63] I. M. Lips, H. Dehnad, C. H. van Gils, A. E. Boeken Kruger, U. A. van der Heide, and M. van Vulpen, "High-dose intensity-modulated radiotherapy for prostate cancer using daily fiducial marker-based position verification: acute and late toxicity in 331 patients," *Radiation Oncology*, vol. 3, no. 1, article 15, 2008.

[64] J. S. Jones, "Radiorecurrent prostate cancer: an emerging and largely mismanaged epidemic," *European Urology*, vol. 60, no. 3, pp. 411–412, 2011.

[65] B. S. Chera, C. Rodriguez, C. G. Morris et al., "Dosimetric comparison of three different involved nodal irradiation techniques for stage ii hodgkin's lymphoma patients: conventional radiotherapy, intensity-modulated radiotherapy, and three-dimensional proton radiotherapy," *International Journal of Radiation Oncology Biology Physics*, vol. 75, no. 4, pp. 1173–1180, 2009.

[66] J. A. Efstathiou, P. J. Gray, and A. L. Zietman, "Proton beam therapy and localised prostate cancer: current status and controversies," *British Journal of Cancer*, vol. 108, no. 6, pp. 1225–1230, 2013.

[67] P. J. Gray and J. A. Efstathiou, "Proton beam radiation therapy for prostate cancer-is the hype (and the cost) justified?" *Current Urology Reports*, vol. 14, no. 3, pp. 199–208, 2013.

[68] N. C. Sheets, G. H. Goldin, A.-M. Meyer et al., "Intensity-modulated radiation therapy, proton therapy, or conformal radiation therapy and morbidity and disease control in localized prostate cancer," *Journal of the American Medical Association*, vol. 307, no. 15, pp. 1611–1620, 2012.

[69] J. F. Fowler, "The radiobiology of prostate cancer including new aspects of fractionated radiotherapy," *Acta Oncologica*, vol. 44, no. 3, pp. 265–276, 2005.

[70] C. Oliai, R. Lanciano, B. Sprandio et al., "Stereotactic body radiation therapy for the primary treatment of localized prostate cancer," *Journal of Radiation Oncology*, vol. 2, no. 1, pp. 63–70, 2013.

[71] D. J. Brenner and E. J. Hall, "Fractionation and protraction for radiotherapy of prostate carcinoma," *International Journal of Radiation Oncology Biology Physics*, vol. 43, no. 5, pp. 1095–1101, 1999.

[72] T. Seisen, S. J. Drouin, V. Phé et al., "Current role of image-guided robotic radiosurgery (Cyberknife) for prostate cancer treatment," *BJU International*, vol. 111, no. 5, pp. 761–766, 2013.

[73] D. E. Freeman and C. R. King, "Stereotactic body radiotherapy for low-risk prostate cancer: five-year outcomes," *Radiation Oncology*, vol. 6, no. 1, article 3, 2011.

[74] Y. Xie, D. Djajaputra, C. R. King, S. Hossain, L. Ma, and L. Xing, "Intrafractional motion of the prostate during hypofractionated radiotherapy," *International Journal of Radiation Oncology Biology Physics*, vol. 72, no. 1, pp. 236–246, 2008.

[75] N. C. Townsend, B. J. Huth, W. Ding et al., "Acute toxicity after CyberKnife-delivered hypofractionated radiotherapy for treatment of prostate cancer," *American Journal of Clinical Oncology*, vol. 34, no. 1, pp. 6–10, 2011.

[76] D. S. Park, "Current status of brachytherapy for prostate cancer," *Korean Journal of Urology*, vol. 53, no. 11, pp. 743–749, 2012.

[77] P. L. Nguyen, A. V. D'Amico, A. K. Lee, and W. W. Suh, "Patient selection, cancer control, and complications after salvage local therapy for postradiation prostate-specific antigen failure: a systematic review of the literature," *Cancer*, vol. 110, no. 7, pp. 1417–1428, 2007.

[78] M. I. Koukourakis and S. Touloupidis, "External beam radiotherapy for prostate cancer: current position and trends," *Anticancer Research*, vol. 26, no. 1B, pp. 485–494, 2006.

[79] B. Turkbey, P. A. Pinto, and P. L. Choyke, "Imaging techniques for prostate cancer: implications for focal therapy," *Nature Reviews Urology*, vol. 6, no. 4, pp. 191–203, 2009.

[80] A. H. Hou, D. Swanson, and A. B. Barqawi, "Modalities for imaging of prostate cancer," *Advances in Urology*, vol. 2009, Article ID 818065, 12 pages, 2009.

[81] H. Hricak, P. L. Choyke, S. C. Eberhardt, S. A. Leibel, and P. T. Scardino, "Imaging prostate cancer: a multidisciplinary perspective," *Radiology*, vol. 243, no. 1, pp. 28–53, 2007.

[82] A. Abdellaoui, S. Iyengar, and S. Freeman, "Imaging in prostate cancer," *Future Oncology*, vol. 7, no. 5, pp. 679–691, 2011.

[83] E. J. Halpern, "Contrast-enhanced ultrasound imaging of prostate cancer," *Reviews in Urology*, vol. 8, supplement 1, pp. S29–S37, 2006.

[84] M. Mitterberger, W. Horninger, F. Aigner et al., "Ultrasound of the prostate," *Cancer Imaging*, vol. 10, pp. 40–48, 2010.

[85] J. G. Bomers, D. Yakar, C. G. Overduin et al., "MR imaging-guided focal cryoablation in patients with recurrent prostate cancer," *Radiology*, vol. 268, no. 2, pp. 451–460, 2013.

[86] A. Oto, I. Sethi, G. Karczmar et al., "MR imaging-guided focal laser ablation for prostate cancer: phase I trial," *Radiology*, vol. 267, no. 3, pp. 932–940, 2013.

[87] M. Seitz, A. Shukla-Dave, A. Bjartell et al., "Functional magnetic resonance imaging in prostate cancer," *European Urology*, vol. 55, no. 4, pp. 801–814, 2009.

[88] F. Cornud, N. B. Delongchamps, P. Mozer et al., "Value of multiparametric MRI in the work-up of prostate cancer," *Current Urology Reports*, vol. 13, no. 1, pp. 82–92, 2012.

[89] A. Shukla-Dave and H. Hricak, "Role of MRI in prostate cancer detection," *NMR in Biomedicine*, vol. 27, no. 1, pp. 16–24, 2014.

[90] D. G. Engehausen, K. Engelhard, S. A. Schwab et al., "Magnetic resonance image-guided biopsies with a high detection rate of prostate cancer," *The Scientific World Journal*, vol. 2012, Article ID 975971, 6 pages, 2012.

[91] G. Fiard, N. Hohn, J. L. Descotes et al., "Targeted MRI-guided prostate biopsies for the detection of prostate cancer: initial clinical experience with real-time 3-dimensional transrectal ultrasound guidance and magnetic resonance/transrectal ultrasound image fusion," *Urology*, vol. 81, no. 6, pp. 1372–1378, 2013.

[92] A. Krieger, S.-E. Song, N. Bongjoon Cho et al., "Development and evaluation of an actuated MRI-compatible robotic system for MRI-guided prostate intervention," *IEEE/ASME Transactions on Mechatronics*, vol. 18, no. 1, pp. 273–284, 2013.

[93] F. Pinto, A. Totaro, A. Calarco et al., "Imaging in prostate cancer diagnosis: present role and future perspectives," *Urologia Internationalis*, vol. 86, no. 4, pp. 373–382, 2011.

[94] G. Fridman, M. Peddinghaus, H. Ayan et al., "Blood coagulation and living tissue sterilization by floating-electrode dielectric barrier discharge in air," *Plasma Chemistry and Plasma Processing*, vol. 26, no. 4, pp. 425–442, 2006.

[95] G. Daeschlein, S. Scholz, R. Ahmed et al., "Skin decontamination by low-temperature atmospheric pressure plasma jet and dielectric barrier discharge plasma," *Journal of Hospital Infection*, vol. 81, no. 3, pp. 177–183, 2012.

[96] M. G. Kong, "A complementary sterilisation strategy using cold atmospheric plasmas," *Medical Device Technology*, vol. 17, no. 3, pp. 26–28, 2006.

[97] M. G. Kong, "Cold atmospheric plasma destruction of solid proteins on stainless-steel surface and on real surgical instruments," *GMS Krankenhaushygiene Interdisziplinär*, vol. 3, no. 1, Article ID Doc07, 2008.

[98] K. Y. Baik, Y. H. Kim, Y. Hyo et al., "Feeding-gas effects of plasma jets on escherichia coli in physiological solutions," *Plasma Processes and Polymers*, vol. 10, no. 3, pp. 235–242, 2013.

[99] M. Laroussi, C. Tendero, X. Lu, S. Alla, and W. L. Hynes, "Inactivation of bacteria by the plasma pencil," *Plasma Processes and Polymers*, vol. 3, no. 6-7, pp. 470–473, 2006.

[100] K. Fricke, I. Koban, H. Tresp et al., "Atmospheric pressure plasma: a high-performance tool for the efficient removal of biofilms," *PLoS ONE*, vol. 7, no. 8, Article ID e42539, 2012.

[101] M. Y. Alkawareek, Q. T. Algwari, S. P. Gorman et al., "Application of atmospheric pressure nonthermal plasma for the in vitro eradication of bacterial biofilms," *Fems Immunology and Medical Microbiology*, vol. 65, no. 2, pp. 381–384, 2012.

[102] J. J. Cotter, P. Maguire, F. Soberon, S. Daniels, J. P. O'Gara, and E. Casey, "Disinfection of meticillin-resistant Staphylococcus aureus and Staphylococcus epidermidis biofilms using a remote non-thermal gas plasma," *Journal of Hospital Infection*, vol. 78, no. 3, pp. 204–207, 2011.

[103] D. Ziuzina, S. Patil, P. J. Cullen et al., "Atmospheric cold plasma inactivation of Escherichia coli in liquid media inside a sealed package," *Journal of Applied Microbiology*, vol. 114, no. 3, pp. 778–787, 2013.

[104] A. Fernandez, E. Noriega, and A. Thompson, "Inactivation of Salmonella enterica serovar Typhimurium on fresh produce by cold atmospheric gas plasma technology," *Food Microbiology*, vol. 33, no. 1, pp. 24–29, 2013.

[105] M. Laroussi, "Nonthermal decontamination of biological media by atmospheric-pressure plasmas: review, analysis, and prospects," *IEEE Transactions on Plasma Science*, vol. 30, no. 4, pp. 1409–1415, 2002.

[106] E. Garcia-Alcantara, R. López-Callejas, P. R. Morales-Ramírez et al., "In vivo accelerated acute wound healing in mouse skin using combined treatment of argon and helium plasma needle," *Archives of Medical Research*, vol. 44, no. 3, pp. 169–177, 2013.

[107] A. S. Wu, S. Kalghatgi, D. Dobrynin et al., "Porcine intact and wounded skin responses to atmospheric nonthermal plasma," *Journal of Surgical Research*, vol. 179, no. 1, pp. e1–e12, 2013.

[108] R. Sensenig, S. Kalghatgi, E. Cerchar et al., "Non-thermal plasma induces apoptosis in melanoma cells via production of intracellular reactive oxygen species," *Annals of Biomedical Engineering*, vol. 39, no. 2, pp. 674–687, 2011.

[109] X. Yan, Z. Xiong, F. Zou et al., "Plasma-induced death of HepG2 cancer cells: intracellular effects of reactive species," *Plasma Processes and Polymers*, vol. 9, no. 1, pp. 59–66, 2012.

[110] J. Y. Kim, J. Ballato, P. Foy et al., "Apoptosis of lung carcinoma cells induced by a flexible optical fiber-based cold microplasma," *Biosensors and Bioelectronics*, vol. 28, no. 1, pp. 333–338, 2011.

[111] N. K. Kaushik, Y. H. Kim, Y. G. Han et al., "Effect of jet plasma on T98G human brain cancer cells," *Current Applied Physics*, vol. 13, no. 1, pp. 176–180, 2013.

[112] J. Waskoenig, K. Niemi, N. Knake et al., "Atomic oxygen formation in a radio-frequency driven micro-atmospheric pressure plasma jet," *Plasma Sources Science and Technology*, vol. 19, no. 4, Article ID 045018, 2010.

[113] N. Knake, K. Niemi, S. Reuter, V. Schulz-von der Gathen, and J. Winter, "Absolute atomic oxygen density profiles in the discharge core of a microscale atmospheric pressure plasma jet," *Applied Physics Letters*, vol. 93, no. 13, Article ID 131503, 2008.

[114] N. Knake and V. Schulz-von der Gathen, "Investigations of the spatio-temporal build-up of atomic oxygen inside the micro-scaled atmospheric pressure plasma jet," *European Physical Journal D*, vol. 60, no. 3, pp. 645–652, 2010.

[115] D. Maletic, N. Puac, S. Lazović et al., "Detection of atomic oxygen and nitrogen created in a radio-frequency-driven micro-scale atmospheric pressure plasma jet using mass spectrometry," *Plasma Physics and Controlled Fusion*, vol. 54, no. 12, 2012.

[116] L. Packer and H. Sies, Eds., *Methods in Enzymology, Singlet Oxygen, UV-A and Ozone*, vol. 319, Academic Press, New York, NY, USA, 2000.

[117] H. Wiseman and B. Halliwell, "Damage to DNA by reactive oxygen and nitrogen species: role in inflammatory disease and progression to cancer," *Biochemical Journal*, vol. 313, no. 1, pp. 17–29, 1996.

[118] H. Sies, "Oxidative stress: oxidants and antioxidants," *Experimental Physiology*, vol. 82, no. 2, pp. 291–295, 1997.

[119] U. Bandyopadhyay, D. Das, and R. K. Banerjee, "Reactive oxygen species: oxidative damage and pathogenesis," *Current Science*, vol. 77, no. 5, pp. 658–666, 1999.

[120] D. B. Graves, "The emerging role of reactive oxygen and nitrogen species in redox biology and some implications for plasma applications to medicine and biology," *Journal of Physics D*, vol. 45, no. 26, 2012.

[121] M. Laroussi, *Plasma Medicine: Applications of Low-Temperature Gas Plasmas in Medicine and Biology*, Cambridge University Press, Cambridge, UK, 2012.

[122] J. Jaroslav, Q. T. Algwari, D. O'Connell et al., "Experimental-modeling study of an atmospheric-pressure helium discharge propagating in a thin dielectric tube," *Ieee Transactions on Plasma Science*, vol. 40, no. 11, pp. 2912–2919, 2012.

[123] Q. T. Algwari and D. O'Connell, "Electron dynamics and plasma jet formation in a helium atmospheric pressure dielectric barrier discharge jet," *Applied Physics Letters*, vol. 99, no. 12, Article ID 121501, 2011.

[124] J. L. Walsh and M. G. Kong, "Contrasting characteristics of linear-field and cross-field atmospheric plasma jets," *Applied Physics Letters*, vol. 93, no. 11, Article ID 111501, 2008.

[125] D. U. Silverthorn and B. R. Johnson, *HumAn Physiology: An Integrated Approach*, Pearson Education, San Francisco, Calif, USA, 3rd edition, 2004, contributions by Bruce R. Johnson.

[126] T. Murakami, K. Niemi, T. Gans et al., "Chemical kinetics and reactive species in atmospheric pressure helium-oxygen plasmas with humid-air impurities," *Plasma Sources Science & Technology*, vol. 22, no. 1, 2013.

[127] E. Wagenaars, T. Gans, D. O'Connell, and K. Niemi, "Two-photon absorption laser-induced fluorescence measurements of atomic nitrogen in a radio-frequency atmospheric-pressure plasma jet," *Plasma Sources Science & Technology*, vol. 21, no. 4, 2012.

[128] K. Niemi, J. Waskoenig, N. Sadeghi, T. Gans, and D. O'Connell, "The role of helium metastable states in radio-frequency driven helium-oxygen atmospheric pressure plasma jets: measurement and numerical simulation," *Plasma Sources Science and Technology*, vol. 20, no. 5, Article ID 055005, 2011.

[129] C. O'Neill, J. Waskoenig, and T. Gans, "Tailoring electron energy distribution functions through energy confinement in dual radio-frequency driven atmospheric pressure plasmas," *Applied Physics Letters*, vol. 101, no. 15, pp. 154107–154104, 2012.

[130] T. Murakami, K. Niemi, T. Gans, D. O'Connell, and W. G. Graham, "Afterglow chemistry of atmospheric-pressure helium-oxygen plasmas with humid air impurity," *Plasma Sources Science and Technology*, vol. 23, no. 2, Article ID 025005, 2014.

[131] K. Niemi, D. O'Connell, N. de Oliveira et al., "Absolute atomic oxygen and nitrogen densities in radio-frequency driven atmospheric pressure cold plasmas: synchrotron vacuum ultra-violet high-resolution Fourier-transform absorption measurements," *Applied Physics Letters*, vol. 103, no. 3, Article ID 034102, 2013.

[132] J. Waskoenig and T. Gans, "Nonlinear frequency coupling in dual radio-frequency driven atmospheric pressure plasmas," *Applied Physics Letters*, vol. 96, no. 18, Article ID 181501, 2010.

[133] K. Niemi, S. Reuter, L. M. Graham et al., "Diagnostic based modelling of radio-frequency driven atmospheric pressure plasmas," *Journal of Physics D*, vol. 43, no. 12, Article ID 124006, 2010.

[134] K. Niemi, S. Reuter, L. M. Graham, J. Waskoenig, and T. Gans, "Diagnostic based modeling for determining absolute atomic oxygen densities in atmospheric pressure helium-oxygen plasmas," *Applied Physics Letters*, vol. 95, no. 15, Article ID 151504, 2009.

[135] V. Schulz-von der Gathen, L. Schaper, N. Knake et al., "Spatially resolved diagnostics on a microscale atmospheric pressure plasma jet," *Journal of Physics D*, vol. 41, no. 19, Article ID 194004, 2008.

[136] D. Ellerweg, J. Benedikt, A. Von Keudell, N. Knake, and V. Schulz-von der Gathen, "Characterization of the effluent of a He/O$_2$ microscale atmospheric pressure plasma jet by quantitative molecular beam mass spectrometry," *New Journal of Physics*, vol. 12, Article ID 013021, 2010.

[137] G. E. Morfill, M. G. Kong, and J. L. Zimmermann, "Focus on plasma medicine," *New Journal of Physics*, vol. 11, Article ID 115011, 2009.

[138] M. Laroussi and F. Leipold, "Evaluation of the roles of reactive species, heat, and UV radiation in the inactivation of bacterial cells by air plasmas at atmospheric pressure," *International Journal of Mass Spectrometry*, vol. 233, no. 1–3, pp. 81–86, 2004.

[139] G. Fridman, A. D. Brooks, M. Balasubramanian et al., "Comparison of direct and indirect effects of non-thermal atmospheric-pressure plasma on bacteria," *Plasma Processes and Polymers*, vol. 4, no. 4, pp. 370–375, 2007.

[140] R. E. J. Sladek and E. Stoffels, "Deactivation of Escherichia coli by the plasma needle," *Journal of Physics D*, vol. 38, no. 11, pp. 1716–1721, 2005.

[141] S. Perni, G. Shama, J. L. Hobman et al., "Probing bactericidal mechanisms induced by cold atmospheric plasmas with Escherichia coli mutants," *Applied Physics Letters*, vol. 90, no. 7, Article ID 073902, 2007.

[142] M. Moisan, J. Barbeau, S. Moreau, J. Pelletier, M. Tabrizian, and L. Yahia, "Low-temperature sterilization using gas plasmas: a review of the experiments and an analysis of the inactivation mechanisms," *International Journal of Pharmaceutics*, vol. 226, no. 1-2, pp. 1–21, 2001.

[143] Z. L. Petrović, S. Puač, N. Lazović et al., "Biomedical applications and diagnostics of atmospheric pressure plasma," *Journal of Physics*, vol. 356, no. 1, Article ID 012001, 2012.

[144] M. Y. Alkawareek, Q. Th. Algwari, G. Laverty et al., "Eradication of Pseudomonas aeruginosa biofilms by atmospheric pressure non-thermal plasma," *PLoS ONE*, vol. 7, no. 8, Article ID e44289, 2012.

[145] E. Stoffels, R. E. J. Sladek, and I. E. Kieft, "Gas plasma effects on living cells," *Physica Scripta*, vol. 2004, article 79, 2004.

[146] C. Jiang, M.-T. Chen, A. Gorur et al., "Nanosecond pulsed plasma dental probe," *Plasma Processes and Polymers*, vol. 6, no. 8, pp. 479–483, 2009.

[147] G. Isbary, G. Morfill, H. U. Schmidt et al., "A first prospective randomized controlled trial to decrease bacterial load using cold atmospheric argon plasma on chronic wounds in patients," *British Journal of Dermatology*, vol. 163, no. 1, pp. 78–82, 2010.

[148] G. Isbary, J. Heinlin, T. Shimizu et al., "Successful and safe use of 2 min cold atmospheric argon plasma in chronic wounds: results of a randomized controlled trial," *British Journal of Dermatology*, vol. 167, no. 2, pp. 404–410, 2012.

[149] G. Daeschlein, S. Scholz, R. Ahmed et al., "Cold plasma is well-tolerated and does not disturb skin barrier or reduce skin moisture," *Journal der Deutschen Dermatologischen Gesellschaft*, vol. 10, no. 7, pp. 509–515, 2012.

[150] M. B. Witte and A. Barbul, "Role of nitric oxide in wound repair," *American Journal of Surgery*, vol. 183, no. 4, pp. 406–412, 2002.

[151] A. Soneja, M. Drews, and T. Malinski, "Role of nitric oxide, nitroxidative and oxidative stress in wound healing," *Pharmacological Reports*, vol. 57, pp. 108–119, 2005.

[152] G. Fridman, G. Friedman, A. Gutsol, A. B. Shekhter, V. N. Vasilets, and A. Fridman, "Applied plasma medicine," *Plasma Processes and Polymers*, vol. 5, no. 6, pp. 503–533, 2008.

[153] G. Lloyd, G. Friedman, S. Jafri, G. Schultz, A. Fridman, and K. Harding, "Gas plasma: medical uses and developments in

wound care," *Plasma Processes and Polymers*, vol. 7, no. 3-4, pp. 194–211, 2010.

[154] J. Heinlin, G. Morfill, M. Landthaler et al., "Plasma medicine: possible applications in dermatology," *Journal der Deutschen Dermatologischen Gesellschaft*, vol. 8, no. 12, pp. 968–976, 2010.

[155] K. R. Stalder, D. F. McMillen, and J. Woloszko, "Electrosurgical plasmas," *Journal of Physics D*, vol. 38, no. 11, pp. 1728–1738, 2005.

[156] J. Raiser and M. Zenker, "Argon plasma coagulation for open surgical and endoscopic applications: state of the art," *Journal of Physics D*, vol. 39, no. 16, Article ID 3520, 2006.

[157] J. M. Canard and B. Védrenne, "Clinical application of argon plasma coagulation in gastrointestinal endoscopy: has the time come to replace the laser?" *Endoscopy*, vol. 33, no. 4, pp. 353–357, 2001.

[158] B. Geavlete, R. Multescu, M. Dragutescu, M. Jecu, D. Georgescu, and P. Geavlete, "Transurethral resection (TUR) in saline plasma vaporization of the prostate vs standard TUR of the prostate: "The better choice" in benign prostatic hyperplasia?" *BJU International*, vol. 106, no. 11, pp. 1695–1699, 2010.

[159] L. P. Xie, J. Qin, X. Y. Zheng et al., "Transurethral vapor enucleation and resection of prostate with TURis button electrode," *Zhonghua Yi Xue Za Zhi*, vol. 92, no. 22, pp. 1558–1559, 2012.

[160] S. Y. Zhang, H. Hu, X. P. Zhang et al., "Efficacy and safety of bipolar plasma vaporization of the prostate with, "button-type" electrode compared with transurethral resection of prostate for benign prostatic hyperplasia," *Chinese Medical Journal*, vol. 125, no. 21, pp. 3811–3814, 2012.

[161] G. Fridman, A. Shereshevsky, M. M. Jost et al., "Floating electrode dielectric barrier discharge plasma in air promoting apoptotic behavior in Melanoma skin cancer cell lines," *Plasma Chemistry and Plasma Processing*, vol. 27, no. 2, pp. 163–176, 2007.

[162] G.-C. Kim, H. J. Lee, and C.-H. Shon, "The effects of a micro plasma on melanoma (G361) cancer cells," *Journal of the Korean Physical Society*, vol. 54, no. 2, pp. 628–632, 2009.

[163] S. Arndt, E. Wacker, Y. F. Li et al., "Cold atmospheric plasma, a new strategy to induce senescence in melanoma cells," *Experimental Dermatology*, vol. 22, no. 4, pp. 284–289, 2013.

[164] S. Iseki, K. Nakamura, M. Hayashi et al., "Selective killing of ovarian cancer cells through induction of apoptosis by nonequilibrium atmospheric pressure plasma," *Applied Physics Letters*, vol. 100, no. 11, Article ID 113702, 2012.

[165] C.-H. Kim, S. Kwon, J. H. Bahn et al., "Effects of atmospheric nonthermal plasma on invasion of colorectal cancer cells," *Applied Physics Letters*, vol. 96, no. 24, Article ID 243701, 2010.

[166] X. Zhang, M. Li, R. Zhou, K. Feng, and S. Yang, "Ablation of liver cancer cells in vitro by a plasma needle," *Applied Physics Letters*, vol. 93, no. 2, Article ID 021502, 2008.

[167] M. Wang, B. Holmes, X. Cheng et al., "Cold atmospheric plasma for selectively ablating metastatic breast cancer cells," *PLoS ONE*, vol. 8, no. 9, Article ID e73741, 2013.

[168] N. K. Kaushik, P. Attriemail, N. Kaushikemail et al., "A preliminary study of the effect of DBD plasma and osmolytes on T98G brain cancer and HEK non-malignant cells," *Molecules*, vol. 18, no. 5, pp. 4917–4928, 2013.

[169] D. O'Connell, L. J. Cox, W. B. Hyland et al., "Cold atmospheric pressure plasma jet interactions with plasmid DNA," *Applied Physics Letters*, vol. 98, no. 4, Article ID 043701, 2011.

[170] I. E. Kieft, M. Kurdi, and E. Stoffels, "Reattachment and apoptosis after plasma-needle treatment of cultured cells," *IEEE Transactions on Plasma Science*, vol. 34, no. 4, pp. 1331–1336, 2006.

[171] N. Barekzi and M. Laroussi, "Dose-dependent killing of leukemia cells by low-temperature plasma," *Journal of Physics D*, vol. 45, no. 42, 2012.

[172] M. Vandamme, E. Robert, S. Dozias et al., "Response of human glioma U87 xenografted on mice to non thermal plasma treatment," *Plasma Medicine*, vol. 1, no. 1, pp. 27–43, 2011.

[173] O. Volotskova, T. S. Hawley, M. A. Stepp et al., "Targeting the cancer cell cycle by cold atmospheric plasma," *Scientific Reports*, vol. 2, article 636, 2012.

[174] M. Vandamme, E. Robert, S. Lerondel et al., "ROS implication in a new antitumor strategy based on non-thermal plasma," *International Journal of Cancer*, vol. 130, no. 9, pp. 2185–2194, 2012.

[175] G. J. Kim, W. Kim, K. T. Kim, and J. K. Lee, "DNA damage and mitochondria dysfunction in cell apoptosis induced by nonthermal air plasma," *Applied Physics Letters*, vol. 96, no. 2, Article ID 021502, 2010.

[176] M. Thiyagarajan, X. F. Gonzales, and H. Anderson, "Regulated cellular exposure to non-thermal plasma allows preferentially directed apoptosis in acute monocytic leukemia cells," *Studies in Health Technology and Informatics*, vol. 184, pp. 436–442, 2013.

[177] R. M. Walk, J. A. Snyder, P. Srinivasan et al., "Cold atmospheric plasma for the ablative treatment of neuroblastoma," *Journal of Pediatric Surgery*, vol. 48, no. 1, pp. 67–73, 2013.

[178] J. T. Au, T. P. Kingham, K. Jun et al., "Irreversible electroporation ablation of the liver can be detected with ultrasound B-mode and elastography," *Surgery*, vol. 153, no. 6, pp. 787–793, 2013.

[179] J. Fanta, P. Hora'k, J. Marvan et al., "The NanoKnife and two successful cases of intracavitary irreversible electroporation of main bronchus tumours," *Rozhledy v Chirurgii*, vol. 91, no. 11, pp. 625–630, 2012.

[180] G. Onik, P. Mikus, and B. Rubinsky, "Irreversible electroporation: implications for prostate ablation," *Technology in Cancer Research and Treatment*, vol. 6, no. 4, pp. 295–300, 2007.

[181] L. Brulle, M. Vandamme, D. Riès et al., "Effects of a non thermal plasma treatment alone or in combination with gemcitabine in a MIA PaCa2-luc orthotopic pancreatic carcinoma model," *PLoS ONE*, vol. 7, no. 12, Article ID e52653, 2012.

[182] D. Dobrynin, G. Fridman, G. Friedman, and A. Fridman, "Physical and biological mechanisms of direct plasma interaction with living tissue," *New Journal of Physics*, vol. 11, Article ID 115020, 2009.

[183] S. Kalghatgi, G. Friedman, A. Fridman, and A. M. Clyne, "Endothelial cell proliferation is enhanced by low dose nonthermal plasma through fibroblast growth factor-2 release," *Annals of Biomedical Engineering*, vol. 38, no. 3, pp. 748–757, 2010.

[184] D. Hirst and T. Robson, "Targeting nitric oxide for cancer therapy," *Journal of Pharmacy and Pharmacology*, vol. 59, no. 1, pp. 3–13, 2007.

[185] D. J. Stuehr and C. F. Nathan, "Nitric oxide: a macrophage product responsible for cytostasis and respiratory inhibition in tumor target cells," *Journal of Experimental Medicine*, vol. 169, no. 5, pp. 1543–1555, 1989.

[186] A. Korkmaz, S. Oter, M. Seyrek et al., "Molecular, genetic and epigenetic pathways of peroxynitrite-induced cellular toxicity," *Interdisciplinary Toxicology*, vol. 2, no. 4, pp. 219–228, 2009.

[187] J. Fraszczak, M. Trad, N. Janikashvili et al., "Peroxynitrite-dependent killing of cancer cells and presentation of released

# Low Temperature Plasma Causes Double-Strand Break DNA Damage in Primary Epithelial Cells Cultured From a Human Prostate Tumor

Adam M. Hirst, Fiona M. Frame, Norman J. Maitland, and Deborah O'Connell

*Abstract*—Research in the new field of plasma medicine continues to demonstrate the efficacy of low temperature plasmas (LTPs) for numerous biomedical applications. Responses such as reduction in cell viability and cell death for cancer therapy, cell proliferation for wound healing, and bacterial inactivation have been observed as a result of plasma treatment. In this paper, we applied LTP to prostate cancer primary cells derived from patient tumour tissue to inflict irreparable DNA damage.

*Index Terms*—Atmospheric pressure plasma, cells (biology), DNA, oncology.

I N RECENT years, the prognosis for prostate cancer (PCa) patients has improved as a result of early detection and improved treatments. Advances in radiotherapy such as the CyberKnife linear accelerator, and the advent of focal therapies, including photodynamic and cryotherapy, have improved treatment options for patients. However, cancer recurrence and adverse side effects are still common [1]. Low temperature plasmas (LTPs), operated at atmospheric pressure and room temperature, could present a new treatment option for localized PCa, with fewer side effects than current treatment options. The transfer of reactive oxygen and nitrogen species from the core plasma to the cell media, such as $O_3$, NO, $^1O_2$, $O_2^-$, OH, and $H_2O_2$, can lead to adverse cellular effects and ultimately cell death [2]. Here, we present the first steps in treatment development for primary PCa cells with LTP, where we have demonstrated potentially lethal DNA double strand breaks (DSBs) within the cell nucleus.

The LTP used in this paper was a dielectric barrier discharge (DBD) device, operated at 6 kV, 30 KHz. Helium was used as a carrier gas at 2 slm, with 0.3% $O_2$ admixture. The distance from the nozzle to the sample surface was maintained at 10 mm. Treated samples received 5 min exposure to the plasma. Exposure times of up to 10 min did not raise the media temperature beyond 36.5 °C.

The PCa tissue was obtained with patient consent from targeted needle core biopsies following radical prostatectomy. Primary cells were cultured from cancer tissue and plated onto a chamber slide at a density of 10 000 cells per well in 200 $\mu$L of stem cell media [3]. Cells were fixed in paraformaldehyde 30 min after treatment before staining. The treated sample was previously identified as Gleason grade 7 cancer through tissue histopathology.

Immunofluorescence staining clearly demonstrated DNA damage in the plasma-treated primary prostate epithelial cells cultured from a patient tumor. Fig. 1(b) and (c) shows a plasma-treated primary cell and an untreated control cell, respectively. The presence of red $\gamma$-H2AX foci in Fig. 1(b) is indicative of DSB DNA damage in the nucleus of the treated sample. The blue 4', 6-diamidino-2-phenylindole (DAPI) and green phalloidin markers were used to indicate cell nuclei and cell cytoskeleton (cell structure), respectively.

This result is a first demonstration that LTP is capable of causing potentially lethal DSB DNA damage in primary cells cultured from patient cancer tissue. The DSBs are particularly difficult for the cell to repair, and in turn lead to apoptosis (regulated cell suicide). It is anticipated that normal tumor-neighboring prostate cells would also sustain DNA damage; however, this would be a localised effect and would not negatively affect the prostate as a whole. Further, study now needs to be conducted to ascertain, comprehend, and manipulate the exact interaction mechanisms between the plasma and cancer cells; however, this result clearly shows the potential of LTP as a therapeutic for cancer patients.

The authors are from the Department of Physics and Biology, University of York, York, YO10 5DD, U.K. (e-mail: amh508@york. ac.uk; fiona.frame@york.ac.uk; n.j.maitland@york.ac.uk; deborah.oconnell@ york.ac.uk).

## References

[1] A. Jemal, F. Bray, M. M. Center, J. Ferlay, E. Ward, and D. Forman, "Global cancer statistics," *CA Cancer J. Clin.*, vol. 61, no. 2, pp. 69–90, Mar./Apr. 2011.

[2] D. B. Graves, "The emerging role of reactive oxygen and nitrogen species in redox biology and some implications for plasma applications to medicine and biology," *J. Phys. D, Appl. Phys.*, vol. 45, no. 26, Jul. 2012.

[3] A. T. Collins, P. A. Berry, C. Hyde, M. J. Stower, and N. J. Maitland, "Prospective identification of tumorigenic prostate cancer stem cells," *Cancer Res.*, vol. 65, no. 23, pp. 10946–10951, Dec. 2005.
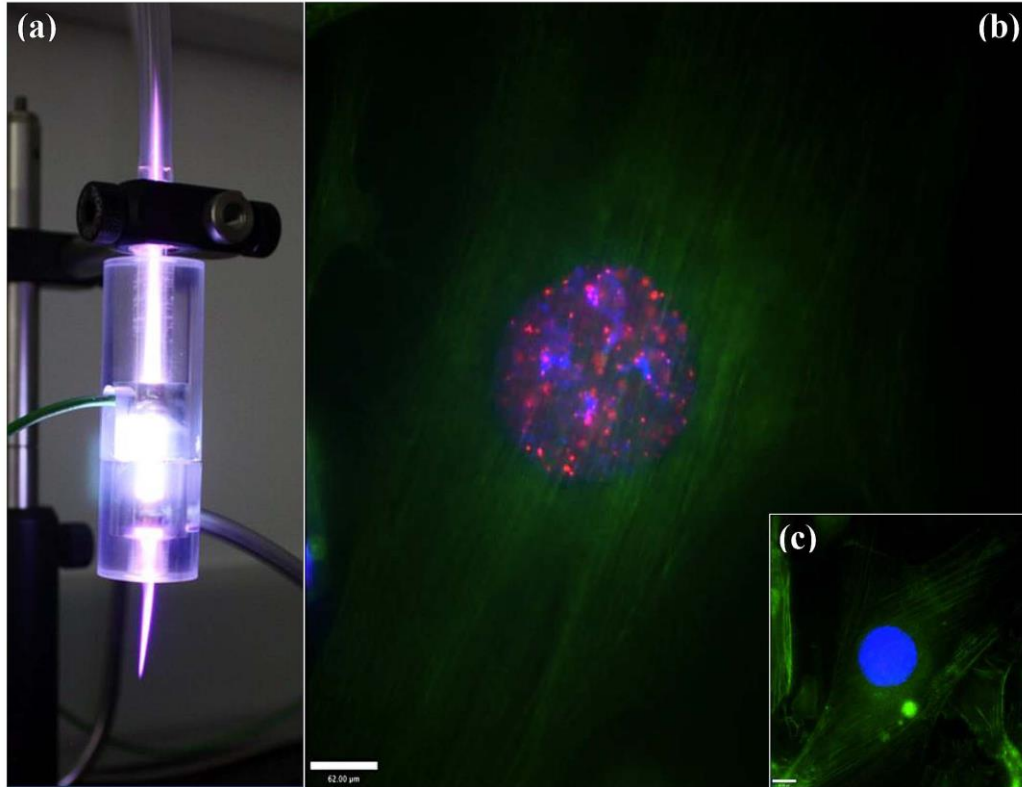
Fig. 1. (a) Primary prostate epithelial cells were treated with low temperature DBD plasma, operated at 6 kV. Helium was used as a carrier gas at 2 slm, with 0.3% $O_2$ admixture. Core discharge is created between the grounded (top) and powered (bottom) electrodes, with the resulting effluent directed onto the cell culture media surface. (b) Cells were cultured from a Gleason grade 7 patient tumor, plated at low density and exposed to 5 min low temperature plasma treatment, or (c) left untreated. Cells were fixed at 30-min posttreatment and stained for $\gamma$-H2AX (red, DNA damage foci), DAPI (blue, cell nucleus), and phalloidin (green, cell actin filament structure). Note the multiple red dots within the cancer cell nucleus after plasma treatment, indicating widespread and potentially lethal damage to the DNA. Scale bars = 62 $\mu$m in both (b) and (c).

# Low-temperature plasma treatment induces DNA damage leading to necrotic cell death in primary prostate epithelial cells

A M Hirst[1], M S Simms[2,3], V M Mann[2,3], N J Maitland[4], D O'Connell[1] and F M Frame[*,4]

[1]York Plasma Institute, Department of Physics, University of York, Heslington, York YO10 5DD, UK; [2]Department of Urology, Castle Hill Hospital, Cottingham, East Yorkshire HU16, 5JQ, UK; [3]Hull York Medical School, University of Hull, Hull, East Yorkshire HU6 7RX, UK and [4]YCR Cancer Research Unit, Department of Biology, University of York, Heslington, York YO10 5DD, UK

**Background:** In recent years, the rapidly advancing field of low-temperature atmospheric pressure plasmas has shown considerable promise for future translational biomedical applications, including cancer therapy, through the generation of reactive oxygen and nitrogen species.

**Method:** The cytopathic effect of low-temperature plasma was first verified in two commonly used prostate cell lines: BPH-1 and PC-3 cells. The study was then extended to analyse the effects in paired normal and tumour (Gleason grade 7) prostate epithelial cells cultured directly from patient tissue. Hydrogen peroxide ($H_2O_2$) and staurosporine were used as controls throughout.

**Results:** Low-temperature plasma (LTP) exposure resulted in high levels of DNA damage, a reduction in cell viability, and colony-forming ability. $H_2O_2$ formed in the culture medium was a likely facilitator of these effects. Necrosis and autophagy were recorded in primary cells, whereas cell lines exhibited apoptosis and necrosis.

**Conclusions:** This study demonstrates that LTP treatment causes cytotoxic insult in primary prostate cells, leading to rapid necrotic cell death. It also highlights the need to study primary cultures in order to gain more realistic insight into patient response.

Despite continual improvement and refinement, long-term treatment for prostate cancer (PCa) is still recognised as inadequate (Jemal *et al*, 2011). In the case of early onset, organ-confined tumours, patients may be treated with a focal therapy (Kasivisvanathan *et al*, 2013; Donaldson *et al*, 2014). Radiotherapy or photodynamic therapy (PDT), which rely on the production of reactive oxygen species (ROS) for cytotoxic effects, are two treatments of choice for localised PCa. However, around a third of patients will experience recurrence of their disease following radiotherapy (Jones, 2011). This may be due to inherent radio-resistance of a small fraction of the tumour – the cancer stem-like cells (Frame *et al*, 2013). Furthermore, numerous side effects are often experienced following treatment (Chen *et al*, 2007; Lips *et al*, 2008), even with more recent technological developments, such as stereotactic body radiation therapy (Cyberknife) (Woo *et al*, 2014).

In recent years, low-temperature plasmas (LTPs) have shown considerable potential as active agents in biomedicine. They are formed by applying a high electric field across a gas, which accelerates electrons into nearby atoms and molecules, leading to a cascade effect of multiple ionisation, excitation and dissociation processes. This creates a complex and unique reactive environment consisting of positive and negative charges, strong localised electric fields, UV radiation, reactive species, and mainly background neutral molecules.

Operated at atmospheric pressure and around room temperature, LTPs produce high concentrations of reactive oxygen and nitrogen species (RONS), including but not limited to: atomic nitrogen (Wagenaars *et al*, 2012) and oxygen (Knake *et al*, 2008; Waskoenig *et al*, 2010; Niemi *et al*, 2013), hydroxyl (OH) (Ninomiya *et al*, 2013), singlet delta oxygen (SDO) (Sousa *et al*, 2011), superoxide (Kang *et al*, 2014), and nitric oxide (NO) (Ma *et al*, 2014). It is now widely

believed that the principal mode of plasma–cell interaction is the delivery of RONS, a key mediator of oxidative damage and cell death in biological systems (Wiseman and Halliwell, 1996; Bandyopadhyay *et al*, 1999), generated in the plasma and transferred to target source (Graves, 2012, 2014).

In contrast, cell death by PDT relies on the generation of ROS, specifically SDO, which is highly cytotoxic (Sharman *et al*, 1999). Nonetheless, strong treatment resistance is encountered in hypoxic tumour regions (Krzykawska-Serda *et al*, 2014). The limitations of both radiotherapy and PDT, combined with the fact that LTPs concurrently produce both a multitude of RONS (Murakami *et al*, 2013) known to be toxic to cells and potentially strong localised electric fields, promotes the potential of LTP as a future cancer therapy, which we have recently reviewed (Hirst *et al*, 2014b).

Many studies now describe the effects of LTPs on various cancer cell lines in culture, with reported effects including reduced cell viability (Cheng *et al*, 2014; Plewa *et al*, 2014), growth arrest (Chang *et al*, 2014), and apoptotic cell death (Keidar *et al*, 2011; Gibson *et al*, 2014; Ishaq *et al*, 2014). We have reported induction of DNA damage by application of LTP treatment to primary prostate epithelial cells (Hirst *et al*, 2014a). Recent *in vivo* studies also revealed that LTP treatment of subcutaneous tumours (grown from cell lines) induced growth arrest and cell death, thus significantly reducing tumour volume in glioblastoma cells (Vandamme *et al*, 2012). Another study showed that short, daily exposure of tumours (squamous cell carcinoma) to LTP causes DNA damage leading to apoptosis (Kang *et al*, 2014). Internal treatment with LTP has also been explored using an endoscopic approach to application (pancreatic and colorectal cells), which demonstrated reduced tumour volume and also invasion capacity (Robert *et al*, 2013). However, the penetrative capability of LTP treatment through solid tissues leading to complete tumour eradication is yet to be established *in vivo*.

Here we first conducted a proof-of-principle study in order to validate the cytopathic effect of LTP treatment on two commonly used prostate cell lines derived from benign disease (BPH-1) and prostate cancer metastasis (PC-3). We then analysed in detail the effect of LTP treatment on a matched pair of primary samples. We cultured prostate epithelial cells from normal prostate and prostate cancer tissue (Gleason grade 7) retrieved from biopsies from a single patient, allowing for direct comparison of the effects of LTP on both normal and cancer cells. We present the first experimental evidence that LTP may be a suitable candidate for focal therapy treatment of patients with early onset prostate cancer through the induction of high levels of DNA damage, leading to a substantial reduction in colony-forming capacity, and ultimately necrotic cell death, in clinically relevant and close-to-patient samples.

## MATERIALS AND METHODS

**Culture of cell lines and primary prostate epithelial cells.** Two prostate cells lines were used in this study: BPH-1 cells, derived from benign prostatic hyperplasia (BPH), and PC-3 cells, derived from PCa bone metastases. BPH-1 cells were cultured in RPMI 1640 medium supplemented with 5% foetal calf serum (FCS) and 1% L-glutamine. PC-3 cells were cultured in Ham's F12 medium, supplemented with 7% FCS and 1% L-glutamine. No antibiotic or antimycotics were added to the cell culture medium. Cells were incubated at 37 °C with 5% $CO_2$.

Primary prostate epithelial cells were cultured from human tissue samples as described previously (Collins *et al*, 2005). Needle core biopsies (14 g) were taken immediately following surgical removal of the prostate. The site of each biopsy was determined by previous pathology, imaging, and palpation. Tissues were transported in RPMI-1640 with 5% FCS and 100 U ml$^{-1}$

antibiotic/antimycotic solution at 4 °C and processed within 6 h. Needle core biopsies were verified as normal or Gleason grade 7 cancer by subsequent pathology, both cores originating from the same patient undergoing radical prostatectomy. Samples were obtained with full ethical permission and patient consent. Primary cells were cultured in stem cell media, based on keratinocyte serum-free media supplemented with L-glutamine, stem cell factor, granulocyte macrophage colony stimulating factor, cholera toxin, bovine pituitary extract, epidermal grown factor and leukaemia inhibitory factor (Collins *et al*, 2005). Significantly, these cells are cultured in media without FCS. Cells were grown on collagen-I-coated 10-cm dishes in the presence of irradiated STO feeder cells and incubated at 37 °C with 5% $CO_2$. No antibiotic or antimycotics were added to the cell culture medium.

**LTP jet configuration and characterisation.** The LTP jet consisted of a quartz glass tube of inner/outer diameter 4/6 mm, with two copper tape electrodes spaced 20 mm apart (Figure 1A). One electrode was powered (6 kV sinusoidal voltage at 30 kHz) and one grounded. Helium was used as a carrier gas at 2 standard litres per minute (SLM), fed with 0.3% molecular oxygen admixture. Cells were exposed to the LTP jet at a distance 15 mm from the end of the bottom electrode for a range of treatment times from 0 to 600 s in centrifuge tubes in a volume of 1.5 ml media. The distance between the end of the glass tube and the media surface was ~2 mm. Hydrogen peroxide ($H_2O_2$, Fisher Scientific, Loughborough, UK) was used throughout as a positive cytoxicity control at a concentration of 1 mM. Using a thermocouple, treatment times of up to 600 s did not raise the surface temperature of culture media above 36.5 °C. The temperature and relative humidity of the laboratory were ~20 °C and ~25% respectively.

Optical emission spectroscopy was performed using an Ocean Optics HR4000CG-UV-NIR spectrometer (Dunedin, FL, USA) (200–1100 nm range) and the Spectra suite analysis software (Dunedin, FL, USA). Integration time and scans to average were set at 6 and 50 s, respectively. A background dark spectrum was obtained and subtracted from subsequent spectra. The optical fibre was aligned directly with the core plasma region and fixed at ~2 cm from the quartz tube.

**Cell viability and clonogenic recovery assays.** Cell viability was determined by use of the alamarBlue assay (Invitrogen, Life Technologies Ltd, Paisley, UK). Cells were treated with LTP and then plated into black-walled 96-well plates in triplicate at a density of 5000 cells per well in 100 µl of media. At 24, 48, 72, and 96 h after treatment, 10 µl of alamarBlue reagent (DAL1025, Invitrogen) was added to each well and incubated for 2 h at 37 °C. Fluorescence was recorded at excitation/emission values of 544/590 nm using a microplate reader (Polarstar Optima, BMG Labtech, Aylesbury, Bucks, UK), with cell viability recorded against normalised untreated samples.

Clonogenic recovery assays were used to measure cellular recovery posttreatment. Cells were treated in suspension and replated in six-well plates in triplicate at a density of 200 disaggregated cells per well. Cells were supplemented with 2 ml of growth media, which was changed every other day. In the case of primary epithelial cell cultures, STO feeder cells were also added. At 12 days after treatment, plates were stained with crystal violet (PBS, 1% crystal violet, 10% ethanol). Only colonies of >50 cells (equating to >5 population doublings) were counted (Francipane *et al*, 2008).

**DNA damage.** LTP-induced DNA damage was quantified using the alkaline comet assay (adapted from Sturmey *et al*, 2009). Cells were treated with LTP in 1.5 ml centrifuge tubes at a density of 20 000 cells in 1.5 ml media suspension. Immediately after treatment, cells were resuspended in 30 µl PBS and mixed with 225 µl low melting point agarose. This was then pipetted onto microscope slides

233
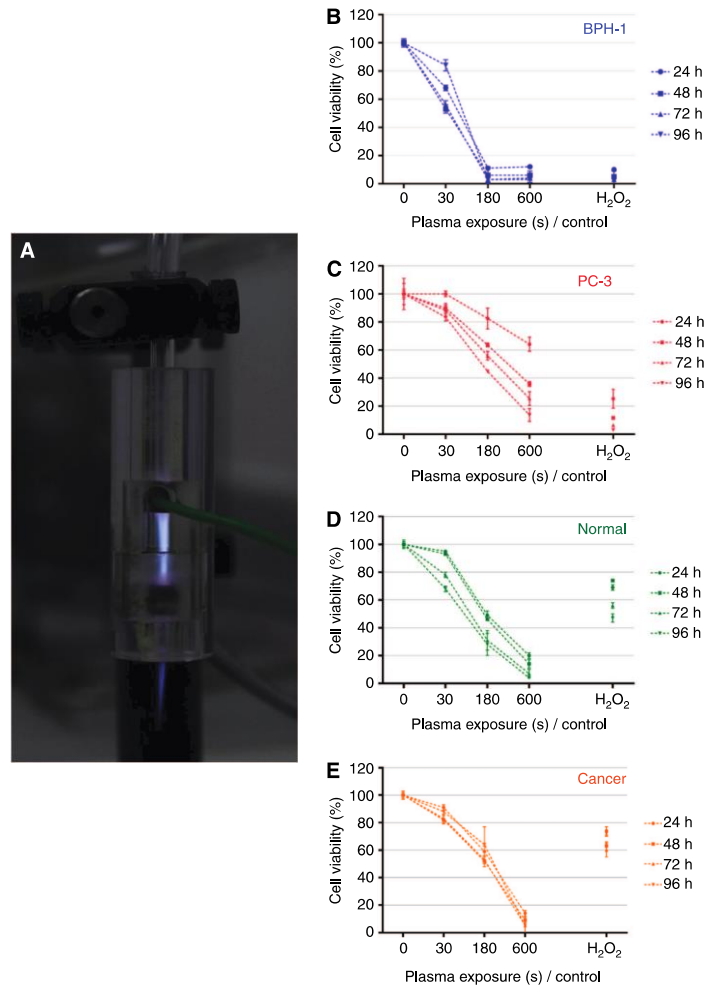
Figure 1. LTP treatment leads to a reduction in cell viability. (**A**) Cells were treated with a dielectric barrier discharge LTP jet, using 2 SLM helium flow rate with 0.3% $O_2$ admixture, operated at 6 kV and 30 kHz. Reduction in cell viability was determined by alamarBlue assay (**B**, **C**) in BPH-1 and PC-3 cells and (**D**, **E**) in normal and cancer primary epithelial cells at 24, 48, 72 and 96 h postexposure.

precoated with high melting point agarose and placed into lysis buffer (2.5 M NaCl, 10 mM Tris, 1 mM EDTA, 10% DMSO, 1% Triton X-100), overnight at 4 °C. The following day, cells were placed in alkaline buffer (0.3 M NaOH, 1 mM EDTA, pH 13) on ice for 40 min, before being electrophoresed at 23–25 V, 300 mA in alkaline buffer for a further 40 min on ice. Slides were then placed into neutralising buffer (0.4 M Tris, pH 7.5) for 2 × 10 min, before DNA was stained using SYBRgold (1 : 10 000 in TE buffer: 10 mM Tris, 1 mM EDTA, pH 7.5). Images were acquired by fluorescence microscopy (Nikon Eclipse TE300 microscope (Nikon, Surrey, UK), × 10 objective lens) using Volocity software (Volocity 6.3, PerkinElmer Inc., Waltham, MA, USA). Autocomet software (Tritek Corp., Sumerduck, VA, USA) was used to analyse cell images, with the median percentage of DNA-in-tail values used to record DNA damage in a minimum of 100 cells per treatment.

**Detection of ROS.** Extracellular $H_2O_2$ formed in the culture media as a result of LTP treatment was detected and quantified using the ROS-Glo $H_2O_2$ assay (Cat. no. G8820, Promega, Southhampton, UK). Cells were treated with LTP, before being plated into black-walled 96-well plates at a density of 10 000 cells in 80 $\mu$l of culture media, before following the manufacturer's protocol. Luminescence intensity was quantified using a microplate reader (Polarstar Optima, BMG Labtech) and normalised to untreated wells.

**Western blotting.** Cells were collected at 2, 4, 8, and 24 h following LTP treatment, and protein lysates were extracted using Cytobuster Protein Extraction Reagent (71009, EMD Millipore, Darmstadt, Germany) with protease inhibitors (cOmplete, EDTA-free Protease Inhibitor Cocktail Tablets, Roche Applied Science, Burgess Hill, West Sussex, UK). Primary antibodies included: cleaved-PARP (Asp214, 1 : 666, Cell Signalling Technology Inc., Hitchin, UK; no. 9541S), anti-LC3B (Ab51520, Abcam, Cambridge, UK; 1 : 3000), and monoclonal anti-$\beta$-actin 1 : 5000 (A5316, Sigma-Aldrich, Gillingham, UK; mouse). Secondary antibodies used

included: anti-rabbit IgG HRP-linked (1 : 5000, Cell Signalling Technology Inc. no. 7074S), and anti-mouse IgG peroxidase (1 : 5000, Sigma-Aldrich A5906). Staurosporine (1 $\mu$M) was used as a positive control for apoptosis (Cell Signalling Technology Inc. no. 9953). Kaleidoscope protein ladder was used as a marker for all gels (161-0375, Bio-Rad). Staurosporine (1 $\mu$M) was used as a positive control for apoptosis (Cell Signalling Technology Inc. no. 9953). The ratio of LC3BII/I band intensity was performed using ImageJ software (Mount Royal, QC, Canada), with all bands quantified against $\beta$-actin loading control lanes and normalised untreated controls.

**Caspase-Glo 3/7 assay.** Cells were treated with LTP and plated into collagen-coated 96-well plates at a density of 20 000 cells per well in 100 $\mu$l. A further 100 $\mu$l of caspase-glo 3/7 detection reagent (Cat. no. G8090, Promega) was immediately added to each well. Cells were incubated at 37 °C, with luminescence intensity (Polarstar Optima, BMG Labtech) recorded at 24 h after treatment. Based on findings from other results, a reduced set of LTP exposures was used for this assay.

**CellTox necrosis assay.** LTP-induced necrosis was quantified using the CellTox green cytoxicity assay (Cat. no. G8741, Promega). Cells were treated with LTP and plated into collagen-coated black-walled 96-well plates at a density of 10 000 cells in 50 $\mu$l of media per well. In addition to $H_2O_2$ and staurosporine, 2 $\mu$l of lysis solution (supplied with assay) was added to necrotic control wells. Fluorescence intensity was recorded using a plate reader (Polarstar Optima, BMG Labtech), at excitation/emission wavelength 485/520 nm, with readings at 2, 4, 8, 12, and 24 h after treatment. Fluorescence was normalised to untreated wells. Complementary fluorescence-brightfield merged microscopy images were also taken (Nikon Eclipse TE300 microscope, × 10 objective lens) at the same posttreatment time intervals.

**Statistical analysis.** All experiments were performed in triplicate, and results are expressed as the mean with associated s.e., with the exception of comet assay data, which shows the median DNA damage value. Plots were constructed and statistical analyses performed using Prism 6 (GraphPad software, San Diego, CA, USA). Statistical significance was determined using unpaired Mann–Whitney test (DNA damage results only) or unpaired $t$-test with Welch's correction (assumes non-equal s.d.) and displayed on figure plots as *$P < 0.05$, **$P < 0.01$, ***$P < 0.001$, and ****$P < 0.0001$.

## RESULTS

**Reduction in cell viability is observed following LTP treatment.** The viability of cells was quantified at 24, 48, 72, and 96 h following LTP treatment (Figure 1). A reduction in viability in both BPH-1 (Figure 1B) and PC-3 (Figure 1C) cell lines was observed. BPH-1 viability was reduced to <20%, whereas viability of PC-3 cells was reduced to <40%. In addition, reduced cell viability was recorded in both normal and primary cells (Figure 1D and E), with 30-s LTP exposure leading to a small decrease in viability and 600-s exposure reducing cell viability to <20%. The positive $H_2O_2$ control was less toxic to both primary samples than the longer LTP exposures (180 and 600 s). The cell lines were more susceptible to 1 mM $H_2O_2$, (up to 90% reduction) than primary cells, which only had a ~30% reduction with $H_2O_2$ alone. Furthermore, the duration posttreatment had little effect on viability in primary samples, with comparable results recorded at 24 and 96 h, particularly in the tumour cells (Figure 1E).

**DNA damage is sustained as a result of LTP exposure.** LTP-induced DNA damage was assessed using the alkaline comet assay, with the percentage of DNA-in-tail recorded for analysis.

Figure 2A and B show the percentage of DNA damage in both BPH-1 and PC-3 cells, respectively, for various exposure times. Each dot represents the DNA-in-tail percentage value from a single cell. Exposures as short as 30 s induced high levels of DNA damage, with a saturation of damage levels occurring from 180 s. This concurs with findings in normal and tumour primary cells (Figure 2C and D). The level of DNA damage from LTP exposure was found to be consistently comparable to the $H_2O_2$ treatment control, and the level of damage in the tumour-derived primary sample (Figure 2D) was marginally higher (but statistically significant, $P < 0.001$) than that recorded for the normal sample (Figure 2C).

**Inhibition of colony-forming capacity as a result of LTP treatment.** Treatment with LTP showed a dose dependent inhibition of cell recovery in both BPH-1 and PC-3 cells, with the cancer cell line being more resistant than the benign cell line (Figure 3A and B). Findings in primary cells showed that treatment with 600-s LTP reduced the surviving fraction to ~20% in both normal and tumour samples (Figure 3E and F). The tumour cells appeared significantly more resistant to the shorter 180-s LTP exposure and to the $H_2O_2$ control than the normal cells.

**Evaluation of $H_2O_2$ formation in cell culture media.** Cells in suspension were treated with LTP for a variety of times before being analysed for the presence of extracellular $H_2O_2$ in the cell culture media, as an indication of LTP-induced ROS production. It is well known that $H_2O_2$ is extremely toxic to cells (Bandyopadhyay et al, 1999), even at micromolar concentrations (Gulden et al, 2010). Figure 3C and D show an increase in the relative concentrations of $H_2O_2$ generated in the culture media with increasing LTP exposure times for BPH-1 and PC-3 cells. $H_2O_2$ production in PC-3 cells was far lower following LTP compared with $H_2O_2$ control, yet 180 and 600-s LTP exposures in BPH-1 cells were comparable to $H_2O_2$ control. In primary samples, a treatment time of 180 s yielded luminescence values comparable
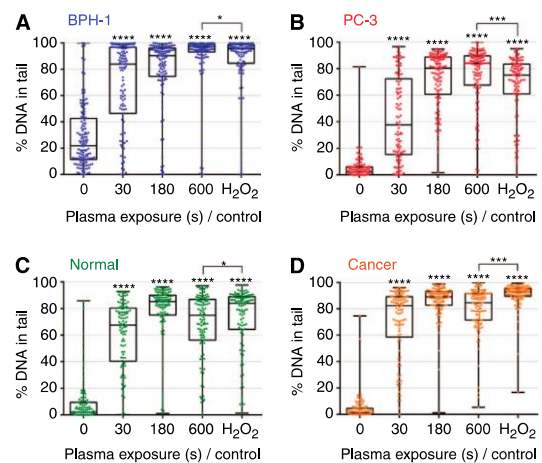
Figure 2. LTP treatment induces high levels of DNA damage in both prostate cell lines and primary epithelial cells. Cells were treated with LTP or $H_2O_2$ control (1 mM). DNA damage levels were measured using the alkaline comet assay and are represented as the percentage of DNA-in-tail in (**A**) BPH-1 and (**B**) PC-3 cells and in (**C**) normal and (**D**) cancer primary epithelial cells. Each dot represents a single cell, with a minimum of 100 cells counted for each exposure. Data are expressed as median ± s.e. and are analysed by Mann–Whitney test. All significance was determined against untreated samples unless otherwise indicated.
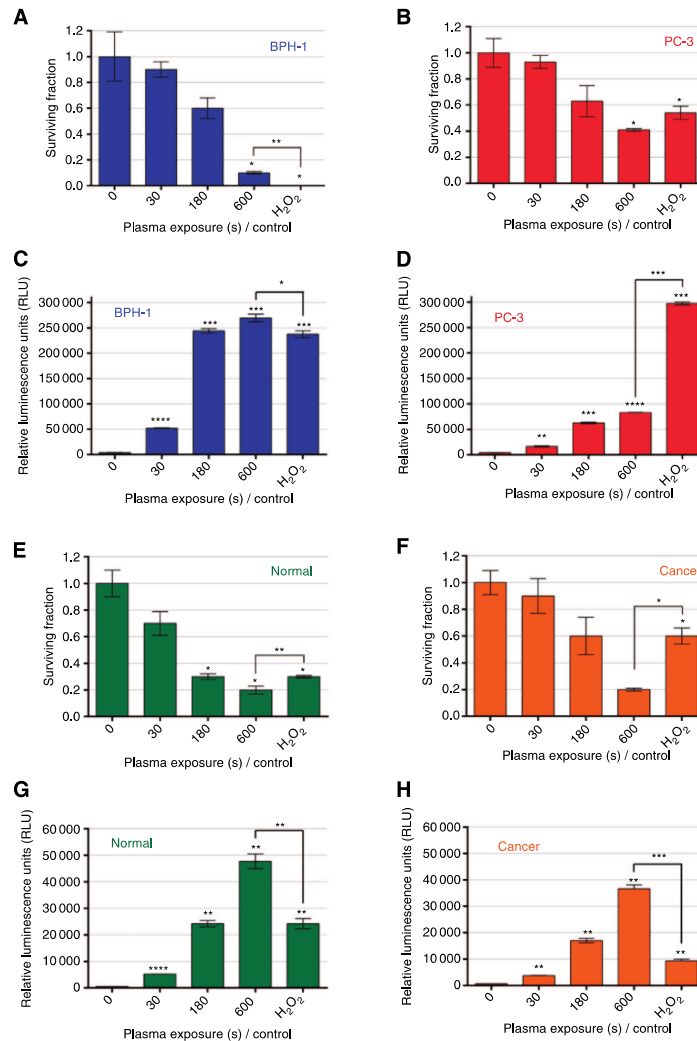
Figure 3. LTP treatment leads to reduction in colony-forming efficiency, and high levels of $H_2O_2$ in cell culture media. Cells were treated with LTP or $H_2O_2$ control (1 mm). Cell recovery was quantified using the colony-forming assays and is represented as surviving fraction posttreatment in (A) BPH-1 and (B) PC-3 cells and in (E) normal and (F) cancer primary epithelial cells. Immediately following treatment, ROS-Glo $H_2O_2$ luminescence assay (Promega) was performed to ascertain $H_2O_2$ levels in the culture media of (C) BPH-1 and (D) PC-3 cells and in (G) normal and (H) cancer primary epithelial cells (Note the different y axis scales). Data are expressed as mean ± s.e., with statistical analysis conducted using unpaired t-test with Welch's correction. All significance was determined against untreated samples unless otherwise indicated.

to 1 mm $H_2O_2$ positive control in normal cells. An exposure time of 600 s corresponded to approximately two-fold of the concentration of a 1 mm $H_2O_2$ positive control in normal cells and three-fold in cancer cells (Figure 3G and H).

**LTP exposure induces different cell death pathways in cells lines and primary prostate epithelial cells.** Our results indicate that LTP exposure causes necrosis in both BPH-1 and PC-3 cell lines, as seen in Figure 4A and B. It is clear that PC-3 cells are more resistant to LTP-induced necrosis than BPH-1 cells. Significantly, necrotic cell death was also observed in both normal and cancer prostate primary cells. Figure 4C and D indicate that 180- and

600-s LTP exposures lead to high levels of necrosis compared with untreated control, with the findings common to both normal and cancer samples. This was verified by supportive fluorescence images taken at 4 h after treatment, which highlighted cells positive for necrosis (green) in 180- and 600-s LTP exposure wells, whereas staurosporine controls were largely negative at this time point.

Initially, the levels of necrosis at 2 h posttreatment were comparable for 180- and 600-s exposures. Cells treated with 600-s LTP showed a marked time-dependent increase in necrosis, whereas values for 180-s samples remained approximately constant. Interestingly, cytopathic effects with the pure $H_2O_2$
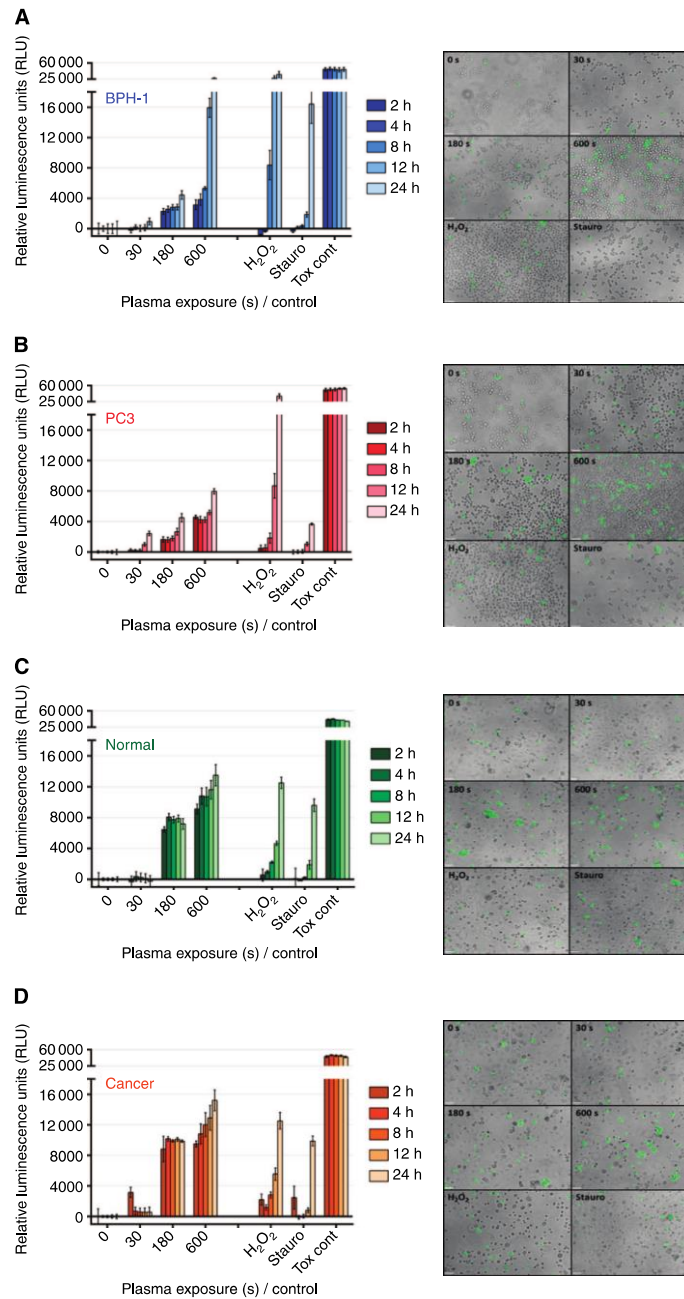
Figure 4. LTP treatment leads to necrotic cell death in both prostate cell lines and primary epithelial cells. Immediately following LTP treatment, the CellTox green cytoxicity assay (Promega) was performed to identify cells with comprimised membrane integrity characteristic of necrosis. In all, 1 mm $H_2O_2$, 1 μm staurosporine, and cell lysing agent (supplied with assay) were used as controls. Fluorescence intensity was quantified at 2, 4, 8, 12, and 24 h following treatment and normalised to untreated control wells in (A) BPH-1 and (B) PC-3 cell lines and in (C) normal and (D) cancer primary epithelial cells. Data are expressed as mean ± s.e. Supporting fluorescence microscopy images (× 10 magnification) taken at 4 h after treatment are also shown for each cell type.

control did not present until around 12–24 h after treatment. Likewise, the staurosporine treatment induced necrosis only at 24 h, indicative of late-stage apoptosis.

In addition to necrosis, a proportion of BPH-1 cells also underwent apoptosis following LTP exposure as verified by western blotting for the presence of cleaved-PARP, whereas PC-3 cells did not (Figure 5A and B). Primary cells treated with LTP did not undergo apoptosis (Figure 5C and D). This was further confirmed by assessment of caspase 3 and 7 activity in primary samples (Caspase-glo 3/7 assay, Promega), where only staurospor-ine-treated positive control cells showed positive expression (Figure 5E). Indeed, LTP-treated primary cells showed apoptotic activity levels below those of untreated control, further verifying

that cell death following LTP exposure occurs through necrosis and not apoptosis.

In addition to apoptosis and necrosis, another cellular response to stress is autophagy, which can serve as a protective mechanism, but also results in cell death. Quantitation of LC3 II/I band intensity revealed that, by 24 h posttreatment, a more than two- and a more than four-fold increase (over untreated controls) was present in the cancer and normal samples, respectively, indicating that an autophagic response occurred following LTP exposure (Figure 5C and D).

## DISCUSSION

In this work, we have shown that treatment with LTP causes DNA damage, a reduction in both cell viability and recovery, and ultimately necrotic cell death in normal and cancer primary prostate epithelial cells. The results indicate that LTP-induced $H_2O_2$ in the culture media is a likely facilitator of these effects. We also observed that, unlike primary cells and the PC-3 cell line, BPH-1 cells also die through apoptotic mechanisms following plasma treatment (Figure 6). Our findings in primary cells highlight the potential of LTP as an alternative to, or for use in conjunction with, other existing treatments for organ-confined prostate cancer. Furthermore, the differential cell death response between cell lines and primary cells stresses the need to study clinically relevant models in order to gain insight into the potential patient response.

LTP exposure is known to cause cytotoxic effects in cells via the delivery of RONS to the liquid environment (Ahn et al, 2014; Ishaq
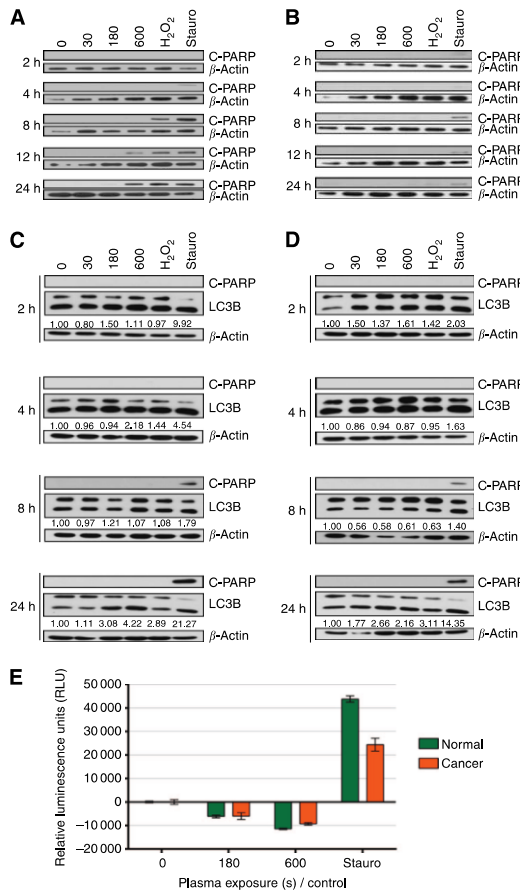


Figure 5. Cell death mechanisms following LTP treatment vary between cell types. Following treatment with LTP, 1 mm $H_2O_2$, or 1 μm staurosporine, protein lysates were harvested. (A) BPH-1 and (B) PC-3 cell line lysates were probed for apoptosis (C-PARP) by western blotting. (C) Normal and (D) cancer primary epithelial lysates were probed for apoptosis (C-PARP) and also autophagy (LC3B I/II). β-Actin was used as a loading control throughout. Band intensity quantification was performed using the ImageJ software. Further analysis of apoptotic activity was conducted in (E) primary epithelial cells using Caspase-glo 3/7 assay (Promega). Immediately following treatment, caspase-glo 3/7 detection reagent was added to all wells, and luminescence intensity was quantified at 24 h. Readings were normalised to untreated control and are expressed as mean ± s.e.
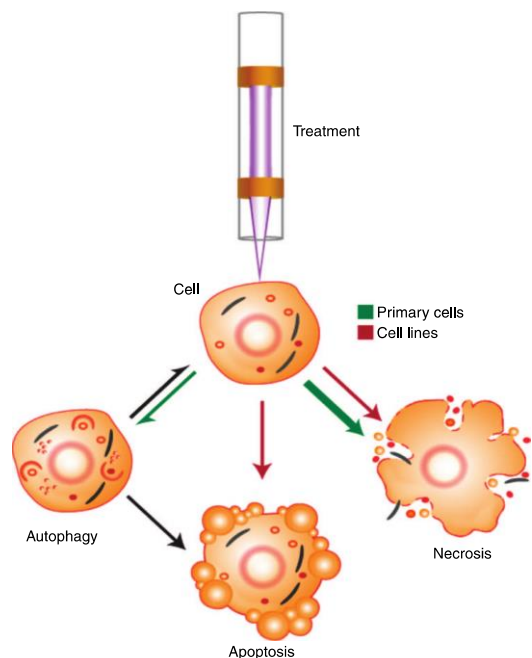


Figure 6. Overview of cellular response mechanism following LTP treatment. As a result of exposure to LTP, cells were observed to undergo (or a combination of) autophagy, apoptosis or necrosis. The relative proportions of, and differences between, cell lines (red arrows) and primary epithelial cells (green arrows) that exhibit these phenomena is emphasised. Adapted from Kepp et al (2011).

*et al*, 2014; Ma *et al*, 2014). Our results indicate that 180-s LTP treatment of prostate primary cells leads to $H_2O_2$ concentrations approximately equal to that of a 1 mM $H_2O_2$ control. Additionally, LTP exposure of 600 s produced statistically significant $H_2O_2$ readings two- to three-fold to those of the control. Interestingly, following exposure to LTP, the levels of $H_2O_2$ recorded in the tumour cells were found to be lower generally than those from the normal cells, resulting in an enhanced colony recovery following treatment at 30- and 180-s LTP treatment times but not at the longest exposure of 600 s. This is in keeping with recent data, suggesting that cancer cells have the ability to quench the effects of ROS more effectively than normal cells (Diehn *et al*, 2009; Gorrini *et al*, 2013). Despite this, cell viability is still strongly reduced following LTP treatments of 180 and 600 s, indicating that any RONS produced initially in the culture medium remain strongly damaging to the primary cells at increased time periods postexposure. In contrast to data from the proof-of-principle study on prostate cell lines (Figure 1B and C), the primary samples appear far more resistant to the $H_2O_2$ control, yet the reduction in viability as a result of LTP exposure is comparable between the different samples (Figure 2C and D). This suggests that the enhanced effect of the plasma is likely to be due to a cumulative effect on the cells of a multitude of reactive species produced in the plasma (the presence of atomic oxygen in the plasma core was verified by optical emission spectroscopy, Supplementary Figure S1), and/or additional plasma components such as electric fields, charges, and UV radiation (Graves, 2012; Kang *et al*, 2014), rather than just solely due to $H_2O_2$. This may also make it unlikely for cancer cells to become resistant to treatment, as increased tolerance to a particular reactive species would not protect against the perceived multi-faceted action of LTP. Because of the added presence of reactive nitrogen species produced by some LTPs (Cheng *et al*, 2014; Gibson *et al*, 2014), this may also present an advantage over radiotherapy, which relies heavily on ROS alone (Palacios *et al*, 2013), and over PDT, which relies predominantly on the single reactive species SDO for its cytotoxic effect (Sharman *et al*, 1999).

A contribution of the cell culture media to the observed effects cannot be discounted. We measured a three-fold increase over control of $H_2O_2$ production after plasma treatment in primary cells. Yet, we see that, in the BPH-1 cell line, the LTP-treated $H_2O_2$ concentrations are broadly similar, and in the PC-3 cell line the $H_2O_2$ concentrations are much lower than the control (Figure 1E and F). It is known that different cell culture media can produce different amounts of $H_2O_2$ (Promega Technical Services, private communication). We therefore considered treating all cell types in a buffered saline solution and re-plating the cells in their optimal culture media. However, a counter-argument is that this would not have been physiological (with respect to treating a patient) and that any cytopathic effect would be likely to be predominantly due to short-lived reactive species, and the prolonged effects of long-lived species would be lost. Significantly, both normal and cancer primary cells used in this study were cultured and treated in identical media without serum, and so media was not a variable factor and the results from these cells can be directly compared.

Differences in $H_2O_2$ levels were recorded in treated media containing cells and treated media only. All plasma-treated samples showed a reduction in $H_2O_2$ production in the presence of cells (*vs* treated media), suggesting that the cells consume, or quench, $H_2O_2$ in the media (Supplementary Figure S2A). This was by far the most pronounced in primary cells, where the $H_2O_2$ level following 180-s LTP exposure was reduced by 78% in the presence of cells. There was far less of a reduction in BPH-1 cells (17%) and PC-3 cells (41%). It was also found that, by 2 h following treatment, the levels of $H_2O_2$ (induced by either 600-s plasma treatment or 1 mM $H_2O_2$) were strongly reduced in both normal and tumour primary cells. This effect was more pronounced in the tumour cells

and demonstrates the strong ROS-quenching capacity of the primary cells (Supplementary Figure S2B and C). The level of $H_2O_2$ formed by the positive control was further reduced to that of the untreated cells by 8 h; however, there were still elevated levels of $H_2O_2$ induced by plasma treatment detected at this time point.

We have found that high levels of DNA damage, which is uniform across all cell types, is inflicted after an LTP exposure of only 30 s. In addition, a reduction in colony-forming ability following LTP treatment was observed, as cells treated with 600-s LTP recovered significantly less than those treated with the $H_2O_2$ control. This is despite the DNA damage values between 600 s and $H_2O_2$ control differing by only a few percent across all samples, in support of the hypothesis that the cytocidal effect of the plasma on cells is not solely due to $H_2O_2$ production. Therefore, *in vitro*, retaining the cells in treated media is necessary to realise a strong anti-proliferative effect (which we investigated and found to be the case; data not shown), as would be seen in tissues. Other LTP-based studies report a selective plasma effect (Wang *et al*, 2013; Guerrero-Preston *et al*, 2014), that is, that the plasma preferentially induces cell death in cancer cells. However, normal and tumour cell lines studied often originate from different sites or hosts or are cultured in different media. We observe similar responses in both primary prostate tumour and normal cells from the same patient, highlighting the necessity for supporting live imaging, for example, MRI, for precise targeted tumour ablation in patients (Sullivan and Crawford, 2009).

Finally, for any progression towards a patient therapy, further elucidation of the mechanism of LTP-induced cell death is required. Following a fatal stimulus, cell death can occur broadly in one of the two ways; apoptosis – a regulated chain of events involving cell shrinkage, blebbing, and ending with the formation of apoptotic bodies that retain membrane integrity (Cohen, 1997), or necrosis – an uncontrolled swelling that leads to membrane rupture and spillage of the cell contents into the surrounding environment, provoking an inflammatory response (Casiano *et al*, 1998). It is clear from our results that primary cells rapidly undergo necrosis, in the almost complete absence of apoptosis. A major advantage of this is that necrotic cell death has the potential to promote immune-activation against tumour cells (Melcher *et al*, 1999). In contrast, apoptotic cell death has been observed to promote an immune-suppressive environment (Voll *et al*, 1997), allowing tumour cells to evade detection by the immune system (Gregory and Pound, 2010). Our findings were common to both normal and cancer primary sample with some subtle differences. Marginally higher levels of necrosis were observed in the cancer cells following 600-s exposure, yet both samples show almost identical recovery from this treatment (20% surviving fraction). Both normal and cancer cells treated with long LTP exposures (180 and 600 s) undergo autophagy: a completely novel finding in LTP studies on human cells. This may be a survival process for cells that do not undergo necrosis. Our observation of higher levels of autophagy in primary normal cells may be attributed to the hypothesis that normal cells have a higher ROS-threshold tolerance than cancer cells (Gorrini *et al*, 2013).

Although this study argues that LTP could become a potential focal therapy for localised PCa, it remains possible that a reduction in metastatic tumour volume could be observed after treatment with LTP, as a result of necrotic cell death and its associated immune response as outlined earlier. Referred to as spontaneous regression, this response has been documented following necrosis-inducing thermal ablation treatments for other cancers (Sanchez-Ortiz *et al*, 2003; Kim *et al*, 2008; Chu and Dupuy, 2014), but the mechanisms responsible are largely unknown. Nevertheless, a proportion of cells survive LTP treatment and are able to proliferate following exposure to LTP, as demonstrated by their residual colony-forming capacity. The reasons for this must be determined and may potentially be overcome by manipulation and

optimisation of the plasma parameters (Cheng *et al*, 2014) and/or pretreatment with a sensitising agent (Frame *et al*, 2013).

Finally, the differences in response we have observed between prostate cell lines and primary cells, particularly in terms of the mechanism of cell death, highlights the importance of studying primary cultures in order to gain an insight into patient efficacy. More specifically, the cell death mechanisms that are triggered following administration of LTP should be elucidated in close-to-patient models.

## CONCLUSIONS

In summary, we have clearly demonstrated the potential of LTP as a future therapy option for localised prostate cancer. Through the formation of reactive species ($H_2O_2$ and more than likely also others, e.g., OH, $O_2^-$) in cell culture media, we observed high levels of DNA damage in primary cells cultured directly from patient tissues, together with reduction in cell viability and colony-forming ability. These ultimately lead to necrotic cell death in both normal and tumour samples. However, further optimisation of the LTP operational parameters needs to be conducted, in order to kill the proportion of cells that remain viable after treatment. In addition, although we have previously outlined a potential approach (Hirst *et al*, 2014b), the feasibility of physically treating patients who have PCa with LTP has yet to be established. This would require some modification of the LTP device itself to deliver the LTP to the tumour bed, sparing normal tissues, perhaps employing existing apparatus for cryotherapy and/or brachytherapy.

We believe that with appropriate imaging techniques to facilitate accurate tumour targeting and spare normal tissues, the multi-faceted action of LTP will provide advantages over other focal therapies. More specifically, therapies such as PDT relies on SDO production to destroy cells; plasmas are known to be able produce a multitude of RONS that are toxic to cells. Given that LTPs can be propagated from tubes $<100\,\mu m$ in diameter (Kim *et al*, 2011), we believe that LTP therapy could be more targeted than radiotherapy and more controlled than ice-ball formation in cryotherapy. LTP would not require additional equipment such as the warming catheters used in cryosurgery. Moreover, LTP treatment should prove far more cost-effective than existing treatments.

## ACKNOWLEDGEMENTS

## REFERENCES

Ahn HJ, Kim KI, Hoan NN, Kim CH, Moon E, Choi KS, Yang SS, Lee JS (2014) Targeting cancer cells with reactive oxygen and nitrogen species generated by atmospheric-pressure air plasma. *PLoS One* **9**: e86173.

Bandyopadhyay U, Das D, Banerjee RK (1999) Reactive oxygen species: oxidative damage and pathogenesis. *Curr Sci* **77**: 658–666.

Casiano CA, Ochs RL, Tan EM (1998) Distinct cleavage products of nuclear proteins in apoptosis and necrosis revealed by autoantibody probes. *Cell Death Differ* **5**: 183–190.

Chang JW, Kang SU, Shin YS, Kim KI, Seo SJ, Yang SS, Lee JS, Moon E, Baek SJ, Lee K, Kim CH (2014) Non-thermal atmospheric pressure plasma induces apoptosis in oral cavity squamous cell carcinoma: Involvement of DNA-damage-triggering sub-G(1) arrest via the ATM/p53 pathway *Arch Biochem Biophys* **545**: 133–140.

Chen MJ, Weltman E, Hanriot RM, Luz FP, Cecilio PJ, Da Cruz JC, Moreira FR, Santos AS, Martins LC, Nadalin W (2007) Intensity modulated radiotherapy for localized prostate cancer: rigid compliance to dose-volume constraints as a warranty of acceptable toxicity? *Radiat Oncol* **2**: 6.

Cheng X, Sherman J, Murphy W, Ratovitski E, Canady J, Keidar M (2014) The effect of tuning cold plasma composition on glioblastoma cell viability. *PLoS One* **9**: e98652.

Chu KF, Dupuy DE (2014) Thermal ablation of tumours: biological mechanisms and advances in therapy. *Nat Rev Cancer* **14**: 199–208.

Cohen GM (1997) Caspases: the executioners of apoptosis. *Biochem J* **326**(Pt 1): 1–16.

Collins AT, Berry PA, Hyde C, Stower MJ, Maitland NJ (2005) Prospective identification of tumorigenic prostate cancer stem cells. *Cancer Res* **65**: 10946–10951.

Diehn M, Cho RW, Lobo NA, Kalisky T, Dorie MJ, Kulp AN, Qian D, Lam JS, Ailles LE, Wong M, Joshua B, Kaplan MJ, Wapnir I, Dirbas FM, Somlo G, Garberoglio C, Paz B, Shen J, Lau SK, Quake SR, Brown JM, Weissman IL, Clarke MF (2009) Association of reactive oxygen species levels and radioresistance in cancer stem cells. *Nature* **458**: 780–783.

Donaldson IA, Alonzi R, Barratt D, Barret E, Berge V, Bott S, Bottomley D, Eggener S, Ehdaie B, Emberton M, Hindley R, Leslie T, Miners A, Mccartan N, Moore CM, Pinto P, Polascik TJ, Simmons L, Van Der Meulen J, Villers A, Willis S, Ahmed HU (2014) Focal therapy: patients, interventions, and outcomes-a report from a consensus meeting. *Eur Urol* **67**(4): 771–777.

Frame FM, Pellacani D, Collins AT, Simms MS, Mann VM, Jones GD, Meuth M, Bristow RG, Maitland NJ (2013) HDAC inhibitor confers radiosensitivity to prostate stem-like cells. *Br J Cancer* **109**: 3023–3033.

Francipane MG, Alea MP, Lombardo Y, Todaro M, Medema JP, Stassi G (2008) Crucial role of interleukin-4 in the survival of colon cancer stem cells. *Cancer Res* **68**: 4022–4025.

Gibson AR, Mccarthy HO, Ali AA, O'connell D, Graham WG (2014) Interactions of a non-thermal atmospheric pressure plasma effluent with PC-3 prostate cancer cells. *Plasma Process Polym* **11**(12): 1142–1149.

Gorrini C, Harris IS, Mak TW (2013) Modulation of oxidative stress as an anticancer strategy. *Nat Rev Drug Discov* **12**: 931–947.

Graves DB (2012) The emerging role of reactive oxygen and nitrogen species in redox biology and some implications for plasma applications to medicine and biology. *J Phys D Appl Phys* **45**: 263001.

Graves DB (2014) Low temperature plasma biomedicine: a tutorial reviewa. *Phys Plasmas* **21**: 080901.

Gregory CD, Pound JD (2010) Microenvironmental influences of apoptosis in vivo and in vitro. *Apoptosis* **15**: 1029–1049.

Guerrero-Preston R, Ogawa T, Uemura M, Shumulinsky G, Valle BL, Pirini F, Ravi R, Sidransky D, Keidar M, Trink B (2014) Cold atmospheric plasma treatment selectively targets head and neck squamous cell carcinoma cells. *Int J Mol Med* **34**: 941–946.

Gulden M, Jess A, Kammann J, Maser E, Seibert H (2010) Cytotoxic potency of H2O2 in cell cultures: impact of cell concentration and exposure time. *Free Radic Biol Med* **49**: 1298–1305.

Hirst AM, Frame FM, Maitland NJ, O'connell D (2014a) Low temperature plasma causes double-strand break DNA damage in primary epithelial cells cultured from a human prostate tumor. *Plasma Sci IEEE Trans* **42**(10): 2740–2741.

Hirst AM, Frame FM, Maitland NJ, O'connell D (2014b) Low temperature plasma: a novel focal therapy for localized prostate cancer? *Biomed Res Int* **2014**: 878319.

Ishaq M, Kumar S, Varinli H, Han ZJ, Rider AE, Evans MD, Murphy AB, Ostrikov K (2014) Atmospheric gas plasma-induced ROS production activates TNF-ASK1 pathway for the induction of melanoma cancer cell apoptosis. *Mol Biol Cell* **25**: 1523–1531.

Jemal A, Bray F, Center MM, Ferlay J, Ward E, Forman D (2011) Global cancer statistics. *CA Cancer J Clin* **61**: 69–90.

Jones JS (2011) Radiorecurrent prostate cancer: an emerging and largely mismanaged epidemic. *Eur Urol* **60**: 411–412.

Kang SU, Cho JH, Chang JW, Shin YS, Kim KI, Park JK, Yang SS, Lee JS, Moon E, Lee K, Kim CH (2014) Nonthermal plasma induces head and neck cancer cell death: the potential involvement of mitogen-activated protein kinase-dependent mitochondrial reactive oxygen species. *Cell Death Dis* **5**: e1056.

Kasivisvanathan V, Emberton M, Ahmed HU (2013) Focal therapy for prostate cancer: rationale and treatment opportunities. *Clin Oncol (R Coll Radiol)* **25**: 461–473.

Keidar M, Walk R, Shashurin A, Srinivasan P, Sandler A, Dasgupta S, Ravi R, Guerrero-Preston R, Trink B (2011) Cold plasma selectivity and the possibility of a paradigm shift in cancer therapy. *Br J Cancer* **105**: 1295–1301.

Kepp O, Galluzzi L, Lipinski M, Yuan J, Kroemer G (2011) Cell death assays for drug discovery. *Nat Rev Drug Discov* **10**: 221–237.

Kim H, Park BK, Kim CK (2008) Spontaneous regression of pulmonary and adrenal metastases following percutaneous radiofrequency ablation of a recurrent renal cell carcinoma. *Korean J Radiol* **9**: 470–472.

Kim JY, Ballato J, Foy P, Hawkins T, Wei Y, Li J, Kim SO (2011) Apoptosis of lung carcinoma cells induced by a flexible optical fiber-based cold microplasma. *Biosens Bioelectron* **28**: 333–338.

Knake N, Niemi K, Reuter S, Schulz-Von Der Gathen V, Winter J (2008) Absolute atomic oxygen density profiles in the discharge core of a microscale atmospheric pressure plasma jet. *Appl Phys Lett* **93**: 131503–131503.

Krzykawska-Serda M, Dabrowski JM, Arnaut LG, Szczygiel M, Urbanska K, Stochel G, Elas M (2014) The role of strong hypoxia in tumors after treatment in the outcome of bacteriochlorin-based photodynamic therapy. *Free Radic Biol Med* **73C**: 239–251.

Lips IM, Dehnad H, Van Gils CH, Boeken Kruger AE, Van Der Heide UA, Van Vulpen M (2008) High-dose intensity-modulated radiotherapy for prostate cancer using daily fiducial marker-based position verification: acute and late toxicity in 331 patients. *Radiat Oncol* **3**: 15.

Ma Y, Ha CS, Hwang SW, Lee HJ, Kim GC, Lee KW, Song K (2014) Non-thermal atmospheric pressure plasma preferentially induces apoptosis in p53-mutated cancer cells by activating ROS stress-response pathways. *PLoS One* **9**: e91947.

Melcher A, Gough M, Todryk S, Vile R (1999) Apoptosis or necrosis for tumor immunotherapy: what's in a name? *J Mol Med (Berl)* **77**: 824–833.

Murakami T, Niemi K, Gans T, O'connell D, Graham WG (2013) Chemical kinetics and reactive species in atmospheric pressure helium-oxygen plasmas with humid-air impurities. *Plasma Sources Sci Technol* **22**: 015003.

Niemi K, O'connell D, Oliveira DE, Joyeux N, Nahon D, Booth L, Gans, T. JP (2013) Absolute atomic oxygen and nitrogen densities in radio-frequency driven atmospheric pressure cold plasmas: synchrotron vacuum ultra-violet high-resolution Fourier-transform absorption measurements. *Appl Phys Lett* **103**: 034102.

Ninomiya K, Ishijima T, Imamura M, Yamahara T, Enomoto H, Takahashi K, Tanaka Y, Uesugi Y, Shimizu N (2013) Evaluation of extra- and intracellular OH radical generation, cancer cell injury, and apoptosis induced by a non-thermal atmospheric-pressure plasma jet. *J Phys D Appl Phys* **46**: 425401.

Palacios DA, Miyake M, Rosser CJ (2013) Radiosensitization in prostate cancer: mechanisms and targets. *BMC Urol* **13**: 4.

Plewa JM, Yousfi M, Frongia C, Eichwald O, Ducommun B, Merbahi N, Lobjois V (2014) Low-temperature plasma-induced antiproliferative effects on multi-cellular tumor spheroids. *N J Phys* **16**: 043027.

Robert E, Vandamme M, Brullé L, Lerondel S, Le Pape A, Sarron V, Riès D, Darny T, Dozias S, Collet G, Kieda C, Pouvesle JM (2013) Perspectives of endoscopic plasma applications. *Clin Plasma Med* **1**: 8–16.

Sanchez-Ortiz RF, Tannir N, Ahrar K, Wood CG (2003) Spontaneous regression of pulmonary metastases from renal cell carcinoma after radio frequency ablation of primary tumor: an in situ tumor vaccine? *J Urol* **170**: 178–179.

Sharman WM, Allen CM, Van Lier JE (1999) Photodynamic therapeutics: basic principles and clinical applications. *Drug Discov Today* **4**: 507–517.

Sousa JS, Niemi K, Cox LJ, Algwari QT, Gans T, O'connell D (2011) Cold atmospheric pressure plasma jets as sources of singlet delta oxygen for biomedical applications. *J Appl Phys* **109**: 123302.

Sturmey RG, Hawkhead JA, Barker EA, Leese HJ (2009) DNA damage and metabolic activity in the preimplantation embryo. *Hum Reprod* **24**: 81–91.

Sullivan KF, Crawford ED (2009) Targeted focal therapy for prostate cancer: a review of the literature. *Ther Adv Urol* **1**: 149–159.

Vandamme M, Robert E, Lerondel S, Sarron V, Ries D, Dozias S, Sobilo J, Gosset D, Kieda C, Legrain B, Pouvesle JM, Pape AL (2012) ROS implication in a new antitumor strategy based on non-thermal plasma. *Int J Cancer* **130**: 2185–2194.

Voll RE, Herrmann M, Roth EA, Stach C, Kalden JR, Girkontaite I (1997) Immunosuppressive effects of apoptotic cells. *Nature* **390**: 350–351.

Wagenaars E, Gans T, O'connell D, Niemi K (2012) Two-photon absorption laser-induced fluorescence measurements of atomic nitrogen in a radio-frequency atmospheric-pressure plasma jet. *Plasma Sources Sci Technol* **21**: 042002.

Wang M, Holmes B, Cheng X, Zhu W, Keidar M, Zhang LG (2013) Cold atmospheric plasma for selectively ablating metastatic breast cancer cells. *PLoS One* **8**: e73741.

Waskoenig J, Niemi K, Knake N, Graham LM, Reuter S, Schulz-Von Der Gathen V, Gans T (2010) Atomic oxygen formation in a radio-frequency driven micro-atmospheric pressure plasma jet. *Plasma Sources Sci Technol* **19**: 045018.

Wiseman H, Halliwell B (1996) Damage to DNA by reactive oxygen and nitrogen species: role in inflammatory disease and progression to cancer. *Biochem J* **313**(Pt 1): 17–29.

Woo JA, Chen LN, Bhagat A, Oermann EK, Kim JS, Moures R, Yung T, Lei S, Collins BT, Kumar D, Suy S, Dritschilo A, Lynch JH, Collins SP (2014) Clinical characteristics and management of late urinary symptom flare following stereotactic body radiation therapy for prostate cancer. *Front Oncol* **4**: 122.

REVIEW

# Low temperature plasmas as emerging cancer therapeutics: the state of play and thoughts for the future

Adam M. Hirst[1] · Fiona M. Frame[2] · Manit Arya[3] · Norman J. Maitland[2] · Deborah O'Connell[1]

**Abstract** The field of plasma medicine has seen substantial advances over the last decade, with applications developed for bacterial sterilisation, wound healing and cancer treatment. Low temperature plasmas (LTPs) are particularly suited for medical purposes since they are operated in the laboratory at atmospheric pressure and room temperature, providing a rich source of reactive oxygen and nitrogen species (RONS). A great deal of research has been conducted into the role of reactive species in both the growth and treatment of cancer, where long-established radio- and chemo-therapies exploit their ability to induce potent cytopathic effects. In addition to producing a plethora of RONS, LTPs can also create strong electroporative fields. From an application perspective, it has been shown that LTPs can be applied precisely to a small target area. On this basis, LTPs have been proposed as a promising future strategy to accurately and effectively control and eradicate tumours. This review aims to evaluate the current state of the literature in the field of plasma oncology and highlight the potential for the use of LTPs in combination therapy. We also present novel data on the effect of LTPs on cancer stem cells, and speculatively outline how LTPs could circumvent treatment resistance encountered with existing therapeutics.

## Introduction

The role of reactive species in cancer initiation, progression and treatment has been intensively researched over the last few decades. The mechanistic actions of radio- and chemo-therapies frequently rely on the formation of reactive species, and they have been proposed as a means to preferentially target malignant cells [1]. Low temperature plasmas are known to generate a plethora of reactive oxygen and nitrogen species [2], and could present an exciting new modality for the treatment of tumours.

Plasmas are ionised gases, comprising a complex environment of charged particles, neutral gas molecules, UV radiation, electric fields and reactive species. They occur widely in nature (for example as lightning or the aurora borealis), yet can also be created in many forms in the laboratory to exploit their unique properties for many varied applications, from surface modification to clean energy production. Due to technological advancements, it has become possible to sustain plasmas at atmospheric pressure and room temperature. This has enabled the use of plasmas in a range of technological and biomedical applications,

Norman J. Maitland and Deborah O'Connell contributed equally to this work.

✉ Deborah O'Connell
deborah.oconnell@york.ac.uk

Adam M. Hirst
amh508@york.ac.uk

Fiona M. Frame
fiona.frame@york.ac.uk

Manit Arya
manit_arya@hotmail.com

Norman J. Maitland
njm9@york.ac.uk

[1] Department of Physics, York Plasma Institute, University of York, Heslington, UK

[2] YCR Cancer Research Unit, Department of Biology, University of York, Heslington, UK

[3] University College London, London, UK

⚝ Springer

and thus the conception of the field of 'plasma medicine' over the last decade. 'Low temperature plasmas' (LTPs) are very weakly ionised; the electrons, which can have temperatures ~$10^4$ K and drive the plasma processes, make up a very small fraction of the plasma (<0.1 %). The bulk of the plasma consists mainly of background neutral gas atoms and molecules, and due to the inefficient energy transfer between the light electrons and 'heavy' neutrals, the global environment remains at room temperature. This aspect allows the application of LTPs to temperature-sensitive materials, such as living tissues.

The general concept of plasmas in medicine is not totally new, as they have been utilised as electrosurgical instruments in medical practice for a number of years and in a range of procedures [3]. Recent innovations include instruments from Plasma Surgical and Arthrocare; hand-held devices capable of vaporising, sealing and dissecting tissues [4, 5]. LTPs are fundamentally different; as their name suggests, they do not utilise thermal effects to induce biological response. Instead, they induce biological response through the production of reactive species and potentially strong electric fields, and are a novel proposition for use in medical procedures. A sketch and photograph of a typical laboratory LTP jet set-up is shown in Fig. 1. Controlled gas flow is fed through glass tubing, around which high-voltage electrodes are positioned. The core plasma is ignited between these electrodes by applying a high voltage (typically up to 20 kV), and a plasma jet then propagates outwards and can interact with the biological sample. It is important to note that Fig. 1 represents only a single example; many different LTP designs and geometries exist that are intended for biomedical applications [7–11].

This review paper aims to highlight recent progress in the field of plasma oncology, and will present LTPs as a promising tool for future focal cancer treatment. Comparisons are made between the mechanisms of existing therapies and how the properties of LTPs could lead to more favourable treatment outcomes. The prospect of combining LTPs with existing therapies and technologies to exploit potential synergies is outlined, as well as a speculative view suggesting how LTPs may be capable of overcoming treatment resistance. We also present novel data on the cytotoxic effect of LTP on cancer stem cells cultured directly from an aggressive prostate tumour. Finally, introduction of LTPs into clinical practice is evaluated, and the logistics of patient treatment is discussed.

## Low temperature plasmas as a source of reactive species

Mounting evidence in the scientific and medical literature suggests that LTPs rely strongly on the formation of reactive species to facilitate cellular responses. Processes such as ionisation, dissociation, excitation and recombination of atoms and molecules within the plasma lead to a chemically rich environment of reactive oxygen species (ROS) including atomic oxygen (O) [12, 13], hydroxyl (OH) [14], superoxide ($O_2^-$)[15], singlet-delta oxygen ($^1O_2$) [16] and hydrogen peroxide ($H_2O_2$) [17]. In addition, depending upon the gas composition and plasma geometry, reactive nitrogen species (RNS) may include atomic nitrogen (N) [18], nitric oxide (NO) [19], peroxynitrite ($ONOO^-$) [20] and other members



Fig. 1 Schematic representation of low temperature plasma formation and application. Gas flow is ignited by high voltage applied across ring electrodes. The core plasma propagates from the end of the tube and is applied into a bulk tumour, causing DNA damage through the formation of reactive oxygen and nitrogen species. Note: this diagram is not to scale; in the accompanying image, the dimensions of central quartz glass tube are 70 × 6 mm. Elements of this figure are modified from Hirst et al. [6]
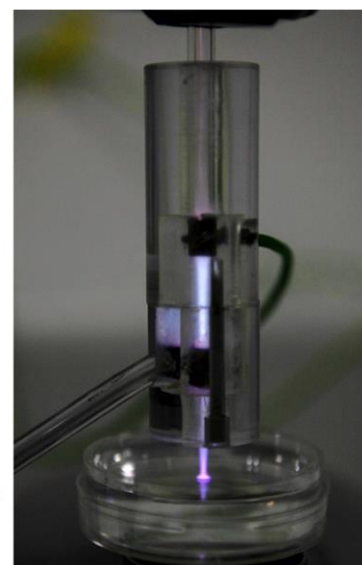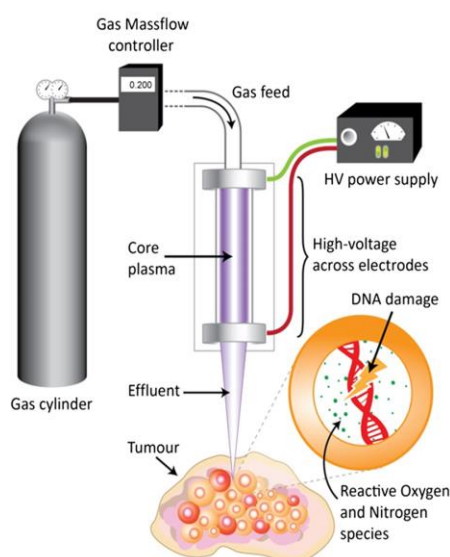
of the $NO_x$ family. The multitude of RONS generated by LTPs could provide significant advantages over other cancer therapies, e.g. radiotherapy and photodynamic therapy, which generally produce only ROS. Indeed, high concentrations of NO has been suggested to preferentially induce apoptosis in tumour cells, implying the action of nitrosative stress could prove crucial to successful cancer therapy [21].

The involvement of ROS in cancer initiation and progression [22], and their therapeutic potential [23] have been actively researched for many years. The cellular threat from low levels of ROS is well tolerated and neutralised through the action of enzymes including super oxide dismutase and catalase [24]. The inherent elevated metabolic activity in malignant cells (Warburg effect) may present a therapeutic window, as they are essentially already at their ROS-tolerance threshold or 'red-line' when compared with neighbouring normal cells [1, 25]. The creation of high levels of ROS is the mechanism by which long-established anti-tumour strategies, such as radio- [26] and some chemo-therapies [27, 28], operate to induce oxidative stress which result in cytopathic cellular responses. Given that LTPs create a multitude of reactive oxygen *and* nitrogen species (RONS) [29], they are an obvious candidate for cancer therapy; potentially being more efficacious than treatments which only involve ROS. This concept is discussed further in the context of treatment resistance in a later section.

The application of LTP to cells or tissues is a multi-phase process, which begins with an initial ignition and steady-state core plasma, followed by an afterglow plasma phase, leading to a diffusive interface with a liquid-like layer or environment. The liquid environment can either be represented by treatment of the cell culture media in laboratory experiments, or more physiologically the fluid within and surrounding a tumour in a clinical plasma application. This plasma-modified liquid environment then influences the cells and tissues around it. An illustrative overview of this process is depicted in Fig. 2, along with approximate time-scales for various phenomena in the plasma and liquid phases, and subsequent biological interaction.

The dynamics of the chemistry within the plasma core are extremely complex. Global models have been developed to capture this, which comprise in excess of 60 different species, involved in ~1000 different reactions [2]. Translation to the liquid environment and ultimately a precise understanding of the specific extra- and intra-cellular RONS involved in both cellular effect and response, and their concentrations is vastly more so. Predictive numerical models have attempted to resolve and understand this complexity, including both the variation in chemistry between the gas-liquid-tissue phases [30], the fluxes of different reactive species at the tissue surface [31], and the influence of different molecular gas admixtures [13, 18, 32]. The mechanistic effects of LTPs on cells are presented in the following section.

## Mechanisms of LTP—cell interaction and response

LTPs create and transfer numerous RONS to the cellular environment, as discussed earlier. Current evidence implies that the production of RONS is primarily responsible for cytopathic effects of the plasma. However, other facets of LTPs may contribute to ultimate cell fate and treatment outcome.

LTPs have been applied to a range of different malignant cell lines in culture with extremely promising results. A range of common cellular responses have been documented including DNA damage [33, 34], decreased cell viability and clonogenicity [35, 36], reduced proliferation [37] and cell cycle arrest [38, 39]. From the growing literature, it would appear the cell death mechanism following LTP treatment varies with both the cell type and plasma source used. The vast majority of studies report apoptosis [19, 37, 40–43]; however, senescence [44] and non-apoptotic cell death [36] have also been presented. A summary of experimental approaches to cell treatment and subsequent cell death mechanism is given in Table 1. The studies presented therein were selected to reflect the different types of plasma, exposure times and approaches to treatment adopted within the field, and how these might relate to the observed outcomes. Elevated RONS levels are continually cited as the likely perpetrators of plasma-induced effects, leading to the activation of apoptotic pathways including TNF-ASK1 [46], ATM/p53 [19] and MAPK [15]. Furthermore, LTP effects have been shown to be (at least partially) alleviated by the use of various RONS scavengers [19, 47], further confirming the central role of reactive species produced by LTPs. Despite this, strong electric fields produced by some LTPs may play an important, synergistic role in plasma-cell interaction [48] and are discussed further in a later section.

Many investigators report a selective effect following LTP treatment, i.e. the plasma-effect preferentially targets tumour cells and leaves normal cells relatively unscathed [36, 49]. This is without doubt a highly desirable, 'gold standard' outcome. One explanation may be the rapidly dividing nature of tumour cells, increasing their vulnerability to DNA damage in M-phase [50], and/or the different tolerances of normal and cancer cells to elevated ROS levels [25] as alluded to earlier. The latter may explain a recent observation of an elevated autophagic response of normal cells when compared to tumour cells [17]. However, a more simple explanation may be the comparison of different cell types, for example normal fibroblasts with epithelial cancer cells, which may have quite different response profiles.

LTPs have also been applied to three-dimensional cell line models including spheroids and murine xenografts. Surface treatment of glioma xenografts with LTP showed a significant reduction in tumour volume, facilitated by ROS-induced caspase-3-dependent cell death [45]. In an earlier study, the same group showed that LTP treatment of tumours resulted in a 58 %
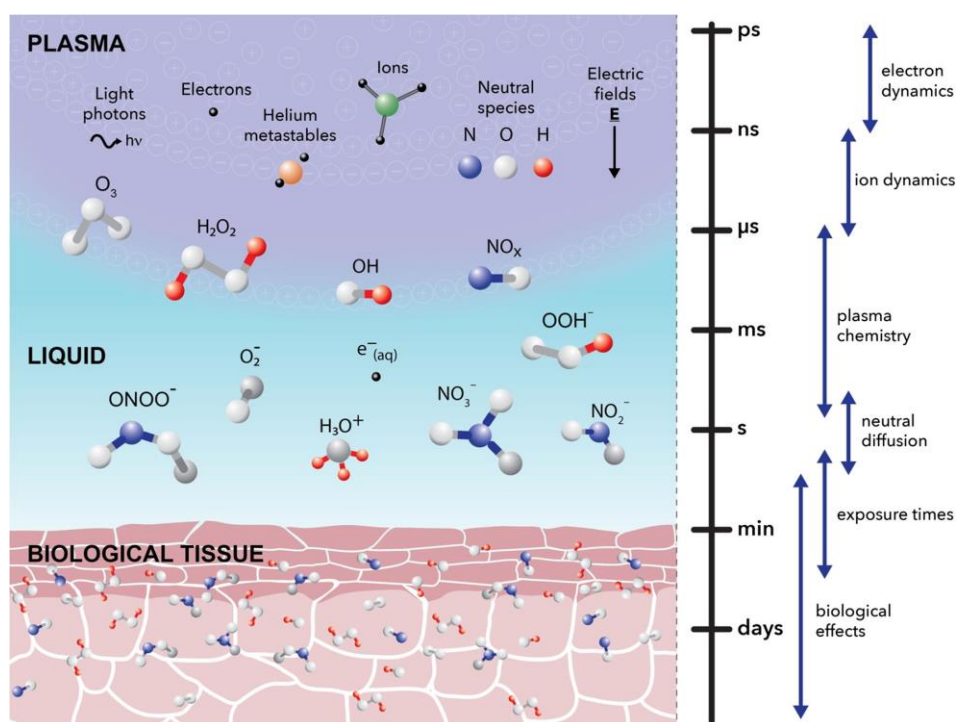
**Fig. 2** An illustrative representation of the multi-phase transfer of plasma species towards a biological sample. The main components of the plasma phase, including ions, photons and neutral species, are shown, leading to the creation of various RONS across the plasma-liquid interface and their propagation towards and diffusion through an arbitrary tissue layer. In addition, approximate timescales governing various phenomena across the plasma-liquid phases and biological interaction are outlined

**Table 1** LTP treatment induces different paths to cell death. Summary of assorted cell treatment methods and associated death mechanisms for a range of malignancies

| Cancer type | Method of treatment | Treatment duration | Cell death mechanism | Reference |
|---|---|---|---|---|
| Prostate cancer cell lines: PC-3 and LNCaP | In suspension, 500 μl volume | 10 s | Apoptosis | Weiss et al. [37] |
| Glioma cell lines: U87, U373, A172 | Adherent cells, 96-well plates, ~40 % confluence | Up to 180 s | Apoptosis/necrosis | Siu et al. [40] |
| Lymphoma cell line: U937 | Adherent cells, 10 cm plates, 5 ml volume | Up to 480 s | Apoptosis | Kaushik et al. [42] |
| Malignant cell lines from various sites | Adherent cells, 35 mm plates | 30–60 s, up to 10 repeated exposures | Apoptosis | Ma et al. [19] |
| Colorectal cancer cell lines: Caco2, HCT116, SW480 and HT29 | Adherent cells in various multi-well culture plates | Up to 30 s | Apoptosis | Ishaq et al. [41] |
| Glioma and colorectal cancer cell lines: U87MG-Luc2 and HCT-116-Luc2. | Adherent cells, 24-well plates, 500 μl volume | Up to 30 s | Apoptosis | Vandamme et al. [45] |
| Glioma xenografts: U87MG-Luc2 | Subcutaneous tumours | 6 min daily for 5 consecutive days | Apoptosis | |
| Head and neck cancer cell lines: FaDu, SNU1041, SNU899 and HN9 | In suspension, 6 cm plates, 3 ml volume | 1 s at either 2 or 4 kV | Apoptosis | Kang et al. [15] |
| FaDu xenografts | Subcutaneous tumours | 20 s daily for 20 days | Apoptosis | |
| Various melanoma cell lines | Adherent cells, assorted culture plates, without culture medium | Up to 120 s | Senescence | Arndt et al. [44] |
| Prostate cancer primary epithelial cells | In suspension, 1.5 ml volume | Up to 600 s | Necrosis, autophagy | Hirst et al. [17] |

increased lifespan over untreated mice [51]. Application of LTP in an in vivo head and neck cancer cell line model showed significant reduction in tumour mass and volume, verified by DNA fragmentation and caspase-3 positive staining, indicative of apoptosis through activation of p38 and JNK [15].

A recent study showed that primary prostate cells, cultured directly from patient tissue samples, rapidly underwent necrosis following exposure to LTP [17]. In addition, the effect on both normal and cancer prostate cells from the same patient was largely comparable. These findings imply that (a) primary cells may respond quite differently to LTP treatment than the broadly apoptotic response found in various cell lines, and (b) selective plasma effects may be less pronounced when LTP is applied to patients. Clearly, further verification of primary cells and primary xenografts from various tumour sites will provide further insight into patient response to LTP. The safe application of LTP to cancerous ulcers has been demonstrated for palliative purposes, but also showed partial tumour remission in some patients [52].

Direct and uniform exposure of all cells within a bulk tumour population to LTP treatment would be extremely technically challenging. However, it is conceivable that cell-to-cell communication will play a role in LTP treatment of a tumour. Radiation-induced bystander effects (RIBEs) are well documented following DNA damaging events and associated elevation in ROS levels in irradiated cells, which lead to extra-cellular stress-signalling to neighbouring non-irradiated cells [53]. Given that LTPs are known to inflict comparable initial cytotoxic effects on tumour cells, it would therefore seem logical to anticipate a similar plasma-induced bystander effect following LTP treatment [54].

Although much of the focus of plasma medicine studies centre around elevated ROS levels and their effects, the formation of strong localised electric fields by LTPs can also occur. These may interact directly with cell membranes and thus cause similar effects to those of emerging electroporative cancer therapies. Electroporation treatments utilise strong electric fields to irreversibly compromise cell membranes to provoke a cytocidal response. Nanoknife technology has been proposed for focal treatment of pancreatic [55], prostate [56] and renal cancers [57]. Numerical modelling has suggested that LTPs may create electric fields in the hundreds of kilovolt/centimetre (kV/cm) range [58], capable of penetrating a few cell layers, and generating sufficiently high fields within individual cells for electroporative effects [59]. The geometry and type of plasma will determine the presence and strength of the electric field. Novel methods and diagnostic techniques have quantified average field strengths of around 10–20 kV/cm within LTPs, but locally these may rise towards 100 kV/cm [60, 61]. Crucially, electric field strength has recently been determined for plasmas propagating through elongated capillaries [48]; the importance of which is discussed later. Electroporative effects have indeed been demonstrated biologically following plasma treatment [62], which may irreversibly damage cell membranes

and aid the transfer of RONS into the cell, as well as permitting leakage of intra-cellular components. In some circumstances, plasmas can also generate focussed shockwaves that propagate through solutions (and into tissues), which have been shown to induce cell death in vivo [63].

## Combination of LTP treatment with existing cancer therapies to exploit synergistic gains

Whilst LTPs show clear potential to be an effective future cancer therapy in their own right, their efficacy could be further enhanced by combining them with existing treatment modalities. A recent study showed that a low temperature plasma gun was more effective than the chemotherapeutic agent gemcitabine in reducing both tumour volume and mass in an orthotopic pancreatic cancer model [64]. However, alternating plasma treatment with the drug saw further significant increases in treatment efficacy. This poses the possibility of combining plasma treatments with current standard treatment modalities, which may exploit potential additive or synergistic effects, leading to improved treatment outcomes.

LTPs may also be considered as an alternative option to treat malignancies that are resistant to the conventional treatment approaches. One example is temozolomide (TMZ), the standard initial chemotherapeutic agent prescribed to glioblastoma patients. However, tumours which express high levels of the enzyme O6-methylguanine-DNA methyltransferase (MGMT) show high resistance to TMZ [65]. When treated with LTP, glioblastoma cell lines (including MGMT-positive cells) showed reduced viability and clonogenicity, cell-cycle arrest, and ultimately apoptosis far in excess of TMZ-treated control cells [66]. A similar finding was observed in a chemo-resistant hepatocarcinoma model, where treatment with LTP lead to significant cytotoxic effects [67]. This demonstrates the potential for the use of LTPs as a salvage treatment option for patients who have failed the standard treatment approach, or perhaps pre-emptively in tumours that are known to be resistant to certain agents.

Recent studies have demonstrated the use of gold nanoparticles (AuNPs) for targeted delivery into tumour cells as drug carriers [68] or radiosensitisers [69]. AuNPs may also provide a means to effectively target cancer stem cells (CSCs) [70], a small population of cells believed by many to be the root of treatment resistance and recurrence, which is discussed further in the following section. The potential of AuNPs has led plasma physicists to investigate their use in conjunction with LTPs [71]. When utilised together, the combination AuNPs with LTP treatment enhanced efficacy beyond that of either agent alone in glioblastoma cells [72]. Treatment with LTP may also increased the uptake of AuNPs into malignant cells [73]. The amalgamation of LTPs and AuNPs may also present an opportunity to increase the cytotoxic selectivity of LTP towards tumour cells [74, 75].

The exact mechanism of plasma-induced cytopathic effects could prove crucial to the long-term success of any prospective anti-cancer treatment, broadly speaking: apoptosis or necrosis. Apoptotic cell death is potentially immunosuppressive and thus can assist immune system evasion of the tumour [76, 77]. However, in several pre-clinical studies addressing the combination of radio- and immuno-therapies to improve therapeutic potential [78], it has been shown that necrotic cell death can increase tumour immunogenicity through induction of heat shock protein expression [79]. Moreover, necrosis is induced by thermally ablative treatments such as cryotherapy [80], radiofrequency ablation [81] and HIFU [82], and is known to cause local inflammation at the treatment site. As mentioned previously, it has recently been demonstrated that prostate cancer cells cultured directly from patient tissue samples and treated with LTP rapidly initiate necrotic cell death [17]. This speculatively raises the question of immune activation against the tumour following plasma application, and the possibility of spontaneous regression of metastatic tumours, as has been occasionally recorded following radiotherapy [83], radiofrequency ablation [84, 85] and cryotherapy [86]. Direct combination with immunotherapy may present further synergistic prospects [87]. As a result, it may be argued that plasma-induced cell death via necrosis *could* provide the most effective long-term treatment outcome. Should this be the case, immune checkpoint inhibitors (such as nivolumab, which has very recently demonstrated efficacy in the treatment of advanced nonsquamous non-small-cell lung cancer and metastatic melanoma [88, 89]) may present an interesting prospect for future use in conjunction with LTP to boost tumour immunogenicity. Another thought-provoking concept is the direct stimulation of immune cells with LTPs, potentially increasing the efficacy of macrophages against tumour cells [90].

## Overcoming resistance to conventional treatments with low temperature plasmas

As with any prospective new treatment, there are questions regarding potential treatment resistance, as commonly experienced with some currently applied cancer therapies. Tumour hypoxia has been identified as one probable factor in radio- and chemo-therapeutic resistance and tumour invasiveness [91]. Supporting evidence has been reported recently in many different malignancies including those of the lung [92], liver [93], breast [94, 95] and brain [96]. Whilst direct DNA damage is inflicted by energetic particles, secondary damage following radiotherapy is caused by the production of oxygen radicals from the interaction of ionising X-rays and molecular $O_2$ in tissues and the local environment. As a result, in oxygen-deficient regions of the tumour, lethal DNA damage may not be achieved [97]. Hypoxia may not be so much of an issue for LTP therapy, since the majority of LTP cancer studies feed small admixtures of molecular oxygen (or nitrogen) into the main gas flow to aid the production of oxidative (and nitrosative) radicals. As such, LTP treatment could provide oxygen radicals directly to the treatment site, circumventing the need for endogenous $O_2$ in the tissue (as with radiotherapy), which may surmount the issue of hypoxic resistance. The success of this theory would depend strongly on the means of treatment administration and reactive species penetration, which are discussed in the subsequent section.

CSCs have been proposed to be the root of both disease initiation [98] and recurrence [99]. They have been widely implicated in both radio- and chemo-resistance [100–103]. One reason for this may be higher levels of heterochromatin in CSCs compared to the bulk population, affording added protection against DNA damaging treatments [104]. It is also thought that CSCs have higher levels of ROS-quenching enzymes in order to alleviate toxicity effects from reactive species formation [105] more effectively than their differentiated counterparts. Overloading CSCs with an abundance of RONS generated by LTPs may overcome this protective shield.

Our own experimental evidence suggests that LTP can be delivered in cytotoxic doses to CSCs. Figure 3 shows high levels of DNA damage (quantified using the Comet assay, based on [108]) following LTP jet treatment [17], irrespective of cellular sub-population. Here, the cells treated with plasma were primary prostate epithelial cells, cultured directly from an aggressive Gleason grade 9 tumour. The cells were sorted into sub-populations [106] and treated in suspension. Whilst this is very preliminary data, its inclusion serves to demonstrate the potential of LTP to induce highly significant cytotoxic effects in cells that are thought to be a causal factor in treatment resistance and relapse.
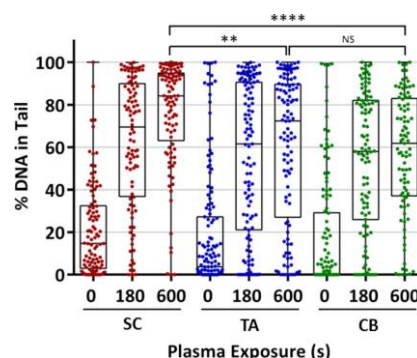


**Fig. 3** LTP induces DNA damage in cancer stem cells. Prostate cancer stem cells (*SC*), transit amplifying (*TA*) and committed basal (*CB*) cells were cultured and fractionated [106, 107] from a Gleason grade 9 metastatic tumour, and treated as described in Hirst et al. [17]. Statistical analysis of plasma treatments was calculated using Mann–Whitney test against untreated samples and showed $P < 0.0001$ significance, unless otherwise indicated (**$P < 0.01$, ****$P < 0.0001$)

## Progress towards the clinical use of low temperature plasmas

Many different plasma designs and geometries exist across academic institutions, e.g. [6, 7], demonstrating a broad versatility, but also highlighting the fact that direct data comparison can be problematic. Standardised 'reference' plasma jets are being developed across research centres to help unravel the fundamental plasma physics and chemistry. It is also possible that different LTP sources will ultimately find different clinical uses. Some proposed uses include intra-operative treatment of potentially positive surgical margins following tumour excision by surgery [37], injection of plasma-activated media into the tumour [109, 110], and decontamination of ulcerations in advanced head and neck cancer patients as mentioned earlier [52].

The majority of published studies in the field of plasma oncology focus on the direct application of LTPs to tumour cells. To fully eradicate solid tumours, the cytotoxic effect of plasma application must be capable of penetrating several layers of cells. A recent study on colorectal cancer cells, cultured as spheroids in suspension and treated with an LTP jet, showed a reduction in growth rate at low exposures and a complete growth arrest at longer plasma exposures of [111]. However, only the first few outer layers of the spheroid showed γH2AX-positive foci, suggesting that plasma-induced cell damage was surface-limited. Another report used agarose gel as a tissue-substitute to model the transfer of RONS across a biologically relevant interface. Reactive species were detected in the liquid regardless of whether the plasma jet was in direct contact with the agarose or not, and even after the plasma had extinguished [112]. This suggested that RONS were released from the agarose, created in the liquid environment as secondary reactions, or both, even after treatment. This simple model shows that reactive species produced by LTPs can cross a tissue-like interface (at least up to a few mm), which when combined with a potential plasma-induced bystander effect gives hope for cytopathic plasma-effects in solid tumours. Despite several in vivo studies showing promising levels of tumour reduction following LTP application [15, 45, 113], complete tumour eradication and long-term disease-free outcome remains to be proven.

The most successful method of realising an effective, focal and minimally invasive surgical approach is likely to be penetration of the plasma into the tumour core, to destroy the cancer radially outwards. Although many tumours are multi-focal, it has been argued that targeted treatment to only the index lesion of a localised tumour is sufficient to provide satisfactory disease control [114], in addition to limiting treatment invasiveness. The concept of inserting the plasma transperineally into the centre of a prostate tumour was proposed in a recent review article [6], and is expanded for an arbitrary solid malignancy in Fig. 4. We propose that this
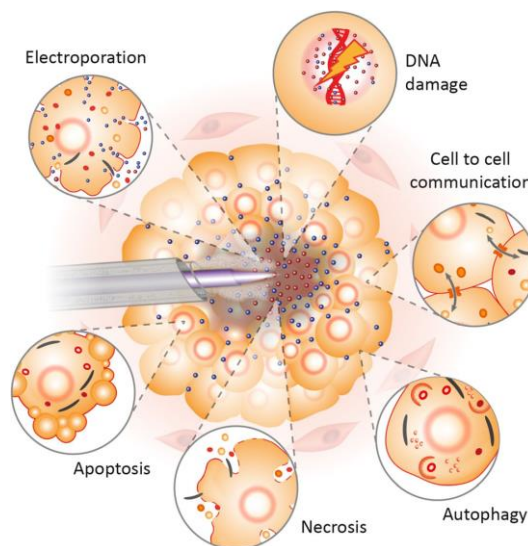


**Fig. 4** Illustration of LTP treatment of a tumour. In the proposed approach, the LTP probe is inserted under needle guidance into the core of the tumour. The plasma is then ignited, creating short-lived reactive species (*red dots*) that induce DNA damage, necrosis and potentially electroporative effects to cells in the immediate vicinity. The diffusion of longer-lived species (*blue dots*) to the tumour periphery is shown, contributing to apoptotic and plasma-induced bystander effects. Proposed cellular effects and responses are estimated based on their proximity to the plasma source. Gas extraction is also indicated through a co-axial configuration in the LTP probe. Elements of this figure are adapted from Hirst et al. [17]

concept should ensure enhanced targeted treatment of a tumour, compared to conventional surgical or radiotherapy techniques, and more controlled tumour volume destruction than is feasible with alternative ablative techniques such as RFA or cryotherapy.

Assuming the effects of LTP could propagate beyond a few cell layers (be it directly or via bystander effects), precisely monitored plasma ablation should also enable a satisfactory clearance zone to be achieved. This implies that damage to normal cells is not necessarily a negative feature, as a degree of collateral damage is a more favourable consequence than incomplete tumour ablation. Clearance margins of ~1 cm have been suggested in some cases [115], to maximise long-term disease-free outcome.

The propagation of LTPs in liquid environments has been demonstrated experimentally [116], where, depending on the operating parameters, the plasma may adopt either a bush- or tree-like formation after generation [117]. Clearly, the degree of relative moisture within the tumour environment will play a role in the plasma propagation and chemistry, and is likely to vary from tumour to tumour. Delivery of the plasma to areas that are potentially difficult to access and penetration inside the tumour are two of the main technical hurdles with this

proposition; nevertheless, evidence within the literature suggests both can be overcome. As plasmas can be propagated along tubes of metres in length [118], precise LTP delivery even to tumours deep within the body should be possible in principle. In shorter tubes, plasmas have been sustained in tubes as small as ~10 μm in diameter [119]. Internal plasma application has already been evaluated as effective and well-tolerated in a pancreatic in vivo model [113]. As some internal applications may require longer tubing lengths than others, the inherently short lifetimes of the most reactive (and thus most damaging) species may curtail their journey from source to target. However, provided an active plasma emerges from the end of the tube where electrons are present, short-lived species will be created locally at the application site. This concept is illustrated in Fig. 4, but largely depends on the plasma source used. Regardless, a rigorous knowledge of the RONS densities emerging from the specific aperture used for application is essential. It has recently been suggested that control and selectivity towards different reactive species may be achievable by using different feed gases [120]. Maximal lethality of treatment is likely to be found by tuning the plasma operating conditions including voltage waveform parameters, gas composition and treatment duration [121]. Finally, some form of gas flow extraction (as highlighted in Fig. 4) during LTP treatment would almost certainly be necessary to minimise the risk of embolisms, and could be combined with cyclic LTP application.

## Conclusions

Earlier diagnosis and accurate targeting, combined with minimal damage to surrounding tissues and reduced patient side effects, has led to increased popularity of tumour treatment with thermal and non-thermal ablative focal therapies. Over the last decade, LTPs have demonstrated their potential as a novel approach in the targeted treatment of cancer. Both in vitro and in vivo studies have shown promising results in a wide range of different malignancies. In addition, both modelling and experimental studies are beginning to unravel the complex interplay of plasma-liquid-cell interphases. Through precise application and accurate monitoring, LTPs could offer defined and effective treatment for many tumours, whilst minimising side effects to the patient. This review has highlighted the multifaceted action of LTPs, through the formation of a rich chemistry containing RONS and the possible contribution of strong electric fields in biological response. It has also speculatively outlined the potential for the application of LTPs as a combination therapy in conjunction with other current approaches, and how they may be able to overcome treatment resistance. Finally, a plausible treatment approach is presented, demonstrating how LTPs might be applied to any arbitrary solid mass, to achieve maximum lethality to the target lesion. It is hoped that the evidence and concepts presented in this paper have conveyed the undeniable promise of LTP technology for the future treatment of cancer.

**Compliance with ethical standards**

**Conflicts of interest** None

## References

1. Gorrini C, Harris IS, Mak TW. Modulation of oxidative stress as an anticancer strategy. Nat Rev Drug Discov. 2013;12(12):931–47.
2. Murakami T, Niemi K, Gans T, O'Connell D, Graham WG. Chemical kinetics and reactive species in atmospheric pressure helium-oxygen plasmas with humid-air impurities. Plasma Sources Sci Technol 2013; 22(1):015003.
3. Stalder KR, McMillen DF, Woloszko J. Electrosurgical plasmas. J Phys D Appl Phys. 2005;38(11):1728–38.
4. Butler-Manuel S, Lippiatt J, Madhuri TK. Interval debulking surgery following neo-adjuvant chemotherapy for stage IVB ovarian cancer using neutral argon plasma (PlasmaJet). Gynecol Oncol. 2014;135(3):622–3.
5. Woloszko J, Stalder KR, Brown IG. Plasma characteristics of repetitively-pulsed electrical discharges in saline solutions used for surgical procedures. IEEE Trans Plasma Sci. 2002;30(3):1376–83.
6. Hirst AM, Frame FM, Maitland NJ, O'Connell D. Low temperature plasma: a novel focal therapy for localized prostate cancer? BioMed Res Int. 2014;2014:878319.
7. Weltmann KD, Polak M, Masur K, von Woedtke T, Winter J, Reuter S. Plasma processes and plasma sources in medicine. Contrib Plasma Phys. 2012;52(7):644–54.
8. Kim C-H, Bahn JH, Lee S-H, Kim G-Y, Jun S-I, Lee K, et al. Induction of cell growth arrest by atmospheric non-thermal plasma in colorectal cancer cells. J Biotechnol. 2010;150(4):530–8.
9. Julák J, Scholtz V. Decontamination of human skin by low-temperature plasma produced by cometary discharge. Clin Plasma Med. 2013;1(2):31–4.
10. Huang J, Li H, Chen W, Lv G-H, Wang X-Q, Zhang G-P, et al. Dielectric barrier discharge plasma in Ar/O2 promoting apoptosis

behavior in A549 cancer cells. Appl Phys Lett. 2011;99(25): 253701.

11. Fridman G, Shereshevsky A, Jost MM, Brooks AD, Fridman A, Gutsol A, et al. Floating electrode dielectric barrier discharge plasma in air promoting apoptotic behavior in melanoma skin cancer cell lines. Plasma Chem Plasma Process. 2007;27(2):163–76.

12. Waskoenig J, Niemi K, Knake N, Graham LM, Reuter S, Schulz-von der Gathen V, et al. Atomic oxygen formation in a radio-frequency driven micro-atmospheric pressure plasma jet. Plasma Sources Science and Technology. 2010;19(4):045018.

13. Niemi K, O'Connell D, de Oliveira N, Joyeux D, Nahon L, Booth JP, et al. Absolute atomic oxygen and nitrogen densities in radio-frequency driven atmospheric pressure cold plasmas: synchrotron vacuum ultra-violet high-resolution Fourier-transform absorption measurements. Appl Phys Lett. 2013;103(3):034102.

14. Xu D, Liu D, Wang B, Chen C, Chen Z, Li D, et al. In situ OH generation from $O_2^-$ and $H_2O_2$ plays a critical role in plasma-induced cell death. PLoS One. 2015;10(6):e0128205.

15. Kang SU, Cho JH, Chang JW, Shin YS, Kim KI, Park JK, et al. Nonthermal plasma induces head and neck cancer cell death: the potential involvement of mitogen-activated protein kinase-dependent mitochondrial reactive oxygen species. Cell Death Dis 2014;5:e1056.

16. Sousa JS, Niemi K, Cox LJ, Algwari QT, Gans T, O'Connell D. Cold atmospheric pressure plasma jets as sources of singlet delta oxygen for biomedical applications. J Appl Phys 2011;109(12): 123302–123302-8.

17. Hirst AM, Simms MS, Mann VM, Maitland NJ, O'Connell D, Frame FM. Low-temperature plasma treatment induces DNA damage leading to necrotic cell death in primary prostate epithelial cells. Br J Cancer. 2015;112(9):1536–45.

18. Wagenaars E, Gans T, O'Connell D, Niemi K. Two-photon absorption laser-induced fluorescence measurements of atomic nitrogen in a radio-frequency atmospheric-pressure plasma jet. Plasma Sources Sci Technol 2012;21(4).

19. Ma Y, Ha CS, Hwang SW, Lee HJ, Kim GC, Lee KW, et al. Non-thermal atmospheric pressure plasma preferentially induces apoptosis in p53-mutated cancer cells by activating ROS stress-response pathways. PLoS One. 2014;9(4):e91947.

20. Lukes P, Dolezalova E, Sisrova I, Clupek M. Aqueous-phase chemistry and bactericidal effects from an air discharge plasma in contact with water: evidence for the formation of peroxynitrite through a pseudo-second-order post-discharge reaction of $H_2O_2$ and $HNO_2$. Plasma Sources Sci Technol. 2014;23(1):015019.

21. Hirst D, Robson T. Targeting nitric oxide for cancer therapy. J Pharm Pharmacol. 2007;59(1):3–13.

22. Klaunig JE, Kamendulis LM. The role of oxidative stress in carcinogenesis. Annu Rev Pharmacol Toxicol. 2004;44:239–67.

23. Pelicano H, Carney D, Huang P. ROS stress in cancer cells and therapeutic implications. Drug Resist Updat. 2004;7(2):97–110.

24. Tovmasyan A, Maia CG, Weitner T, Carballal S, Sampaio RS, Lieb D, et al. A comprehensive evaluation of catalase-like activity of different classes of redox-active therapeutics. Free Radic Biol Med. 2015; 86:308–21.

25. Trachootham D, Alexandre J, Huang P. Targeting cancer cells by ROS-mediated mechanisms: a radical therapeutic approach? Nat Rev Drug Discov. 2009;8(7):579–91.

26. Yoshida T, Goto S, Kawakatsu M, Urata Y, Li TS. Mitochondrial dysfunction, a probable cause of persistent oxidative stress after exposure to ionizing radiation. Free Radic Res. 2012;46(2):147–53.

27. Sangeetha P, Das UN, Koratkar R, Suryaprabha P. Increase in free radical generation and lipid peroxidation following chemotherapy in patients with cancer. Free Radic Biol Med. 1990;8(1):15–9.

28. Conklin KA. Chemotherapy-associated oxidative stress: impact on chemotherapeutic effectiveness. Integr Cancer Ther. 2004;3(4):294–300.

29. Graves DB. The emerging role of reactive oxygen and nitrogen species in redox biology and some implications for plasma applications to medicine and biology. J Phys D Appl Phys 2012;45(26).

30. Chen C, Liu DX, Liu ZC, Yang AJ, Chen HL, Shama G, et al. A model of plasma-biofilm and plasma-tissue interactions at ambient pressure. Plasma Chem Plasma Process. 2014;34(3):403–41.

31. Babaeva NY, Kushner MJ. Reactive fluxes delivered by dielectric barrier discharge filaments to slightly wounded skin. J Phys D Appl Phys. 2013;46(2):025401.

32. Van Gaens W, Iseni S, Schmidt-Bleker A, Weltmann K, Reuter S, Bogaerts A. Numerical analysis of the effect of nitrogen and oxygen admixtures on the chemistry of an argon plasma jet operating at atmospheric pressure. New J Phys. 2015;17(3):033003.

33. Hirst AM, Frame FM, Maitland NJ, O'Connell D. Low temperature plasma causes double-strand break DNA damage in primary epithelial cells cultured from a human prostate tumor. IEEE Trans Plasma Sci. 2014;42(10):2740–1.

34. Han X, Klas M, Liu Y, Stack MS, Ptasinska S. DNA damage in oral cancer cells induced by nitrogen atmospheric pressure plasma jets. Appl Phys Lett. 2013;102(23):233703.

35. Wende K, Williams P, Dalluge J, Gaens WV, Aboubakr H, Bischof J, et al. Identification of the biologically active liquid chemistry induced by a nonthermal atmospheric pressure plasma jet. Biointerphases. 2015;10(2):029518.

36. Guerrero-Preston R, Ogawa T, Uemura M, Shumulinsky G, Valle BL, Pirini F, et al. Cold atmospheric plasma treatment selectively targets head and neck squamous cell carcinoma cells. Int J Mol Med. 2014;34(4):941–6.

37. Weiss M, Gumbel D, Hanschmann EM, Mandelkow R, Gelbrich N, Zimmermann U, et al. Cold atmospheric plasma treatment induces anti-proliferative effects in prostate cancer cells by redox and apoptotic signaling pathways. PLoS One. 2015;10(7): e0130350.

38. Nakai N, Fujita R, Kawano F, Takahashi K, Ohira T, Shibaguchi T, et al. Retardation of C2C12 myoblast cell proliferation by exposure to low-temperature atmospheric plasma. J Physiol Sci. 2014;64(5):365–75.

39. Chang JW, Kang SU, Shin YS, Kim KI, Seo SJ, Yang SS, et al. Non-thermal atmospheric pressure plasma induces apoptosis in oral cavity squamous cell carcinoma: Involvement of DNA-damage-triggering sub-G(1) arrest via the ATM/p53 pathway. Arch Biochem Biophys. 2014;545:133–40.

40. Siu A, Volotskova O, Cheng X, Khalsa SS, Bian K, Murad F, et al. Differential effects of cold atmospheric plasma in the treatment of malignant glioma. PLoS One. 2015;10(6):e0126313.

41. Ishaq M, Evans MD, Ostrikov KK. Atmospheric pressure gas plasma-induced colorectal cancer cell death is mediated by Nox2-ASK1 apoptosis pathways and oxidative stress is mitigated by Srx-Nrf2 anti-oxidant system. Biochim Biophys Acta. 2014;1843(12):2827–37.

42. Kaushik N, Kumar N, Kim CH, Kaushik NK, Choi EH. Dielectric barrier discharge plasma efficiently delivers an apoptotic response in human monocytic lymphoma. Plasma Process Polym. 2014;11(12).

43. Gibson AR, McCarthy HO, Ali AA, O'Connell D, Graham WG. Interactions of a non-thermal atmospheric pressure plasma effluent with PC-3 prostate cancer cells. Plasma Process Polym. 2014;11(12):1142–9.

44. Arndt S, Wacker E, Li YF, Shimizu T, Thomas HM, Morfill GE, et al. Cold atmospheric plasma, a new strategy to induce senescence in melanoma cells. Exp Dermatol. 2013;22(4):284–9.

45. Vandamme M, Robert E, Lerondel S, Sarron V, Ries D, Dozias S, et al. ROS implication in a new antitumor strategy based on non-thermal plasma. Int J Cancer. 2012;130(9):2185–94.

46. Ishaq M, Kumar S, Varinli H, Han ZJ, Rider AE, Evans MD, et al. Atmospheric gas plasma-induced ROS production activates TNF-ASK1 pathway for the induction of melanoma cancer cell apoptosis. Mol Biol Cell. 2014;25(9):1523–31.

47. Kaushik N, Uddin N, Sim GB, Hong YJ, Baik KY, Kim CH, et al. Responses of solid tumor cells in DMEM to reactive oxygen species generated by non-thermal plasma and chemically induced ROS systems. Sci Rep. 2015;5:8587.

48. Robert E, Darny T, Dozias S, Iseni S, Pouvesle JM. New insights on the propagation of pulsed atmospheric plasma streams: from single jet to multi jet arrays. Phys Plasmas. 2015;22(12):122007.

49. Wang M, Holmes B, Cheng X, Zhu W, Keidar M, Zhang LG. Cold atmospheric plasma for selectively ablating metastatic breast cancer cells. PLoS One. 2013;8(9):e73741.

50. Hubenak JR, Zhang Q, Branch CD, Kronowitz SJ. Mechanisms of injury to normal tissue after radiotherapy: a review. Plast Reconstr Surg. 2014;133(1):49e–56.

51. Vandamme M, Robert E, Doziaz S, Sobilo J, Lerondel S, Le Pape A, et al. Response of human glioma U87 xenografted on mice to non thermal plasma treatment. Plasma Med. 2011;1(1):27–43.

52. Metelmann H.-R, Nedrelow DS, Seebauer C, Schuster M, von Woedtke T, Weltmann K.-D et al. Head and neck cancer treatment and physical plasma. Clin Plasma Med 2015.

53. Klammer H, Mladenov E, Li F, Iliakis G. Bystander effects as manifestation of intercellular communication of DNA damage and of the cellular oxidative status. Cancer Lett. 2015;356(1):58–71.

54. Graves DB. Oxy-nitroso shielding burst model of cold atmospheric plasma therapeutics. Clin Plasma Med. 2014;2(2):38–49.

55. Zhang Z, Li W, Procissi D, Tyler P, Omary RA, Larson AC. Rapid dramatic alterations to the tumor microstructure in pancreatic cancer following irreversible electroporation ablation. Nanomedicine. 2014;9(8):1181–92.

56. Valerio M, Dickinson L, Ali A, Ramachandran N, Donaldson I, Freeman A, et al. A prospective development study investigating focal irreversible electroporation in men with localised prostate cancer: Nanoknife Electroporation Ablation Trial (NEAT). Contemp Clin Trials. 2014;39(1):57–65.

57. Wendler JJ, Porsch M, Nitschke S, Kollermann J, Siedentopf S, Pech M, et al. A prospective Phase 2a pilot study investigating focal percutaneous irreversible electroporation (IRE) ablation by NanoKnife in patients with localised renal cell carcinoma (RCC) with delayed interval tumour resection (IRENE trial). Contemp Clin Trials. 2015;43:10–9.

58. Jansky J, Algwari QT, O'Connell D, Bourdon A. Experimental–modeling study of an atmospheric-pressure helium discharge propagating in a thin dielectric tube. IEEE Trans Plasma Sci. 2012;40(11):2912–9.

59. Babaeva NY, Tian W, Kushner MJ. The interaction between plasma filaments in dielectric barrier discharges and liquid covered wounds: electric fields delivered to model platelets and cells. J Phys D Appl Phys. 2014;47(23):235201.

60. Goran BS, Ivan BK, Vesna VK, Bratislav MO, Milorad MK. Spatio-temporally resolved electric field measurements in helium plasma jet. J Phys D Appl Phys. 2014;47(10):102001.

61. Begum A, Laroussi M, Pervez MR. Atmospheric pressure He-air plasma jet: breakdown process and propagation phenomenon. AIP Adv. 2013;3(6):062117.

62. Leduc M, Guay D, Leask R, Coulombe S. Cell permeabilization using a non-thermal plasma. New J Phys. 2009;11(11):115021.

63. Lukes P, Zeman J, Horak V, Hoffer P, Pouckova P, Holubova M, et al. In vivo effects of focused shock waves on tumor tissue visualized by fluorescence staining techniques. Bioelectrochemistry. 2015;103:103–10.

64. Brulle L, Vandamme M, Ries D, Martel E, Robert E, Lerondel S, et al. Effects of a non thermal plasma treatment alone or in combination with gemcitabine in a MIA PaCa2-luc orthotopic pancreatic carcinoma model. PLoS One. 2012;7(12):e52653.

65. Sarkaria JN, Kitange GJ, James CD, Plummer R, Calvert H, Weller M, et al. Mechanisms of chemoresistance to alkylating agents in malignant glioma. Clin Cancer Res. 2008;14(10):2900–8.

66. Koritzer J, Boxhammer V, Schafer A, Shimizu T, Klampfl TG, Li YF, et al. Restoration of sensitivity in chemo-resistant glioma cells by cold atmospheric plasma. PLoS One. 2013;8(5):e64498.

67. Yang H, Lu R, Xian Y, Gan L, Lu X, Yang X. Effects of atmospheric pressure cold plasma on human hepatocarcinoma cell and its 5-fluorouracil resistant cell line. Phys Plasmas. 2015;22(12):122006.

68. Patra CR, Bhattacharya R, Mukhopadhyay D, Mukherjee P. Fabrication of gold nanoparticles for targeted therapy in pancreatic cancer. Adv Drug Deliv Rev. 2010;62(3):346–61.

69. Jeremic B, Aguerri AR, Filipovic N. Radiosensitization by gold nanoparticles. Clin Trans Oncol. 2013;15(8):593–601.

70. Sun TM, Wang YC, Wang F, Du JZ, Mao CQ, Sun CY, et al. Cancer stem cell therapy using doxorubicin conjugated to gold nanoparticles via hydrazone bonds. Biomaterials. 2014;35(2):836–45.

71. Kong M, Keidar M, Ostrikov K. Plasmas meet nanoparticles—where synergies can advance the frontier of medicine. J Phys D Appl Phys. 2011;44(17):174018.

72. Cheng X, Murphy W, Recek N, Yan D, Cvelbar U, Vesel A, et al. Synergistic effect of gold nanoparticles and cold plasma on glioblastoma cancer therapy. J Phys D Appl Phys. 2014;47(33):335402.

73. Cheng X, Rajjoub K, Sherman J, Canady J, Recek N, Yan D et al. Cold plasma accelerates the uptake of gold nanoparticles into glioblastoma cells. Plasma Process Polym 2015, n/a-n/a.

74. Choi BB, Kim MS, Song KW, Kim UK, Hong JW, Lee HJ, et al. Targeting NEU protein in melanoma cells with non-thermal atmospheric pressure plasma and gold nanoparticles. J Biomed Nanotechnol. 2015;11(5):900–5.

75. Kim G, Park SR, Kim GC, Lee JK. Targeted cancer treatment using anti-EGFR and -TFR antibody-conjugated gold nanoparticles stimulated by nonthermal air plasma. Plasma Med. 2011;1(1):45–54.

76. Voll RE, Herrmann M, Roth EA, Stach C, Kalden JR, Girkontaite I. Immunosuppressive effects of apoptotic cells. Nature. 1997;390(6658):350–1.

77. Gregory CD, Pound JD. Microenvironmental influences of apoptosis in vivo and in vitro. Apoptosis. 2010;15(9):1029–49.

78. Teng F, Kong L, Meng X, Yang J, Yu J. Radiotherapy combined with immune checkpoint blockade immunotherapy: achievements and challenges. Cancer Lett. 2015; 365(1):23–9

79. Melcher A, Todryk S, Hardwick N, Ford M, Jacobson M, Vile RG. Tumor immunogenicity is determined by the mechanism of cell death via induction of heat shock protein expression. Nat Med. 1998;4(5):581–7.

80. Baust JG, Gage AA. The molecular basis of cryosurgery. BJU Int. 2005;95(9):1187–91.

81. McGahan JP, Gu WZ, Brock JM, Tesluk H, Jones CD. Hepatic ablation using bipolar radiofrequency electrocautery. Acad Radiol. 1996;3(5):418–22.

82. Alkhorayef M, Mahmoud MZ, Alzimami KS, Sulieman A, Fagiri MA. High-intensity focused ultrasound (HIFU) in localized prostate cancer treatment. Pol J Radiol. 2015;80:131–41.

83. Camphausen K, Moses MA, Menard C, Sproull M, Beecken WD, Folkman J, et al. Radiation abscopal antitumor effect is mediated through p53. Cancer Res. 2003;63(8):1990–3.

84. Sanchez-Ortiz RF, Tannir N, Ahrar K, Wood CG. Spontaneous regression of pulmonary metastases from renal cell carcinoma after radio frequency ablation of primary tumor: an in situ tumor vaccine? J Urol. 2003;170(1):178–9.

85. Kim H, Park BK, Kim CK. Spontaneous regression of pulmonary and adrenal metastases following percutaneous radiofrequency ablation of a recurrent renal cell carcinoma. Korean J Radiol. 2008;9(5):470–2.

86. Shah TT, Ahmed H, Kanthabalan A, Lau B, Ghei M, Maraj B, et al. Focal cryotherapy of localized prostate cancer: a systematic review of the literature. Expert Rev Anticancer Ther. 2014;14(11): 1337–47.

87. Frey B, Rubner Y, Kulzer L, Werthmoller N, Weiss EM, Fietkau R, et al. Antitumor immune responses induced by ionizing irradiation and further immune stimulation. Cancer Immunol Immunother. 2014;63(1):29–36.

88. Borghaei H, Paz-Ares L, Horn L, Spigel DR, Steins M, Ready NE et al. Nivolumab versus docetaxel in advanced nonsquamous non-small-cell lung cancer. N Engl J Med 373:1627–1639.

89. Larkin J, Chiarion-Sileni V, Gonzalez R, Grob JJ, Cowey CL, Lao CD, et al. Combined nivolumab and ipilimumab or monotherapy in untreated melanoma. New Engl J Med. 2015;373(1):23–34.

90. Miller V, Lin A, Fridman A, Why target immune cells for plasma treatment of cancer. Plasma Chem Plasma Process. 2015;36(1): 259–268

91. Harris AL. Hypoxia—a key regulatory factor in tumour growth. Nat Rev Cancer. 2002;2(1):38–47.

92. Brustugun OT. Hypoxia as a cause of treatment failure in non-small cell carcinoma of the lung. Semin Radiat Oncol. 2015;25(2):87–92.

93. Luo D, Wang Z, Wu J, Jiang C, Wu J. The role of hypoxia inducible factor-1 in hepatocellular carcinoma. BioMed Res Int. 2014;2014:409272.

94. Wang W, He YF, Sun QK, Wang Y, Han XH, Peng DF, et al. Hypoxia-inducible factor 1alpha in breast cancer prognosis. Clin Chim Acta. 2014;428:32–7.

95. Zhang J, Li L, Lu Y. Effects of hypoxia, surrounding fibroblasts, and p16 expression on breast cancer cell migration and invasion. J Cancer. 2015;6(5):430–7.

96. Joseph JV, Conroy S, Pavlov K, Sontakke P, Tomar T, Eggens-Meijer E, et al. Hypoxia enhances migration and invasion in glioblastoma by promoting a mesenchymal shift mediated by the HIF1alpha-ZEB1 axis. Cancer Lett. 2015;359(1):107–16.

97. Gomez-Millan J, Lara MF, Correa Generoso R, Perez-Rozos A, Lupianez-Perez Y, Medina Carmona JA. Advances in the treatment of prostate cancer with radiotherapy. Crit Rev Oncol Hematol. 2015;95(2):144–53.

98. Maitland NJ, Collins AT. Prostate cancer stem cells: a new target for therapy. J Clin Oncol. 2008;26(17):2862–70.

99. Bao S, Wu Q, McLendon RE, Hao Y, Shi Q, Hjelmeland AB, et al. Glioma stem cells promote radioresistance by preferential activation of the DNA damage response. Nature. 2006;444(7120):756–60.

100. Huang R, Wang G, Song Y, Tang Q, You Q, Liu Z et al. Colorectal cancer stem cell and chemoresistant colorectal cancer cell phenotypes and increased sensitivity to Notch pathway inhibitor. Mol Med Rep. 2015;12(2):2417–24

101. Dean M, Fojo T, Bates S. Tumour stem cells and drug resistance. Nat Rev cancer. 2005;5(4):275–84.

102. Gorelik E, Lokshin A, Levina V. Lung cancer stem cells as a target for therapy. Anti Cancer Agents Med Chem. 2010;10(2):164–71.

103. Kumazawa S, Kajiyama H, Umezu T, Mizuno M, Suzuki S, Yamamoto E, et al. Possible association between stem-like hallmark and radioresistance in human cervical carcinoma cells. J Obstet Gynaecol Res. 2014;40(5):1389–98.

104. Frame FM, Pellacani D, Collins AT, Simms MS, Mann VM, Jones GD, et al. HDAC inhibitor confers radiosensitivity to prostate stem-like cells. Br J Cancer. 2013;109(12):3023–33.

105. Diehn M, Cho RW, Lobo NA, Kalisky T, Dorie MJ, Kulp AN, et al. Association of reactive oxygen species levels and radioresistance in cancer stem cells. Nature. 2009;458(7239): 780–3.

106. Collins AT, Berry PA, Hyde C, Stower MJ, Maitland NJ. Prospective identification of tumorigenic prostate cancer stem cells. Cancer Res. 2005;65(23):10946–51.

107. Richardson GD, Robson CN, Lang SH, Neal DE, Maitland NJ, Collins AT. CD133, a novel marker for human prostatic epithelial stem cells. J Cell Sci. 2004;117(Pt 16):3539–45.

108. Sturmey RG, Hawkhead JA, Barker EA, Leese HJ. DNA damage and metabolic activity in the preimplantation embryo. Hum Reprod. 2009;24(1):81–91.

109. Yan D, Sherman JH, Cheng X, Ratovitski E, Canady J, Keidar M. Controlling plasma stimulated media in cancer treatment application. Appl Phys Lett. 2014;105(22):224101.

110. Utsumi F, Kajiyama H, Nakamura K, Tanaka H, Mizuno M, Ishikawa K, et al. Effect of indirect nonequilibrium atmospheric pressure plasma on anti-proliferative activity against chronic chemo-resistant ovarian cancer cells in vitro and in vivo. PLoS One. 2013;8(12):e81576.

111. Plewa J-M, Yousfi M, Frongia C, Eichwald O, Ducommun B, Merbahi N, et al. Low-temperature plasma-induced antiproliferative effects on multi-cellular tumor spheroids. New J Phys. 2014;16(4):043027.

112. Szili EJ, Oh J-S, Hong S-H, Hatta A, Short RD. Probing the transport of plasma-generated RONS in an agarose target as surrogate for real tissue: dependency on time, distance and material composition. J Phys D Appl Phys. 2015;48(20):202001.

113. Robert E, Vandamme M, Brullé L, Lerondel S, Le Pape A, Sarron V, et al. Perspectives of endoscopic plasma applications. Clin Plasma Med. 2013;1(2):8–16.

114. Ahmed HU, Dickinson L, Charman S, Weir S, McCartan N, Hindley R. G et al. Focal ablation targeted to the index lesion in multifocal localised prostate cancer: a prospective development study. Eur Urol. 2015;68(6):927–36

115. Mala T, Samset E, Aurdal L, Gladhaug I, Edwin B, Soreide O. Magnetic resonance imaging-estimated three-dimensional temperature distribution in liver cryolesions: a study of cryolesion characteristics assumed necessary for tumor ablation. Cryobiology. 2001;43(3):268–75.

116. Marinov I, Guaitella O, Rousseau A, Starikovskaia S. Cavitation in the vicinity of the high-voltage electrode as a key step of nanosecond breakdown in liquids. Plasma Sources Sci Technol. 2013;22(4):42001–6.

117. Marinov I, Guaitella O, Rousseau A, Starikovskaia S. Modes of underwater discharge propagation in a series of nanosecond successive pulses. J Phys D Appl Phys. 2013;46(46):464013.

118. Polak M, Winter J, Schnabel U, Ehlbeck J, Weltmann K-D. Innovative plasma generation in flexible biopsy channels for inner-tube decontamination and medical applications. Plasma Process Polym. 2012;9(1):67–76.

119. Kim JY, Ballato J, Foy P, Hawkins T, Wei Y, Li J, et al. Apoptosis of lung carcinoma cells induced by a flexible optical fiber-based cold microplasma. Biosens Bioelectron. 2011;28(1):333–8.

120. Dai XJ, Corr CS, Ponraj SB, Maniruzzaman M, Ambujakshan AT, Chen Z et al. Efficient and selectable production of reactive species using a nanosecond pulsed discharge in gas bubbles in liquid. Plasma Process Polym 2015, n/a-n/a.

121. Cheng X, Sherman J, Murphy W, Ratovitski E, Canady J, Keidar M. The effect of tuning cold plasma composition on glioblastoma cell viability. PLoS One. 2014;9(5):e98652.

# List of Abbreviations

| | |
|---|---|
| **%** | Percentage |
| **°C** | Degrees celcius |
| **$^{103}$Pd** | Radioisotope of Palladium |
| **$^{125}$I** | Radioisotope of Iodine |
| **$^{131}$Cs** | Radioisotope of Caesium |
| **$^1$O$_2$** | Singlet delta oxygen |
| **2D** | Two-dimensional |
| **3D** | Three-dimensional |
| **α** | Degree of ionisation |
| **ε$_0$** | Permittivity of free space |
| **κ** | Rate constant |
| **λ** | Mean free path |
| **λ$_D$** | Debye length |
| **μ-APPJ** | Micro-scaled atmospheric pressure plasma jet |
| **μg** | Micro gram |
| **μl** | Micro litre |
| **μM** | Micro molar |
| **ν** | Collision frequency |
| **σ** | Collision cross section |
| **τ** | Average time between collisions |
| **ω$_p$** | Plasma frequency |

| | |
|---|---|
| **ABM** | Anti-biotic anti-mycotic |
| **AC** | Alternating current |
| **ADT** | Androgen deprivation therapy |
| **AFS** | Anterior fibromuscular stroma |
| **AR** | Androgen receptor |
| **ASK1** | Apoptosis signal-regulating kinase 1 |
| **ATCC** | American type culture collection |
| **ATM** | Ataxia telangiectasia mutated |
| **ATP** | Adenosine Triphosphate |
| **BCA** | Bioinchoinic acid |
| **BM** | Basement membrane |
| **BPE** | Bovine pituitary extract |
| **BPH** | Benign prostatic hyperplasia |
| **BSA** | Bovine serum albumin |
| **CB** | Committed basal |
| **CCP** | Capacitively coupled plasma |
| **CFE** | Colony forming efficiency |
| **CK** | Cytokeratin |
| **C-PARP** | Cleaved- poly (ADP-ribose) polymerase |
| **cm** | Centimetre |
| **CO$_2$** | Carbon dioxide |
| **COST** | Co-operation in science and technology |
| **CRPC** | Castrate resistant prostate cancer |

| | |
|---|---|
| **CSC** | Cancer stem cell |
| **CZ** | Central zone |
| **dH$_2$O** | Distilled water |
| **ddH$_2$O** | Double distilled water |
| **DAPI** | 4',6-diamidino-2-phenylindole |
| **DBD** | Dielectric barrier discharge |
| **DMEM** | Dulbecco's modified eagle medium |
| **DMSO** | Dimethyl sulfoxide |
| **DNA** | Deoxyribonucleic acid |
| **DRE** | Digital rectal exam |
| **DTT** | Dithiothreitol |
| **e** | Electronic charge |
| **ECL** | Enhanced chemiluminescence |
| **EDTA** | Ethylenediaminetetraacetic acid |
| **EEDF** | Electron energy distribution function |
| **EGF** | Epidermal growth factor |
| **EU** | European Union |
| **eV** | Electronvolt |
| **FE-DBD** | Floating electrode dielectric barrier discharge |
| **FGF** | Fibroblast growth factor |
| **GM-CSF** | Granulocyte macrophage colony stimulating factor |
| **g** | Gram |
| **Gy** | Gray |

| | |
|---|---|
| **h** | Hour |
| **H2AX** | H2A histone family member X |
| **H$_2$O$_2$** | Hydrogen peroxide |
| **H7** | Ham's F12 medium + 7% FCS + 2 mM L-Glutamine |
| **HBSS** | Hank's balanced saline solution |
| **HCl** | Hydrogen chloride |
| **He** | Helium |
| **HIFU** | High-intensity focussed ultrasound |
| **HRP** | Horseradish peroxidase |
| **IC$_{50}$** | Half maximal inhibitory concentration |
| **ID** | Inner diameter |
| **IF** | Immunofluorescence |
| **IR** | Ionising radiation |
| **IgG** | Immunoglobulin G |
| **IU** | International units |
| **K** | Kelvin |
| **K2** | KSFM media + 2% FCS + 2 mM L-Glutamine + BPE + EGF |
| **kHz** | kilohertz |
| **kV** | kilovolt |
| **KSFM** | Keratinocyte serum free medium |
| **L** | System length scale |
| **LIF** | Leukaemia inhibitory factor |
| **LTP** | Low temperature plasma |

| | |
|---|---|
| **MAPK** | Mitogen-activated protein kinase |
| **MHz** | Megahertz |
| **ml** | Millilitre |
| **mm** | Millimetre |
| **mM** | Millimolar |
| **MRI** | Magnetic resonance imaging |
| **N** | Atomic nitrogen |
| **n** | Plasma density |
| **$n_e$** | Electron density |
| **$n_i$** | Ion density |
| **$n_g$** | Density of background gas |
| **NaCl** | Sodium chloride |
| **NaOH** | Sodium hydroxide |
| **NGS** | Normal goat serum |
| **NO** | Nitric oxide |
| **nm** | Nanometre |
| **NP40** | nonylphenoxypolyethoxyethanol |
| **O** | Atomic oxygen |
| **$O_2^-$** | Superoxide |
| **$O_3$** | Ozone |
| **OD** | Outer diameter |
| **OES** | Optical emission spectroscopy |
| **OH** | Hydroxyl |

| | |
|---|---|
| **ONOO⁻** | Peryoxynitrite |
| **P** | P-value |
| **PAP** | Prostatic acid phosphatase |
| **PARP** | Poly (ADP-ribose) polymerase |
| **PBS** | Phosphate-buffered saline |
| **PCa** | Prostate cancer |
| **pd** | Product of pressure (p) and electrode separation distance (d) |
| **PFA** | Paraformaldehyde |
| **PI** | Propidium iodide |
| **PIN** | Prostatic intraepithelial neoplasia |
| **PDT** | Photodynamic therapy |
| **PTM** | Plasma treated media |
| **PSA** | Prostate-specific antigen |
| **PZ** | Peripheral zone |
| **R5** | RPMI + 5% FCS + 2 mM L-Glutamine |
| **RP** | Radical prostatectomy |
| **RPMI** | Roswell Park Memorial Institute medium |
| **RF** | Radio frequency |
| **RONS** | Reactive oxygen and nitrogen species |
| **ROS** | Reactive oxygen species |
| **RNS** | Reactive nitrogen species |
| **RT** | Radiotherapy |
| **SBRT** | Stereotactic body radiation therapy |

| | |
|---|---|
| **s** | Second |
| **SC** | Stem cell |
| **SCCM** | Standard cubic centimetres per minute |
| **SCF** | Stem cell factor |
| **SCM** | Stem cell medium |
| **SDO** | Singlet delta oxygen |
| **SDS** | Sodium dodecyl sulphate |
| **SDS-PAGE** | Sodium dodecyl sulphate polyacrylamide gel electrophoresis |
| **SE** | Standard error |
| **SF** | Surviving fraction |
| **SLM** | Standard Litres per minute |
| **Stauro** | Staurosporine |
| **STO** | Continuous line of SIM mouse embryonic fibroblasts |
| **SV40** | Simian vacuolating virus 40 |
| **TA** | Transit-amplifying |
| **TBS** | Tris buffered saline |
| **TBS-T** | Tris buffered saline + Tween-20 |
| **TE** | Tris-EDTA buffer |
| **TNF** | Tumour necrosis factor |
| **Tox Cont** | Toxicity control |
| **TRUS** | Trans-rectal ultrasound |
| **TURP** | Transurethral resection of the prostate |
| **TZ** | Transition zone |

| | |
|---|---|
| **U** | Unit |
| **Unt** | Untreated |
| **UV** | Ultraviolet |
| **v/v** | Volume per volume |
| $\mathbf{V_B}$ | Breakdown voltage |
| **w/v** | Weight per volume |
| $\mathbf{Wcm^{-2}}$ | Watts per square centimetre |

# References

1.      McNeal, J. E., The zonal anatomy of the prostate. *Prostate* **1981,** 2, (1), 35-49.

2.      McNeal, J. E.; Redwine, E. A.; Freiha, F. S.; Stamey, T. A., Zonal distribution of prostatic adenocarcinoma. Correlation with histologic pattern and direction of spread. *The American journal of surgical pathology* **1988,** 12, (12), 897-906.

3.      De Marzo, A. M.; Platz, E. A.; Sutcliffe, S.; Xu, J.; Gronberg, H.; Drake, C. G.; Nakai, Y.; Isaacs, W. B.; Nelson, W. G., Inflammation in prostate carcinogenesis. *Nature reviews. Cancer* **2007,** 7, (4), 256-69.

4.      Wadhera, P., An introduction to acinar pressures in BPH and prostate cancer. *Nat Rev Urol* **2013,** 10, (6), 358-366.

5.      Lilja, H.; Abrahamsson, P. A., Three predominant proteins secreted by the human prostate gland. *Prostate* **1988,** 12, (1), 29-38.

6.      Maitland, N. J.; Collins, A. T., Prostate cancer stem cells: a new target for therapy. *J Clin Oncol* **2008,** 26, (17), 2862-70.

7.      Bonkhoff, H.; Remberger, K., Widespread distribution of nuclear androgen receptors in the basal cell layer of the normal and hyperplastic human prostate. *Virchows Archiv. A, Pathological anatomy and histopathology* **1993,** 422, (1), 35-8.

8.      Collins, A. T.; Maitland, N. J., Prostate cancer stem cells. *European journal of cancer* **2006,** 42, (9), 1213-8.

9.      Oldridge, E. E.; Pellacani, D.; Collins, A. T.; Maitland, N. J., Prostate cancer stem cells: are they androgen-responsive? *Molecular and cellular endocrinology* **2012,** 360, (1-2), 14-24.

10.     Liu, A. Y., Expression of CD44 in prostate cancer cells. *Cancer letters* **1994,** 76, (1), 63-9.

11.     Signoretti, S.; Waltregny, D.; Dilks, J.; Isaac, B.; Lin, D.; Garraway, L.; Yang, A.; Montironi, R.; McKeon, F.; Loda, M., p63 is a prostate basal cell marker and is required for prostate development. *The American journal of pathology* **2000,** 157, (6), 1769-75.

12.     Hudson, D. L.; Guy, A. T.; Fry, P.; O'Hare, M. J.; Watt, F. M.; Masters, J. R. W., Epithelial Cell Differentiation Pathways in the Human Prostate: Identification of Intermediate Phenotypes by Keratin Expression. *Journal of Histochemistry & Cytochemistry* **2001,** 49, (2), 271-278.

13. Sherwood, E. R.; Theyer, G.; Steiner, G.; Berg, L. A.; Kozlowski, J. M.; Lee, C., Differential expression of specific cytokeratin polypeptides in the basal and luminal epithelia of the human prostate. *Prostate* **1991,** 18, (4), 303-14.

14. Bonkhoff, H.; Stein, U.; Remberger, K., Endocrine-paracrine cell types in the prostate and prostatic adenocarcinoma are postmitotic cells. *Human pathology* **1995,** 26, (2), 167-70.

15. Abrahamsson, P. A., Neuroendocrine cells in tumour growth of the prostate. *Endocrine-related cancer* **1999,** 6, (4), 503-19.

16. Bostwick, D. G.; Dousa, M. K.; Crawford, B. G.; Wollan, P. C., Neuroendocrine differentiation in prostatic intraepithelial neoplasia and adenocarcinoma. *The American journal of surgical pathology* **1994,** 18, (12), 1240-6.

17. Hall, J. A.; Maitland, N. J.; Stower, M.; Lang, S. H., Primary prostate stromal cells modulate the morphology and migration of primary prostate epithelial cells in type 1 collagen gels. *Cancer Res* **2002,** 62, (1), 58-62.

18. Berry, P. A.; Maitland, N. J.; Collins, A. T., Androgen receptor signalling in prostate: effects of stromal factors on normal and cancer stem cells. *Molecular and cellular endocrinology* **2008,** 288, (1-2), 30-7.

19. Krieger, J. N.; Nyberg, L., Jr.; Nickel, J. C., NIH consensus definition and classification of prostatitis. *JAMA* **1999,** 282, (3), 236-7.

20. Krieger, J. N., Classification, epidemiology and implications of chronic prostatitis in North America, Europe and Asia. *Minerva urologica e nefrologica = The Italian journal of urology and nephrology* **2004,** 56, (2), 99-107.

21. Stevermer, J. J.; Easley, S. K., Treatment of prostatitis. *American family physician* **2000,** 61, (10), 3015-22, 3025-6.

22. Kramer, G.; Marberger, M., Could inflammation be a key component in the progression of benign prostatic hyperplasia? *Curr Opin Urol* **2006,** 16, (1), 25-9.

23. Kramer, G.; Mitteregger, D.; Marberger, M., Is benign prostatic hyperplasia (BPH) an immune inflammatory disease? *Eur Urol* **2007,** 51, (5), 1202-16.

24. Berry, S. J.; Coffey, D. S.; Walsh, P. C.; Ewing, L. L., The development of human benign prostatic hyperplasia with age. *J Urol* **1984,** 132, (3), 474-9.

25. Lepor, H., Pathophysiology, epidemiology, and natural history of benign prostatic hyperplasia. *Rev Urol* **2004,** 6 Suppl 9, S3-S10.

26. Schroder, F. H.; Blom, J. H., Natural history of benign prostatic hyperplasia (BPH). *The Prostate. Supplement* **1989,** 2, 17-22.

27.    Rane, J. K.; Greener, S.; Frame, F. M.; Mann, V. M.; Simms, M. S.; Collins, A. T.; Berney, D. M.; Maitland, N. J., Telomerase Activity and Telomere Length in Human Benign Prostatic Hyperplasia Stem-like Cells and Their Progeny Implies the Existence of Distinct Basal and Luminal Cell Lineages. *Eur Urol* **2015**.

28.    Shin, H. J.; Ro, J. Y., Prostatic intraepithelial neoplasia: a potential precursor lesion of prostatic adenocarcinoma. *Yonsei medical journal* **1995,** 36, (3), 215-31.

29.    Bostwick, D. G.; Liu, L.; Brawer, M. K.; Qian, J., High-grade prostatic intraepithelial neoplasia. *Rev Urol* **2004,** 6, (4), 171-9.

30.    Torre, L. A.; Bray, F.; Siegel, R. L.; Ferlay, J.; Lortet-Tieulent, J.; Jemal, A., Global cancer statistics, 2012. *CA Cancer J Clin* **2015,** 65, (2), 87-108.

31.    UK, C. R., UK Cancer Incidence and Mortality Summary 2012. **2012**.

32.    Jemal, A.; Bray, F.; Center, M. M.; Ferlay, J.; Ward, E.; Forman, D., Global cancer statistics. *CA Cancer J Clin* **2011,** 61, (2), 69-90.

33.    Li, J.; Djenaba, J. A.; Soman, A.; Rim, S. H.; Master, V. A., Recent trends in prostate cancer incidence by age, cancer stage, and grade, the United States, 2001-2007. *Prostate Cancer* **2012,** 2012, 691380.

34.    Lesko, S. M.; Rosenberg, L.; Shapiro, S., Family history and prostate cancer risk. *American journal of epidemiology* **1996,** 144, (11), 1041-7.

35.    Lichtenstein, P.; Holm, N. V.; Verkasalo, P. K.; Iliadou, A.; Kaprio, J.; Koskenvuo, M.; Pukkala, E.; Skytthe, A.; Hemminki, K., Environmental and heritable factors in the causation of cancer--analyses of cohorts of twins from Sweden, Denmark, and Finland. *The New England journal of medicine* **2000,** 343, (2), 78-85.

36.    Shen, M. M.; Abate-Shen, C., Molecular genetics of prostate cancer: new prospects for old challenges. *Genes & development* **2010,** 24, (18), 1967-2000.

37.    Taylor, R. A.; Toivanen, R.; Frydenberg, M.; Pedersen, J.; Harewood, L.; Australian Prostate Cancer, B.; Collins, A. T.; Maitland, N. J.; Risbridger, G. P., Human Epithelial Basal Cells Are Cells of Origin of Prostate Cancer, Independent of CD133 Status. *STEM CELLS* **2012,** 30, (6), 1087-1096.

38.    De Marzo, A. M.; Meeker, A. K.; Epstein, J. I.; Coffey, D. S., Prostate Stem Cell Compartments: Expression of the Cell Cycle Inhibitor p27Kip1 in Normal, Hyperplastic, and Neoplastic Cells. *The American journal of pathology* **1998,** 153, (3), 911-919.

39.     Tannock, I. F.; de Wit, R.; Berry, W. R.; Horti, J.; Pluzanska, A.; Chi, K. N.; Oudard, S.; Théodore, C.; James, N. D.; Turesson, I.; Rosenthal, M. A.; Eisenberger, M. A., Docetaxel plus Prednisone or Mitoxantrone plus Prednisone for Advanced Prostate Cancer. *New Engl J Med* **2004,** 351, (15), 1502-1512.

40.     de Bono, J. S.; Logothetis, C. J.; Molina, A.; Fizazi, K.; North, S.; Chu, L.; Chi, K. N.; Jones, R. J.; Goodman, O. B.; Saad, F.; Staffurth, J. N.; Mainwaring, P.; Harland, S.; Flaig, T. W.; Hutson, T. E.; Cheng, T.; Patterson, H.; Hainsworth, J. D.; Ryan, C. J.; Sternberg, C. N.; Ellard, S. L.; Fléchon, A.; Saleh, M.; Scholz, M.; Efstathiou, E.; Zivi, A.; Bianchini, D.; Loriot, Y.; Chieffo, N.; Kheoh, T.; Haqq, C. M.; Scher, H. I., Abiraterone and Increased Survival in Metastatic Prostate Cancer. *New Engl J Med* **2011,** 364, (21), 1995-2005.

41.     Makinen, T.; Tammela, T. L.; Hakama, M.; Stenman, U. H.; Rannikko, S.; Aro, J.; Juusela, H.; Maattanen, L.; Auvinen, A., Tumor characteristics in a population-based prostate cancer screening trial with prostate-specific antigen. *Clinical cancer research : an official journal of the American Association for Cancer Research* **2003,** 9, (7), 2435-9.

42.     Gulati, R.; Gore, J. L.; Etzioni, R., Comparative effectiveness of alternative prostate-specific antigen--based prostate cancer screening strategies: model estimates of potential benefits and harms. *Ann Intern Med* **2013,** 158, (3), 145-53.

43.     Nadler, R. B.; Humphrey, P. A.; Smith, D. S.; Catalona, W. J.; Ratliff, T. L., Effect of inflammation and benign prostatic hyperplasia on elevated serum prostate specific antigen levels. *J Urol* **1995,** 154, (2 Pt 1), 407-13.

44.     Hou, A. H.; Swanson, D.; Barqawi, A. B., Modalities for imaging of prostate cancer. *Adv Urol* **2009**, 818065.

45.     Turkbey, B.; Pinto, P. A.; Choyke, P. L., Imaging techniques for prostate cancer: implications for focal therapy. *Nat Rev Urol* **2009,** 6, (4), 191-203.

46.     Harvey, C. J.; Pilcher, J.; Richenberg, J.; Patel, U.; Frauscher, F., Applications of transrectal ultrasound in prostate cancer. *Br J Radiol* **2012,** 85 Spec No 1, S3-17.

47.     Gleason, D. F., Classification of prostatic carcinomas. *Cancer chemotherapy reports. Part 1* **1966,** 50, (3), 125-8.

48.     Epstein, J. I., An update of the Gleason grading system. *J Urol* **2010,** 183, (2), 433-40.

49.     Miki, J.; Rhim, J. S., Prostate cell cultures as in vitro models for the study of normal stem cells and cancer stem cells. *Prostate cancer and prostatic diseases* **2007,** 11, (1), 32-39.

50.     Izadpanah, R.; Kaushal, D.; Kriedt, C.; Tsien, F.; Patel, B.; Dufour, J.; Bunnell, B. A., Long-term In vitro Expansion Alters the Biology of Adult Mesenchymal Stem Cells. *Cancer Research* **2008,** 68, (11), 4229-4238.

51.     Frame, F. M.; Maitland, N. J., Cancer stem cells, models of study and implications of therapy resistance mechanisms. In *Human Cell Transformation*, Springer: 2012; pp 105-118.

52.     Scardino, P. T., Early detection of prostate cancer. *The Urologic clinics of North America* **1989,** 16, (4), 635-55.

53.     Chodak, G. W.; Thisted, R. A.; Gerber, G. S.; Johansson, J. E.; Adolfsson, J.; Jones, G. W.; Chisholm, G. D.; Moskovitz, B.; Livne, P. M.; Warner, J., Results of conservative management of clinically localized prostate cancer. *The New England journal of medicine* **1994,** 330, (4), 242-8.

54.     Johansson, J. E.; Andren, O.; Andersson, S. O.; Dickman, P. W.; Holmberg, L.; Magnuson, A.; Adami, H. O., Natural history of early, localized prostate cancer. *JAMA* **2004,** 291, (22), 2713-9.

55.     Palacios, D. A.; Miyake, M.; Rosser, C. J., Radiosensitization in prostate cancer: mechanisms and targets. *BMC Urol* **2013,** 13, (1), 4.

56.     Johns, H. E., The physicist in cancer treatment and detection. *Int J Radiat Oncol Biol Phys* **1981,** 7, (6), 801-8.

57.     Radford, I. R., Evidence for a general relationship between the induced level of DNA double-strand breakage and cell-killing after X-irradiation of mammalian cells. *Int J Radiat Biol Relat Stud Phys Chem Med* **1986,** 49, (4), 611-20.

58.     Ward, J. F., Biochemistry of DNA lesions. *Radiat Res Suppl* **1985,** 8, S103-11.

59.     Cho, Y. M.; Kim, Y. S.; Kang, M. J.; Farrar, W. L.; Hurt, E. M., Long-term recovery of irradiated prostate cancer increases cancer stem cells. *Prostate* **2012,** 72, (16), 1746-56.

60.     Ogawa, K.; Yoshioka, Y.; Isohashi, F.; Seo, Y.; Yoshida, K.; Yamazaki, H., Radiotherapy targeting cancer stem cells: current views and future perspectives. *Anticancer Res* **2013,** 33, (3), 747-54.

61.     Chargari, C.; Moncharmont, C.; Levy, A.; Guy, J. B.; Bertrand, G.; Guilbert, M.; Rousseau, C.; Vedrine, L.; Alphonse, G.; Toillon, R. A.; Rodriguez-Lafrasse, C.;

Deutsch, E.; Magne, N., [Cancer stem cells, cornerstone of radioresistance and perspectives for radiosensitization: glioblastoma as an example]. *Bull Cancer* **2012,** 99, (12), 1153-60.

62.     Cheng, X.; Sherman, J.; Murphy, W.; Ratovitski, E.; Canady, J.; Keidar, M., The effect of tuning cold plasma composition on glioblastoma cell viability. *PLoS One* **2014,** 9, (5), e98652.

63.     Hummel, S.; Simpson, E. L.; Hemingway, P.; Stevenson, M. D.; Rees, A., Intensity-modulated radiotherapy for the treatment of prostate cancer: a systematic review and economic evaluation. *Health Technol Assess* **2010,** 14, (47), 1-108, iii-iv.

64.     Kupelian, P.; Kuban, D.; Thames, H.; Levy, L.; Horwitz, E.; Martinez, A.; Michalski, J.; Pisansky, T.; Sandler, H.; Shipley, W.; Zelefsky, M.; Zietman, A., Improved biochemical relapse-free survival with increased external radiation doses in patients with localized prostate cancer: the combined experience of nine institutions in patients treated in 1994 and 1995. *Int J Radiat Oncol Biol Phys* **2005,** 61, (2), 415-9.

65.     Trada, Y.; Plank, A.; Martin, J., Defining a dose-response relationship for prostate external beam radiotherapy. *J Med Imaging Radiat Oncol* **2013,** 57, (2), 237-46.

66.     Chen, M. J.; Weltman, E.; Hanriot, R. M.; Luz, F. P.; Cecilio, P. J.; da Cruz, J. C.; Moreira, F. R.; Santos, A. S.; Martins, L. C.; Nadalin, W., Intensity modulated radiotherapy for localized prostate cancer: rigid compliance to dose-volume constraints as a warranty of acceptable toxicity? *Radiat Oncol* **2007,** 2, 6.

67.     Lips, I. M.; Dehnad, H.; van Gils, C. H.; Boeken Kruger, A. E.; van der Heide, U. A.; van Vulpen, M., High-dose intensity-modulated radiotherapy for prostate cancer using daily fiducial marker-based position verification: acute and late toxicity in 331 patients. *Radiat Oncol* **2008,** 3, 15.

68.     Jones, J. S., Radiorecurrent prostate cancer: an emerging and largely mismanaged epidemic. *Eur Urol* **2011,** 60, (3), 411-2.

69.     Freeman, D. E.; King, C. R., Stereotactic body radiotherapy for low-risk prostate cancer: five-year outcomes. *Radiat Oncol* **2011,** 6, 3.

70.    Xie, Y.; Djajaputra, D.; King, C. R.; Hossain, S.; Ma, L.; Xing, L., Intrafractional motion of the prostate during hypofractionated radiotherapy. *Int J Radiat Oncol Biol Phys* **2008,** 72, (1), 236-46.

71.    Oliai, C.; Lanciano, R.; Sprandio, B.; Yang, J.; Lamond, J.; Arrigo, S.; Good, M.; Mooreville, M.; Garber, B.; Brady, L. W., Stereotactic body radiation therapy for the primary treatment of localized prostate cancer. *J Radiat Oncol* **2013,** 2, (1), 63-70.

72.    Seisen, T.; Drouin, S. J.; Phe, V.; Parra, J.; Mozer, P.; Bitker, M. O.; Cussenot, O.; Roupret, M., Current role of image-guided robotic radiosurgery (Cyberknife((R)) ) for prostate cancer treatment. *BJU Int* **2013**.

73.    Park, D. S., Current status of brachytherapy for prostate cancer. *Korean J Urol* **2012,** 53, (11), 743-9.

74.    Nguyen, P. L.; D'Amico, A. V.; Lee, A. K.; Suh, W. W., Patient selection, cancer control, and complications after salvage local therapy for postradiation prostate-specific antigen failure: a systematic review of the literature. *Cancer* **2007,** 110, (7), 1417-28.

75.    Sanda, M. G.; Dunn, R. L.; Michalski, J.; Sandler, H. M.; Northouse, L.; Hembroff, L.; Lin, X.; Greenfield, T. K.; Litwin, M. S.; Saigal, C. S.; Mahadevan, A.; Klein, E.; Kibel, A.; Pisters, L. L.; Kuban, D.; Kaplan, I.; Wood, D.; Ciezki, J.; Shah, N.; Wei, J. T., Quality of Life and Satisfaction with Outcome among Prostate-Cancer Survivors. *New Engl J Med* **2008,** 358, (12), 1250-1261.

76.    Nam, R. K.; Cheung, P.; Herschorn, S.; Saskin, R.; Su, J.; Klotz, L. H.; Chang, M.; Kulkarni, G. S.; Lee, Y.; Kodama, R. T.; Narod, S. A., Incidence of complications other than urinary incontinence or erectile dysfunction after radical prostatectomy or radiotherapy for prostate cancer: a population-based cohort study. *Lancet Oncol* **2014,** 15, (2), 223-31.

77.    Gandaglia, G.; Sammon, J. D.; Chang, S. L.; Choueiri, T. K.; Hu, J. C.; Karakiewicz, P. I.; Kibel, A. S.; Kim, S. P.; Konijeti, R.; Montorsi, F.; Nguyen, P. L.; Sukumar, S.; Menon, M.; Sun, M.; Trinh, Q. D., Comparative effectiveness of robot-assisted and open radical prostatectomy in the postdissemination era. *J Clin Oncol* **2014,** 32, (14), 1419-26.

78. Klotz, L., Active surveillance versus radical treatment for favorable-risk localized prostate cancer. *Current Treatment Options in Oncology* 7, (5), 355-362.

79. Siegel, R.; Naishadham, D.; Jemal, A., Cancer statistics, 2012. *CA Cancer J Clin* **2012,** 62, (1), 10-29.

80. Eggener, S.; Salomon, G.; Scardino, P. T.; De la Rosette, J.; Polascik, T. J.; Brewster, S., Focal therapy for prostate cancer: possibilities and limitations. *Eur Urol* **2010,** 58, (1), 57-64.

81. Ahmed, H. U.; Dickinson, L.; Charman, S.; Weir, S.; McCartan, N.; Hindley, R. G.; Freeman, A.; Kirkham, A. P.; Sahu, M.; Scott, R.; Allen, C.; Van der Meulen, J.; Emberton, M., Focal Ablation Targeted to the Index Lesion in Multifocal Localised Prostate Cancer: a Prospective Development Study. *Eur Urol* **2015**.

82. Kang, S. U.; Cho, J. H.; Chang, J. W.; Shin, Y. S.; Kim, K. I.; Park, J. K.; Yang, S. S.; Lee, J. S.; Moon, E.; Lee, K.; Kim, C. H., Nonthermal plasma induces head and neck cancer cell death: the potential involvement of mitogen-activated protein kinase-dependent mitochondrial reactive oxygen species. *Cell Death Dis* **2014,** 5.

83. Liu, T.; Wu, L. Y.; Choi, J. K.; Berkman, C. E., Targeted photodynamic therapy for prostate cancer: inducing apoptosis via activation of the caspase-8/-3 cascade pathway. *Int J Oncol* **2010,** 36, (4), 777-84.

84. Sharman, W. M.; Allen, C. M.; van Lier, J. E., Photodynamic therapeutics: basic principles and clinical applications. *Drug Discov Today* **1999,** 4, (11), 507-517.

85. Klotz, L. O.; Kroncke, K. D.; Sies, H., Singlet oxygen-induced signaling effects in mammalian cells. *Photochem Photobiol Sci* **2003,** 2, (2), 88-94.

86. Schiff, L. J.; Eisenberg, W. C.; Dziuba, J.; Taylor, K.; Moore, S. J., Cytotoxic effects of singlet oxygen. *Environ Health Perspect* **1987,** 76, 199-203.

87. Briviba, K.; Klotz, L. O.; Sies, H., Toxic and signaling effects of photochemically or chemically generated singlet oxygen in biological systems. *Biol Chem* **1997,** 378, (11), 1259-65.

88. Moore, C. M.; Emberton, M.; Bown, S. G., Photodynamic therapy for prostate cancer--an emerging approach for organ-confined disease. *Lasers Surg Med* **2011,** 43, (7), 768-75.

89. Arumainayagam, N.; Moore, C. M.; Ahmed, H. U.; Emberton, M., Photodynamic therapy for focal ablation of the prostate. *World J Urol* **2010,** 28, (5), 571-6.

90. Bozzini, G.; Colin, P.; Nevoux, P.; Villers, A.; Mordon, S.; Betrouni, N., Focal therapy of prostate cancer: energies and procedures. *Urol Oncol* **2012**.

91. Lepor, H., Vascular targeted photodynamic therapy for localized prostate cancer. *Rev Urol* **2008,** 10, (4), 254-61.

92. Nomura, T.; Mimata, H., Focal therapy in the management of prostate cancer: an emerging approach for localized prostate cancer. *Adv Urol* **2012,** 2012, 391437.

93. Zisman, A.; Pantuck, A. J.; Cohen, J. K.; Belldegrun, A. S., Prostate cryoablation using direct transperineal placement of ultrathin probes through a 17-gauge brachytherapy template-technique and preliminary results. *Urology* **2001,** 58, (6), 988-93.

94. De La Taille, A.; Benson, M. C.; Bagiella, E.; Burchardt, M.; Shabsigh, A.; Olsson, C. A.; Katz, A. E., Cryoablation for clinically localized prostate cancer using an argon-based system: complication rates and biochemical recurrence. *BJU Int* **2000,** 85, (3), 281-6.

95. Cohen, J. K.; Miller, R. J., Thermal protection of urethra during cryosurgery of prostate. *Cryobiology* **1994,** 31, (3), 313-6.

96. Derakhshani, P.; Neubauer, S.; Braun, M.; Zumbe, J.; Heidenreich, A.; Engelmann, U., Cryoablation of localized prostate cancer. Experience in 48 cases, PSA and biopsy results. *Eur Urol* **1998,** 34, (3), 181-7.

97. Chin, J. L.; Lim, D.; Abdelhady, M., Review of primary and salvage cryoablation for prostate cancer. *Cancer Control* **2007,** 14, (3), 231-7.

98. Izawa, J. I.; Ajam, K.; McGuire, E.; Scott, S.; von Eschenbach, A. C.; Skibber, J.; Pisters, L. L., Major surgery to manage definitively severe complications of salvage cryotherapy for prostate cancer. *J Urol* **2000,** 164, (6), 1978-81.

99. Gangi, A.; Tsoumakidou, G.; Abdelli, O.; Buy, X.; de Mathelin, M.; Jacqmin, D.; Lang, H., Percutaneous MR-guided cryoablation of prostate cancer: initial experience. *Eur Radiol* **2012,** 22, (8), 1829-1835.

100. Bihrle, R.; Foster, R. S.; Sanghvi, N. T.; Donohue, J. P.; Hood, P. J., High intensity focused ultrasound for the treatment of benign prostatic hyperplasia: early United States clinical experience. *J Urol* **1994,** 151, (5), 1271-5.

101. Madersbacher, S.; Pedevilla, M.; Vingers, L.; Susani, M.; Marberger, M., Effect of high-intensity focused ultrasound on human prostate cancer in vivo. *Cancer Res* **1995,** 55, (15), 3346-51.

102. Ter Haar, G. R., et al., Trackless surgery using focused ultrasound: Technique and case report. *Min Inv Ther* **1991,** 1, (1), 13-19.

103. Orsi, F.; Arnone, P.; Chen, W.; Zhang, L., High intensity focused ultrasound ablation: a new therapeutic option for solid tumors. *J Cancer Res Ther* **2010,** 6, (4), 414-20.

104. Lindner, U.; Trachtenberg, J.; Lawrentschuk, N., Focal therapy in prostate cancer: modalities, findings and future considerations. *Nat Rev Urol* **2010,** 7, (10), 562-71.

105. Napoli, A.; Anzidei, M.; De Nunzio, C.; Cartocci, G.; Panebianco, V.; De Dominicis, C.; Catalano, C.; Petrucci, F.; Leonardo, C., Real-time magnetic resonance-guided high-intensity focused ultrasound focal therapy for localised prostate cancer: preliminary experience. *Eur Urol* **2013,** 63, (2), 395-8.

106. Madersbacher, S.; Kratzik, C.; Szabo, N.; Susani, M.; Vingers, L.; Marberger, M., Tissue ablation in benign prostatic hyperplasia with high-intensity focused ultrasound. *European Urology* **1993,** 23, 39-43.

107. Bomers, J. G.; Sedelaar, J. P.; Barentsz, J. O.; Futterer, J. J., MRI-guided interventions for the treatment of prostate cancer. *AJR Am J Roentgenol* **2012,** 199, (4), 714-20.

108. El Fegoun, A. B.; Barret, E.; Prapotnich, D.; Soon, S.; Cathelineau, X.; Rozet, F.; Galiano, M.; Sanchez-Salas, R.; Vallancien, G., Focal therapy with high-intensity focused ultrasound for prostate cancer in the elderly. A feasibility study with 10 years follow-up. *Int Braz J Urol* **2011,** 37, (2), 213-9; discussion 220-2.

109. Cordeiro, E. R.; Cathelineau, X.; Thuroff, S.; Marberger, M.; Crouzet, S.; de la Rosette, J. J., High-intensity focused ultrasound (HIFU) for definitive treatment of prostate cancer. *BJU Int* **2012,** 110, (9), 1228-42.

110. Mearini, L.; Porena, M., Transrectal high-intensity focused ultrasound for the treatment of prostate cancer: past, present, and future. *Indian J Urol* **2010,** 26, (1), 4-11.

111. Chaussy, C.; Thuroff, S., The status of high-intensity focused ultrasound in the treatment of localized prostate cancer and the impact of a combined resection. *Curr Urol Rep* **2003,** 4, (3), 248-52.

112. Spencer, G. M.; Rubens, D. J.; Roach, D. J., Hypoechoic fat: a sonographic pitfall. *AJR American journal of roentgenology* **1995,** 164, (5), 1277-80.

113. Sumitomo, M.; Asakuma, J.; Yoshii, H.; Sato, A.; Horiguchi, A.; Ito, K.; Nagakura, K.; Asano, T., Anterior perirectal fat tissue thickness is a strong predictor of recurrence after high-intensity focused ultrasound for prostate cancer. *Int J Urol* **2010,** 17, (9), 776-82.

114. Hirst, A. M.; Frame, F. M.; Maitland, N. J.; O'Connell, D., Low Temperature Plasma: A Novel Focal Therapy for Localized Prostate Cancer? *BioMed research international* **2014,** 2014, 878319.

115. Chen, F. F., *Introduction to plasma physics and controlled fusion*. 2nd ed. ed.; Plenum: New York ; London, 1984.

116. Paschen, F., Ueber die zum Funkenübergang in Luft, Wasserstoff und Kohlensäure bei verschiedenen Drucken erforderliche Potentialdifferenz. *Annalen der Physik* **1889,** 273, (5), 69-96.

117. Shishoo, R., *Plasma technologies for textiles*. Elsevier: 2007.

118. Morent, R.; De Geyter, N.; Verschuren, J.; De Clerck, K.; Kiekens, P.; Leys, C., Non-thermal plasma treatment of textiles. *Surface and Coatings Technology* **2008,** 202, (14), 3427-3449.

119. Haruhiko, A.; Masahiro, Y.; Nobuo, F., Developments of Plasma Etching Technology for Fabricating Semiconductor Devices. *Japanese Journal of Applied Physics* **2008,** 47, (3R), 1435.

120. Williams, P., *Plasma processing of semiconductors*. Springer Science & Business Media: 2013; Vol. 336.

121. Niemi, K.; O'Connell, D.; de Oliveira, N.; Joyeux, D.; Nahon, L.; Booth, J. P.; Gans, T., Absolute atomic oxygen and nitrogen densities in radio-frequency driven atmospheric pressure cold plasmas: Synchrotron vacuum ultra-violet high-resolution Fourier-transform absorption measurements. *Appl Phys Lett* **2013,** 103, (3), 034102.

122. Qing, X.; Anton Yu, N.; Manuel Á, G.; Christophe, L.; Xin Pei, L., Characterization of an atmospheric helium plasma jet by relative and absolute optical emission spectroscopy. *Plasma Sources Science and Technology* **2013,** 22, (1), 015011.

123. Coburn, J. W.; Chen, M., Optical emission spectroscopy of reactive plasmas: A method for correlating emission intensities to reactive particle density. *J Appl Phys* **1980,** 51, (6), 3134-3136.

124. Smirnov, B. M., *Physics of Atoms and Ions*. 1 ed.; Springer-Verlag New York: 2003; p 443.

125. Electrical breakdown of gases. By J. M. Meek and J. D. Craggs. Oxford (Clarendon Press), 1953. Pp. vii, 507; 320 Figs., 82 tables. 60s. *Quarterly Journal of the Royal Meteorological Society* **1954,** 80, (344), 282-283.

126. Raether, H., *Electron avalanches and breakdown in gases*. Butterworths: London, 1964.

127. Raizer, Y. P.; Allen, J. E., *Gas discharge physics*. Springer Berlin: 1997; Vol. 2.

128. Algwari, Q. T. Plasma jet formation and interactions between atmospheric pressure dielectric barrier discharge jets. Queen's University of Belfast, 2011.

129. Walsh, J. L.; Iza, F.; Janson, N. B.; Law, V. J.; Kong, M. G., Three distinct modes in a cold atmospheric pressure plasma jet. *Journal of Physics D: Applied Physics* **2010,** 43, (7), 075201.

130. Fridman, G.; Peddinghaus, M.; Ayan, H.; Fridman, A.; Balasubramanian, M.; Gutsol, A.; Brooks, A.; Friedman, G., Blood coagulation and living tissue sterilization by floating-electrode dielectric barrier discharge in air. *Plasma Chem Plasma P* **2006,** 26, (4), 425-442.

131. Daeschlein, G.; Scholz, S.; Ahmed, R.; von Woedtke, T.; Haase, H.; Niggemeier, M.; Kindel, E.; Brandenburg, R.; Weltmann, K. D.; Juenger, M., Skin decontamination by low-temperature atmospheric pressure plasma jet and dielectric barrier discharge plasma. *J Hosp Infect* **2012,** 81, (3), 177-83.

132. Kong, M. G., A complementary sterilisation strategy using cold atmospheric plasmas. *Med Device Technol* **2006,** 17, (3), 26-8.

133. Kong, M. G., Cold atmospheric plasma destruction of solid proteins on stainless-steel surface and on real surgical instruments. *GMS Krankenhhyg Interdiszip* **2008,** 3, (1), Doc07.

134. Baik, K. Y.; Kim, Y. H.; Ryu, Y. H.; Kwon, H. S.; Park, G.; Uhm, H. S.; Choi, E. H., Feeding-Gas Effects of Plasma Jets on Escherichia coli in Physiological Solutions. *Plasma Process Polym* **2013,** 10, (3), 235-242.

135. Laroussi, M.; Tendero, C.; Lu, X.; Alla, S.; Hynes, W. L., Inactivation of Bacteria by the Plasma Pencil. *Plasma Process Polym* **2006,** 3, 470-473.

136. Fricke, K.; Koban, I.; Tresp, H.; Jablonowski, L.; Schroder, K.; Kramer, A.; Weltmann, K. D.; von Woedtke, T.; Kocher, T., Atmospheric pressure plasma: a high-performance tool for the efficient removal of biofilms. *PLoS One* **2012,** 7, (8), e42539.

137. Alkawareek, M. Y.; Algwari, Q. T.; Gorman, S. P.; Graham, W. G.; O'Connell, D.; Gilmore, B. F., Application of atmospheric pressure nonthermal plasma for the in vitro eradication of bacterial biofilms. *Fems Immunol Med Mic* **2012,** 65, (2), 381-384.

138. Cotter, J. J.; Maguire, P.; Soberon, F.; Daniels, S.; O'Gara, J. P.; Casey, E., Disinfection of meticillin-resistant Staphylococcus aureus and Staphylococcus epidermidis biofilms using a remote non-thermal gas plasma. *Journal of Hospital Infection* **2011,** 78, (3), 204-207.

139. Ziuzina, D.; Patil, S.; Cullen, P. J.; Keener, K. M.; Bourke, P., Atmospheric cold plasma inactivation of Escherichia coli in liquid media inside a sealed package. *J Appl Microbiol* **2013,** 114, (3), 778-87.

140. Fernandez, A.; Noriega, E.; Thompson, A., Inactivation of Salmonella enterica serovar Typhimurium on fresh produce by cold atmospheric gas plasma technology. *Food Microbiol* **2013,** 33, (1), 24-9.

141. Laroussi, M., Non-Thermal Decontamination of Biological Media by Atmospheric Pressure Plasmas: Review, Analysis, and Prospects. *Ieee T Plasma Sci* **2002,** 30, (4), 1409-1415.

142. Garcia-Alcantara, E.; Lopez-Callejas, R.; Morales-Ramirez, P. R.; Pena-Eguiluz, R.; Fajardo-Munoz, R.; Mercado-Cabrera, A.; Barocio, S. R.; Valencia-Alvarado, R.; Rodriguez-Mendez, B. G.; Munoz-Castro, A. E.; Piedad-Beneitez, A. D.; Rojas-Olmedo, I. A., In Vivo Accelerated Acute Wound Healing in Mouse Skin Using Combined Treatment of Argon and Helium Plasma Needle. *Arch Med Res* **2013**.

143. Wu, A. S.; Kalghatgi, S.; Dobrynin, D.; Sensenig, R.; Cerchar, E.; Podolsky, E.; Dulaimi, E.; Paff, M.; Wasko, K.; Arjunan, K. P.; Garcia, K.; Fridman, G.; Balasubramanian, M.; Ownbey, R.; Barbee, K. A.; Fridman, A.; Friedman, G.; Joshi, S. G.; Brooks, A. D., Porcine intact and wounded skin responses to atmospheric nonthermal plasma. *J Surg Res* **2013,** 179, (1), e1-e12.

144. Sensenig, R.; Kalghatgi, S.; Cerchar, E.; Fridman, G.; Shereshevsky, A.; Torabi, B.; Arjunan, K. P.; Podolsky, E.; Fridman, A.; Friedman, G.; Azizkhan-Clifford,

J.; Brooks, A. D., Non-thermal plasma induces apoptosis in melanoma cells via production of intracellular reactive oxygen species. *Ann Biomed Eng* **2011,** 39, (2), 674-87.

145. Yan, X.; Xiong, Z. L.; Zou, F.; Zhao, S. S.; Lu, X. P.; Yang, G. X.; He, G. Y.; Ostrikov, K., Plasma-Induced Death of HepG2 Cancer Cells: Intracellular Effects of Reactive Species. *Plasma Process Polym* **2012,** 9, (1), 59-66.

146. Kim, J. Y.; Ballato, J.; Foy, P.; Hawkins, T.; Wei, Y.; Li, J.; Kim, S. O., Apoptosis of lung carcinoma cells induced by a flexible optical fiber-based cold microplasma. *Biosens Bioelectron* **2011,** 28, (1), 333-8.

147. Kaushik, N. K.; Kim, Y. H.; Han, Y. G.; Choi, E. H., Effect of jet plasma on T98G human brain cancer cells. *Current Applied Physics* **2013,** 13, (1), 176-180.

148. Stalder, K. R.; McMillen, D. F.; Woloszko, J., Electrosurgical plasmas. *J Phys D Appl Phys* **2005,** 38, (11), 1728-1738.

149. Raiser, J.; Zenker, M., Argon plasma coagulation for open surgical and endoscopic applications: state of the art. *Journal of Physics D: Applied Physics* **2006,** 39, (16), 3520.

150. Canard, J. M.; Vedrenne, B., Clinical application of argon plasma coagulation in gastrointestinal endoscopy: Has the time come to replace the laser? *Endoscopy* **2001,** 33, (4), 353-357.

151. Geavlete, B.; Multescu, R.; Dragutescu, M.; Jecu, M.; Georgescu, D.; Geavlete, P., Transurethral resection (TUR) in saline plasma vaporization of the prostate vs standard TUR of the prostate: 'the better choice' in benign prostatic hyperplasia? *BJU International* **2010,** 106, (11), 1695-1699.

152. Xie, L. P.; Qin, J.; Zheng, X. Y.; Mao, Q. Q.; Zhang, P.; Huang, X.; Tan, F. Q.; Liu, B., [Transurethral vapor enucleation and resection of prostate with TURis button electrode]. *Zhonghua Yi Xue Za Zhi* **2012,** 92, (22), 1558-9.

153. Zhang, S. Y.; Hu, H.; Zhang, X. P.; Wang, D.; Xu, K. X.; Na, Y. Q.; Huang, X. B.; Wang, X. F., Efficacy and safety of bipolar plasma vaporization of the prostate with "button-type" electrode compared with transurethral resection of prostate for benign prostatic hyperplasia. *Chin Med J (Engl)* **2012,** 125, (21), 3811-4.

154. Graves, D. B., The emerging role of reactive oxygen and nitrogen species in redox biology and some implications for plasma applications to medicine and biology. *J Phys D Appl Phys* **2012,** 45, (26).

155. Laroussi, M., *Plasma medicine : applications of low-temperature gas plasmas in medicine and biology*. Cambridge University Press: Cambridge, 2012.

156. Jaroslav, J.; Algwari, Q. T.; O'Connell, D.; Bourdon, A., Experimental-Modeling Study of an Atmospheric-Pressure Helium Discharge Propagating in a Thin Dielectric Tube. *Ieee T Plasma Sci* **2012,** 40, (11), 2912-2919.

157. Algwari, Q. T.; O'Connell, D., Electron dynamics and plasma jet formation in a helium atmospheric pressure dielectric barrier discharge jet. *Appl Phys Lett* **2011,** 99, (12), 121501-3.

158. Walsh, J. L.; Kong, M. G., Contrasting characteristics of linear-field and cross-field atmospheric plasma jets. *Appl Phys Lett* **2008,** 93, (11), 111501-3.

159. Murakami, T.; Niemi, K.; Gans, T.; O'Connell, D.; Graham, W. G., Chemical kinetics and reactive species in atmospheric pressure helium-oxygen plasmas with humid-air impurities. *Plasma Sources Sci T* **2013,** 22, (1).

160. Wagenaars, E.; Gans, T.; O'Connell, D.; Niemi, K., Two-photon absorption laser-induced fluorescence measurements of atomic nitrogen in a radio-frequency atmospheric-pressure plasma jet. *Plasma Sources Sci T* **2012,** 21, (4).

161. Niemi, K.; Waskoenig, J.; Sadeghi, N.; Gans, T.; Connell, D. O., The role of helium metastable states in radio-frequency driven helium–oxygen atmospheric pressure plasma jets: measurement and numerical simulation. *Plasma Sources Science and Technology* **2011,** 20, (5), 055005.

162. Maletic, D.; Puac, N.; Lazovic, S.; Malovic, G.; Gans, T.; Schulz-von der Gathen, V.; Petrovic, Z. L., Detection of atomic oxygen and nitrogen created in a radio-frequency-driven micro-scale atmospheric pressure plasma jet using mass spectrometry. *Plasma Phys Contr F* **2012,** 54, (12).

163. O'Neill, C.; Waskoenig, J.; Gans, T., Tailoring electron energy distribution functions through energy confinement in dual radio-frequency driven atmospheric pressure plasmas. *Appl Phys Lett* **2012,** 101, (15), 154107-4.

164. Schaper, L.; Waskoenig, J.; Kong, M. G.; Schulz-von der Gathen, V.; Gans, T., Electron Dynamics in a Radio-Frequency-Driven Microatmospheric Pressure Plasma Jet. *Ieee T Plasma Sci* **2011,** 39, (11), 2370-2371.

165. Waskoenig, J.; Niemi, K.; Knake, N.; Graham, L. M.; Reuter, S.; Schulz-von der Gathen, V.; Gans, T., Atomic oxygen formation in a radio-frequency driven micro-atmospheric pressure plasma jet. *Plasma Sources Science and Technology* **2010,** 19, (4), 045018.

166. Waskoenig, J.; Niemi, K.; Knake, N.; Graham, L. M.; Reuter, S.; Schulz-von der Gathen, V.; Gans, T., Diagnostic-based modeling on a micro-scale atmospheric-pressure plasma jet. *Pure Appl Chem* **2010,** 82, (6), 1209-1222.

167. Waskoenig, J.; Gans, T., Nonlinear frequency coupling in dual radio-frequency driven atmospheric pressure plasmas. *Appl Phys Lett* **2010,** 96, (18).

168. Niemi, K.; Reuter, S.; Graham, L. M.; Waskoenig, J.; Knake, N.; Schulz-von der Gathen, V.; Gans, T., Diagnostic based modelling of radio-frequency driven atmospheric pressure plasmas. *J Phys D Appl Phys* **2010,** 43, (12).

169. Niemi, K.; Reuter, S.; Graham, L. M.; Waskoenig, J.; Gans, T., Diagnostic based modeling for determining absolute atomic oxygen densities in atmospheric pressure helium-oxygen plasmas. *Appl Phys Lett* **2009,** 95, (15).

170. Schulz-von der Gathen, V.; Schaper, L.; Knake, N.; Reuter, S.; Niemi, K.; Gans, T.; Winter, J., Spatially resolved diagnostics on a microscale atmospheric pressure plasma jet. *Journal of Physics D: Applied Physics* **2008,** 41, (19).

171. Ellerweg, D.; Benedikt, J.; von Keudell, A.; Knake, N.; Schulz-von der Gathen, V., Characterization of the effluent of a He/O-2 microscale atmospheric pressure plasma jet by quantitative molecular beam mass spectrometry. *New J Phys* **2010,** 12.

172. Golda, J.; Held, J.; Redeker, B.; Konkowski, M.; Beijer, P.; Sobota, A.; Kroesen, G.; Braithwaite, N. S. J.; Reuter, S.; Turner, M. M.; Gans, T.; O'Connell, D.; Gathen, V. S.-v. d., Concepts and characteristics of the 'COST Reference Microplasma Jet'. *Journal of Physics D: Applied Physics* **2016,** 49, (8), 084003.

173. Klaunig, J. E.; Kamendulis, L. M., The role of oxidative stress in carcinogenesis. *Annual review of pharmacology and toxicology* **2004,** 44, 239-67.

174. Pelicano, H.; Carney, D.; Huang, P., ROS stress in cancer cells and therapeutic implications. *Drug resistance updates : reviews and commentaries in antimicrobial and anticancer chemotherapy* **2004,** 7, (2), 97-110.

175. Tovmasyan, A.; Maia, C. G.; Weitner, T.; Carballal, S.; Sampaio, R. S.; Lieb, D.; Ghazaryan, R.; Ivanovic-Burmazovic, I.; Radi, R.; Reboucas, J. S.; Spasojevic, I.; Benov, L.; Batinic-Haberle, I., A comprehensive Evaluation of catalase-like activity of different classes of redox-active therapeutics. *Free Radic Biol Med* **2015**.

176. Gorrini, C.; Harris, I. S.; Mak, T. W., Modulation of oxidative stress as an anticancer strategy. *Nat Rev Drug Discov* **2013,** 12, (12), 931-47.

177. Trachootham, D.; Alexandre, J.; Huang, P., Targeting cancer cells by ROS-mediated mechanisms: a radical therapeutic approach? *Nat Rev Drug Discov* **2009,** 8, (7), 579-91.

178. Yoshida, T.; Goto, S.; Kawakatsu, M.; Urata, Y.; Li, T. S., Mitochondrial dysfunction, a probable cause of persistent oxidative stress after exposure to ionizing radiation. *Free radical research* **2012,** 46, (2), 147-53.

179. Sangeetha, P.; Das, U. N.; Koratkar, R.; Suryaprabha, P., Increase in free radical generation and lipid peroxidation following chemotherapy in patients with cancer. *Free Radic Biol Med* **1990,** 8, (1), 15-9.

180. Conklin, K. A., Chemotherapy-associated oxidative stress: impact on chemotherapeutic effectiveness. *Integrative cancer therapies* **2004,** 3, (4), 294-300.

181. Xu, D.; Liu, D.; Wang, B.; Chen, C.; Chen, Z.; Li, D.; Yang, Y.; Chen, H.; Kong, M. G., In Situ OH Generation from O2- and H2O2 Plays a Critical Role in Plasma-Induced Cell Death. *PLoS One* **2015,** 10, (6), e0128205.

182. Sousa, J. S.; Niemi, K.; Cox, L. J.; Algwari, Q. T.; Gans, T.; O'Connell, D., Cold atmospheric pressure plasma jets as sources of singlet delta oxygen for biomedical applications. *J Appl Phys* **2011,** 109, (12).

183. Hirst, A. M.; Simms, M. S.; Mann, V. M.; Maitland, N. J.; O'Connell, D.; Frame, F. M., Low-temperature plasma treatment induces DNA damage leading to necrotic cell death in primary prostate epithelial cells. *Br J Cancer* **2015,** 112, (9), 1536-45.

184. Ma, Y.; Ha, C. S.; Hwang, S. W.; Lee, H. J.; Kim, G. C.; Lee, K. W.; Song, K., Non-Thermal Atmospheric Pressure Plasma Preferentially Induces Apoptosis in p53-Mutated Cancer Cells by Activating ROS Stress-Response Pathways. *PLoS One* **2014,** 9, (4), e91947.

185. Lukes, P.; Dolezalova, E.; Sisrova, I.; Clupek, M., Aqueous-phase chemistry and bactericidal effects from an air discharge plasma in contact with water: evidence for the formation of peroxynitrite through a pseudo-second-order post-discharge reaction of H2O2 and HNO2. *Plasma Sources Science and Technology* **2014,** 23, (1), 015019.

186. Hirst, D. G.; Robson, T., Nitrosative stress as a mediator of apoptosis: implications for cancer therapy. *Current pharmaceutical design* **2010,** 16, (1), 45-55.

187.    Gorbanev, Y.; O'Connell, D.; Chechik, V., Non-Thermal Plasma in Contact with Water: The Origin of Species. *Chemistry–A European Journal* **2016**.

188.    Hirst, A. M.; Frame, F. M.; Arya, M.; Maitland, N. J.; O'Connell, D., Low temperature plasmas as emerging cancer therapeutics: the state of play and thoughts for the future. *Tumour biology : the journal of the International Society for Oncodevelopmental Biology and Medicine* **2016**.

189.    Chen, C.; Liu, D. X.; Liu, Z. C.; Yang, A. J.; Chen, H. L.; Shama, G.; Kong, M. G., A Model of Plasma-Biofilm and Plasma-Tissue Interactions at Ambient Pressure. *Plasma Chem Plasma P* **2014,** 34, (3), 403-441.

190.    Babaeva, N. Y.; Kushner, M. J., Reactive fluxes delivered by dielectric barrier discharge filaments to slightly wounded skin. *Journal of Physics D: Applied Physics* **2013,** 46, (2), 025401.

191.    Van Gaens, W.; Iseni, S.; Schmidt-Bleker, A.; Weltmann, K.; Reuter, S.; Bogaerts, A., Numerical analysis of the effect of nitrogen and oxygen admixtures on the chemistry of an argon plasma jet operating at atmospheric pressure. *New J Phys* **2015,** 17, (3), 033003.

192.    Hirst, A. M.; Frame, F. M.; Maitland, N. J.; O'Connell, D., Low Temperature Plasma Causes Double-Strand Break DNA Damage in Primary Epithelial Cells Cultured From a Human Prostate Tumor. *Plasma Science, IEEE Transactions on* **2014,** 42, (10), 2740-2741.

193.    Han, X.; Klas, M.; Liu, Y.; Stack, M. S.; Ptasinska, S., DNA damage in oral cancer cells induced by nitrogen atmospheric pressure plasma jets. *Appl Phys Lett* **2013,** 102, (23), 233703.

194.    Wende, K.; Williams, P.; Dalluge, J.; Gaens, W. V.; Aboubakr, H.; Bischof, J.; von Woedtke, T.; Goyal, S. M.; Weltmann, K. D.; Bogaerts, A.; Masur, K.; Bruggeman, P. J., Identification of the biologically active liquid chemistry induced by a nonthermal atmospheric pressure plasma jet. *Biointerphases* **2015,** 10, (2), 029518.

195.    Guerrero-Preston, R.; Ogawa, T.; Uemura, M.; Shumulinsky, G.; Valle, B. L.; Pirini, F.; Ravi, R.; Sidransky, D.; Keidar, M.; Trink, B., Cold atmospheric plasma treatment selectively targets head and neck squamous cell carcinoma cells. *International journal of molecular medicine* **2014,** 34, (4), 941-6.

196.    Weiss, M.; Gumbel, D.; Hanschmann, E. M.; Mandelkow, R.; Gelbrich, N.; Zimmermann, U.; Walther, R.; Ekkernkamp, A.; Sckell, A.; Kramer, A.;

Burchardt, M.; Lillig, C. H.; Stope, M. B., Cold Atmospheric Plasma Treatment Induces Anti-Proliferative Effects in Prostate Cancer Cells by Redox and Apoptotic Signaling Pathways. *PLoS One* **2015,** 10, (7), e0130350.

197. Nakai, N.; Fujita, R.; Kawano, F.; Takahashi, K.; Ohira, T.; Shibaguchi, T.; Nakata, K.; Ohira, Y., Retardation of C2C12 myoblast cell proliferation by exposure to low-temperature atmospheric plasma. *The journal of physiological sciences : JPS* **2014,** 64, (5), 365-75.

198. Chang, J. W.; Kang, S. U.; Shin, Y. S.; Kim, K. I.; Seo, S. J.; Yang, S. S.; Lee, J. S.; Moon, E.; Baek, S. J.; Lee, K.; Kim, C. H., Non-thermal atmospheric pressure plasma induces apoptosis in oral cavity squamous cell carcinoma: Involvement of DNA-damage-triggering sub-G(1) arrest via the ATM/p53 pathway. *Archives of biochemistry and biophysics* **2014,** 545, 133-40.

199. Cotter, T. G., Apoptosis and cancer: the genesis of a research field. *Nature Reviews Cancer* **2009,** 9, (7), 501-507.

200. Grooten, J.; Goossens, V.; Vanhaesebroeck, B.; Fiers, W., Cell membrane permeabilization and cellular collapse, followed by loss of dehydrogenase activity: early events in tumour necrosis factor-induced cytotoxicity. *Cytokine* **1993,** 5, (6), 546-555.

201. Fiers, W.; Beyaert, R.; Declercq, W.; Vandenabeele, P., More than one way to die: apoptosis, necrosis and reactive oxygen damage. *Oncogene* **1999,** 18, (54), 7719-7730.

202. Siu, A.; Volotskova, O.; Cheng, X.; Khalsa, S. S.; Bian, K.; Murad, F.; Keidar, M.; Sherman, J. H., Differential Effects of Cold Atmospheric Plasma in the Treatment of Malignant Glioma. *PLoS One* **2015,** 10, (6), e0126313.

203. Ishaq, M.; Evans, M. D.; Ostrikov, K. K., Atmospheric pressure gas plasma-induced colorectal cancer cell death is mediated by Nox2-ASK1 apoptosis pathways and oxidative stress is mitigated by Srx-Nrf2 anti-oxidant system. *Biochimica et biophysica acta* **2014,** 1843, (12), 2827-37.

204. Kaushik, N.; Kumar, N.; Kim, C. H.; Kaushik, N. K.; Choi, E. H., Dielectric Barrier Discharge Plasma Efficiently Delivers an Apoptotic Response in Human Monocytic Lymphoma. *Plasma Process Polym* **2014**.

205. Arndt, S.; Wacker, E.; Li, Y. F.; Shimizu, T.; Thomas, H. M.; Morfill, G. E.; Karrer, S.; Zimmermann, J. L.; Bosserhoff, A. K., Cold atmospheric plasma, a

new strategy to induce senescence in melanoma cells. *Experimental dermatology* **2013,** 22, (4), 284-9.

206.    Ishaq, M.; Kumar, S.; Varinli, H.; Han, Z. J.; Rider, A. E.; Evans, M. D.; Murphy, A. B.; Ostrikov, K., Atmospheric gas plasma-induced ROS production activates TNF-ASK1 pathway for the induction of melanoma cancer cell apoptosis. *Molecular biology of the cell* **2014,** 25, (9), 1523-31.

207.    Kaushik, N.; Uddin, N.; Sim, G. B.; Hong, Y. J.; Baik, K. Y.; Kim, C. H.; Lee, S. J.; Kaushik, N. K.; Choi, E. H., Responses of solid tumor cells in DMEM to reactive oxygen species generated by non-thermal plasma and chemically induced ROS systems. *Sci Rep* **2015,** 5, 8587.

208.    Zhang, Z.; Li, W.; Procissi, D.; Tyler, P.; Omary, R. A.; Larson, A. C., Rapid dramatic alterations to the tumor microstructure in pancreatic cancer following irreversible electroporation ablation. *Nanomedicine* **2014,** 9, (8), 1181-92.

209.    Valerio, M.; Dickinson, L.; Ali, A.; Ramachandran, N.; Donaldson, I.; Freeman, A.; Ahmed, H. U.; Emberton, M., A prospective development study investigating focal irreversible electroporation in men with localised prostate cancer: Nanoknife Electroporation Ablation Trial (NEAT). *Contemporary clinical trials* **2014,** 39, (1), 57-65.

210.    Wendler, J. J.; Porsch, M.; Nitschke, S.; Kollermann, J.; Siedentopf, S.; Pech, M.; Fischbach, F.; Ricke, J.; Schostak, M.; Liehr, U. B., A prospective Phase 2a pilot study investigating focal percutaneous irreversible electroporation (IRE) ablation by NanoKnife in patients with localised renal cell carcinoma (RCC) with delayed interval tumour resection (IRENE trial). *Contemporary clinical trials* **2015,** 43, 10-19.

211.    Jansky, J.; Algwari, Q. T.; O'Connell, D.; Bourdon, A., Experimental&#x2013;Modeling Study of an Atmospheric-Pressure Helium Discharge Propagating in a Thin Dielectric Tube. *Plasma Science, IEEE Transactions on* **2012,** 40, (11), 2912-2919.

212.    Babaeva, N. Y.; Tian, W.; Kushner, M. J., The interaction between plasma filaments in dielectric barrier discharges and liquid covered wounds: electric fields delivered to model platelets and cells. *Journal of Physics D: Applied Physics* **2014,** 47, (23), 235201.

213. Goran, B. S.; Ivan, B. K.; Vesna, V. K.; Bratislav, M. O.; Milorad, M. K., Spatio-temporally resolved electric field measurements in helium plasma jet. *Journal of Physics D: Applied Physics* **2014,** 47, (10), 102001.

214. Begum, A.; Laroussi, M.; Pervez, M. R., Atmospheric pressure He-air plasma jet: Breakdown process and propagation phenomenon. *AIP Advances* **2013,** 3, (6), 062117.

215. Leduc, M.; Guay, D.; Leask, R.; Coulombe, S., Cell permeabilization using a non-thermal plasma. *New J Phys* **2009,** 11, (11), 115021.

216. Vandamme, M.; Robert, E.; Doziaz, S.; Sobilo, J.; Lerondel, S.; Le Pape, A.; Pouvesle, J.-M., Response of Human Glioma U87 Xenografted on Mice to Non Thermal Plasma Treatment. *Plasma Medicine* **2011,** 1, (1), 27-43.

217. Volotskova, O.; Hawley, T. S.; Stepp, M. A.; Keidar, M., Targeting the cancer cell cycle by cold atmospheric plasma. *Sci Rep* **2012,** 2, 636.

218. Vandamme, M.; Robert, E.; Lerondel, S.; Sarron, V.; Ries, D.; Dozias, S.; Sobilo, J.; Gosset, D.; Kieda, C.; Legrain, B.; Pouvesle, J. M.; Pape, A. L., ROS implication in a new antitumor strategy based on non-thermal plasma. *Int J Cancer* **2012,** 130, (9), 2185-94.

219. Kim, G. J.; Kim, W.; Kim, K. T.; Lee, J. K., DNA damage and mitochondria dysfunction in cell apoptosis induced by nonthermal air plasma. *Appl Phys Lett* **2010,** 96, (2), 021502-3.

220. Thiyagarajan, M.; Gonzales, X. F.; Anderson, H., Regulated cellular exposure to non-thermal plasma allows preferentially directed apoptosis in acute monocytic leukemia cells. *Stud Health Technol Inform* **2013,** 184, 436-42.

221. Walk, R. M.; Snyder, J. A.; Srinivasan, P.; Kirsch, J.; Diaz, S. O.; Blanco, F. C.; Shashurin, A.; Keidar, M.; Sandler, A. D., Cold atmospheric plasma for the ablative treatment of neuroblastoma. *J Pediatr Surg* **2013,** 48, (1), 67-73.

222. Hayward, S. W.; Dahiya, R.; Cunha, G. R.; Bartek, J.; Deshpande, N.; Narayan, P., Establishment and characterization of an immortalized but non-transformed human prostate epithelial cell line: BPH-1. *In Vitro Cell Dev Biol - Animal* **1995,** 31, (1), 14-24.

223. Maitland, N. J.; Macintosh, C. A.; Hall, J.; Sharrard, M.; Quinn, G.; Lang, S., In vitro models to study cellular differentiation and function in human prostate cancers. *Radiation research* **2001,** 155, (1 Pt 2), 133-142.

224. Kaighn, M. E.; Narayan, K. S.; Ohnuki, Y.; Lechner, J. F.; Jones, L. W., Establishment and characterization of a human prostatic carcinoma cell line (PC-3). *Investigative urology* **1979,** 17, (1), 16-23.

225. Collins, A. T.; Berry, P. A.; Hyde, C.; Stower, M. J.; Maitland, N. J., Prospective identification of tumorigenic prostate cancer stem cells. *Cancer Res* **2005,** 65, (23), 10946-51.

226. Engelmann, J.; Volk, J.; Leyhausen, G.; Geurtsen, W., ROS formation and glutathione levels in human oral fibroblasts exposed to TEGDMA and camphorquinone. *Journal of biomedical materials research. Part B, Applied biomaterials* **2005,** 75, (2), 272-6.

227. Zhang, X. D.; Gillespie, S. K.; Hersey, P., Staurosporine induces apoptosis of melanoma by both caspase-dependent and -independent apoptotic pathways. *Molecular cancer therapeutics* **2004,** 3, (2), 187-97.

228. Chae, H. J.; Kang, J. S.; Byun, J. O.; Han, K. S.; Kim, D. U.; Oh, S. M.; Kim, H. M.; Chae, S. W.; Kim, H. R., Molecular mechanism of staurosporine-induced apoptosis in osteoblasts. *Pharmacological research* **2000,** 42, (4), 373-81.

229. Belmokhtar, C. A.; Hillion, J.; Segal-Bendirdjian, E., Staurosporine induces apoptosis through both caspase-dependent and caspase-independent mechanisms. *Oncogene* **2001,** 20, (26), 3354-62.

230. Sturmey, R. G.; Hawkhead, J. A.; Barker, E. A.; Leese, H. J., DNA damage and metabolic activity in the preimplantation embryo. *Human reproduction* **2009,** 24, (1), 81-91.

231. Francipane, M. G.; Alea, M. P.; Lombardo, Y.; Todaro, M.; Medema, J. P.; Stassi, G., Crucial role of interleukin-4 in the survival of colon cancer stem cells. *Cancer Res* **2008,** 68, (11), 4022-5.

232. Ettinger, A.; Wittmann, T., Fluorescence live cell imaging. *Methods in cell biology* **2014,** 123, 77-94.

233. Bromfield, G. P.; Meng, A.; Warde, P.; Bristow, R. G., Cell death in irradiated prostate epithelial cells: role of apoptotic and clonogenic cell kill. *Prostate cancer and prostatic diseases* **2003,** 6, (1), 73-85.

234. Lee, D. I.; Sumbilla, C.; Lee, M.; Natesavelalar, C.; Klein, M. G.; Ross, D. D.; Inesi, G.; Hussain, A., Mechanisms of resistance and adaptation to thapsigargin in androgen-independent prostate cancer PC3 and DU145 cells. *Archives of biochemistry and biophysics* **2007,** 464, (1), 19-27.

235. Rokhlin, O. W.; Hostager, B. S.; Bishop, G. A.; Sidorenko, S. P.; Glover, R. A.; Gudkov, A. V.; Cohen, M. B., Dominant nature of the resistance to Fas- and tumor necrosis factor-alpha-mediated apoptosis in human prostatic carcinoma cell lines. *Cancer Res* **1997,** 57, (18), 3941-3.

236. Ulukaya, E.; Frame, F. M.; Cevatemre, B.; Pellacani, D.; Walker, H.; Mann, V. M.; Simms, M. S.; Stower, M. J.; Yilmaz, V. T.; Maitland, N. J., Differential cytotoxic activity of a novel palladium-based compound on prostate cell lines, primary prostate epithelial cells and prostate stem cells. *PLoS One* **2013,** 8, (5), e64278.

237. Pfeiffer, M. J.; Schalken, J. A., Stem cell characteristics in prostate cancer cell lines. *Eur Urol* **2010,** 57, (2), 246-54.

238. Winterbourn, C. C., Reconciling the chemistry and biology of reactive oxygen species. *Nature chemical biology* **2008,** 4, (5), 278-86.

239. Kramarenko, G. G.; Hummel, S. G.; Martin, S. M.; Buettner, G. R., Ascorbate Reacts with Singlet Oxygen to Produce Hydrogen Peroxide. *Photochemistry and photobiology* **2006,** 82, (6), 1634-1637.

240. Tainer, J. A.; Getzoff, E. D.; Richardson, J. S.; Richardson, D. C., Structure and mechanism of copper, zinc superoxide dismutase. *Nature* **1983,** 306, (5940), 284-287.

241. Helleday, T.; Lo, J.; van Gent, D. C.; Engelward, B. P., DNA double-strand break repair: from mechanistic understanding to cancer treatment. *DNA repair* **2007,** 6, (7), 923-35.

242. Bonner, W. M.; Redon, C. E.; Dickey, J. S.; Nakamura, A. J.; Sedelnikova, O. A.; Solier, S.; Pommier, Y., GammaH2AX and cancer. *Nature reviews. Cancer* **2008,** 8, (12), 957-67.

243. Kuo, L. J.; Yang, L. X., Gamma-H2AX - a novel biomarker for DNA double-strand breaks. *In Vivo* **2008,** 22, (3), 305-9.

244. Judee, F.; Fongia, C.; Ducommun, B.; Yousfi, M.; Lobjois, V.; Merbahi, N., Short and long time effects of low temperature Plasma Activated Media on 3D multicellular tumor spheroids. *Sci Rep* **2016,** 6, 21421.

245. Klotz, L., Active surveillance versus radical treatment for favorable-risk localized prostate cancer. *Curr Treat Options Oncol* **2006,** 7, (5), 355-62.

246. Stoffels, E.; Kieft, I.; Sladek, R., Superficial treatment of mammalian cells using plasma needle. *Journal of Physics D: Applied Physics* **2003,** 36, (23), 2908.

247. Robert, E.; Vandamme, M.; Brullé, L.; Lerondel, S.; Le Pape, A.; Sarron, V.; Riès, D.; Darny, T.; Dozias, S.; Collet, G.; Kieda, C.; Pouvesle, J. M., Perspectives of endoscopic plasma applications. *Clinical Plasma Medicine* **2013,** 1, (2), 8-16.

248. Keidar, M.; Walk, R.; Shashurin, A.; Srinivasan, P.; Sandler, A.; Dasgupta, S.; Ravi, R.; Guerrero-Preston, R.; Trink, B., Cold plasma selectivity and the possibility of a paradigm shift in cancer therapy. *Br J Cancer* **2011,** 105, (9), 1295-301.

249. Kim, S. J.; Chung, T., Cold atmospheric plasma jet-generated RONS and their selective effects on normal and carcinoma cells. *Scientific reports* **2016,** 6.

250. Panngom, K.; Baik, K.; Nam, M.; Han, J.; Rhim, H.; Choi, E., Preferential killing of human lung cancer cell lines with mitochondrial dysfunction by nonthermal dielectric barrier discharge plasma. *Cell Death Dis* **2013,** 4, (5), e642.

251. Wang, M.; Holmes, B.; Cheng, X.; Zhu, W.; Keidar, M.; Zhang, L. G., Cold atmospheric plasma for selectively ablating metastatic breast cancer cells. *PLoS One* **2013,** 8, (9), e73741.

252. Lee, J.-H.; Om, J.-Y.; Kim, Y.-H.; Kim, K.-M.; Choi, E.-H.; Kim, K.-N., Selective Killing Effects of Cold Atmospheric Pressure Plasma with NO Induced Dysfunction of Epidermal Growth Factor Receptor in Oral Squamous Cell Carcinoma. *PloS one* **2016,** 11, (2), e0150279.

253. Gibson, A. R.; McCarthy, H. O.; Ali, A. A.; O'Connell, D.; Graham, W. G., Interactions of a Non-Thermal Atmospheric Pressure Plasma Effluent with PC-3 Prostate Cancer Cells. *Plasma Process Polym* **2014,** 11, (12), 1142-1149.

254. Ninomiya, K.; Ishijima, T.; Imamura, M.; Yamahara, T.; Enomoto, H.; Takahashi, K.; Tanaka, Y.; Uesugi, Y.; Shimizu, N., Evaluation of extra- and intracellular OH radical generation, cancer cell injury, and apoptosis induced by a non-thermal atmospheric-pressure plasma jet. *J Phys D Appl Phys* **2013,** 46, (42).

255. Partecke, L. I.; Evert, K.; Haugk, J.; Doering, F.; Normann, L.; Diedrich, S.; Weiss, F.-U.; Evert, M.; Huebner, N. O.; Guenther, C., Tissue tolerable plasma (TTP) induces apoptosis in pancreatic cancer cells in vitro and in vivo. *BMC cancer* **2012,** 12, (1), 473.

256. Tuhvatulin, A.; Sysolyatina, E.; Scheblyakov, D.; Logunov, D. Y.; Vasiliev, M.; Yurova, M.; Danilova, M.; Petrov, O.; Naroditsky, B.; Morfill, G., Non-thermal plasma causes p53-dependent apoptosis in human colon carcinoma cells. *Acta naturae* **2012,** 4, (3), 82-87.

257. Iseki, S.; Nakamura, K.; Hayashi, M.; Tanaka, H.; Kondo, H.; Kajiyama, H.; Kano, H.; Kikkawa, F.; Hori, M., Selective killing of ovarian cancer cells through induction of apoptosis by nonequilibrium atmospheric pressure plasma. *Appl Phys Lett* **2012,** 100, (11), 113702.

258. Conway, G. E.; Casey, A.; Milosavljevic, V.; Liu, Y.; Howe, O.; Cullen, P. J.; Curtin, J. F., Non-thermal atmospheric plasma induces ROS-independent cell death in U373MG glioma cells and augments the cytotoxicity of temozolomide. *Br J Cancer* **2016,** 114, (4), 435-43.

259. Frame, F. M.; Savoie, H.; Bryden, F.; Giuntini, F.; Mann, V. M.; Simms, M. S.; Boyle, R. W.; Maitland, N. J., Mechanisms of growth inhibition of primary prostate epithelial cells following gamma irradiation or photodynamic therapy include senescence, necrosis, and autophagy, but not apoptosis. *Cancer medicine* **2016,** 5, (1), 61-73.

260. Saito, K.; Asai, T.; Fujiwara, K.; Sahara, J.; Koguchi, H.; Fukuda, N.; Suzuki-Karasaki, M.; Soma, M.; Suzuki-Karasaki, Y., Tumor-selective mitochondrial network collapse induced by atmospheric gas plasma-activated medium. *Oncotarget* **2016.**

261. Ishaq, M.; Evans, M. M.; Ostrikov, K. K., Effect of atmospheric gas plasmas on cancer cell signaling. *Int J Cancer* **2014,** 134, (7), 1517-28.

262. Kalghatgi, S.; Kelly, C. M.; Cerchar, E.; Torabi, B.; Alekseev, O.; Fridman, A.; Friedman, G.; Azizkhan-Clifford, J., Effects of non-thermal plasma on mammalian cells. *PLoS One* **2011,** 6, (1), e16270.

263. Li, W.; Yu, K. N.; Bao, L.; Shen, J.; Cheng, C.; Han, W., Non-thermal plasma inhibits human cervical cancer HeLa cells invasiveness by suppressing the MAPK pathway and decreasing matrix metalloproteinase-9 expression. *Sci Rep* **2016,** 6, 19720.

264. Iseki, S.; Nakamura, K.; Hayashi, M.; Tanaka, H.; Kondo, H.; Kajiyama, H.; Kano, H.; Kikkawa, F.; Hori, M., Selective killing of ovarian cancer cells through induction of apoptosis by nonequilibrium atmospheric pressure plasma. *Appl Phys Lett* **2012,** 100, (11).

265. Hanus, J.; Zhang, H.; Wang, Z.; Liu, Q.; Zhou, Q.; Wang, S., Induction of necrotic cell death by oxidative stress in retinal pigment epithelial cells. *Cell Death Dis* **2013,** 4, e965.

266. Hirst, D.; Robson, T., Targeting nitric oxide for cancer therapy. *J Pharm Pharmacol* **2007,** 59, (1), 3-13.

267. Lechner, M.; Lirk, P.; Rieder, J., Inducible nitric oxide synthase (iNOS) in tumor biology: the two sides of the same coin. *Seminars in cancer biology* **2005,** 15, (4), 277-89.

268. Szabo, C.; Ohshima, H., DNA damage induced by peroxynitrite: subsequent biological effects. *Nitric oxide : biology and chemistry / official journal of the Nitric Oxide Society* **1997,** 1, (5), 373-85.

269. Sidorkina, O.; Espey, M. G.; Miranda, K. M.; Wink, D. A.; Laval, J., Inhibition of poly(ADP-RIBOSE) polymerase (PARP) by nitric oxide and reactive nitrogen oxide species. *Free Radic Biol Med* **2003,** 35, (11), 1431-8.

270. Hubenak, J. R.; Zhang, Q.; Branch, C. D.; Kronowitz, S. J., Mechanisms of injury to normal tissue after radiotherapy: a review. *Plastic and reconstructive surgery* **2014,** 133, (1), 49e-56e.

271. Iacovelli, R.; Verri, E.; Cossu Rocca, M.; Aurilio, G.; Cullura, D.; De Cobelli, O.; Nole, F., The incidence and relative risk of cardiovascular toxicity in patients treated with new hormonal agents for castration-resistant prostate cancer. *European journal of cancer* **2015,** 51, (14), 1970-7.

272. UK, T. S. P., Private communication. In 2014.

273. Biedler, J. L., Chromosome Abnormalities in Human Tumor Cells in Culture. In *Human Tumor Cells in Vitro*, Fogh, J., Ed. Springer US: Boston, MA, 1975; pp 359-394.

274. Cassio, D., Long term culture of MDCK strains alters chromosome content. *BMC Research Notes* **2013,** 6, (1), 1-7.

275. Ohnuki, Y.; Reddel, R. R.; Bates, S. E.; Lehman, T. A.; Lechner, J. F.; Harris, C. C., Chromosomal changes and progressive tumorigenesis of human bronchial epithelial cell lines. *Cancer genetics and cytogenetics* **1996,** 92, (2), 99-110.

276. Yang, Z.; Klionsky, D. J., Eaten alive: a history of macroautophagy. *Nature cell biology* **2010,** 12, (9), 814-22.

277. Kroemer, G.; Levine, B., Autophagic cell death: the story of a misnomer. *Nature reviews. Molecular cell biology* **2008,** 9, (12), 1004-10.

278.  E., B. D., Targeting of the PI3K/AKT/mTOR pathway in human prostate cancer. **2014**.

279.  Kepp, O.; Galluzzi, L.; Lipinski, M.; Yuan, J.; Kroemer, G., Cell death assays for drug discovery. *Nat Rev Drug Discov* **2011,** 10, (3), 221-37.

280.  Eguchi, Y.; Shimizu, S.; Tsujimoto, Y., Intracellular ATP levels determine cell death fate by apoptosis or necrosis. *Cancer Res* **1997,** 57, (10), 1835-40.

281.  Tsujimoto, Y., Apoptosis and necrosis: intracellular ATP level as a determinant for cell death modes. *Cell death and differentiation* **1997,** 4, (6), 429-34.

282.  Villena, J.; Henriquez, M.; Torres, V.; Moraga, F.; Diaz-Elizondo, J.; Arredondo, C.; Chiong, M.; Olea-Azar, C.; Stutzin, A.; Lavandero, S.; Quest, A. F., Ceramide-induced formation of ROS and ATP depletion trigger necrosis in lymphoid cells. *Free Radic Biol Med* **2008,** 44, (6), 1146-60.

283.  Martins, I.; Wang, Y.; Michaud, M.; Ma, Y.; Sukkurwala, A. Q.; Shen, S.; Kepp, O.; Metivier, D.; Galluzzi, L.; Perfettini, J. L.; Zitvogel, L.; Kroemer, G., Molecular mechanisms of ATP secretion during immunogenic cell death. *Cell death and differentiation* **2014,** 21, (1), 79-91.

284.  Lang, S. H.; Smith, J.; Hyde, C.; Macintosh, C.; Stower, M.; Maitland, N. J., Differentiation of prostate epithelial cell cultures by matrigel/ stromal cell glandular reconstruction. *In vitro cellular & developmental biology. Animal* **2006,** 42, (8-9), 273-80.

285.  Plewa, J.-M.; Yousfi, M.; Frongia, C.; Eichwald, O.; Ducommun, B.; Merbahi, N.; Lobjois, V., Low-temperature plasma-induced antiproliferative effects on multi-cellular tumor spheroids. *New J Phys* **2014,** 16, (4), 043027.

286.  Szili, E. J.; Oh, J.-S.; Hong, S.-H.; Hatta, A.; Short, R. D., Probing the transport of plasma-generated RONS in an agarose target as surrogate for real tissue: dependency on time, distance and material composition. *Journal of Physics D: Applied Physics* **2015,** 48, (20), 202001.

287.  Ahmed, H. U.; Hindley, R. G.; Dickinson, L.; Freeman, A.; Kirkham, A. P.; Sahu, M.; Scott, R.; Allen, C.; Van der Meulen, J.; Emberton, M., Focal therapy for localised unifocal and multifocal prostate cancer: a prospective development study. *Lancet Oncology* **2012,** 13, (6), 622-632.

288.  Klotz, L., Active surveillance: patient selection. *Curr Opin Urol* **2013,** 23, (3), 239-44.

289. Tareen, B.; Godoy, G.; Taneja, S. S., Focal therapy: a new paradigm for the treatment of prostate cancer. *Rev Urol* **2009,** 11, (4), 203-12.

290. Sullivan, K. F.; Crawford, E. D., Targeted focal therapy for prostate cancer: a review of the literature. *Ther Adv Urol* **2009,** 1, (3), 149-59.

291. Martini, L. M.; Dilecce, G.; Scotoni, M.; Tosi, P.; Benedictis, S. D., OH Density Measurements by Time-Resolved Broad Band Absorption Spectroscopy in a He–H2O Dielectric Barrier Discharge with Small O2 Addition. *Plasma Process Polym* **2014,** 11, (3), 232-238.

292. Polak, M.; Winter, J.; Schnabel, U.; Ehlbeck, J.; Weltmann, K.-D., Innovative Plasma Generation in Flexible Biopsy Channels for Inner-Tube Decontamination and Medical Applications. *Plasma Process Polym* **2012,** 9, (1), 67-76.

293. Dai, X. J.; Corr, C. S.; Ponraj, S. B.; Maniruzzaman, M.; Ambujakshan, A. T.; Chen, Z.; Kviz, L.; Lovett, R.; Rajmohan, G. D.; de Celis, D. R.; Wright, M. L.; Lamb, P. R.; Krasik, Y. E.; Graves, D. B.; Graham, W. G.; d'Agostino, R.; Wang, X., Efficient and Selectable Production of Reactive Species Using a Nanosecond Pulsed Discharge in Gas Bubbles in Liquid. *Plasma Process Polym* **2016,** 13, (3), 306-310.

294. Harris, A. L., Hypoxia--a key regulatory factor in tumour growth. *Nature reviews. Cancer* **2002,** 2, (1), 38-47.

295. Joseph, J. V.; Conroy, S.; Pavlov, K.; Sontakke, P.; Tomar, T.; Eggens-Meijer, E.; Balasubramaniyan, V.; Wagemakers, M.; den Dunnen, W. F.; Kruyt, F. A., Hypoxia enhances migration and invasion in glioblastoma by promoting a mesenchymal shift mediated by the HIF1alpha-ZEB1 axis. *Cancer letters* **2015,** 359, (1), 107-16.

296. Brustugun, O. T., Hypoxia as a cause of treatment failure in non-small cell carcinoma of the lung. *Semin Radiat Oncol* **2015,** 25, (2), 87-92.

297. Gomez-Millan, J.; Lara, M. F.; Correa Generoso, R.; Perez-Rozos, A.; Lupianez-Perez, Y.; Medina Carmona, J. A., Advances in the treatment of prostate cancer with radiotherapy. *Crit Rev Oncol Hematol* **2015**.

298. Bao, S.; Wu, Q.; McLendon, R. E.; Hao, Y.; Shi, Q.; Hjelmeland, A. B.; Dewhirst, M. W.; Bigner, D. D.; Rich, J. N., Glioma stem cells promote radioresistance by preferential activation of the DNA damage response. *Nature* **2006,** 444, (7120), 756-60.

299. Huang, R.; Wang, G.; Song, Y.; Tang, Q.; You, Q.; Liu, Z.; Chen, Y.; Zhang, Q.; Li, J.; Muhammand, S.; Wang, X., Colorectal cancer stem cell and chemoresistant colorectal cancer cell phenotypes and increased sensitivity to Notch pathway inhibitor. *Molecular medicine reports* **2015**.

300. Dean, M.; Fojo, T.; Bates, S., Tumour stem cells and drug resistance. *Nature reviews. Cancer* **2005,** 5, (4), 275-84.

301. Gorelik, E.; Lokshin, A.; Levina, V., Lung cancer stem cells as a target for therapy. *Anti-cancer agents in medicinal chemistry* **2010,** 10, (2), 164-71.

302. Kumazawa, S.; Kajiyama, H.; Umezu, T.; Mizuno, M.; Suzuki, S.; Yamamoto, E.; Mitsui, H.; Sekiya, R.; Shibata, K.; Kikkawa, F., Possible association between stem-like hallmark and radioresistance in human cervical carcinoma cells. *The journal of obstetrics and gynaecology research* **2014,** 40, (5), 1389-98.

303. Frame, F. M.; Pellacani, D.; Collins, A. T.; Simms, M. S.; Mann, V. M.; Jones, G. D.; Meuth, M.; Bristow, R. G.; Maitland, N. J., HDAC inhibitor confers radiosensitivity to prostate stem-like cells. *Br J Cancer* **2013,** 109, (12), 3023-33.

304. Diehn, M.; Cho, R. W.; Lobo, N. A.; Kalisky, T.; Dorie, M. J.; Kulp, A. N.; Qian, D.; Lam, J. S.; Ailles, L. E.; Wong, M.; Joshua, B.; Kaplan, M. J.; Wapnir, I.; Dirbas, F. M.; Somlo, G.; Garberoglio, C.; Paz, B.; Shen, J.; Lau, S. K.; Quake, S. R.; Brown, J. M.; Weissman, I. L.; Clarke, M. F., Association of reactive oxygen species levels and radioresistance in cancer stem cells. *Nature* **2009,** 458, (7239), 780-3.

305. Klammer, H.; Mladenov, E.; Li, F.; Iliakis, G., Bystander effects as manifestation of intercellular communication of DNA damage and of the cellular oxidative status. *Cancer letters* **2015,** 356, (1), 58-71.

306. Graves, D. B., Oxy-nitroso shielding burst model of cold atmospheric plasma therapeutics. *Clinical Plasma Medicine* **2014,** 2, (2), 38-49.

307. Voll, R. E.; Herrmann, M.; Roth, E. A.; Stach, C.; Kalden, J. R.; Girkontaite, I., Immunosuppressive effects of apoptotic cells. *Nature* **1997,** 390, (6658), 350-1.

308. Gregory, C. D.; Pound, J. D., Microenvironmental influences of apoptosis in vivo and in vitro. *Apoptosis : an international journal on programmed cell death* **2010,** 15, (9), 1029-49.

309. Teng, F.; Kong, L.; Meng, X.; Yang, J.; Yu, J., Radiotherapy combined with immune checkpoint blockade immunotherapy: Achievements and challenges. *Cancer letters*, (0).

310. Melcher, A.; Todryk, S.; Hardwick, N.; Ford, M.; Jacobson, M.; Vile, R. G., Tumor immunogenicity is determined by the mechanism of cell death via induction of heat shock protein expression. *Nature medicine* **1998,** 4, (5), 581-7.

311. Baust, J. G.; Gage, A. A., The molecular basis of cryosurgery. *BJU Int* **2005,** 95, (9), 1187-91.

312. Alkhorayef, M.; Mahmoud, M. Z.; Alzimami, K. S.; Sulieman, A.; Fagiri, M. A., High-Intensity Focused Ultrasound (HIFU) in Localized Prostate Cancer Treatment. *Polish journal of radiology / Polish Medical Society of Radiology* **2015,** 80, 131-41.

313. Camphausen, K.; Moses, M. A.; Menard, C.; Sproull, M.; Beecken, W. D.; Folkman, J.; O'Reilly, M. S., Radiation abscopal antitumor effect is mediated through p53. *Cancer Res* **2003,** 63, (8), 1990-3.

314. Sanchez-Ortiz, R. F.; Tannir, N.; Ahrar, K.; Wood, C. G., Spontaneous regression of pulmonary metastases from renal cell carcinoma after radio frequency ablation of primary tumor: an in situ tumor vaccine? *J Urol* **2003,** 170, (1), 178-9.

315. Kim, H.; Park, B. K.; Kim, C. K., Spontaneous regression of pulmonary and adrenal metastases following percutaneous radiofrequency ablation of a recurrent renal cell carcinoma. *Korean journal of radiology : official journal of the Korean Radiological Society* **2008,** 9, (5), 470-2.

316. Shah, T. T.; Ahmed, H.; Kanthabalan, A.; Lau, B.; Ghei, M.; Maraj, B.; Arya, M., Focal cryotherapy of localized prostate cancer: a systematic review of the literature. *Expert review of anticancer therapy* **2014,** 14, (11), 1337-47.

317. Frey, B.; Rubner, Y.; Kulzer, L.; Werthmoller, N.; Weiss, E. M.; Fietkau, R.; Gaipl, U. S., Antitumor immune responses induced by ionizing irradiation and further immune stimulation. *Cancer immunology, immunotherapy : CII* **2014,** 63, (1), 29-36.

318. Borghaei, H.; Paz-Ares, L.; Horn, L.; Spigel, D. R.; Steins, M.; Ready, N. E.; Chow, L. Q.; Vokes, E. E.; Felip, E.; Holgado, E.; Barlesi, F.; Kohlhäufl, M.; Arrieta, O.; Burgio, M. A.; Fayette, J.; Lena, H.; Poddubskaya, E.; Gerber, D. E.; Gettinger, S. N.; Rudin, C. M.; Rizvi, N.; Crinò, L.; Blumenschein, G. R.;

Antonia, S. J.; Dorange, C.; Harbison, C. T.; Graf Finckenstein, F.; Brahmer, J. R., Nivolumab versus Docetaxel in Advanced Nonsquamous Non–Small-Cell Lung Cancer. *New Engl J Med* 0, (0), null.

319. Larkin, J.; Chiarion-Sileni, V.; Gonzalez, R.; Grob, J. J.; Cowey, C. L.; Lao, C. D.; Schadendorf, D.; Dummer, R.; Smylie, M.; Rutkowski, P.; Ferrucci, P. F.; Hill, A.; Wagstaff, J.; Carlino, M. S.; Haanen, J. B.; Maio, M.; Marquez-Rodas, I.; McArthur, G. A.; Ascierto, P. A.; Long, G. V.; Callahan, M. K.; Postow, M. A.; Grossmann, K.; Sznol, M.; Dreno, B.; Bastholt, L.; Yang, A.; Rollin, L. M.; Horak, C.; Hodi, F. S.; Wolchok, J. D., Combined Nivolumab and Ipilimumab or Monotherapy in Untreated Melanoma. *New Engl J Med* **2015,** 373, (1), 23-34.

320. Gathen, V. S.-v. d.; Schaper, L.; Knake, N.; Reuter, S.; Niemi, K.; Gans, T.; Winter, J., Spatially resolved diagnostics on a microscale atmospheric pressure plasma jet. *Journal of Physics D: Applied Physics* **2008,** 41, (19), 194004.

321. Schulz-von der Gathen, V.; Buck, V.; Gans, T.; Knake, N.; Niemi, K.; Reuter, S.; Schaper, L.; Winter, J., Optical Diagnostics of Micro Discharge Jets. *Contributions to Plasma Physics* **2007,** 47, (7), 510-519.

322. Knake, N.; Niemi, K.; Reuter, S.; Schulz-von der Gathen, V.; Winter, J., Absolute atomic oxygen density profiles in the discharge core of a microscale atmospheric pressure plasma jet. *Appl Phys Lett* **2008,** 93, (13), 131503.